THE APPLICATION OF LOW ASPECT RATIO HYDROFOILS TO THE SECURE POSITIONING OF STATIC EQUIPMENT IN TIDAL STREAMS

ALAN OWEN

A thesis submitted in partial fulfilment of the requirements of
The Robert Gordon University
for the degree of degree of Doctor of Philosophy

The research programme was supported by:-
Scottish Enterprise, Aberdeen City Council, Supergen Marine,
The European Marine Energy Centre (Orkney)
The Robin Keir Watson Trust and The Robert Gordon University.

May 2007

"The existing very high cost of fuel, and the prospect that this cost is likely ever to increase, makes tidal power development a commercial possibility and attractive to capital"

A.M.A. Struben, 'Tidal Power', 1921

Abstract

The costs of installing tidal energy technology are high, requiring expensive vessels to drill sockets in the sea bed or to handle gravity based structures of substantial mass, and this impacts on the commercial viability of any proposed marine renewables development.

This thesis offers a viable alternative to socketed or gravity based installations by proposing that the downwards lift force that can be developed from the flow over a hydrofoil can be used to resist the slip and overturning moments applied to a structure by the flow. The fundamental theory of axial and crossflow energy conversion devices is outlined and the current methods of fixing and supporting tidal stream devices are analysed.

The origins of tidal stream flows are discussed and the effects of local topography, bathymetry and system resonance are used to explain the significant differences between real tidal behaviour and the ideal of Newton's equilibrium theory. The idiosyncratic and localised nature of tidal streams is thereby made clear as well as the need for a solid understanding of the resource prior to device design and installation.

The principles of classical hydrodynamics and conformal mapping are used in the context of relating theoretical lift and drag functions to low aspect ratio hydrofoils with endplates, and a numerical model of distributed surface pressures around a hydrofoil is demonstrated. Subsequently, the concept is evaluated using two $1/7^{th}$ scale test devices, one is field tested in a large stream under real flow conditions, and the second in a tow tank under ideal laboratory conditions. The limitations and challenges of model scaling are shown and the semi-empirical Froude method of scaling using residual forces is applied to the towing model. Analysis of the experimental data shows a correlation with normal distribution and extrapolation of the experimental results shows that the Sea Snail can operate with an average lift coefficient of 0.7 and drag coefficient of 0.18. Application of the experimental data to the full scale device demonstrates that the Sea Snail principle is not only valid, but is a significant advance on existing installation methodologies.

Acknowledgements

I am irretrievably indebted to my wife, Janie, and to my children, Ben, George and Tom, for their support and forbearance during the writing of this thesis.

I wish to thank my supervisors, Professor Ian Bryden and Dr David Forehand for their guidance and support, as well as the staff and other researchers (past and present) of the School of Engineering at The Robert Gordon University, for their encouragement during the project.

This has been a wide ranging project both academically and geographically, and my thanks extend to the people and businesses of Orkney who helped with sea trials, in particular Dr Jennifer Norris of the European Marine Energy Centre Ltd and Ralph Stevenson of Hamnavoe Engineering Ltd.

To everyone else who helped, in whatever way, thank you.

Contents

Nomenclature

All mathematical constants and variables are defined locally in the text, as are any acronyms.

List of figures

US 20060140724A1

(19) **United States**

(12) **Patent Application Publication** (10) **Pub. No.: US 2006/0140724 A1**

Owen et al. (43) **Pub. Date: Jun. 29, 2006**

(54) **APPARATUS FOR CONTROLLING UNDERWATER BASED EQUIPMENT**

(75) Inventors: **Alan Owen**, Ellon (GB); **Ian Gordon Bryden**, Aberdeen (GB)

Correspondence Address:
DRINKER BIDDLE & REATH
ATTN: INTELLECTUAL PROPERTY GROUP
ONE LOGAN SQUARE
18TH AND CHERRY STREETS
PHILADELPHIA, PA 19103-6996 (US)

(73) Assignee: **Robert Gordon University**

(21) Appl. No.: **10/526,264**

(22) PCT Filed: **Sep. 5, 2003**

(86) PCT No. **PCT/GB03/03845**

(30) **Foreign Application Priority Data**

Sep. 5, 2002 (GB) 0220626.6

Publication Classification

(51) **Int. Cl.**
E02B 9/00 (2006.01)

(52) **U.S. Cl.** **405/75**

(57) **ABSTRACT**

The apparatus may include a space frame on which is mounted at least one hydrofoil for generating positive or negative lift. The frame is attachable to underwater equipment such as a turbine. The hydrofoils are adapted to produce negative lift when a flow of liquid passes over them and so in use cause the apparatus and attached equipment to sink to the seabed. The flow of water over the hydrofoils continue to produce negative life and so maintain the apparatus on the seabed. In certain embodiments, the hydrofoils can typically be set to a passive configuration in which they flip over when the current flow changes direction. Furthermore, the hydrofoils are selectively rotatable to provide an angle of attack such that they may be adapted to provide positive lift when it is necessary to remove the apparatus from the water.

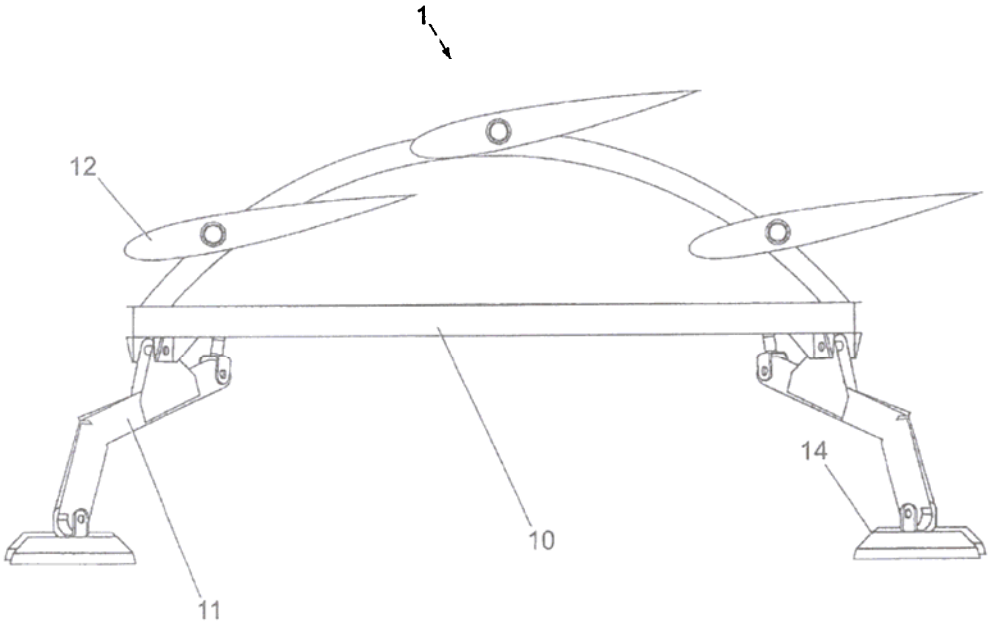

(12) INTERNATIONAL APPLICATION PUBLISHED UNDER THE PATENT COOPERATION TREATY (PCT)

(19) World Intellectual Property Organization
International Bureau

(43) International Publication Date
18 March 2004 (18.03.2004)

PCT

(10) International Publication Number
WO 2004/022856 A1

(51) International Patent Classification[7]: E02B 9/08

(21) International Application Number:
PCT/GB2003/003845

(22) International Filing Date:
5 September 2003 (05.09.2003)

(25) Filing Language:

(26) Publication Language: English

(30) Priority Data:
0220626.6 5 September 2002 (05.09.2002) GB

(71) Applicant *(for all designated States except US)*: **ROBERT GORDON UNIVERSITY** [GB/GB]; Schoolhill, Aberdenn AB10 1FR (GB).

(72) Inventors; and

(75) Inventors/Applicants *(for US only)*: **OWEN, Alan** [GB/GB]; Braeside Schoolhouse, Auchnagatt, Ellon AB41 8YE (GB). **BRYDEN, Ian, Gordon** [GB/GB]; 62 Brentfield Circle, Ellon, Aberdeenshire AB41 9DD (GB).

(74) Agent: **MURGITROYD & COMPANY**; Scotland House, 165-169 Scotland Street, Glasgow G5 8PL (GB).

(81) Designated States *(national)*: AE, AG, AL, AM, AT, AU, AZ, BA, BB, BG, BR, BY, BZ, CA, CH, CN, CO, CR, CU, CZ, DE, DK, DM, DZ, EC, EE, ES, FI, GB, GD, GE, GH, GM, HR, HU, ID, IL, IN, IS, JP, KE, KG, KP, KR, KZ, LC, LK, LR, LS, LT, LU, LV, MA, MD, MG, MK, MN, MW, MX, MZ, NI, NO, NZ, OM, PG, PH, PL, PT, RO, RU, SC, SD, SE, SG, SK, SL, SY, TJ, TM, TN, TR, TT, TZ, UA, UG, US, UZ, VC, VN, YU, ZA, ZM, ZW.

(84) Designated States *(regional)*: ARIPO patent (GH, GM, KE, LS, MW, MZ, SD, SL, SZ, TZ, UG, ZM, ZW), Eurasian patent (AM, AZ, BY, KG, KZ, MD, RU, TJ, TM), European patent (AT, BE, BG, CH, CY, CZ, DE, DK, EE, ES, FI, FR, GB, GR, HU, IE, IT, LU, MC, NL, PT, RO, SE, SI, SK, TR), OAPI patent (BF, BJ, CF, CG, CI, CM, GA, GN, GQ, GW, ML, MR, NE, SN, TD, TG).

Published:
— *with international search report*
— *before the expiration of the time limit for amending the claims and to be republished in the event of receipt of amendments*

For two-letter codes and other abbreviations, refer to the "Guidance Notes on Codes and Abbreviations" appearing at the beginning of each regular issue of the PCT Gazette.

(54) Title: APPARATUS FOR CONTROLLING UNDERWATER BASED EQUIPMENT

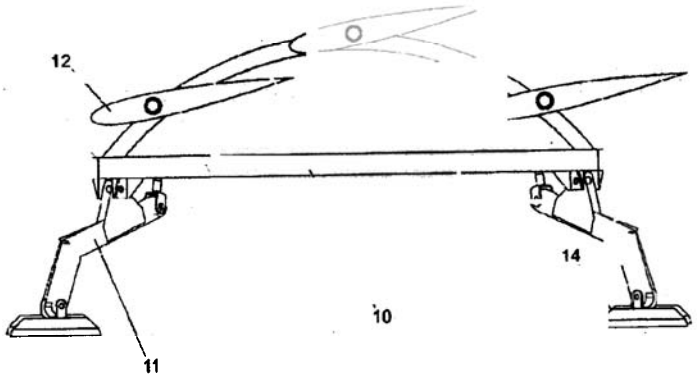

(57) Abstract: The apparatus may include a space frame (10, 110) on which is mounted at least one hydrofoil (12, 112) for generating positive or negative lift. The frame (10, 110) is attachable to underwater equipment such as a turbine. The hydrofoils (12, 112) are adapted to produce negative lift when a flow of liquid passes over them and so in use cause the apparatus (10, 110) and attached equipment to sink to the seabed. The flow of water over the hydrofoils continue to produce negative lift and so maintain the apparatus (1, 100) on the seabed. In certain embodiments, the hydrofoils (12) can typically be set to a passive configuration in which they flip over when the current flow changes direction. Furthermore, the hydrofoils (12) are selectively rotatable to provide an angle of attack such that they may be adapted to provide positive lift when it is necessary to remove the apparatus (1) from the water.

WO 2004/022856 A1

Preface

The following work demonstrates the concept of the Sea Snail, a hydrodynamic device for securing equipment in fast moving flows. The basic model was initiated by Professor Ian Bryden and the ensuing proposal was funded by the Scottish Enterprise Proof of Concept (POC) fund, a support mechanism for demonstration of the commercial potential of research proposals. The author of this thesis developed the Sea Snail from Professor Bryden's fundamental mathematical model into a fully operational 20 tonne device, subsequently deployed for sea trials in Orkney during the summer of 2005. In addition, the author is the lead inventor responsible for, and substantially the author of, the patent that protects the concept in Europe, with patents pending in the United States and Australia.

The project received £159,000 in funding from the POC fund and an additional £30,000 from the Robert Gordon University's Research Development Initiative and Aberdeen City Council, with operational and in-kind support kindly given by The European Marine Energy Centre in Orkney and Ross-Deeptech Initiatives of Stonehaven.

The author was responsible for all aspects of the research, project management, system specification, structural and systems design, budgetary control, sub-contractor negotiations, site selection, licences and permits applications, site surveys, environmental impact assessment and sea trials management. Additionally, the river test model and the tow tank model were designed, built and instrumented by the author who also published an outline paper of the concept in the journals of the Institute of Mechanical Engineers and has presented aspects of the concept at a number of international conferences.

The project achieved a considerable output on a very small budget and, though not every aspect went to plan, valuable experience has been gained in the cost effective fabrication and deployment of a device which is capable of making a substantial contribution to the early stage development of tidal stream energy.

Introduction

The generation of electrical power from tidal streams is similar to run-of – river power generation in that the kinetic energy of the moving flow is converted first to mechanical energy in the turbine and subsequently to electrical energy in the generator driven by the turbine. The principal hydrodynamic similarity is that passage through the turbine is not the only route that the water can follow, unlike tidal barrages and freshwater hydro dam schemes where turbines are positioned within a tube or duct. The flow within a tidal stream is free to find its own path, within the strictures of the local space and time dependent hydrodynamic regime, and pressure variations will permit some of the flow to circumvent the turbine disc.

A broad spectrum of tidal energy devices based on cross flow, axial flow and oscillating wings have been proposed in recent years, and, whilst many of them have yet to progress further than a speculative internet web page, there are some serious attempts to address the considerable engineering challenges of tidal stream energy. Energy conversion requires that the force applied by a moving fluid to an actuator must be resisted by an equal and opposite reaction and this inescapable fact is the essence of this thesis; how can a substantial device be installed quickly, at low cost, whilst offering minimal environmental impact and relative ease of maintenance? The Sea Snail proposal is that hydrofoils can be used to enhance the inherent weight of a structure and thus enable the structure to resist overturning and slippage. The Sea Snail concept is introduced in Chapter 1 and discussed in relation to existing tidal stream device moorings and support structures.

The operational integrity of any tidal device, (including the Sea Snail) is heavily influenced by the characteristics of the flow in which it is expected to operate. Chapter 2 offers an introduction to the driving forces and modifiers of tidal streams and considers present knowledge gaps in the understanding of the flow behaviour. A sound understanding of the tidal stream resource is of fundamental importance in the design process that will ensure the long term viability and survivability of deployed devices.

Chapter 3 outlines the fundamental hydrodynamic theory required for modelling the drag and lift forces applicable to hydrofoils and tubulars, both of which are important in the present embodiment of the Sea Snail. The use of semi-empirical Low-Aspect-Ratio hydrofoil theory is discussed and the numerical solution of a distributed surface pressure over a NACA0013 hydrofoil model is shown.

In Chapter 4, the Sea Snail concept is taken from its fundamental mathematical basis and tested both as a tow tank model and under field conditions in a real stream flow at $1/7^{th}$ scale. The experimental results are analysed and presented along with details of the data acquisition equipment used in the experiments. The implications and challenges of scale model testing are discussed and the scale testing results are extrapolated up to full size.

The experimental and theoretical results are discussed in Chapter 5 and the justification of the Sea Snail is presented prior to a short, bullet-pointed list of conclusions.

Chapter 1 Tidal devices and fixings

1.0 Chapter introduction

This text is concerned with advancing the commercial exploitation of the kinetic energy available in tidal streams, though recent work [**1**] suggests that the actual energy extracted is a combination of kinetic and potential energy, and MacKay [**2**] argues that tidal stream energy should be modelled as wave energy.

Tidal devices presently fall into two basic types, axial flow and vertical axis crossflow, and the wide range of proposals is somewhat reminiscent of the explosion of concepts for wind energy conversion in the mid-twentieth century, many of which now seem most unlikely in hindsight.

The actuator motion on tidal stream devices can be oscillatory (e.g. The Engineering Business Ltd, Stingray [**3**]), rotational or flexural and power conversion can be direct electrical or hydraulic, or even operationally distanced from the point of energy extraction (e.g. Rochester Venturi).

Though much research and development effort has been directed toward the energy conversion methodologies, with a few notable exceptions [**4**,**5**], fixing and anchoring techniques have received little attention.

The commercial exploitation of tidal stream energy is dependent on an appropriate device being installed at minimum cost, with maximum security and long term reliability, and capable of swift decommissioning with low remediation requirements. This chapter introduces the concept of the Sea Snail prior to reviewing the existing fixing and installation methodologies and subsequently developing the conceptual design of the Sea Snail.

1.1 The Sea Snail concept

The concept of the Sea Snail is that a negatively buoyant structure requires no fixing when there are no lateral forces acting on it, and that the flow itself can be utilised as a means of providing the necessary restorative forces when lateral forces are acting on the structure.

The fundamental operating principle of the Sea Snail is based on the familiar upturned aerofoil found in motor sport to increase downforce. A number of hydrofoils are mounted on a frame in such a way as to induce a lift force, in a downward sense, from the stream flow. As the flow speed increases so does the overturning moment applied to the structure and the lift force on the hydrofoils. Provided that the ratio of hydrofoil to turbine surface areas is such that the total restorative moment generated exceeds the overturning moment, then the Sea Snail will remain in position. Similarly, if the combination of self-mass and downforce exceeds the horizontal drag force applied, then the Sea Snail will remain in place provided that sufficient friction acts at its interface with the seabed.

At slack water, the Sea Snail, being negatively buoyant, will remain in place since no external moving or overturning force is acting on it, and its hydrofoils, being positively buoyant, will align themselves vertically, tail up. As the speed of the flow increases, the stream flow will overcome the hydrofoils' inherent buoyancy and rotate the hydrofoil about its shaft until it reaches its limit stops. Once at its limit stops, the hydrofoil applies downforce to the frame and creates a reaction to both the lateral drag and overturning moments applied to the frame by the current.

As the stream flow velocity reduces, the forces on the frame and hydrofoils reduce in proportion to the square of the velocity until the hydrofoils natural buoyancy is again greater then the forces applied. At the reversal of the tidal stream, the hydrofoils are passively self-reversing and will accept the flow from the opposite direction until the next slack water when the whole process is repeated.

As can be seen in Figure 1-1, given a certain minimal level of negative buoyancy, there are only two principal forces to be resisted by the structure; an overturning moment and a lateral slip.

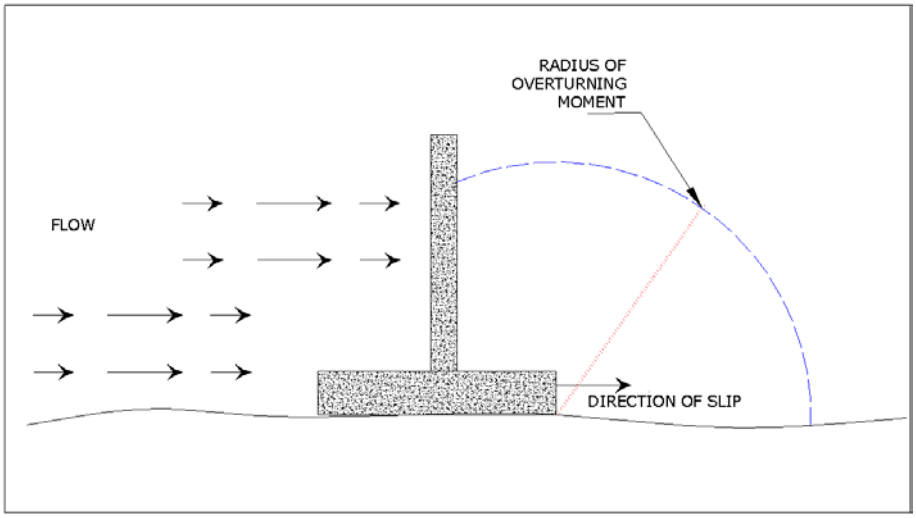

Figure 1-1: Forces and overturning moments on a simple structure placed in a flow

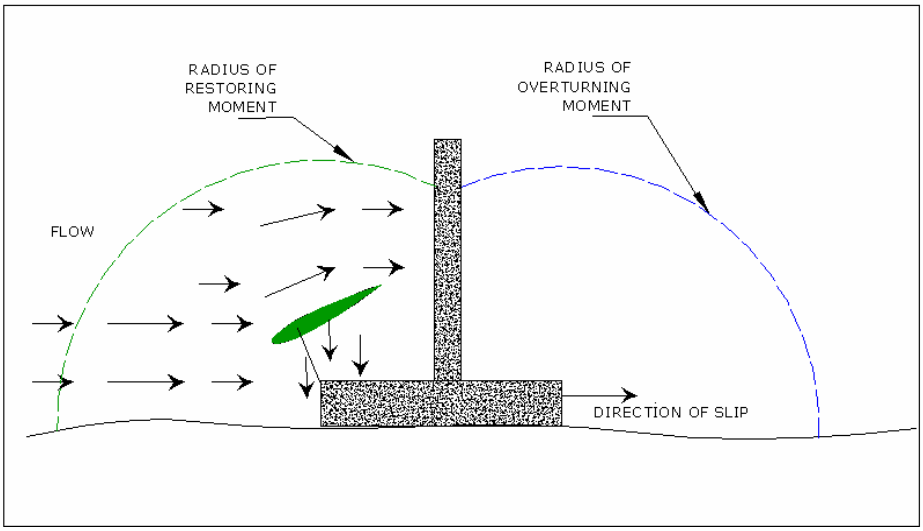

Figure 1-2: Restorative forces applied to the structure via a hydrofoil

By mounting a hydrofoil attached to the structure in an upstream position (Figure 1-2), the overturning moment is restored and the lateral slip is resisted by an increase in the downwards force applied by the structure to the seabed. Provided that the restoring moment exceeds the overturning moment and that the force applied by the structure to the seabed is sufficient

to maintain the no–slip condition required by the laws of Coulomb friction, then the device will remain in position.

Other than establishing that the seabed is reasonably level, no seabed work is required, and since no physical attachment is made to the seabed, the device is easily decommissioned and removed.

Figure 1-3: Sea Snail assembled for deployment

There are no theoretical depth limitations to its use and the Sea Snail can be installed using a readily available working boat, typical hire cost (2005) being £3,000 per day.

The Sea Snail is designed to minimise the structural form and skin drag, and its configuration illustrated here (Figure 1-3) is suitable for predominantly bi-directional streams with minimal side forces. An omni-directional Sea Snail concept is presently under development. To place the Sea Snail into its proper context, the existing devices and their fixing/mooring methodologies are discussed, prior to developing the Sea Snail conceptual design on page 46.

1.2 Devices

The essential requirement of any tidal stream energy conversion device is to cause the kinetic energy of the moving water to move an actuator and thus to produce a transmissible power output. The mode of transmissibility need not necessarily be electrical, and the transmission distance may only need to be minimal if onboard storage or energy vector conversion is available. The actuator device itself may be axially aligned with the mean flow vector, crossflow relative to the mean flow vector, or oscillating in either a vertical or horizontal sense. The preferred options have, so far, tended to follow the lead of wind power, in that a two or three bladed horizontal axis turbine or a crossflow Darrieus type turbine has been the dominant feature in most proposals. The only demonstrably viable alternative to date is the oscillating hydroplane "Stingray", which has been withdrawn by its developers.

In order to extract energy from the moving fluid, the actuator device must be supported by a structure capable of providing an equal and opposite reaction, in accordance with Newton's 3rd law. Whatever form the structure takes, it has to be fabricated, securely installed and maintained, all within a commercially acceptable budget. The operational location of the device may be considered to be surface, sub-surface or bottom mounted, but the eventual reaction point will ultimately be the seabed or shoreline, thereby introducing the local geology and sediments as material considerations.

Conversion efficiency is an important attribute of any energy conversion device and a wide variety of claims are made by the developers of tidal energy conversion devices. However, to properly evaluate the efficacy of any device proposal, it is desirable that agreed conventions are stipulated for device testing [**6**]. A draft device performance protocol is currently in preparation by the University of Edinburgh on behalf of the UK Department of Trade and Industry, though this is not yet in the public domain.

The economic exploitation of tidal streams will require that a range of Tidal Stream Energy Converters (TSEC) is available, suitably optimised for different water depths and stream flow characteristics and capable of being deployed in large arrays at appropriate spacing. In bi-directional flows it may

be possible to employ relatively tight unit spacing perpendicular to the flow, but, due to the persistence of turbulent eddies in water (discussed on page 86), streamwise spacing will be at considerable distances.

Other than extracting energy from a moving fluid, and sharing some basic conceptual architecture, wind turbines and tidal devices have little in common. The structural blade loading for a horizontal axis TSEC is flapwise bending in the axial direction and, for a crossflow axis TSEC, spanwise bending in the radial direction. But a horizontal axis wind turbine will experience much greater centrifugal and gravitational loadings which will also negate some of the flapwise bending forces [**7**]. The use of water as the working fluid also introduces the possibility of cavitation, where local pressure on the downstream face of the turbine blade drops to the point of vaporisation and the boundary layer separates from the blade surface. As well as limiting performance, cavitation also causes damage to the blade surface, reducing blade life, and, since cavitation is pressure related, the maximum blade tip speed is therefore partially governed by the turbine's minimum proximity to the free surface. Much work has been carried out on the fluid dynamics of wind turbines, hydro turbines and ship's propellers, but these fields only partially overlap the characteristics of tidal energy extraction, they do not fully encompass them. For the purposes of comparison, the structures and moorings will be assumed to be carrying a load equivalent to 5 m diameter turbine with a rated coefficient of power (C_P) of 0.4 with its rotational axis 6 m above the seabed (or mid-depth for buoyant devices) in 30 m depth of water, generating 100 kW output at a flow velocity of 3 m/s.

1.2.1 Axial flow actuator

A submerged axial flow turbine will have its principal rotational axis parallel to the free stream velocity vector, and present an array of two or more hydrofoil section blades which rotate about that axis. The blade profile will generally be asymmetric if the blade's attitude can be altered to accept flow

from different directions, and symmetric if the blade is to accept flow from two opposing directions.

The most hydrodynamically efficient tidal stream energy converters (TSEC) use a hydrofoil section blade to create a lift force (as compared with the drag force applied to a panemone) given by,

$$F_L = 0.5 C_L \rho A U^2 \qquad \textbf{(1-1)}$$

Where, F_L is the lift force, ρ is the fluid density (typically 1025 kg/m^3 for seawater), U is the free stream velocity (m/s), A is the area of lift surface apparent to the mean flow vector, and C_L is the lift coefficient

The theoretical power output of a TSEC is governed by the same fundamental equation as that of a wind turbine,

$$P = 0.5 C_p \rho A U^3 \qquad \textbf{(1-2)}$$

Where, P is power, A is the swept area of the device, and C_p is the power coefficient, which describes the device's energy capture efficiency (thought to be approximately 0.3 [**8**] for tidal turbines, though Marine Current Turbines Ltd are quoting a C_P of 0.45. [**9**]). The derivation of C_P is discussed on p8. This lift/power relationship holds for both horizontal axis and crossflow rotating devices, as well as for oscillating devices [**10**].

From equation ***(1-1)*** the forces applied to a tidal turbine are a function of the area that it presents normal to the flow. However, as will be demonstrated in Chapter 2, the flow is not consistently well behaved and steady and as a result, nor are the forces. The blades of an axial flow tidal turbine are subject to flapwise bending moments, changes in static pressure, and dynamic pressure fluctuations from turbulence and wave action (see 2.4.3). Additionally, the drag forces F_D given by ***(1-3)*** will act upon the support structure, the turbine blades and any mooring or umbilical systems.

$$F_D = 0.5 C_D \rho A U^2 \qquad \textbf{(1-3)}$$

where C_D is the drag coefficient of the component concerned. The basic coefficients of thrust force C_F, power C_P, and torque C_T of axial flow tidal turbines can be defined using linear momentum theory. The definitions of C_L and of C_D are discussed in Chapter 3.

Linear Momentum Theory

An axial flow turbine can be simply modelled [**11**] as a hypothetical actuator disc which decelerates an inviscid fluid from its freestream velocity U_1 to a downstream velocity U_3. Referring to Figure 1-4, the kinetic energy per unit time in the tidal stream E_K is given by $E_K = 0.5\rho A U_1^3$ where U_1 is the free stream velocity, which will vary considerably with turbulence, shear, and the vertical distance from seabed to free surface (see section 2.4.3), but for present purposes is assumed to be steady and uniform across the turbine face. A represents any arbitrary area chosen through which the tidal stream flows. For basic turbine modelling, this area is usually the swept area of the turbine, considered to be an actuator disc across which a change of pressure occurs as energy is extracted from the flow. The decrease in the momentum of the flow caused by energy extraction can be used to find the thrust force F_T upon the turbine from,

$$F_T = \dot{m}U_1 - \dot{m}U_3 \qquad \textbf{(1-4)}$$

where $\dot{m} = \rho A_2 U_2$ and the power extracted from the tidal stream by the turbine P_T is given by,

$$P_T = \dot{m}(U_1 - U_3)U_2 \qquad \textbf{(1-5)}$$

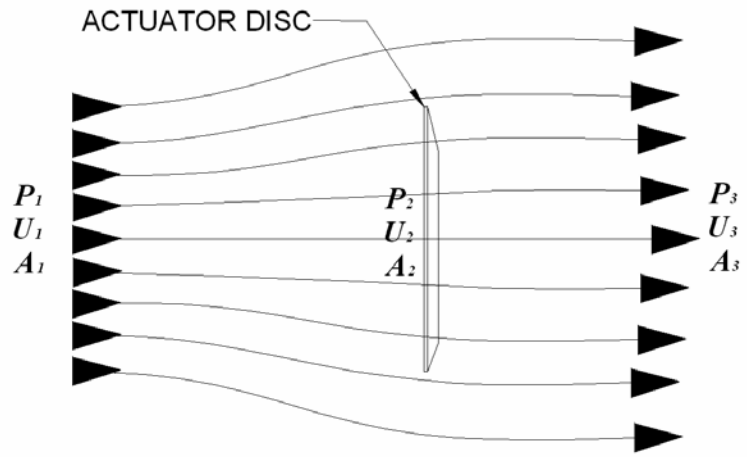

Figure 1-4: Actuator disc model of axial turbine

and the loss in energy per unit time from the tidal stream P_{TS} is,

$$P_{TS} = 0.5\dot{m}\left(U_1^2 - U_3^2\right) \qquad \textbf{(1-6)}$$

Substituting for $\dot{m}$ in ***(1-6)*** gives

$$P_T = \rho A_2 U_2{}^2 (U_1 - U_3) \qquad \textbf{(1-7)}$$

Now, equating ***(1-5)*** and ***(1-6)*** leaves

$$U_2 = \left(\frac{U_1 + U_3}{2} \right) \qquad \textbf{(1-8)}$$

Therefore, from linear momentum theory, the flow speed through the actuator disc must be $>0.5U_1$. Rearranging ***(1-8)*** for U_3 and applying the result to (1-7) leaves

$$P_T = \rho A_2 U_2{}^2 (U_1 - (2U_2 - U_1)) = \rho A_2 U_2{}^2 2(U_1 - U_2)) \qquad \textbf{(1-9)}$$

A dimensionless factor referred to as the interference factor a represents the fractional drop in flow velocity at the turbine, given by,

$$a = \left(\frac{U_1 - U_2}{U_1} \right) \qquad \textbf{(1-10)}$$

from which,

$$U_2 = (1 - a) U_1 \qquad \textbf{(1-11)}$$

so,

$$P_T = 2\rho A_2 (1-a)^2 U_1{}^2 (U_1 - (1-a)U_1) = \{4a(1-a)^2\} 0.5 \rho A_2 U_1{}^3 \qquad \textbf{(1-12)}$$

the power coefficient C_P is defined as,

$$C_P = 4a(1-a)^2 \qquad \textbf{(1-13)}$$

and is therefore a function of the freestream velocity and the stream velocity at the actuator disc. Plotting C_P against a gives a maximum value of C_P=0.59 at a = 0.33 approximately, Figure 1-5, and is known as the Betz limit when applied to wind turbines.

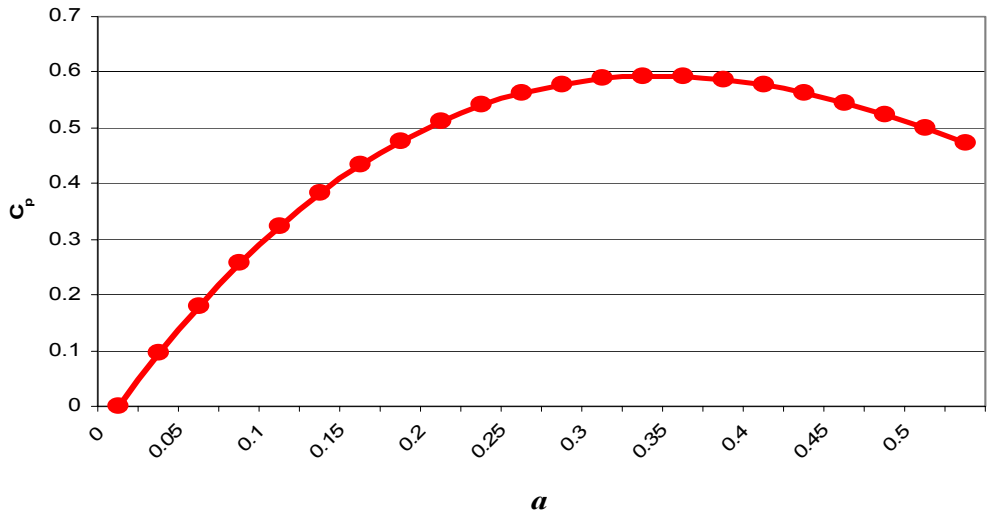

Figure 1-5: C_p as a function of interference factor, a

As discussed, the linear momentum theory assumes an incompressible flow operating on a hypothetical energy extraction device which is an infinite distance from any constraining boundary [**12**], and this is not necessarily the case for a tidal stream turbine, the flow through which is constrained at least by the seabed and the free surface, and often by the channel sides as well. Thus use of the Betz limit is therefore not necessarily applicable to tidal turbines, but technology and fluid mechanics are likely to be the performance limiting factors for the foreseeable future, rather than a hypothetical flow velocity limitation.

Thrust Coefficient

Using the same actuator disc approach as before, a tidal turbine will create a pressure difference across the thickness of the actuator disc. Referring again to Figure 1-4, if no energy is extracted at this stage, then from Bernoulli, taking g as gravity and z_1 and z_2 as the vertical displacements,

$$\frac{P_1}{\rho_1 g}+\frac{U_1^{\,2}}{2g}+z_1=\frac{P_2}{\rho_2 g}+\frac{U_2^{\,2}}{2g}+z_2 \qquad \textbf{(1-14)}$$

Assuming that no significant change of depth occurs (i.e. z_1=z_2) for any of the fluid and that the fluid is homogenous (i.e. ρ_1=ρ_2), then,

$$P_1 - P_2 = \Delta p = \left(U_1^{\,2} - U_2^{\,2}\right)\rho / 2 \qquad \textbf{(1-15)}$$

where the left hand terms, P_1-P_2 represent static pressure and the right-hand terms represent dynamic pressure. Equation ***(1-15)*** reaches a maximum as the value of U_2 approaches zero, which equates to the actuator disc being an impermeable boundary, and thus the maximum thrust force on an impermeable disc is,

$$F_{thrust} = \rho A_2 U_1^{\,2} \qquad \textbf{(1-16)}$$

Equating this to the loss of momentum by the tidal stream ***(1-4***), and substituting as before gives,

$$F_{thrust} = 0.5\rho A_2 U_1^{\,2}\left(4a\left(1-a\right)\right) \qquad \textbf{(1-17)}$$

From which, the thrust coefficient, C_F

$$C_F = 4a\left(1-a\right) \qquad \textbf{(1-18)}$$

which has a maximum value of 1 when a=0.5,

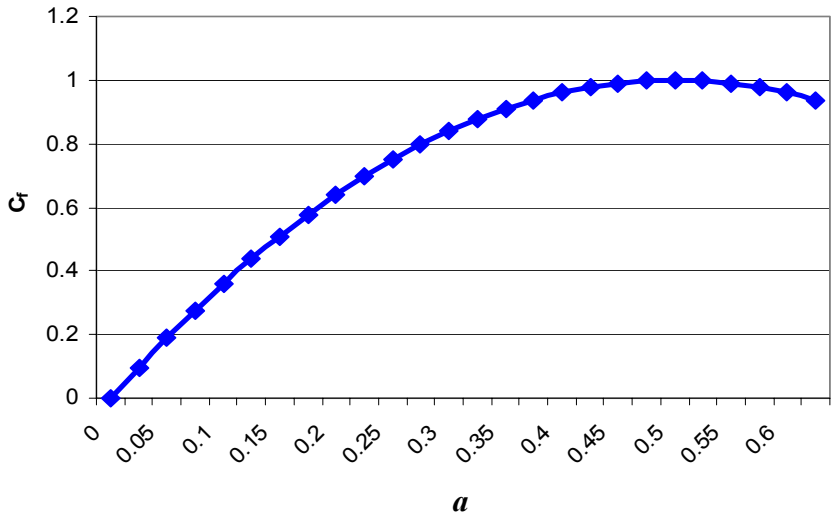

Figure 1-6: Thrust coefficient as a function of interference factor, a

Torque Coefficient

For a turbine of radius, r, the maximum applicable torque assumes that the maximum thrust F_{max} is applied at the blade tip,

$$T_{max} = F_{max} r \qquad \textbf{(1-19)}$$

and the torque coefficient (C_T) is defined as the torque available (T) at the shaft as a proportion of the maximum torque (T_{max}) that is theoretically possible.

$$C_T = \frac{T}{T_{max}} \qquad \textbf{(1-20)}$$

The tip-speed-ratio TSR is defined as the ratio of the instantaneous blade tip tangential velocity V_T and the free stream velocity of the tidal stream that is driving the turbine U_1, i.e.

$$TSR = \frac{V_T}{U_1} = \frac{\omega r}{U_1} \qquad \textbf{(1-21)}$$

where ω is the angular frequency. Rearranging ***(1-21)*** for r and substituting, along with ***(1-16***) into ***(1-19***), gives

$$T_{max} = F_{max} r = P_{TS} \frac{TSR}{\omega} \qquad \textbf{(1-22)}$$

The delivered power at the turbine shaft from ***(1-12)*** is,

$$P_T = 0.5 C_P \rho A_2 U_1^{\,3} = T\omega \qquad \textbf{(1-23)}$$

So,

$$C_P P_{TS} = C_T T_{max} \omega \qquad \textbf{(1-24)}$$

and, from ***(1-22***)

$$C_P = C_T TSR \qquad \textbf{(1-25)}$$

For optimal energy extraction, the turbine requires to be dynamically matched to its environment via the TSR and the number of blades n, but a reasonable approximation of the optimal value of TSR is given by [**13**], as

$$TSR_{opt} = \frac{4\pi}{n} \qquad \textbf{(1-26)}$$

The solidity of a turbine is defined as the ratio of the blade area perpendicular to the flow and the turbine disc swept area.

Having reviewed the fundamental theory of the operation of axial flow devices, there now follows a brief discussion of some of the more advanced proposals. The objective here is to illustrate the range of energy conversion machines that could be installed using a Sea Snail structure.

Axial flow projects

The axial flow turbine is commonly found amongst tidal stream energy proposals, but is yet to establish the dominance that its three-bladed wind-driven equivalents have achieved. The balance of forces that three blades offer to wind turbines is less of an issue in seawater, where buoyancy considerations can be utilised to reduce the blade's submerged weight. The small number of sea-trialled projects and the commercially sensitive nature of real data offer little material for turbine optimisation at this point in time.

The floating turbine demonstrated in the Corran Narrows of Loch Linnhe in 1994, by IT Power Ltd, can be considered to be the originator of the present drive to exploit the energy in tidal streams.

Figure 1-7: 1994 Loch Lihnne rotor (Courtesy of Marine Current Turbines Ltd)

The Loch Linnhe turbine demonstrated the fundamental viability of tidal stream energy, and gave an early indication of the substantial technological barriers that would need to be surmounted in years to come. Amongst these

challenges is the secure mooring of floating devices, particularly if attached to unsecured power cables, and their susceptibility to torsional forces and entanglement. The 3.5 m turbine was suspended below a catamaran pontoon and is reported to have generated 15 kW in a 2.5 m/s stream. [**14**].

The UEK turbine (Figure 1-8) utilises a ducted turbine combined with a diffuser to improve the flow through the turbine and claims to have the potential to achieve an efficiency of 57.1% [**15**]. The device was deployed as a 3 m diameter unit in the DeQew (Ontario) hydro station in 2000, though no indication is given regarding the anchorage system that secured the device.

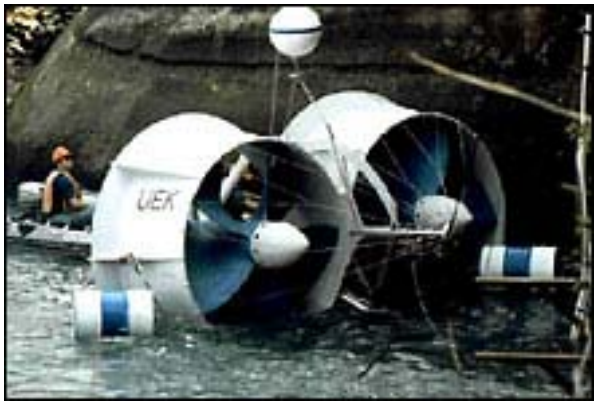

Figure 1-8: Abacus Controls Kite, (Courtesy of UEK Corporation)

The Marine Current Turbines (MCT) Ltd Seaflow project is by far the most advanced and rigorously tested tidal energy device yet installed in the field. It has been operating off North Devon since May 2003, generating up to 300 kW and dissipating the generated power as heat via a resistive load cooled by the surrounding seawater.

The device consists of a twin bladed rotor attached to the gearbox/generator assembly which is supported on a surface piercing, tubular steel pile grouted into a pre-drilled socket in the seabed. By means of equipment housed within the steel pile, the rotor and power train can be hydraulically raised above the free surface for maintenance, and lowered for installation and running.

Figure 1-9: Artist's impression of SeaGen (Courtesy of Marine Current Turbines Ltd)

The powertrain components (epicyclic gearbox and generator) are essentially marinised versions of existing equipment, but the 11 m diameter rotor is a bespoke composite design. Each blade can be rotated through 180^{o} to accept bi-directional flow and is formed around a carbon fibre skeleton that transmits the forces from the hydrodynamic surface to the blade root [**16**] and thence to the shaft. The present version of the technology is the Seagen project (Figure 1-9), a twin rotored 1 MW rated concept, built on the experience of the earlier 300 kW Seaflow device and planned for deployment in Strangford Lough Narrows, Northern Ireland.

1.2.2 Crossflow actuator

Frequently described as vertical axis turbines, because they are usually mounted vertically, these turbines are more accurately described as crossflow, since the flow must cross their axis of rotation, which could be horizontal as well as vertical. In 1976, the Intermediate Technology Development Group, forerunners of IT Power and MCT Ltd, installed a 3 m diameter Darrieus turbine in the Nile River, mounted beneath a pontoon. This

device worked successfully for two years, pumping 50 m^3 of irrigation water daily through a head of 7 m [5]. A Darrieus turbine was also proposed for use in low-head barrage systems in Japan in 1998 [**17**]. The vertical axis application of crossflow concept has the advantage of removing any requirement for directional positioning of the turbine relative to the flow. There have been some surface mounted proposals using paddle wheels, and these would constitute crossflow turbines in the strict sense, but they are drag-based machines rather than lift-based machines.

The Darrieus turbine consists of a number of symmetrical section hydrofoils distributed tangentially around a common axis.

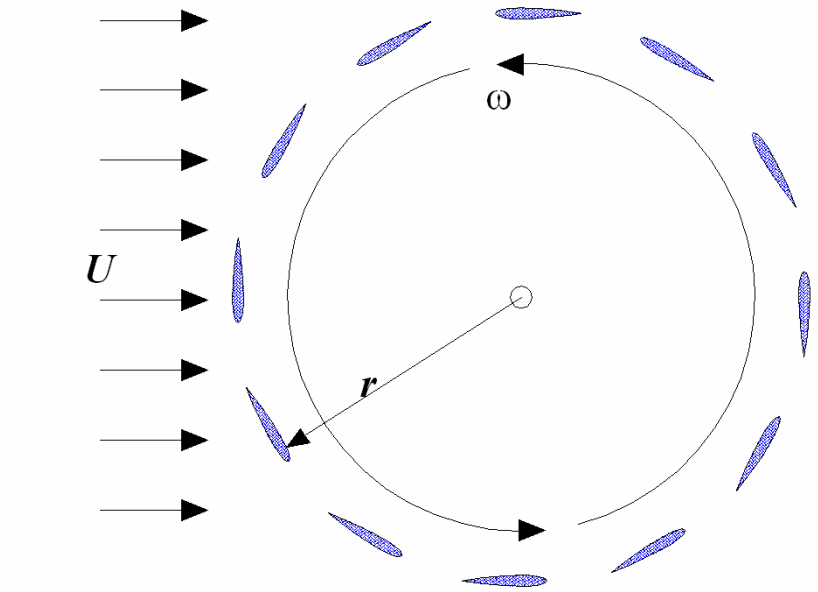

Figure 1-10: Fixed pitch Darrieus turbine schematic

The hydrofoils are fixed and rely on their rotation relative to the flow stream to bring them into two periods of variable lift throughout 360°. The optimal lift is generated at two positions relative to the flow for a duration dependant on the stream flow velocity and the turbine tip speed, which in water is necessarily relatively slow. As a result, fixed pitch Darrieus type turbines are poor self-starters, and, since the hydrofoils spend most of their rotational transit in a stalled mode, are therefore generally limited to a maximum C_p of 0.2 according to Salter [**18**], though this value is contradicted by Kiho [**19**]

with a C_P claim of 0.56. For tip speed ratio (TSR)>1, there will also exist two locations where the flow and the blade are in direct opposition, and at these points, a zero angle of attack and minimised drag is required.

Crossflow actuator theory

The crossflow turbine can be simply evaluated using the same linear momentum theory outlined for the axial flow machines on page 8. An idealised model is presented here using the distributed surface pressures (DSP) model developed in Chapter 3. Taking 12 o'clock and 6 o'clock from Figure 1-10, as 0° and 180° respectively, the values of C_L and C_D are given by the model as in Figure 1-11. It should be noted that the model is restricted to a maximum value of $\alpha \approx 20°$ in a real flow due to flow separation.

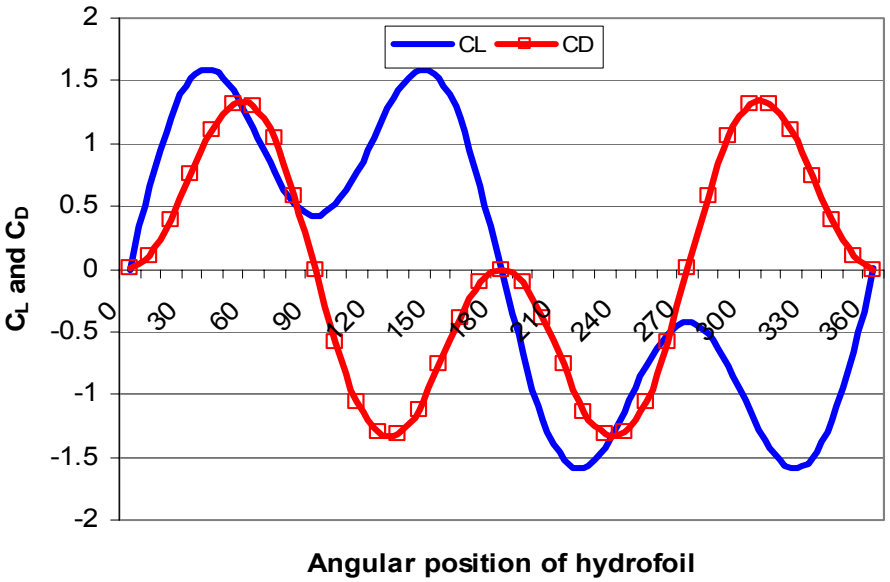

Figure 1-11: C_L and C_D of NACA0013 hydrofoils on a Darrieus Turbine

This model gives a net motive force of 26 N, and the reason for this low torque is that as the DSP model shows, for a static position the lift and drag forces almost cancel each other out. The DSP model does not allow for the fact that when the hydrofoils are rotating relative to the flow stream the flow seen by the hydrofoils is the apparent flow (Figure 1-12) rather than the static situation shown in Figure 1-10, and it is the sum of the relative flow

vectors from each hydrofoil that generate the motive force. From this it follows that the fixed blade crossflow turbine is sensitive to tip-speed ratio.

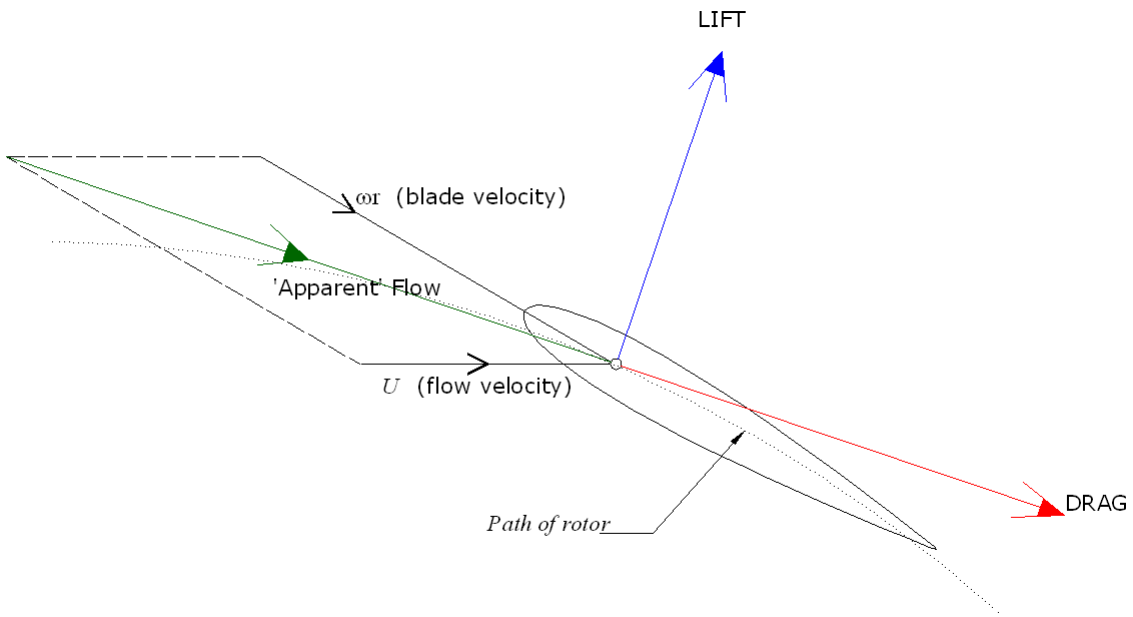

Figure 1-12: Apparent flow as seen by the hydrofoil.

The lack of substantial starting torque is therefore the significant difficulty with fixed blade Darrieus turbines, often requiring a short period of motoring of the rotor to initiate rotation. Other difficulties with the fixed blade Darrieus rotors include cavitation at high rotational speeds and a narrow band of efficient operational speeds.

There are a number of alternative approaches, all of which utilise some form of blade pitch control during the rotational cycle to increase the starting torque and the overall efficiency.

Crossflow actuator projects

The Davis turbine [**20**] is a development of the expired 1927 patent on the crossflow wind turbine proposed by Georges Darrieus. The Davis Turbine, renamed the Blue Energy Ocean Turbine, is a free stream device, claiming a generating capability of 6 kW/m^2 of turbine CSA in a 3 m/s stream flow, implying a C_P of 0.43, but no generator cut-in flow velocity is given so an evaluation of performance over a range of flow velocities is not possible. In

its tidal fence configuration, each module of the Davis Turbine consists of four fixed hydrofoil blades connected to a rotor that drives a unified gearbox and electrical generator assembly. The unit is mounted in a concrete marine caisson which anchors the unit to the ocean floor, directs the water flow through the turbine and supports the coupler, gearbox, and generator above. However, no mention is made of the fluctuating pressure and dynamic loads, nor if the structure is susceptible to resonance with so many rotating devices.

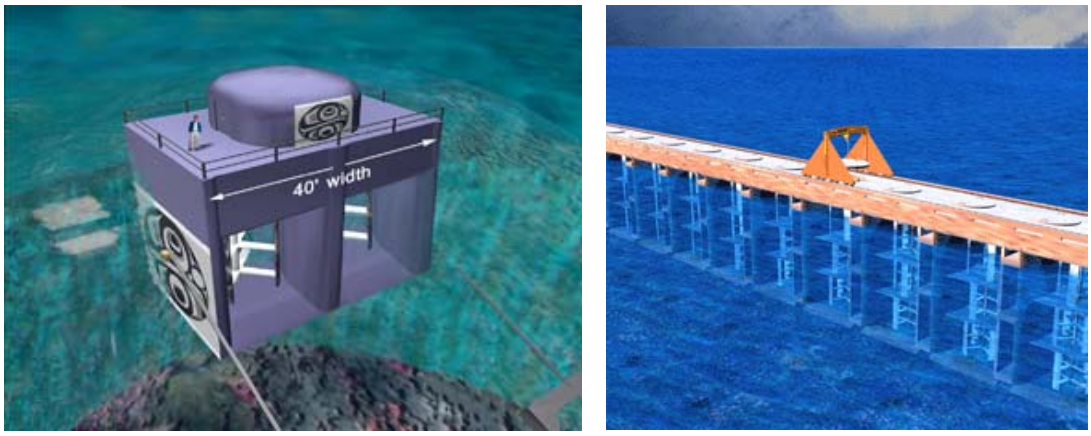

Figure 1-13: Blue Energy concept. (Courtesy of Blue Energy, Canada)
Left: 250 kW unit Right: Tidal fence array

Self aligning pitch devices

A four blade Darrieus type turbine, patented as the Kobold turbine [**21**] has offered a solution to the starting torque difficulty by allowing the hydrofoils to freely oscillate by up to 10^{o}, thus increasing lift and decreasing drag differentially at certain hydrofoil position's in the rotation. The Enermar project [**22**], has carried out field research and experiments by installing a platform equipped with a Kobold turbine in the Strait of Messina. The Kobold turbine is a variation on the Darrieus theme, with asymmetrical hydrofoil section blades (HILIFT 18) that can self align in order to maximise lift forces and minimise drag forces.

The 6 m diameter turbine uses three blades with a vertical height of 5 m and a chord length of 0.4 m. The blade pitch is controlled by means of balancing masses which alter the centre of gravity of the blade and thereby modify the

turbine performance. The device, fully described in [**21**], is claimed to have generated 20 kW in a flow speed of 1.8 m/s and to have achieved an overall efficiency of around 23%, though as in many proof of concept trials, the start and end points of system efficiency are not carefully defined. The turbine is currently installed and generating power in the Strait of Messina.

Other crossflow axis concepts such as the Flettner Rotor and Turbosails ™ have been modelled by other investigators [**23**] and found to be unlikely to offer any advantages over existing Darrieus-based devices.

Cyclic Pitch devices

The controlled cyclic pitch device is similar to the Voith Schneider mechanism that has been exploited as a ship propulsion system.

The angle of attack of a fixed blade crossflow device varies cyclically with the turbine rotation, and any control mechanism that seeks to improve the useful lift duration must adjust the angle of attack cyclically. If the flow through the turbine perpendicular to the rotational axis is considered to be made up of a finite but large number of streamtubes, then, neglecting the tangential streamtubes at the very periphery of the rotor, each blade passes through each streamtube twice per revolution. The lift (and drag) imparted to each hydrofoil by each streamtube can be integrated over one full cycle to give the total applied torque at the axis.

Cyclic pitch control seeks to optimise this relative position for as many hydrofoils as possible and for the greatest continuous period of rotation. One solution, comprehensively described in [**24**], suggests that a hydraulic control mechanism, powered by the turbine's own rotation, can be used to enforce a cyclic motion on each blade so that its angle of attack is altered relative to its position in the turbine ring and the flow direction. A tow tank model has been tested and results showed fair correlation with the streamtube model and demonstrated a TSR of 1.2. Alternative mechanisms are possible but mechanical linkages are prone to fouling, corrosion and wear, and electrically powered actuation requires some form of on board generator and is also prone to corrosion in salt water. Hydraulics additionally

offers the option of using freshwater as a working fluid, thus removing any concerns over leaks and contamination.

Devices summary

There is no shortage of energy conversion proposals for tidal streams, but many are unproven, most are very complex and almost all are expensive. There is a wide range of efficiency claims, but there is no formal definition of efficiency or its relation to C_P and this factor makes turbine comparison very difficult. Also, cut-in speed is an important consideration that is rarely discussed in tidal-turbine literature; without it, no reasonable calculation of delivered power can be made. The fact that 1 kWh of energy will not provide the same market-driven profit as its equivalent measure of oil means that for tidal stream energy to be successful, the turbine must be cheap to build. In addition, the turbine geometry needs to be sufficiently robust to operate efficiently within a broad tolerance range otherwise the surface geometry of a tidal stream device relative to the flow is totally dependent on the accuracy of the support structures' installation. The supporting structure must be capable of maintaining the optimal orientation of the turbine relative to the flow since poor positional control may place unforeseen loads on the device, which in turn will place additional demands on the support structure and moorings. It is ultimately the moorings that will control the support structure position and therefore the position of the turbine relative to the flow.

The next section will examine and evaluate the range of mooring fixings available for supporting tidal devices.

1.3 Mooring Systems

The adequate fixing and restraint of tidal stream energy converters is probably the least developed technology area within the fledgling tidal energy industry. A significant proportion of the installation cost is consumed by the fixing methodology and the success of the device is inextricably bound to the success of its attachment to the seabed. There are a number of requirements that a fixing system should meet, and the following are adapted from proposals for wave energy converters, [**25**],

- To maintain the device in position under normal operating conditions and pre-defined storm surge conditions.
- To withstand all the loadings applied to the structure and to do so at a cost effective rate.
- To withstand corrosion and biofouling, and to inherently provide sufficient strength and durability to outlast the service life of the device which it is securing.
- To incorporate sufficient redundancy to minimise the probability of catastrophic failure.
- To permit regular inspection of all components, and particularly those subject to cyclic loads.
- To permit cost effective decommissioning and require minimal subsequent remediation.

The basic fixing systems appropriate for securing TSEC are, gravity base, gravity anchor, rock bolts and suction/driven/drilled pile anchors, and the advantages and disadvantages of each method are discussed. The development of the Sea Snail, a novel, dynamic, combined fixing and support structure concept, (see page 46) is a direct response to these difficulties and is particularly applicable to shallow tidal streams.

1.3.1 Gravity base

The gravity base is a body of sufficient mass to adequately resist the vertical loads, and horizontal loads applied to a TSEC, with an acceptable factor of safety. The mass itself can be precast, e.g. concrete, or liquid slurry pumped into a containing shell that forms part of the device to be secured. Precast concrete mass is relatively quick and simple to deploy, but handling can be awkward, especially if consideration is given to the fact that the mass footprint needs to be substantial in order to maximise the seabed friction. In addition, due to its different properties in compression and tension, concrete used as a tether block can only hold an embedded bail with a maximum force equivalent to that of half the mass of the block. Therefore 1 m^3 of concrete with a dry mass of about 2600 kg, will weigh approximately 1600 kg due to its buoyancy in water, and can only be used to secure 12700 N. This makes non-reinforced precast concrete gravity anchors poor holding value for a given volume handled, as will be demonstrated shortly.

Pumped slurry can be used to transfer dense negative value material into a void from which the water can drain, leaving the denser material behind. If the material is environmentally benign e.g. quarry waste, and no setting agent or cement has been used, then there exists the possibility that the void can be evacuated at the end of the device's service life, leaving the shell to be recovered as deployed.

The sliding friction that can be resisted by the block will depend on the friction coefficient between the two contact faces. This may be substantial, e.g. where scouring or settlement allows the gravity anchor to sink below its original installation level, or minimal, e.g. where a square faced gravity anchor is resting on an exposed uneven rock bed. When the possibility of combined tidal stream and swell forces are considered, a high safety factor will be necessary for a satisfactory confidence level, especially for buoyant submerged devices. For a gravity base to be effective, the seabed must be reasonably level, thereby requiring preparation in advance if it is not already suitable.

A gravity base uses the same principle as a deadweight anchor and its effectiveness can be modelled from a free body diagram [**26**]. The maximum securing force that a gravity base can exert is given by,

$$W = B + T\,sin(\phi) + T\,cos(\phi)\left[\frac{\mu\,sin(\theta) + cos(\theta)}{\mu\,cos(\theta) - sin(\theta)}\right] \qquad \textbf{(1-27)}$$

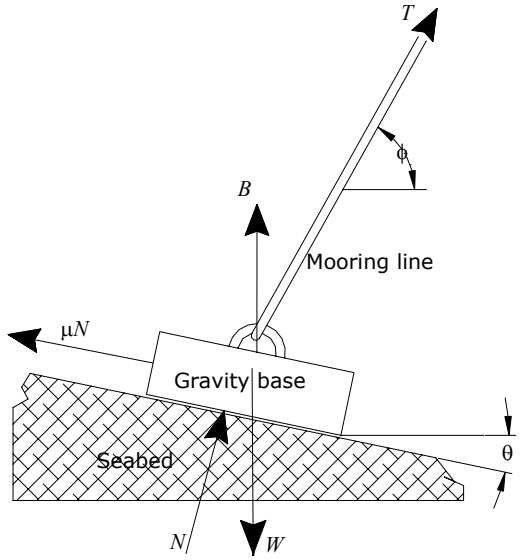

Figure 1-14: Forces applicable to gravity base object

The limiting case for a gravity base on a sloping seabed is when $\theta = a\,tan(\mu)$, at which point the anchor is sliding down the slope. For a horizontal seabed,

$$W = B + T\,sin(\phi) + \frac{T\,cos(\phi)}{\mu} \qquad \textbf{(1-28)}$$

Thus the maximum horizontal component that can be applied is inversely proportional to the value of the coefficient of friction (μ) and therefore, in spite of being cheap and easy to make, the applicability of the gravity anchor is restricted to vertical (or near vertical) loads on a flat stable seabed.

The ability of a gravity base to resist overturning moments due to flow is a function of the base length co-linear with the applied moment as well as the net value of W.

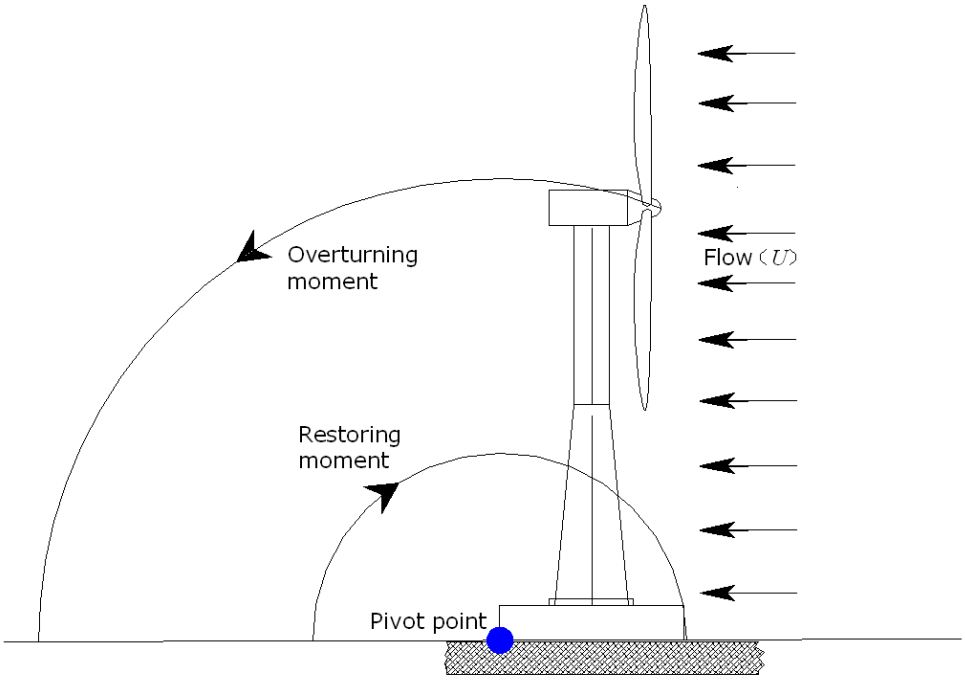

Figure 1-15: Gravity base moments

In addition to the overturning moment, a turbine reaction moment will also be applied by the power generating torque created by the turbine blades, which will be perpendicular to the flow, so the net moment will be a resultant and therefore will not be collinear with the flow velocity, U.

The key constraints on a gravity base will be,

- increasing the base planform area will improve moment resistance but make handling and cranage difficult
- increasing the base height will increase the mass and improve cranage but will also increase the overturning moment applied by the turbine unless the tower is shortened to compensate
- the turbine reaction moment will be at a maximum under the same flow conditions that the overturning moment will be at a maximum and any additional surge could destabilise the system, shifting it from its designed position
- undermining by scour will affect the position and therefore the dynamic response of the complete structure.

As introduced previously, for general comparisons between the various mooring types, a hypothetical 5 m diameter turbine positioned 6 m above the

seabed will be used to demonstrate the loading applied to the mooring. The turbine mast is 400 mm x 20 mm CHS tubular steel and the gravity base is assumed to be concrete. A hypothetical safety factor of 3 is applied to allow for surge loading and allowing for tensile loading of concrete requires an additional multiplier of 2.

Table 1-1: Gravity base parameters

Gravity base							
Turbine Cp	0.4		Gravity base sizes	Width (m)			6
Turbine TSR	3			Length (m)			6
Turbine diameter (m)	5			Height (m)			2.25
Tower outer diameter (m)	0.4			Factor of safety			2
Tower inner diameter (m)	0.36			Submerged Mass (tonne)			128
Tower height (m)	3.75			Moment arm (m)			3.20
Total height (m)	6			Ixy (m^4)			0.00043
Water density (kg/m^3)	1025			E (N/m^2)			2.1E+11
Density concrete (kg/m^3)	2600			Dry mass (tonnes)			211
mass of mast (kg)	698			Cranage (tonne metres)			1479
Flow velocity (m/s)	0	0.5	1	1.5	2	2.5	3
Axial force on turbine (N)	0	2516	10063	22642	40252	62893	90566
Torque reaction (Nm)	0	335	1342	3019	5367	8386	12075
Overturning moment (Nm)	0	15094	60377	135849	241510	377359	543397
ω (radians/sec)	0.00	0.60	1.20	1.80	2.40	3.00	3.60
Maximum torque (Nm)	0	6289	25157	56604	100629	157233	226416
Shaft Torque (Nm)	0	839	3354	7547	13417	20964	30189
Power (kW)	0.00	0.50	4.03	13.58	32.20	62.89	108.68
Net moment (Nm)	0	15098	60392	135883	241570	377452	543532
Mast deflection (m)	0.00	0.00	0.01	0.02	0.03	0.05	0.07
Slip force as % of weight	0.0%	0.35%	1.41%	3.17%	5.64%	8.82%	12.70%
Restorative moment (kNm)	4032						
Net restorative moment (kNm)	4032	4002	3911	3760	3549	3277	2945

For the hypothetical case, a gravity base of 81 m^3 of concrete is required to maintain position in a 3 m/s flow. With the steel tower, this represents a dry mass of 211 tonnes (no turbine or generator mass is included as this is assumed to be consistent for all cases). The device is unlikely to slip since at 3 m/s the slip force is only 13% of the submerged weight of the device. The main point of interest here is the cranage capability required; allowing 4 m

for manoeuvring space in addition to half of the width of the gravity base gives a cranage capability requirement of 1479 tonne metres.

The long-term security of a gravity base will require the existence or preparation of suitable seabed conditions. However, gravity bases are cheap and quick to install compared to socket drilling.

1.3.2 Rock bolts

Rock bolts are available with a variety of fixing mechanisms. The simplest approach is a mechanical expansion shell that grips the sides of a drilled hole. The vertical forces attempting to withdraw the bolt are resisted by the friction between the rock bolt shell and the rock, for as long as the applied force does not exceed the fracture strength of the rock into which it is inserted. Similarly, horizontal forces are resisted by the shear strength of the bolt material and the crushing strength of the rock.

The holding capacity of the rock bolt is dependent on the qualities of the geology into which it is inserted. If the rock is soft or fractured, the rock bolt's holding capacity can be improved with polyester resin or cement grouting. An additional benefit of cement grouting is that a socket can be drilled oversize and the grout will allow minor realignment of the socket and the bolt axes.

For a rock bolt fixing to be able to withstand fluctuating forces, it is a necessary condition that the item to be fixed and the rock surface are in good surface contact over as large an area as possible. Since it would be very difficult to adequately mate the surfaces of the seabed rock and the base of a device, it is this requirement that makes rock bolts inappropriate for tidal stream energy device fixing. In addition, rock bolts need to be installed by divers, or possibly by remotely operated vehicle (ROV), neither of which are unable to work satisfactorily in strong flows, so rock bolts will not be considered further here.

1.3.3 Suction/Driven/Drilled Pile anchors

Suction anchors and piled foundations form the principal methodology of installation for existing offshore platforms, and it therefore seems appropriate at first glance to use them for tidal devices. Suction anchors require a depth of sediment, the quality of which may vary from soft silt to stiff clay, which will give sufficient depth of insertion to generate the resistive forces necessary for the anchor to hold reliably under operational conditions. These anchors are potentially applicable to sites where the tidal stream flow is relatively slow and sufficient depth of sediment exists, but high velocity channels (where the flow exceeds 2 m/s regularly) are generally scoured clean. Suction pile anchors are relatively quick and cheap to install in situations where a high degree of positional accuracy of the anchor is not critical to the installation. An analysis of suction pile capabilities is given in [**27**].

Piled anchors can either be drilled or driven into the seabed depending on the seabed geology and the ultimate compressive axial load bearing capacity of a piled foundation (P_p) is given by [**28**],

$$P_p = F_{sf} A_p + F_g A_e \qquad \textbf{(1-29)}$$

Where F_{sf} is the skin friction force between the cylindrical surface of the driven pile and the geology, A_p is the cylindrical area of the pile, F_g is the load bearing capacity of the geology and A_e is the end area of the pile. The axial tensile capacity of a driven pile (P_{po})is given by,

$$P_{po} = F_{sf} A_p \qquad \textbf{(1-30)}$$

The friction limit of a drilled and grouted pile (f) is governed by the equation,

$$f = \frac{D_p}{D_s} P_b \qquad \textbf{(1-31)}$$

where D_p is the pile diameter, D_s is the socket diameter, and P_b is the allowable bond stress of the grouting material. Typical values from the offshore industry are of the order of 150 kPa. The limiting value for a drilled and grouted pile is the crushing strength of the grout and its surrounding

geology. When the flow applies a lateral pressure to the turbine, the pile is required to provide the reaction force at its junction with the geology. A well fitted pile distributes much of the pressure evenly over its grouted interface, but there still exist areas of very high stress, and the reliability of the installation depends on the crushing strength of the grout and immediate geology at these points. Of course, at the reversal of the flow, the opposite side of the socket is subjected to similar loading.

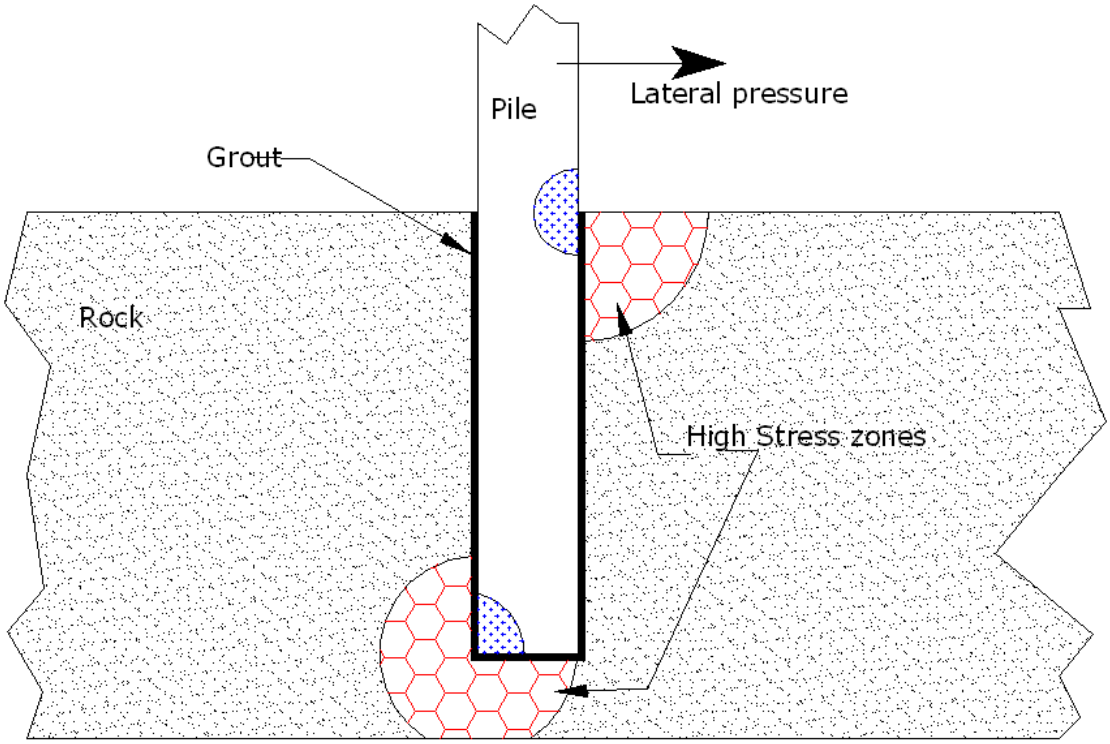

Figure 1-16: Schematic of lateral pressure applied to a grouted socket

The high stress zones in the geology are matched by high stress zones in the pile tubular and allowance must be made for this in the design.

Using the same tubular dimensions as those for the gravity installation and socketing the tower by 1/3rd of its visible length i.e. an additional 2 m, gives a total tower length of 8 m for a 6 m rise and wall dimensions of 20 mm thick by 0.4 m diameter. The maximum axial turbine force F_a is given as 90566 N at U=3 m/s, giving a force at the seabed/pile interface of,

$$\frac{8\,m}{2\,\mathrm{m}} F_a = 362264\ N \approx 360\ kN$$

Assuming that the grout is homogenous and that all components are perfectly round, the initial contact area bearing the pressure Pg will be half of the circumference c at opposing bottom and top halves of the socket d varying with the cosine of the angle θ (Figure 1-17) between the applied force and the circumferential position of the pressure point.

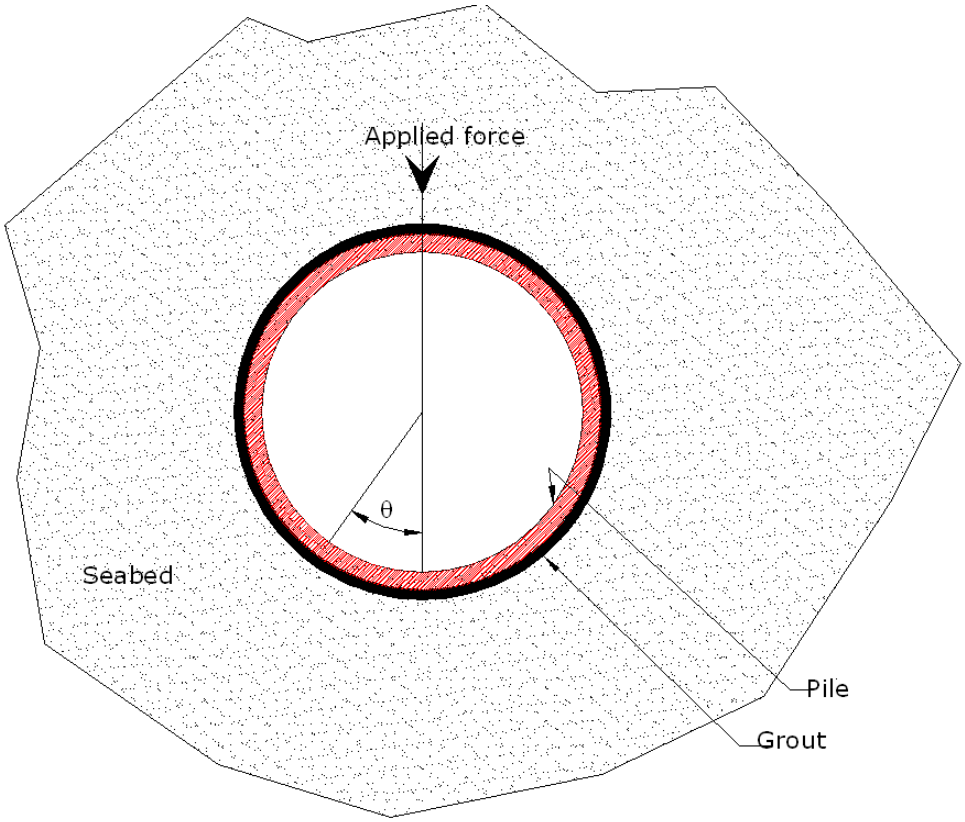

Figure 1-17: Grouted socket, plan view

The applied pressure is given by,

$$Pg = \int_{\frac{-\pi}{2}}^{\frac{\pi}{2}} \frac{F_a}{cd} cos(\theta) d\theta = 576 kPa \qquad \textbf{(1-32)}$$

i.e. four times the recommended grout bond stress given previously, so drilled and grouted sockets for tidal turbines require a stronger grout or a larger diameter pile over which to distribute the lateral loading.

In addition to the forces applied to a socketed monopile that have been discussed, there will be additional wind and wave loading from meteorological influences. Whilst wind loading is relatively small compared to the tidal stream loading, the addition of wave loading (discussed on p85) is a significant factor for a surface piercing monopile.

The drilled socket approach is a development of the rock bolt method up to a much larger scale, whereby the rock bolt effectively becomes a single, circular steel pile that can be inserted from a surface vessel. The drilling of the socket requires an appropriately equipped workboat capable of holding station in vigorous flows whilst drilling. As well as competent physical anchoring systems, most modern workboats are equipped with Global Positioning Systems (GPS), which, when linked with the boat's 360^{o} thruster propulsion system, can maintain position to very close tolerances. Naturally, these capabilities require significant financial commitment.

The drilling of the seabed socket is easily within the capabilities of present technology, though the operation is sensitive to weather conditions and has a maximum operational water depth of about 35 m. Since the cost of installing the pile is believed to be of the order of £500,000, then a minimum size of turbine is required to generate sufficient power to make the installation economically viable. This limitation effectively constrains the minimum water depth to be about 20 m, and this water depth window of 20 m – 35 m greatly restricts the number of sites that can be exploited, at present, using the socketed monopile installation technology.

1.4 Support Structures

A tidal stream device and all associated plant needs to be transported from shore to the installation site, where it will be manoeuvred into position, fixed in place and connected to its power take-off system. Tidal stream devices will be positioned in sites of varying characteristics at both macro and micro levels (flow, depth, geology and sediments) and versatility of the support structure is important. It is unlikely that a 'one concept fits all' situation will dominate the tidal energy industry in the same way that the tubular tower, three-blade, horizontal axis concept has come to dominate the wind industry.

In addition to any lift forces applied to the energy conversion actuator, the tidal stream will apply a considerable drag force F_D to any structure in its path based on,

$$F_D = \frac{1}{2} C_D \rho A U^2 \qquad \textbf{(1-33)}$$

Where *A* is the area of structure apparent to the mean flow vector and C_D is the drag coefficient. The total drag is made up of the pressure or form drag which depends on the profile shape as presented to the flow, and the skin or surface drag which depends on the surface finish and level of turbulence pre-existing within the flow. These properties are discussed in greater depth in Chapter 3.

The turbine C_p is reduced with greater proximity to the free surface. The gravitational effect of the free surface prevents the full wake expansion, thereby reducing the pressure drop across the turbine and the corresponding thrust and power coefficients. The turbine wake will also produce free-surface waves against the force of gravity and this further contributes to power losses. It follows from this, that for scaling purposes, the hydrodynamic forces applied to a tidal stream device, and by association, to its support structure, must be a function of Froude Number (inertia/gravity) and/or Reynolds Number (inertia/viscosity) and these coefficients are discussed in greater depth under section 4.3.1.

The drag load on the support structure will depend on a number of factors, some of which are constant features and can be controlled by careful design,

whilst others are dynamic and inherent within the operational environment e.g.

- stream flow velocity (dynamic)
- blade count, geometry and subsequent vortex shedding (design)
- structural section profiles (design)
- actuator area perpendicular to the mean flow vector (design)
- surface finish (design)
- amount and type of biofouling (environmental)
- significant turbulence and shear within the flow (dynamic)

The effect of the structure's drag on the upstream flow is to advance the stagnation point created by the structure and, as a result, affect the flow over the TSEC working surfaces. The drag loading will also vary with depth for any given depth-averaged stream velocity due to the depthwise velocity profile. If this profile is assumed to follow a $1/7^{th}$ power law [**29**], then there may exist variations of up to 0.5 m/s over a 20 m depth, a factor which is negligible for a vertical axis crossflow device with hydrofoils of 5 m length, but which may carry considerable structural loading implications for a horizontal axis turbine.

1.4.1 Installation Cost Components

In addition to providing secure positioning and minimal drag resistance for the duration of the installed life of the device, the support system must offer a cost effective and safe methodology for fabrication, installation, maintenance and eventual decommissioning, coupled with a minimal effect on the marine environment.

The cost areas (materials, fabrication, installation, maintenance and decommissioning) common to all support concepts are based on the methodology outlined in [**30**] and it is assumed that a generic energy conversion actuator can be attached equally well to any of the support structures. A number of device support solutions have been developed, and

each of the current support systems will be examined against these cost areas, along with a brief description of its operational principles.
The individual cost areas can be itemised as follows:-

Materials

Steel – In spite of its tendency to corrode, especially in marine situations, steel is most likely to be employed as the principal structural material. There is a wealth of experience in its use and it is readily available. Stainless steel alloys will be necessary for demountable fixings.
Concrete – The offshore oil and gas industry has used a wide range of concrete and derivative products for piles, gravity bases and fixing grouts. For tidal stream device structures any substantial concrete component would need to be reinforced, probably with steel.
Composites – Wind turbine supports intended for offshore use in the USA have been fabricated from composite materials [**31**] and these may well become important in submerged marine devices.
Negative value materials – quarry waste, dredged sand and similar materials may prove useful as ballast for injection into structural cavities for gravity bases.

Fabrication

Kit form - the support structure needs to be fabricated in transportable units for assembly at the quayside or on site. This requires a consistent degree of accuracy in the design and manufacture stage.
Surface finish – A range of surface finishes are available and there may be some distinction required, e.g. high levels of suspended sediment in a vigorous flow may require a particularly durable surface protection
Standards- All installed equipment will need to be verified against an accepted standard governing the quality of fabrication work [**32**].

Installation

Survey - an initial seabed survey will require multiple ROV transits, the time available for which will be limited by the characteristics of the stream flow,

and a large site will occupy a survey vessel for some considerable time. The Crown Estate and environmental non-governmental organisations (NGO) require a detailed survey of the immediate and surrounding seabed prior to any licences or permits being granted. The output of the survey will provide the initial input into the Environmental Impact Assessment (EIA) scoping study.

Preparation - assuming that licences and permits are approved, site levelling may be necessary for some structures, particularly for large footprint gravity base proposals. Pre-installation preparations such as vessel moorings will need to be carried out in advance of installation.

Installation – this is the biggest single component cost and very sensitive to weather difficulties. The complexity and timescale of each stage is different for individual concepts but essentially is made up of vessel mobilisation, transport/towage, lifting and fixing. Vessel costs are somewhat distorted by the current high value of offshore oil and gas, and marine renewables are not yet in a position to command the same price for their product, though recently one tidal energy developer has been unable to hire installation barges due to the rapid expansion of offshore wind sites.

Completion – commissioning of the support structure, confirmation surveys of the structure and surrounding seabed, removal of any installation related debris and remediation of the seabed. Scour protection may be required for some concepts.

Maintenance

The support structure maintenance component has two strands – the first is the influence that the support structure has over the maintenance of the energy converter, and the second is the maintenance requirement of the support structure itself.

Access - ease of access to the energy converter over its service life is a major component of the operating and service costs attributable to a device.

Downtime – length of the service and maintenance downtime required to access the energy converter.

Complexity – most of the existing support structure concepts have a mechanism for retrieving the energy converter to the surface. This mechanism will itself require maintenance and repair.
Support structure surface topography – Tidal streams carry a lot of debris entrained within their flow. A complex surface with multiple trap points will soon become loaded in unpredictable ways.

Decommissioning

The level of decommissioning required for tidal energy converters on completion of their service lifetime is, as yet, not clear. There are arguments for returning the seabed to its virgin state, or as close as is possible to it, but this may not be desirable if the site has been profitably delivering energy for the lifetime of the installed technology and the operator wishes to replace the generator rather than just remove it. It is also well known that the ocean environment is very quick to colonise and absorb new intrusions, and the base of a tidal energy device may become a particularly rich habitat, being a place of shelter within the powerful flow. For the time being, particularly with regard to overall project costing, it is considered preferable to assume that the device will need to be removed and that full remediation of the site is required.

1.4.2 Socketed Monopile

The forces applied to the socketed monopile have been discussed previously on p28.

Materials

The socketed monopile is a circular, hollow section, high strength steel tubular of sufficient thickness to withstand cyclic and vibration loading, and any material losses due to corrosion. The Seaflow concept uses a hydraulic mechanism to raise and lower the turbine/powertrain assembly and this will require some components to be fabricated using high grade stainless steels to withstand the long term corrosion and biofouling.

Fabrication

The fabrication of the steel monopile is a straightforward engineering task and it could employ a specially produced section profile, or rolled and welded depending on the level of ovality that is acceptable in the design process. The demands of the hydraulic mechanism previously referred to will be the principal arbiter of tolerances here. The maximum length of any one section will be around 14 m to allow for transportation by road, and the complete pile will need to be assembled prior to being placed on a barge for towing to site

Installation

A socketed monopile can only be installed where suitable rock strata exist that can support the socket. The local bathymetry can be recorded using readily available sonar techniques, and seismic reflection can be employed to determine the geometry, structure and configuration of the geological strata [**33**]. Most tidal stream sites with sufficient flow to be of immediate interest will be relatively sediment free though a considerable depth of rocks and boulders is still possible. However, the actual physical and mechanical properties of the rock can only be ascertained with any degree of accuracy by taking core samples. The MCT Ltd Seaflow installation required a steel sleeve [**34**] to be inserted due the fractured nature of the seabed geology. Soft geological structures, such as the Old Devonian Sandstones which make up much of the seabed off the north of Scotland, may also require primary sleeving to prevent the erosion of the socket by the cyclic, lateral, opposing forces applied by the tides.

The drilling of the rock socket is carried out by an appropriately equipped jack-up vessel which can maintain position against strong currents. The casing shoe which acts as a template through which all the subsequent operations are carried out, is located on the seabed along with its conductor tube, and seated into position in the rock surface. The coring drill is then lowered down into the conductor tube and the rock socket is drilled to the required depth.

Figure 1-18: 2003, SeaFlow's monopile. (Courtesy of Marine Current Turbines Ltd)

The drill is withdrawn along with the conductor tube and the casing shoe is left in position. At this point, any remediation of the socket that may be required is applied, including extra sleeving.

On completion of the socket, the pile is floated out to site and lowered into the socket, the annulus is filled with grout and the pile held in position whilst the grout cures. Handling a steel pile of up to 50 m in length is awkward, and poses a challenge for a single, surface lift. Similar sized offshore wind turbine towers are assembled on site in unitary lengths.

Operation

The socketed monopile is a very stiff structure and is capable of sustaining substantial operational thrust loads and rotodynamic vibration for long periods, in addition to the applied wave loading that results from its surface-piercing nature.

The Seaflow design incorporates a single turbine axially aligned with the prevailing Spring flow and perpendicular to the axis of the vertically aligned

support pile. The pile itself is circular and therefore has a drag coefficient in the range approximately 0.3 to 1.0 depending on flow velocity. When the flow approaches the turbine from the direction upstream of the turbine, then the pile has very little effect on the flow though the turbine, but when the flow approaches from the pile side, there will be a considerable wake from the pile creating large pulses of force applied to the turbine. This effect is exacerbated by the twin-bladed nature of the Seaflow turbine, since both blades will enter and exit the wake simultaneously. This undesirable shadow effect will be largely mitigated by the next generation Seagen design, which carries twin turbines on streamlined horizontal spars, clear of the vertical pile.

Maintenance

The monopile structure, being surface piercing and rigidly fixed to the seabed, coupled with a capability to hydraulically raise the complete operational unit above sea level, offers a safe working environment for service and maintenance of the turbine and powertrain, though it is expected that major overhauls will require the turbine/generator unit be returned to base. The hydraulic system does create an additional layer of complexity requiring high grade materials to provide long term reliable service and the system may prove susceptible to long term biofouling.

Decommissioning

Removal of the structure from site will require appropriate lifting technology and subsea cutting equipment, whilst removal of the reinforcing sleeve may be more problematic. Though it is not yet clear what level of remediation will be required by the Crown Estate in its capacity as custodian of the seabed, it is reasonable to assume that the socket may need to be backfilled and returned to its original state in terms of seabed levels and basic habitat support.

1.4.3 Positively Buoyant (Floating and sub-surface)

The positively buoyant installation can be modelled as a single or multi-line mooring system as appropriate and a detailed analysis of such systems is given by Berteaux [**35**]. The full dynamic analysis of such a device is a major undertaking, and an outline of the static model with velocity only will be offered here.

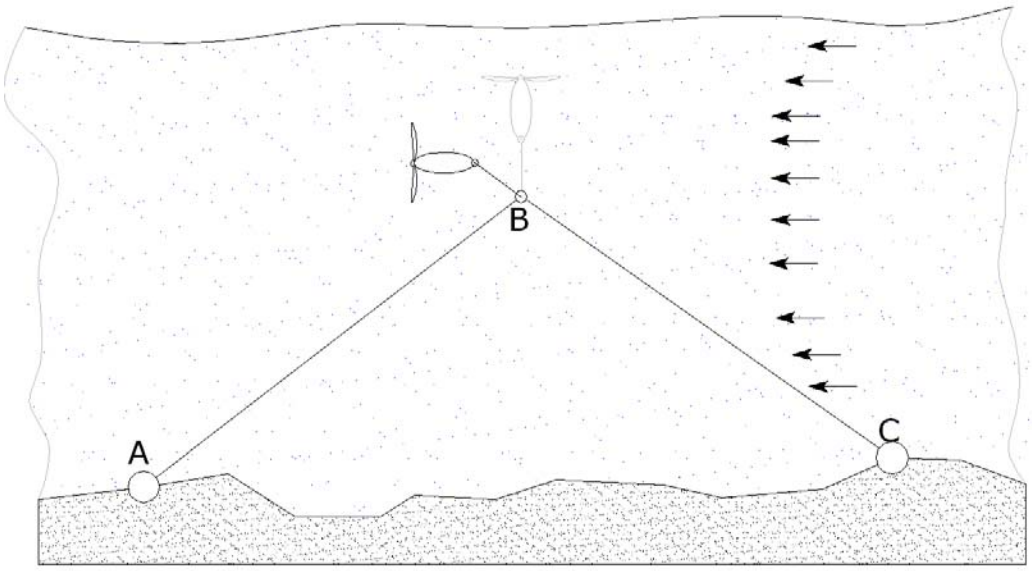

Figure 1-19: Schematic of positively buoyant device

When there is no flow, the positively buoyant generator (greyed out) will apply a vertical tension Ty to mooring lines AB and BC. If these lines are initially considered to be massless then the sum of the horizontal and vertical force vectors at mooring point A and mooring point C will be equal to the sum of the horizontal and vertical vectors at B. Since B is subjected to a pure vertical tension of Ty then the sum of the vectors at A and C will also be Ty. As the flow applies a force to the turbine, the forces applied to C will be the vector sum of the vertical buoyancy force (Ty) and the flow induced horizontal tension forces (Tx). If Tx exceeds Ty then mooring point C will be subject to the resultant of Tx and Ty and mooring point A will be redundant. At the change of tidal stream direction the situation will be reversed. However, if Tx is significantly greater than Ty, then the device may be driven into the

seabed. Since in reality the mooring lines will have mass (ML_m) and applied drag (ML_d) in addition to Tx and Ty, then further forces are added to the system. When the system is generating the vector sum at C will be,

$$C_x = Tx + MLd$$

$$C_y = Ty - MLm$$

Using the 5 m turbine model as before, the axial force on the turbine (Tx) will be 90566 N and assuming that the turbine is mid-depth at 15 m and the mooring points A and C are 40 m apart then the mooring lines are 25 m in length. Tx is equivalent to a static load of 9.2 tonnes, applying a safety factor of 3 gives 27.6 tonnes cable capacity which requires a plastic-coated wire rope of 25 mm OD. At 3 m/s Re = 7.6x10^4 giving a C_D ~0.95 and a drag force on the mooring lines (ML_d) of 5477 N, therefore,

$$C_x = Tx + MLd = 90566\,N + 5477\,N = 96043\,N$$

Assuming that the mass of the generator is counteracted by sufficient buoyancy, it may be neglected. The system must provide buoyancy to maintain position against the flow, at say 12 m above seabed level, and to support the mooring lines. 25 mm OD plastic coated cable has a mass per metre of approximately 12 kg, so 50 m represents a weight of MLm ≈5900 N. Since the distance from C to the turbine is 25 m then if the vertical depth is to be maintained at 12 m and the magnitude of C_x is 96043 N, the tension in the mooring line is 109481 N and the vertical tension C_y is 52554 N. Now $C_y = Ty - MLm$ so Ty =5900N+52554N=58454N which must be provided by buoyancy within the generator housing, and 58454 N requires around 5.8 m^3 of buoyancy, in addition to whatever is required to carry the turbine/gearbox/generator train. From equation ***(1-28***), the weight W of a gravity anchor on a flat seabed is given by,

$$W = B + T\,sin(\phi) + \frac{T\,cos(\phi)}{\mu}$$

So the weight of gravity anchor required, assuming μ=1 is,

52554 N + 96043 N =148597 N

i.e. a submerged mass of concrete of 15.15 tonnes which equates to almost 25 tonnes dry mass. Applying the safety factor of 3 gives a gravity mooring of 75 tonnes at each end of the system and this figure is doubled to allow for tensile forces in concrete. A mass with dimensions of around 4 m x 4 m x 4 m would suffice, giving a cranage requirement of 900 tonne metres. If the seabed is unable to provide a value of μ=1 then the mass will multiply inversely with the change in μ.

Materials

A positively buoyant mooring system comprises a buoyant body secured by a number of mooring lines to anchor assemblies. Mooring lines are typically wire ropes or chains, and the use of rubber as a component of the mooring line is now being advocated by Joosten [**36**]. A flexible component of the mooring line can reduce some the cyclic loading on chains and cables, but careful design is required to avoid resonance. Some systems may use multiple chain/anchor assemblies with a spreader beam to gain some directional control and offer a degree of redundancy to the structure. The anchor itself may be gravity, rock bolts or a drilled socket with a grouted insert.

Fabrication

The fabrication of the mooring system is very simple, requiring only cut length mooring lines, spreader beam and shackles, with the additional benefit that the support structure for a turbine structure assembly can be carried by road.

Installation

Until recently, drilled sockets were the proposed installation methodology for anchoring these devices, but cost implications have forced a reconsideration of this approach. Since drilled anchorage sockets would be subject to the same depth limitations as the monopile installation, floating or sub-surface installations are restricted to employing gravity base or rock bolt anchors in waters exceeding 35 m in depth. As has been discussed under 1.3.1 , the

horizontal forces applied by the flow to the turbine, in addition to the applied wave loading and the buoyancy forces of the turbine assembly, will tend to drag gravity anchors together and the device may well surface autonomously and unexpectedly.

Floating and sub-surface devices rely on a tether to provide a reaction force for the turbine against the stream flow and the tether also provides the route to a secure position for power take off. The locus of the tether restricts the spacing of floating devices because tidal streams have a tendency to swirl and shear during the periods immediately before, and just after, slack water.

Operation

The buoyancy components of the device are inherent within its structure and the principal design difficulty here is the dynamic position control of a rigid body device with static buoyancy characteristics operating in six degrees of freedom. The moorings will behave as tensioned moorings and will be subject to the wave loading and current loading acting on the moorings themselves in addition to the surge, sway, heave, roll, pitch and yaw loadings applied by the device itself [**37**].

The tether connection to these devices may be either cable or chain, both of which are vulnerable to cyclic fatigue loading. In the case of a cable tether, the cyclic loading on cables will very quickly weaken the tether. The net result is a relatively short installed tether lifespan, and the device may be lost.

Figure 1-20: Navigational buoy mooring chain, (Courtesy Datawell BV, The Netherlands)

For a mooring chain, the constant grinding action between the links and suspended sediment coupled with the frequent torsional loading applied by tidal streams quickly wears the chain away. Rubber is a potential solution to this difficulty and applications are discussed in [**36**].

Publicly available test data does not indicate the system response if one turbine of a contra-rotating pair should fail nor indicate how the positively buoyant system will respond dynamically to such an imbalance of forces. Devices that are tethered by a pair of cables or chains fixed to one anchorage point can be considered as an equivalent system to a person flying a two string kite, and, as anyone who has ever done so will know, this is an active dynamic process requiring constant monitoring and adjustment to maintain control. For a tidal device, sufficient restorative positioning force can only be applied statically by a substantial buoyancy component and/or dynamically by lateral wings of sufficient size to provide a suitable reaction force.

However, in order to generate sufficient static or dynamic restorative positioning force, the tether will also have to resist a considerable lift force and this will need to be accounted for in the anchorage capabilities. After a period of installation, the tether will attract a significant level of biofouling

which can substantially increase the tether drag and therefore the associated dynamic load.

Maintenance

Being on the surface or easily recovered to the surface, positively buoyant devices themselves can be very cost effective to service and maintain. Replacement generator units can be installed quickly and with a readily available workboat. The tether system itself will however need frequent cleaning and maintenance and will also need to be replaced at fairly short intervals. The servicing and maintenance costs of the system may well negate any savings accrued in accelerating the installation process and minimising the support structure material costs.

Decommissioning

The system can be removed from its anchorages without difficulty and, if gravity bases are used, these can be retrieved as the reversal of installation. Fixings that have been grouted into sockets may prove more difficult to remove and their effective lifespan is yet to be fully appraised.

1.5 The Sea Snail

The Sea Snail concept addresses the problem of a cost effective, secure and environmentally acceptable system for installing tidal energy turbines in relatively shallow and fast running tidal streams. The initial project was funded for two years by the Scottish Enterprise Proof of Concept scheme, which seeks to develop and showcase Scottish inventiveness, and bring forward potentially profitable ideas from partially validated research.

The flow of seawater over a hydrofoil is shown in Chapter 3 to be theoretically suitable for inducing a lift force oriented in the downward direction, and understanding of the physical characteristics of the hydrofoils was the earliest consideration in the design process. The Sea Snail concept is a novel arrangement of existing technologies designed to enhance the inherent weight of the structure and thus resist the applied overturning moments and the slip forces, by means of hydrofoils creating a lift force from the flow stream. The overall structure dimensions were limited by available funding, but it was desired that the device be proportioned at appropriate dimensions to undergo meaningful sea trials. The short time frame constraint meant that, in many areas, the development of different components and concepts were continuous parallel processes, and the following discussion of the project should not be construed as a single timeline. An overview of the design and testing of the Sea Snail is presented in [**38**].

1.5.1 Conceptual design

The initial requirements were maximum lift and minimal drag from an inexpensive, easily fabricated structure requiring minimal moving parts yet fully functional in a chosen marine environment. Harbourside assembly and placing the device in the water would require a crane, and crane capabilities are defined by the combination of mass and reach, if the Sea Snail is excessively wide, it would require a larger crane to deploy it and large cranes tend to be expensive and difficult to source in remote locations. Additionally, the Sea Snail would need to possess sufficient mass to make security of

positioning a reasonable certainty, but not so much mass that the concept would remain unproven at applicable flow velocities.

A range of Low Aspect Ratio (LAR) hydrofoils of different section, chord and span dimensions were considered, and the NACA0013 chosen as it offers the best Lift/Drag ratio of the symmetrical sections (LAR theory is discussed under section 3.3.1. Early research indicated that an angle of attack, α=15^{o} would give the best lift force without substantial risk of stall, consequently the modelling in Chapters 3 and 4 is based on the same value for α.

Initial mathematical modelling indicated that a structure that gave the largest practicable lateral distance from its seabed contact points, to a centrally placed turbine (assumed to be 5 m diameter), would offer best resistance to overturning in the direction of the freestream. Referring to Figure 1-21, the product of the lift on the hydrofoils ($L1, L2$ & $L3$), and the distance from the pivot point (P_p) about the rearmost feet must exceed the sum of, the overturning moment applied by $D_{turbine}$, the hydrofoil drag forces ($D1, D2, D3$) and the general drag moments applied over the complete structure about P_p. Skin friction resistance is neglected at this stage.

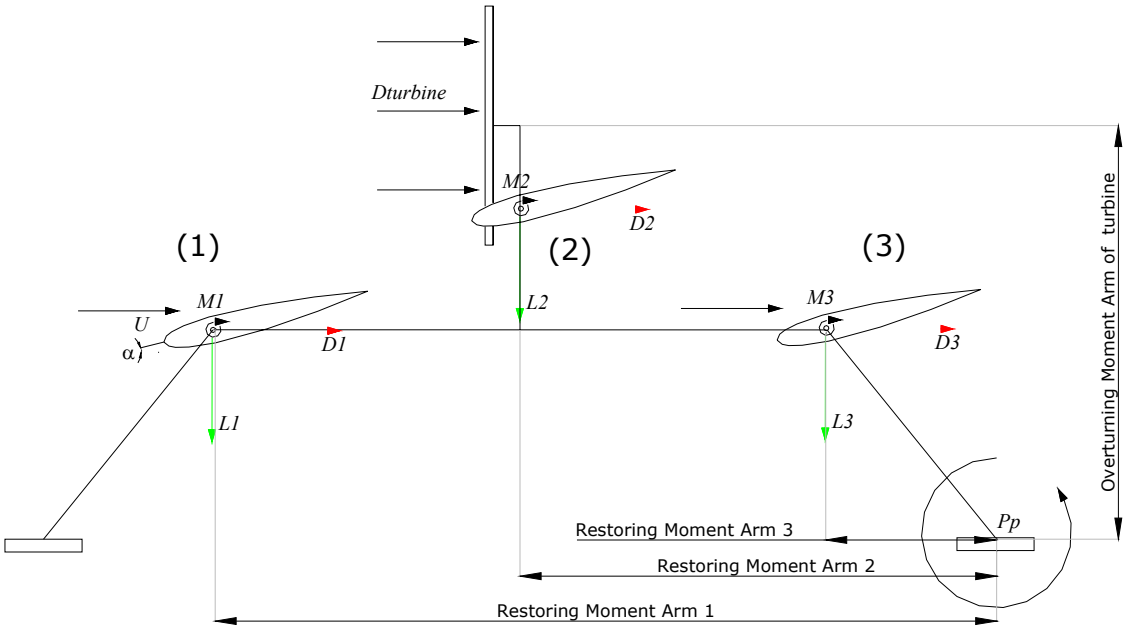

Figure 1-21: Operational concept of the Sea Snail

Until experimental data were generated, the wake interactions remained unknown, but could still be considered. It was therefore assumed that the wake from an upstream hydrofoil would reduce the lift coefficient of the following hydrofoil by a factor of 0.8 for the upper middle hydrofoil and 0.6 for the trailing hydrofoil.

The hydrofoil lift distribution was intuitively assessed as follows:- The lead hydrofoil pair (1), with an assumed C_L of 0.7, would be the largest contributors to the restoring moment, with some support from the central hydrofoils (2) which were assumed to have C_L= 0.8*0.7=0.56. The trailing hydrofoil pair (3), C_L= 0.6*0.7=0.42 would be expected to contribute relatively little to the restoring moment. However, when the tidal stream reverses, the trailing hydrofoil pair (3) becomes the lead hydrofoil pair and therefore the principle contributors to the restoring moment. Thus the operational layout of the Sea Snail was determined at an early stage and strategies were developed to utilise this layout.

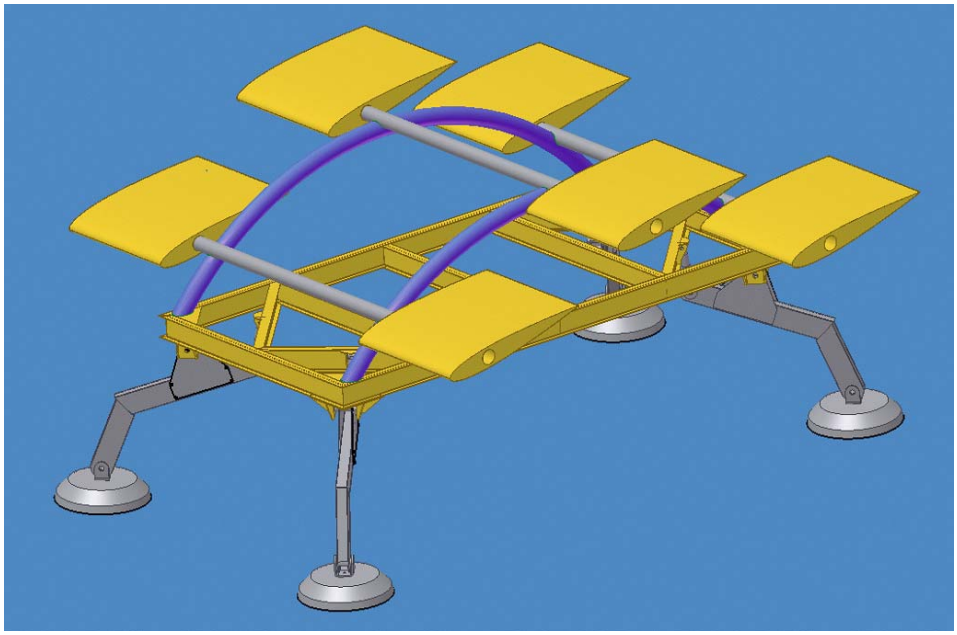

Figure 1-22: Sea Snail support frame, concept 1

Support frame concepts were developed, with off-the-shelf mild steel sections preferred for structural strength, ease of fabrication and cost effectiveness.

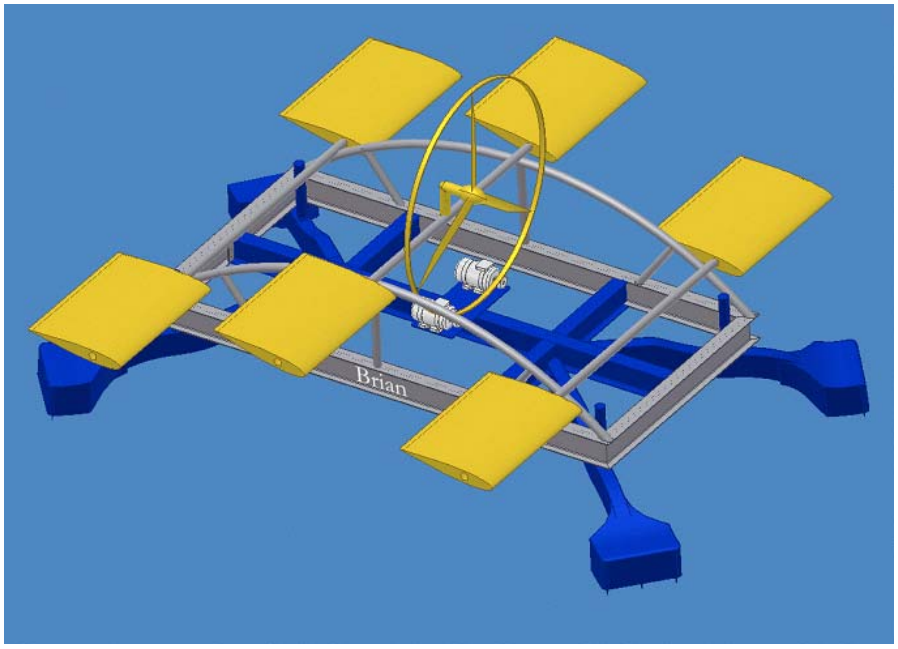

Figure 1-23: Sea Snail support frame, concept 2

The structure would also require a mechanism for reversing the hydrofoils at the change of tidal stream direction. Again, a range of options were considered, including some with powered mechanisms that would allow for the possibility of an on-board control for optimisation of the angle of attack.

An early conceptual model is shown in Figure 1-22, with formed tubing proposed as the upper frame carrier members. Incidentally, the similarity of the curved shapes of the tubulars to the shape of a Citroen 2CV (alias 'The Tin Snail'), are what gave rise to the 'Sea Snail' name.

Formed tubing is an elegant solution to the demands for structural strength with minimal material usage, and the formed tubing solution was carried forward into the second stage concept, Figure 1-23, which also looked at options for power generation and the influence of the centres of mass and buoyancy.

The hydrofoils are sized at 2.5 m span and 3.0 m chord, giving a planform area of 7.5 m^2 each, and thus a total for six hydrofoils of 45 m^2. The

structural tubing was approximated as being equivalent to a frontal area of 3 m^2, and the mathematical model included a 5 m diameter turbine (3 m diameter is shown on the assembly drawings) to simulate power extraction. It is further calculated that the submerged mass of the Sea Snail will be approximately 8 tonnes (78.5 kN) and its centre of mass will be at the longitudinal mid-point between the supporting legs, i.e. 7.25 m from the rearmost feet.

The first run model, using the values for C_L as discussed previously for the hydrofoils and C_D = 0.85 for the entire device, gave the no slip limits as 1.8 m/s for the assembly without hydrofoils and 2.6 m/s for the assembly with hydrofoils, and the results are plotted in Figure 1-24.

Table 1-2: Summary of initial model parameters.

Parameter	Value		Parameter	Value
C_L (lead)	0.7		Hydrofoil area (x6)	7.5 m^2
C_L (central)	0.56		Inherent restoring moment	7.25 m x 78.5 kN
C_L (trailing)	0.42		Frontal area (frame)	3 m^2
C_D (overall)	0.85		Turbine area	7.1 m^2

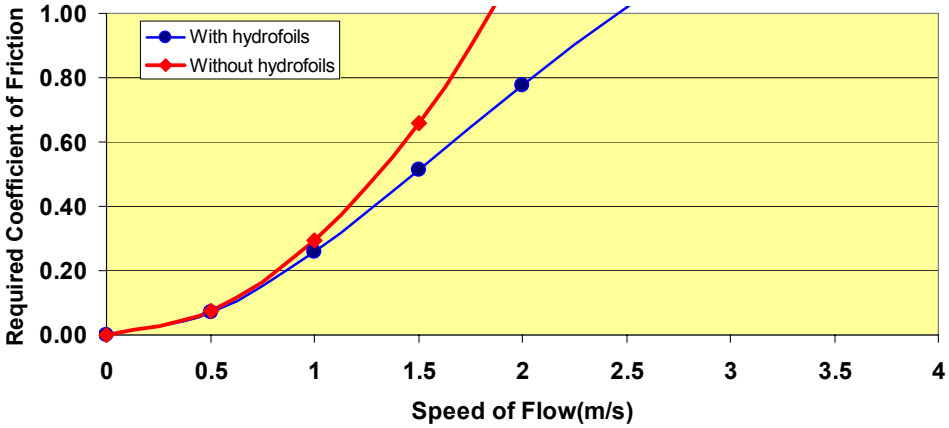

Figure 1-24: Comparison of No-Slip limits

Based on these assumptions it was established that the hydrofoils would improve the no-slip condition but further work would be required to reduce the overall drag and/or to improve the lift force.

The overturning limits were calculated by approximation of the frontal area and height of turbine centre and the results are shown in Figure 1-25.

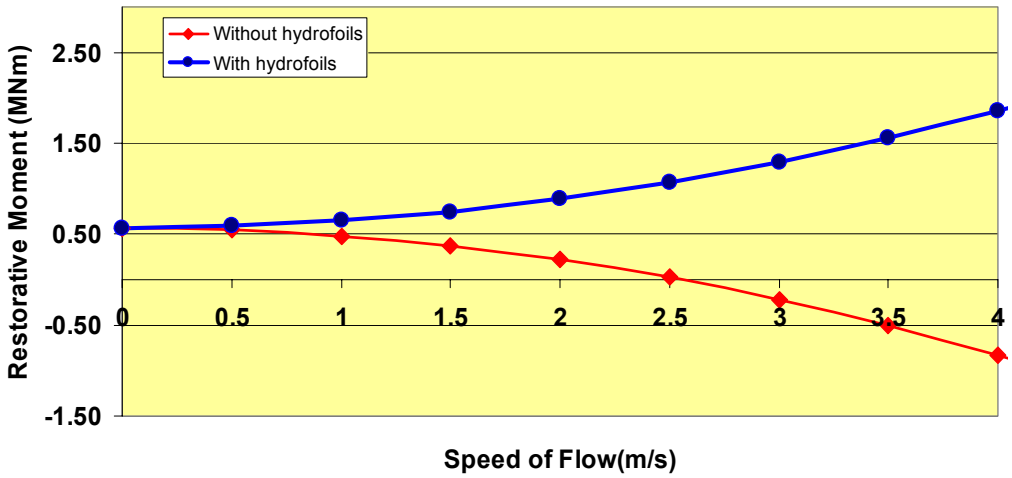

Figure 1-25: Evaluation of overturning moments

The plot shows that, without hydrofoils the flow will overturn the structure at 2.5 m/s, so slippage or overturning are both possible at relatively low flow velocities.

The Sea Snail does not require the same 3x safety factor applied to gravity anchors, since any surge force will apply to the hydrofoils as well as to the turbine, thus maintaining equality between restorative and overturning forces. Using the same parameters as those used for gravity anchors, (see page 23) the cranage required will be of the order of 180 tonne meters instead of 702 tonne meters required for handling equivalent gravity anchors.

Having established that the outline design is mathematically and structurally feasible, and that hydrofoils can be used to augment the structures inherent weight, the project moved to the detailed design phase (4.1), and subsequently sought to develop a more accurate operational mathematical model (4.2).

Materials

The materials required by the Sea Snail system are deliberately low cost and readily available. The frame is entirely made up of stock sizes of steel

tubulars and plate, and the hydrofoils are glass reinforced polyester resin filled with polyurethane foam.

Fabrication

The Sea Snail structure is easily fabricated with minimal machining requirements and broad tolerances, making it appropriate for deployment and maintenance in parts of the world where advanced engineering facilities are scarce.

Installation

The device is towed into position on air filled buoyancy tanks which are then flooded by means of a control umbilical running from the Sea Snail to the installation vessel, thus allowing the device to sink. If this is done as the tidal stream starts to run, with the installation vessel upstream of the Sea Snail, then, for narrow, bi-directional streams, the device will be self-aligning to the principal flow vector. Once the tanks are fully flooded and the Sea Snail is positioned on the seabed, the umbilical is sealed off and attached to a small recovery buoy. Installation duration from arrival on site is approximately one hour.

Operation

The structure is susceptible to the same biofouling hazards as the alternative installation systems and the performance of the hydrofoils can be degraded by excessive surface contamination. The bi-directional mechanism is passive, being driven by the reversing tidal stream flow and will be subject to wear over long periods of deployment.

Maintenance

The Sea Snail can be recovered by evacuating the integral buoyancy tanks and returning the complete structure to the surface for cleaning, maintenance and repair. Alternatively, since the structure is very cost effective, it is envisaged that a serviced unit can simply be swapped in for a

recovered unit requiring maintenance, and the recovered unit either returned to shore or serviced on deck whilst en route to the next site.

Decommissioning

Decommissioning of a Sea Snail is the reverse of installation and the device leaves no footprint, empty socket, or debris from its presence.

1.6 Environmental factors

As well as being constantly abraded by the suspended sediments, tidal stream devices will be subject to collision damage from marine debris, fouling from animal and plant growth, corrosion due to the electrochemical nature of seawater and fatigue as a result of the cyclic loadings applied to the structure. The structure must be able to withstand the constant environmental attacks for the lifetime of the attached energy converter and enable the converter itself to be maintained at low frequency intervals and with minimal downtime. Thus the entire assembly must be thought of as a contiguous system; the support structure is as technically demanding as the energy converter.

1.6.1 Bio- Fouling

Any object submerged or partially submerged in seawater will attract the growth of organisms on its surface, creating opportunities for corrosion, increased drag on support structures and reduced hydrodynamic efficiency of the actuator surfaces. The light intensity at different depths will influence the species and quantity of organisms, as will the temperature of the tidal stream itself, which will often have different thermal characteristics to the surrounding mass of water. In addition to the increased drag, biofouling is often the cause of sensor failure [**39**] and can initiate a new food chain around the structure, increasing the probability of fish bites and other predatory attacks on cables and hydraulic lines. Increased levels of equipment protection are required and the inhibition of biofouling is likely to pose considerable environmental difficulties given the toxic nature of commonly available anti-fouling agents.

Over 2000 biofouling species have been identified and a highly detailed review of biofouling is given in [**40**]. The tidal stream energy industry, given its green heritage and environmentally friendly image, is unlikely to wish to pursue highly toxic coatings which are indiscriminately harmful to the marine environment, such as tributyl tin self-polishing copolymers, (TBT-SPC

paints). These coatings are estimated to cover 70% of the world's shipping fleet [**40**] but have been shown to cause defective shell growth in oysters, sexual disorders in dog whelks and reduction of immunological defences in fish. The development of less harmful coatings is actively being pursued with the approaching phase-out date for TBT-SPC paints by 1st January 2008.

1.7 Chapter summary

Parity of evaluation of the different turbine concepts is difficult; principally due to the lack of any consistency from developer to developer. Claims are made regarding C_P, but a related TSR is not mentioned, nor is the cut-in speed. The efficacy of a turbine over a range of flow velocities and rotational speeds is what determines its economic output, not claims of C_p=0.56. Tidal energy is unlikely to carry the same market value per kWh of its hydrocarbon equivalents, and cannot therefore justify the same installation, maintenance and de-commissioning costs as North Sea engineering projects.

The engineering challenges of tidal stream energy are therefore very clear; the installation of tidal turbines whether they are of axial or crossflow rotor configuration requires a reliable and cost effective structure that can withstand both the routine forces applied by the flow and the 100 year storm surge, whatever that may prove to be. Gravity anchors are relatively cheap and long-lived, but the quantity of mass required to restrain the turbine is substantial, with the result that the boat hire and cranage costs soon consume the economic benefit of the gravity anchor fabrication.

The drilled and grouted pile is rigid and, provided the pile diameter is correctly chosen and the geology is sound, will remain in position for many decades. Indeed one pile will probably need to support two or three generations of turbine to make its installation economically viable.

Based on the conceptual model, the Sea Snail should be cheap and easy to fabricate, easily transported to site and effective in use. It is also capable of supporting either crossflow or axial turbines and can be recovered easily.

The comparative models used in this introductory chapter were based on a uniform and steady flow of 3 m/s, but tidal streams are neither uniform nor steady. The next chapter examines the origin and characteristics of tidal streams and offers a more realistic view of the tidal stream environment.

Chapter 2 The origin of tidal streams

2.0 Chapter introduction

The Earth's basic tidal system consists essentially of two wave crests, one on each side of the planet, beneath which the Earth rotates. These tidal waves are principally of astronomical origin and have no connection with a tsunami; an event that is often erroneously referred to as a tidal wave.

Tidal streams are generally driven by two connected bodies of water equalising their level differences, resulting in a flow of water from an area of high pressure head to an area of lower pressure head. If the pressure head differences exist at opposite ends of a channel or similar restriction, then substantial flow speeds frequently result through relatively small cross-sectional areas and it is this high speed flow that makes tidal streams attractive for power generation. This chapter examines the forces that drive these potential differences as well as the topographical and bathymetrical features that influence the flow characteristic of the resulting streams.

Not all tidal streams occur at the connections between large bodies of water; many streams exist as a result of the filling and emptying of basins and estuaries, the resonant dimensions of which can affect the flow behaviour. Meteorological events and processes can play a part in enhancing or reducing flows and the Coriolis forces change the flow behaviour according to the stream's flow direction relative to the Earth's rotation.

The tidal systems that move the oceans are regular, reliable and highly complex gravitational, centrifugal and resonance driven systems, and should not be confused with other oceanic flows such as the Gulf Stream and the Global Conveyor (Figure 2-1), which rely principally on thermohaline induced density variations for their motive force. That being said, the two types of system do interact in certain locations around the globe.

In addition, the North Atlantic and South Atlantic gyres are examples of non tidal currents which are driven by their respective hemispherical trade winds [**41**] and, as such, are repositories of solar heat energy and not gravitationally induced kinetic energy.

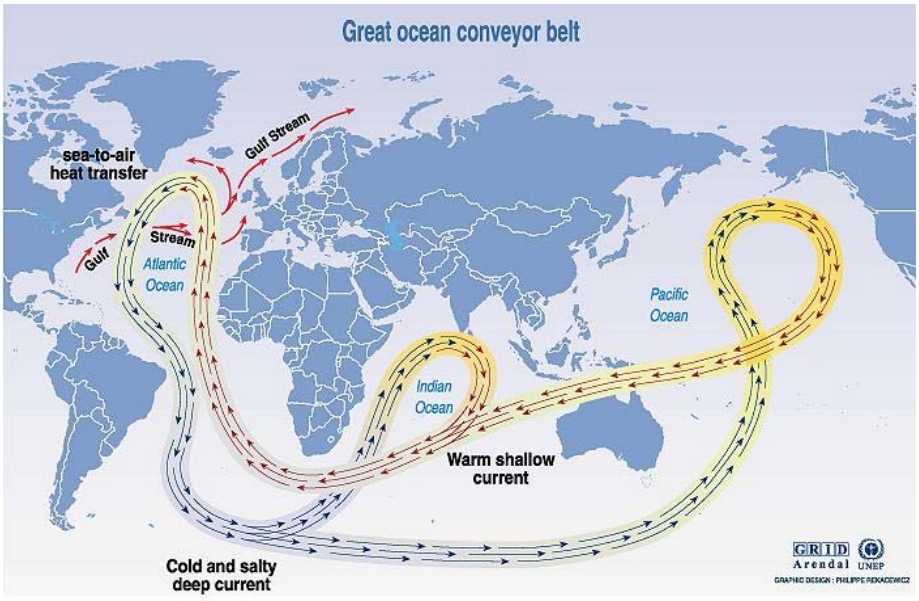

Figure 2-1: The Global Conveyor [42]

Over the centuries, a number of ideas have been developed with the intention of describing and predicting tidal behaviour at any given location. It would have been clear to early mariners, that the tides are spatially inconsistent but essentially temporally reliable at any point on the Earth's surface, and that, in some locations, knowledge of the tides is a pre-requisite to safe passage. A comprehensive and detailed history of the mathematics of the Earth's tidal system is available in [**43**].

Both Kepler and Newton are credited with early development of explanatory proposals, and although these were somewhat simplistic and clearly did not explain the observed phenomena very well, Newton was essentially correct and his work formed the basis of tidal force generation theory. In 1738, the Academy of Sciences of Paris offered tidal theory as a subject for a prize, among the recipients of which were Bernoulli and Euler, both of whom adopted Newton's approach [**44**]. Laplace contributed in 1774, demonstrating that the rotational movement of the Earth itself is also a significant factor and developing the Dynamical Theory of tides. Laplace put forward the idea that the tides are a pair of forced waves corresponding to the constituents of the periodic gravitational forces. However, this approach as yet has no analytical solution, though some numerical advances have been made [**45**].

The final essential component of understanding was delivered by Lord Kelvin who postulated that the application of harmonic analysis would be appropriate to the problem and this idea was further developed by George Darwin [**46**].

Until recently, understanding and prediction of tidal behaviour was based principally on the harmonic analysis of the various constituent waves contained within the measurements of the rise and fall of the water level. However, application of Fourier Spectral Analysis to the tidal records [**47**] has led to the Response Method, which indicates the level of non-astronomical components within the tidal drivers and offers a more powerful analytical approach.

2.1 Astronomical Drivers

The basic astronomical and rotational movements that govern the gravitational tidal cycles are the rotation of the Earth about its own axis once every solar day (24 hours), the elliptical revolution of the Moon about the Earth/Moon centre of mass in a period of 29.5 solar days and the elliptical revolution of the Earth/Moon system around the Sun in 365.25 solar days.

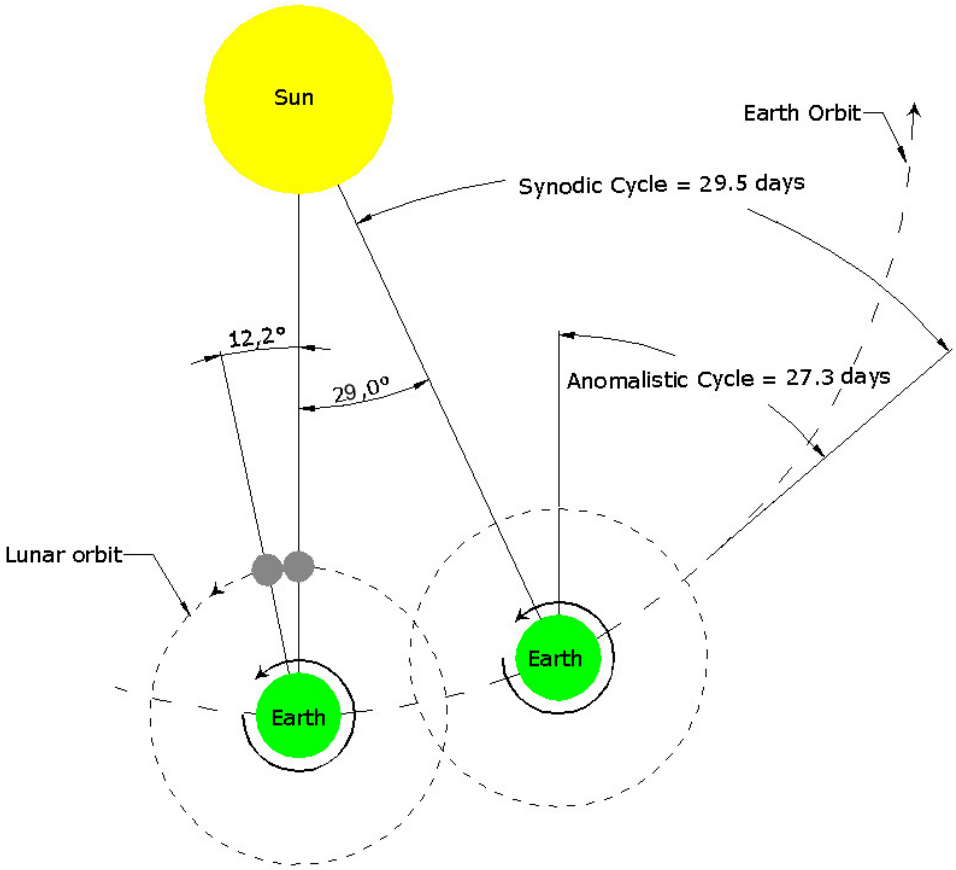

Figure 2-2: Lunar cycles

The plane of the Earth's path around the Sun is known as the ecliptic, from which the Earth's axis is inclined 66°30' and the Moon's orbit is inclined 5°9', which, in combination allow the Moon's declination to reach 28°30' every 18.6 years. It is these offsets, in combination with the superimposed rotational patterns of the Earth/Moon/Sun system that create the highly complex forces which drive the Earth's tides.

The solar system also encompasses other large bodies, which are responsible for relatively insignificant gravitational effects in terms of the equilibrium theory and will therefore be neglected in this analysis.

The Moon is responsible for the largest proportion of the tidal forces applied to the Earth but it is not independent in its influence, since not only does the Sun also affect the tidal forces, but the Moon's own tidal influence is modified by the Sun's gravitational field. These cycles are themselves modified by the evective influence of the Sun, and occasionally other planets within our solar system, depending on their relative positions.

The fundamental lunar cycles in relation to the Earth are; the Synodic cycle, which has a period of 29.53 days (New Moon to New Moon) and the Anomalistic cycle (perigee to perigee) which is 27.5 days (see Figure 2-2).

Solar gravitational influence is greatest at perihelion (when the Earth is closest to the Sun) in January, and least at aphelion, in July.

Newton's equilibrium theory assumes that only gravitational forces are responsible for tidal movements, and, for the time being, that assumption is sufficient.

2.2 Newton's equilibrium theory

Newton's Law of Gravitation states that any body of mass m_1 exerts an attractive force F on a neighbouring body of mass m_2, which is a product of their individual masses and inversely proportional to the square of the distance between their centres of mass, r, as given in

$$F = G\frac{m_1 m_2}{r^2} \qquad \textbf{(2-1)}$$

where G represents the universal gravitational constant, the value of which in SI units is 6.67 x 10^{-11} Nm^2kg^{-2}. The physical constants applicable to the Earth/Moon/Sun system are given in Table 2-1.

Table 2-1: Astronomical constants.

Astronomical Constants applicable to the Earth/Moon/Sun system			
		Dimension	**Symbol**
The Earth	Mass	5.97 x 10^{24} kg	M_E
	Equatorial Radius	6378 km	a
	Mean distance from the Sun	149.6 x 10^6 km	R_E
	Distance from Earth centre to Earth/Moon mass centre	4671 km	
The Moon	Mass	7.35 x 10^{22} kg	M_M
	Radius	1738 km	
	Mean distance from the Earth	384400 km	R_M
The Sun	Mass	1.99 x 10^{30} kg	M_S
	Radius	696000 km	

Newton proposed the Equilibrium Theory as a first attempt to quantify and explain the application of gravitationally induced body forces to a perfect, non-rotating sphere, completely covered by inviscid water of constant depth and density which responds instantaneously to the applied forces. Although it is convenient, and sufficiently accurate for calculation purposes, to take the distance between two bodies as the distance between their centres of mass, in actuality the forces in question are those forces acting between each

particle and every other particle within the two bodies. Thus, the particles which make up the three bodies of the Earth/Moon/Sun system are attracting one another individually as well as collectively and the resulting gravitational force is the net result of the interactions of all the particles within the system.

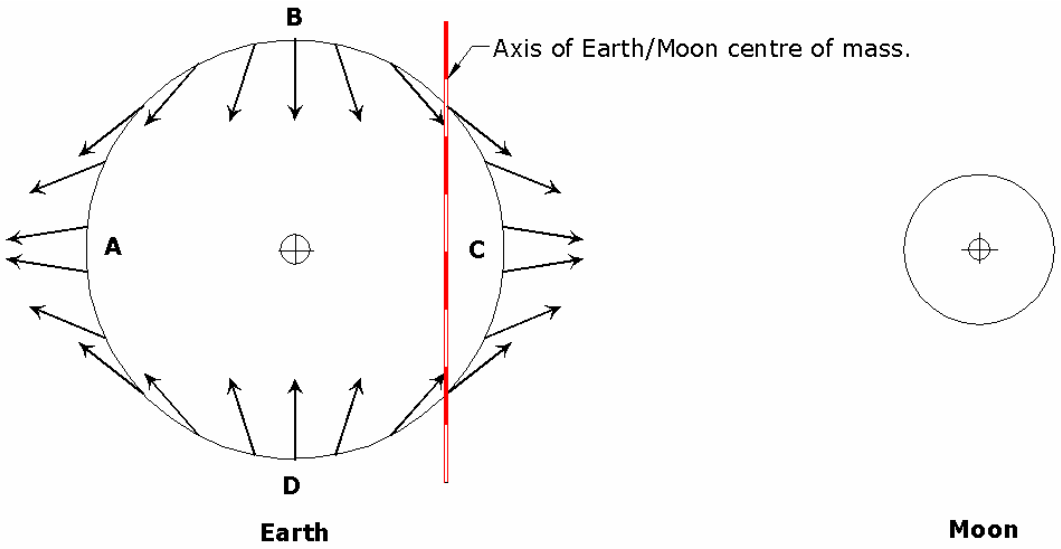

Figure 2-3: Idealised oceanic response to lunar gravity

Referring to Figure 2-3, the gravitational forces exerted by the Moon on the Earth's ocean are not the same for all particles in all locations. The force applied on a fluid particle (of mass κ) at **B** is given by ***(2-1)***, setting

$$m_1 = \kappa \qquad m_2 = M_M \qquad r = R_M$$

and dividing through by M_E to obtain force per unit mass.

$$F_B = \frac{G\kappa M_M}{M_E R_M^{\,2}} = \frac{GM_M}{R_M^{\,2}} \qquad \textbf{(2-2)}$$

The force (per unit mass) applied on the same particle at **C**, will be different by virtue of being one Earth's radius closer to the Moon, hence,

$$F_C = \frac{G\kappa M_M}{M_E (R_M - a)^2} = \frac{GM_M}{(R_M - a)^2} \qquad \textbf{(2-3)}$$

However, in this equilibrium model, the Earth moves without itself rotating (Figure 2-4), about an axis of common centre of mass with the Moon, so

each particle of the Earth will move in a circle of constant radius and the driving force of this circular movement is the Earth/Moon gravitational system.

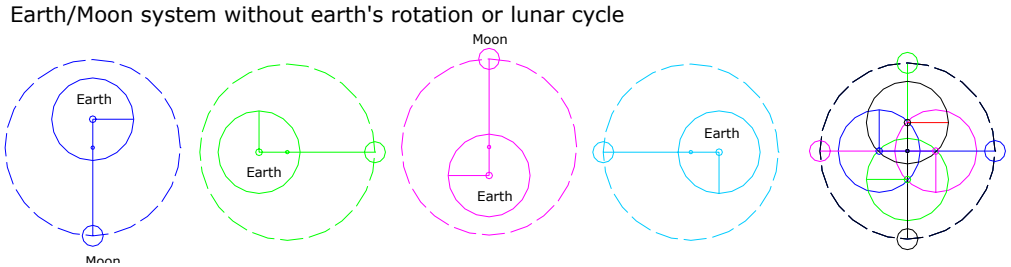

Figure 2-4: Rotational pattern of the Earth Moon system, with a non-rotating Earth.

The particles that lie between the common centre of mass and the Moon will experience a force at **C** (F_C) greater than that required to maintain the orbit, whilst those particles more distant will experience a reduced force at **B** (F_B). It is the difference between the experienced forces and the orbital requirements that produce the tidal forces [**48**].

$$TideForce_C = F_C - F_B = \left[\frac{GM_M}{(R_M - a)^2} - \frac{GM_M}{R_M{}^2}\right] \qquad \textbf{(2-4)}$$

Where

$$(R_M - a)^2 = R_M{}^2\left(1 - \frac{2a}{R_M} + \frac{a^2}{R_M{}^2}\right) = R_M{}^2\left(1 - \frac{a}{R_M}\right)^2$$

Application of binomial series and neglecting small terms gives,

$$TideForce_C \approx \frac{GM_M}{R_M{}^2}\left[1 + \frac{2a}{R_M}\right] - \frac{G_E M_M}{R_M{}^2} \qquad \textbf{(2-5)}$$

this gives a net tide raising force at **C** of,

$$TideForce_C \approx \frac{2aGM_M}{R_M{}^3} \qquad \textbf{(2-6)}$$

Similarly, the tide raising force at **A** is given by,

(2-7)

$$TideForce_A \approx -\frac{2aGM_M}{R_M{}^3}$$

whilst the forces at **B** and **D** are given by,

$$TideForce_B = TideForce_D \approx \frac{GM_M}{R_M{}^2 + a^2} * \frac{a}{(R_M{}^2 + a^2)^{1/2}} \quad \textbf{(2-8)}$$

$$\approx \frac{GM_M a}{(R_M{}^2 + a^2)^{3/2}} \approx \frac{GM_M a}{R_M{}^3} \quad \textbf{(2-9)}$$

The tractive forces applied by the Moon to the ocean on the Earth satisfactorily explains the displacement away from the Earth that occurs on a line between their centres of mass, but the corresponding displacement on the opposite side of the Earth is due to the centrifugal forces generated by the Earth/Moon pair rotating about their common axis. This axis is below the Earth's surface at a distance of 4671 km from the Earth's axis of rotation. Thus the Moonward displacement balances the gravitational attraction of the Earth/Moon system and the opposite displacement balances the centrifugal forces created by the two bodies rotating about their common centre of mass and thus the system remains in equilibrium. At the same time, particles at **B** and **D** are displaced toward the Earth's centre.

The net result of this simplistic model is an elliptical body of water moving relative to the Earth following the orbital path of the Moon, governed by the mass of the Moon, the radius of the Earth, and the inverse cube of the distance between their centres of mass.

By introducing one rotation of the Earth about its axis to be one sidereal day, and setting the Moon's rotational period about the Earth to be 29.5 sidereal days in the same sense and plane, it is possible to illustrate the fundamental semi-diurnality of the tidal drivers.

While the Earth rotates once, the Moon makes 1/29.5 of an orbital about the Earth and, since there exists a diametrically opposed displacement of water away from the Earth, two tides will have been observed during 1 sidereal

day. The total net force experienced by the Earth as a result of the Moon's gravitation on a line of centres is given by

$$\frac{2GM_E M_M a}{R_M{}^3} = 6.571 \times 10^{18}\, N \qquad \textbf{(2-10)}$$

Therefore, the acceleration experienced by a particle of unit mass, κ, in terms of the Earth's standard gravity, g, is

$$2\kappa\left(\frac{M_M}{M_E}\right)\left(\frac{a}{R_M}\right)^3 g = 1.12 * 10^{-7} g \qquad \textbf{(2-11)}$$

A result which is apparently unlikely to generate the vertical movements observed in the oceans. However, the vertical movements are not created by the vertical component of the tide generating force, they are the result of the tractive, or locally horizontal force, acting tangentially to the Earth's surface over a large area. The motion has been compared to that of a stiff shafted pendulum, whereby vertical movement is impossible, but minimal force is required to impart a measurable horizontal movement. Early attempts to measure the tide generating force by means of a pendulum were defeated by the fact that the Earth's crust is also subject to the same force and therefore it is impossible to measure any relative motion between the Earth's surface and any apparatus attached to it.

An estimate of the tidal range due to the Moon on a uniformly water covered Earth can be made as follows. At some point, the total gravitational effects of the Earth and Moon on the water will achieve equilibrium and the water will rise (or fall, at the poles) from its mean level, to this point, *h.* Taking g as gravitational force per unit mass, given by

$$g = \frac{GM_E}{a^2} \qquad \textbf{(2-12)}$$

Then the gravitational force g_h at height $a + h$ will be,

(2-13)

$$g_h = \frac{GM_E}{(a+h)^2} = \frac{GM_E}{a^2}\left(1 - \frac{2h}{a}\right)$$

The water surface will rise until equilibrium is achieved, for example at point **C** (Figure 2-3), on the line of centres and dividing by the mass of the Earth to obtain tide producing force per unit mass,

$$g = g_h + \frac{TideForce_C}{M_E} = g_h + 2\frac{GM_M a}{R_M{}^3} \qquad \textbf{(2-14)}$$

Substituting ***(2-12)*** and ***(2-13)*** into ***(2-14)***

$$\frac{GM_E}{a^2} = \frac{GM_E}{a^2}\left(1 - \frac{2h}{a}\right) + 2\frac{GM_M a}{R_M{}^3} \qquad \textbf{(2-15)}$$

Solving for h and simplifying gives the height, h_C, at **C**

$$h_C = \frac{M_M}{M_E}\frac{a^4}{R_M{}^3} \qquad \textbf{(2-16)}$$

Application of the same reasoning to the forces at **B**, gives the height h_C at **B**;

$$h_B = -\frac{M_M}{M_E}\frac{a^4}{2R_M{}^3} \qquad \textbf{(2-17)}$$

The total range is given by the sum of the two heights, h_B and h_C ,

$$\frac{M_M}{M_E}\frac{a^4}{R_M{}^3} + \frac{M_M}{M_E}\frac{a^4}{2R_M{}^3} = 0.538\,m \qquad \textbf{(2-18)}$$

Up to this point, it has been assumed that the Moon acts alone, but the forces applied by all other celestial bodies are calculated in the same way as for the Moon.

The Sun, though much more massive than the Moon, is much further away, with the net result that its influence is about 0.47 of that of the Moon. It is also assumed at this stage that the Earth, Moon and the Sun are within the same ecliptic plane, with their rotational axes normal to that plane, and that the Moon's orbit about the Earth/Moon centre of mass and the Earth/Moon system's orbit about the Moon are both circular.

When the Earth/Moon/Sun are aligned (Syzygy), the combined tractive forces applied to the oceans will be approximately greater than that of the Moon alone by a factor of 1.47. When the Moon is perpendicular to the Sun/Earth alignment (Quadrature), the resultant factor is approximately 1.09 and, the tractive forces will vary between these values twice during the Synodic cycle, giving rise to the Spring/Neap cycle of tides on Earth, Figure 2-5.

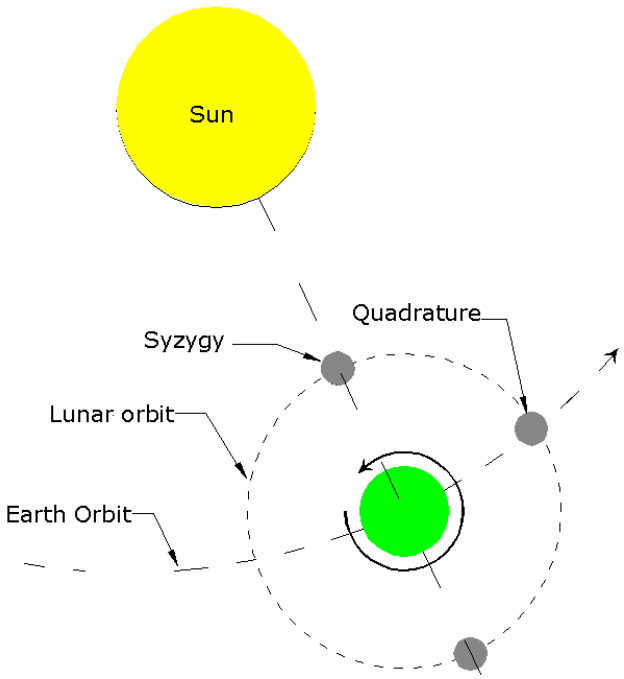

Figure 2-5: Spring and neap tides

The Equilibrium Theory, developed by Newton et al, clearly describes the fundamental semi-diurnal and Synodic cycles observed in the system, but appears to make little headway when applied to actual observed tidal events. The reasons for the observed variations, both spatial and temporal are examined in the next section.

2.3 Analysing tides

The inviscid water assumed to cover the Earth to a regular depth, would respond instantaneously to the tractive forces and high water would, at all times, be directly beneath and opposite to the Moon. But the Earth is not covered to regular depth by a perfect fluid and the time of high water is often at considerable variance with the passage of the Moon over the meridian, and this observed delay (known as the "age of the tide" or phase lag) is consistent at any location. The fact that the paths of the Moon around the Earth and the Earth/Moon pair around the Sun are not circular but elliptic, the Earth's axis is at 66.5^{o} to the solar ecliptic, the Moon orbits the Earth at 5.9^{o} to the solar ecliptic, and that these cycles have different periods, means that the resulting force patterns are highly complex. The three principal cycles associated with the lunar forces are:

- **The Lunar Declinational**, which varies with the Moon's position relative to the Earth's equatorial plane, (27.32 solar days).
- **The Perigean** tides where the Moon's elliptical orbit brings it closest to the Earth (27.55 solar days).
- **The Apogean** tides where the Moon is at the furthest point in its elliptical path (27.55 solar days)

The Sun will induce similar patterns on the tides which will be superposed onto the lunar cycles and the resulting combinations of cycles mean that for most tide prediction purposes the limiting periodicity is generally taken as the 18.6 year cycle of the lunar nodal regression, i.e. the point at which the Moon crosses the ecliptic plane in its passage from a maximum declination of 28.5^{o} to a minimum declination of 18.5^{o} [**49**].

2.3.1 Harmonic Analysis

By recording the tide at regular intervals in one location, a complex curve is mapped, which is a combination of all of the simple harmonics of different

periods, phases and amplitudes. The taking of measurements over a sufficiently lengthy period makes it possible to predict tidal behaviour into the future with reasonable accuracy. The technique was used historically to predict tides at any location, long before the idea of harmonic analysis was introduced. It is of particular importance to note that the tidal height constituents are not necessarily of the same relative proportion as the forcing constituents.

The local bathymetry and topography both play a significant role in how the water responds to the forcing constituents in any one location. The local tide record will reflect these response variances and provide illustrative numerical values where a purely analytical approach may not. Figure 2-6, shows a typical UK semi-diurnal record taken over one synodic cycle (29.53 days) and the superposition of the two fundamental frequencies is obvious.

The level of accuracy of any analysis and, therefore any prediction, will depend on the number and type of constituents used in the analysis.

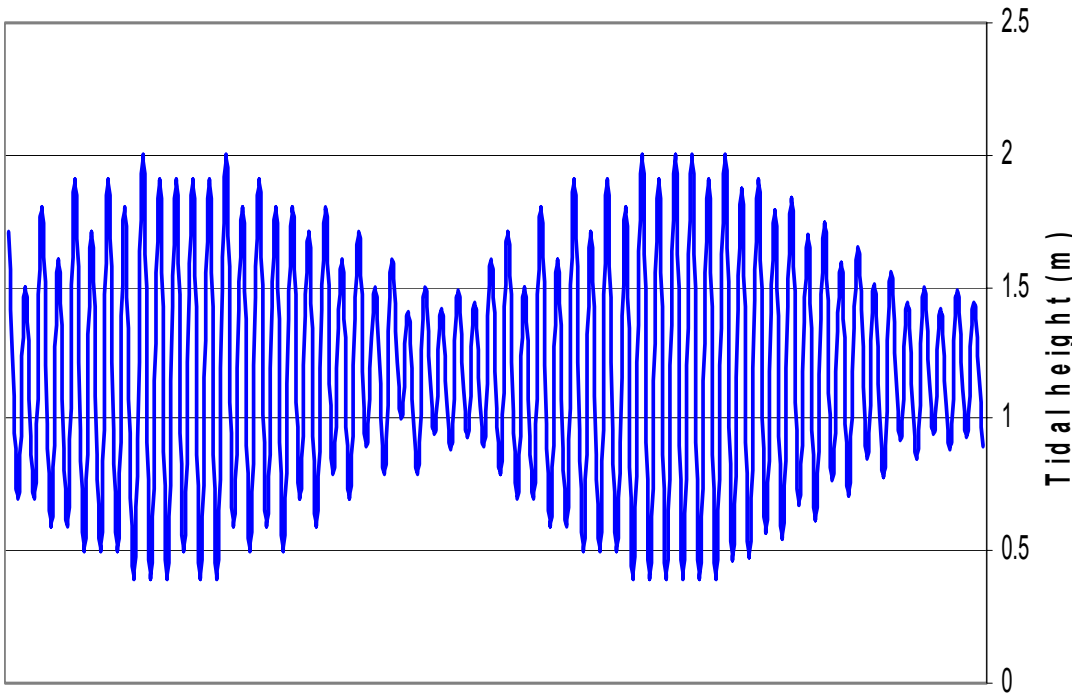

Figure 2-6: A generic semi-diurnal tidal height plot

Any sampling must be with regard to the Nyquist frequency of the highest frequency component to be considered. The solar and lunar cycles are well known and the resulting tide producing forces can be modelled as the sum of simple harmonics constituents. The periods of some of the principal tide producing force constituents are given in Table 2-2.

Table 2-2: Characteristics of the principal tidal constituents

Constituent Symbol	Description	Period (solar hours)
M6	Shallow water overtides of principal lunar	4.140
S4	Shallow water overtides of principal solar	6.0000
MS4	Compound tide of M2 & S2	6.103
M4	Shallow water overtides of principal lunar	6.210
K2	Lunisolar semi-diurnal	11.967
S2	Principal solar semi diurnal	12.0000
M2	Principal lunar semi-diurnal	12.421
N2	Larger lunar elliptic semi diurnal	12.659
K1	Lunisolar diurnal	23.935
S1	Solar diurnal	24.000
P1	Solar diurnal	24.067
O1	Lunar Diurnal	25.819
Mf	Lunar fortnightly	327.869

A list of common harmonic constituents, overtides and compound tides is given in appendix 1. The actual number of constituents that are important is a function of the particular situation to be modelled, with up to 65 individual constituents being appropriate in some cases.

The diurnal and semi-diurnal harmonics of the astronomical drivers are modified locally by ocean basin resonance and the resulting tidal pattern can be characterised by their principal response mode into diurnal, semi-diurnal or mixed tides. A typical diurnal response is one high water and one low water per day; semi-diurnal will give two, roughly equal high water levels and two roughly equal low water levels per day, and mixed tides present a high high water, a low low water, a low high water and a high low water. In some locations a mixed tide can become semi-diurnal for a sub-period of its cycle. Phase lead (or lag) is also a location specific feature with spring tides leading (or lagging) Syzygy and neap tides leading (or lagging) Quadrature.

A more systematic classification of tides employs a form function [**50**], described by,

$$Form = \frac{(K1 + O1)}{(M2 + S2)} \qquad \textbf{(2-19)}$$

where the ratio of the sum of the amplitudes of the principal diurnal constituents and the sum of the amplitudes of the principal semi-diurnal constituents can be used to give four classes of tide, Table 2-3.

Table 2-3: Classes of tide

Classes of tide	
F = 0.00 ⟶ 0.25	A semi-diurnal tide with two roughly equal high and low waters daily.
F = 0.25 ⟶ 1.5	Mixed, primarily semi-diurnal tide with significant inequalities in tidal range and time.
F = 1.5 ⟶ 3.0	Mixed, primarily diurnal tide
F = >3.0	Fully diurnal tide

2.3.2 Response Method

This is a further method of tidal analysis that is more accurate than harmonic analysis and is capable of showing an improved level of accuracy whilst employing fewer components [**51**]. It treats the ocean as a black box system, using the astronomical forces of the equilibrium tide as input and the measured tidal heights or flow speeds as the output. The Response method can operate on relatively short records and can incorporate radiational effects and shallow water effects as well as the standard gravitational input.

The harmonic analysis method remains the preferred methodology, principally for its conceptual simplicity and ease of application to computer analysis.

2.4 Ocean Tides: Drivers of tidal streams

The Equilibrium Theory demonstrated that the tide producing forces are fundamentally astronomically based, but that other factors need to be considered when examining the resultant tide height at any one location. In fact, the actual tidal behaviour appears, in places, to be completely different from the behaviour predicted by Equilibrium Theory. For example, without land masses, there would be two symmetrical tidal bulges, directly beneath and diametrically opposed to the Moon and Sun positions, each producing a maximum equatorial tidal range of about 0.5 m. The individual high tides would track around the globe from east to west as the planet rotated beneath them. Clearly these conditions are not in agreement with the observed patterns of the tides. In reality, the tides spread from their home oceans onto the surrounding continental shelves where they can generate tidal ranges of over 10 m. The principal drivers of these contrary and complex tidal patterns are mainly due to the presence of continental land masses, which are generally arranged in a north/south alignment at right angles to the Equilibrium Theory travelling waves.

The ocean basins each have their own natural modes of oscillation and can respond to a variety of forcing frequencies. The complete ocean system appears to be close to resonance with the semi-diurnal forces and the resulting tidal ranges are much larger than the Equilibrium Theory suggests. The overall response to diurnal forcing is much weaker, but local conditions in some areas will favour diurnal over semi-diurnal. The development of standing waves in a resonant ocean basin explains how the tides sometimes appear to travel the ‘wrong’ way.

The tidal waves propagate as long waves, and their speed is dependent on water depth. A typical wave in an average ocean of 4000 m depth would travel at about 200 m/s. This compares with the equatorial lunar speed of about 450 m/s, thus demonstrating that the Earth’s oceans simply cannot keep up with the lunar track.

The Earth is a rotating spheroid and not a flat sheet. In order to comply with gravity the oceans must constantly accelerate which requires an additional force at right angles to the imposed motion. These forces are described by Coriolis and result in waves with a slope in two directions, described as Kelvin waves.

The Earth itself is elastically modified by the gravitational pull and it is known that continental land masses sink as well as rise in response to this tidal loading.

The results of the tide-producing, astronomical forces can easily be measured at the shoreline, and tabulated data has been produced for hundreds of years at certain sites, particularly those of interest to the Admiralty. Use of harmonic analysis, which has been substantially accelerated by the application of digital processing, allows appropriate tidal predictions to be made, which are generally fit for purpose at any one location. However, the height of the shoreline tide is known to be influenced by local topographical and bathymetrical features, and that the tidal elevation in mid-ocean is not the same as at the land/sea interface. Since tidal streams are driven by pressure head differences on each side of a restriction, then the amplitude and phasing of the ocean tides are vital to the stream's energy resource.

2.4.1 Tidal Data

Historically, tidal information has been based entirely on shoreline measurements and this due to a number of factors.

Need: The main effect of tides, as far as shipping is concerned, is whether or not sufficient draught is available to access a port, and, with a few well charted exceptions, this is not generally a concern in the open ocean.

Feasibility: Shoreline locations offer easy access and an effectively fixed datum from which to record observations.

Instrumentation: Without a fixed surface datum, measurement of tidal variations of about 0.5 m relative to a depth of, say 500 m is within an error band of 0.001 and therefore difficult to verify unless the sea is flat calm.

There is very little information yet available on the deep ocean tides, though there is some speculation as to their nature. Theoretically, Laplace's dynamical postulate should provide a method for calculating the tides anywhere in the Earth's oceans, but in reality the ocean boundaries and bathymetry are so complex that no analytical solution is yet available [**52**]. However, the work that has been done using the solutions that can be found from Laplace does give an indication of the tidal behaviour over an area, as opposed to the edges, which is where present models tend to concentrate their efforts. Given sufficient space, and a gyratory motion, the tide producing forces impose a wave that describes a rotary motion about a point known as an amphidromic point or node.

Much of the historic modelling of ocean tides has been based empirically on observed data from ports around the periphery of an ocean. By noting the timing of tide heights and applying a local knowledge of the tidal phase movement along a coast, it has been possible to extrapolate out into the oceans. The resulting co-tidal charts are usually based on the major constituents (M2, S2, K1, O1) etc.

The development of numerically powerful computing systems has allowed other investigators to apply numerical solutions to Laplace's dynamical equations with some degree of success. Using known bathymetry and tidal forces, models have been developed for the open oceans that show reasonable agreement with recorded coastal measurements. The method also allows model constraint by inputting observed data and forcing the model to develop around these points. The numerical solutions have not only confirmed the position and effects of amphidromes, but have also revealed anti-amphidromes where there exists an apparently phaseless region of maximum tidal amplitude [**53**].

Finally, satellite measurements will give a more accurate picture of the ocean tidal waves, a feature which has been almost irrelevant to mankind until the 21st century, but a solid understanding of which is vital for the global tidal energy industry since it is principally these waves and their topographical modifiers that drive the tidal streams of the world.

2.4.2 Creation of tidal streams

For the purposes of this thesis tidal streams are defined as: the periodic movement of water driven principally, though not necessarily exclusively, by a head difference created by out of phase ocean tides at each end of a restriction. Other external and, frequently, non-periodic forces are applied to tidal streams and these will often depend on the local weather patterns (radiational tides), ocean characteristics (internal tides) and geography. The rotation of the Earth is important in that the Coriolis forces modify the flow away from the equator, dependent on the local topography, and the bathymetry at any particular location will affect the bottom friction energy losses as well as the intensity of turbulent mixing.

Tidal streams can be analysed and predicted using the same mathematical techniques as tidal heights. The process of obtaining the initial data from tidal streams is more difficult than that of reading tidal heights, but the introduction of subsea digital electronics has made acquisition of substantial quantities of high-quality tidal stream velocity data relatively straightforward though somewhat expensive.

Long wave characteristics

The oceans are covered in waves, but the generally observed waves are of a short period and are dependent on the wind for their generation. Tidal waves can be observed; in certain areas they create dramatic estuarial bores that can reach far inland, but they are of a long period, on average around 24 hours 50 minutes and 12 hours 25 minutes for diurnal and semi-diurnal respectively. This implies wavelengths of hundreds or thousands of kilometres which makes their wavelength much greater than the water depth and hence they are known as long waves or shallow water waves. For these waves, the speed of propagation c is given by

$$c = \sqrt{gz} \qquad \textbf{(2-20)}$$

Where z is the water depth and g is gravity. Wave length λ and period T are related by,

$$\lambda = \sqrt{gzT} \qquad \textbf{(2-21)}$$

If two waves of the same period and wavelength move in opposite directions and the wave length is twice the basin length then resonance will occur. The fundamental oscillation is given by

$$T = \frac{2\lambda}{c} = \frac{2\lambda}{\sqrt{gZ}} \qquad \textbf{(2-22)}$$

In an open ended basin, such as an estuary or similar funnelling structure, the required ratio is that the wavelength is four times the basin length [**54**] and the body of water is known as a quarter-wave oscillator.

For a standing wave to be maintained some form of external periodic forcing is required and the multiple harmonics within a tidal wave are capable of providing just such a force. The resonance will depend on the integer number (n) of wave periods that correspond to the time taken for the wave to travel the basin length, as in,

$$T_n = \frac{2\lambda}{nc} \qquad \textbf{(2-23)}$$

The net result of resonance, regardless of particular type, is that the waves will interfere in a constructive manner, i.e. the net amplitude will be equal to the sum of the individual wave amplitudes. The additional amplifying effects of bathymetry and topography are discussed on p82.

Radiational tides

Although regular, these effects are not of an astronomical nature in the gravitational sense. Created by the warming effects of the Sun, a variety of meteorological events will apply diurnal and semi-diurnal patterns of pressure and wind to the local ocean surface. The diurnal warming of shallow areas of sea will also create forcing patterns, though these tend to be on more of an annual cycle. Being of a diurnal and semi-diurnal nature, radiational effects are frequently masked by (or confused with) the S2 astronomical harmonics, particularly in the tropics where day length remains essentially constant compared with higher latitudes. This is not to say,

however, that radiational effects are not important at higher latitudes, but that their presence is less easy to explain [**55**].

Internal tides

Internal tides caused by density differences as a result of long-term temperature and salinity variations within the oceans, can produce wave propagation along lines of density gradients. Typical speeds of these internal tides are of the order of 1 m/s, which, out in the open ocean has little influence on coastal tidal streams but on arrival at a continental shelf, may apply considerable forcing effects by virtue of their momentum. The density differences that drive these internal tides are of a fluctuating and irregular nature, and therefore are usually very difficult to identify solely from single site data.

Coriolis forces

Although named after Coriolis (1835) who developed the area of acceleration in a rotating system [**56**], the actual concept is due to Laplace [**57**] in his original study of tides in 1775. The concept can be explained, thus:
If a particle is considered to be at the Earth's equator, it will experience acceleration (due to the curvature of the Earth) and have an angular momentum given by $\omega^2 r$ where r (the radius of motion) is equivalent to the radius of the Earth at the equator and the angular velocity (ω) is given by,

$$\omega = \frac{2\pi}{24 * 3600} rad / s \qquad \textbf{(2-24)}$$

If the particle now travels northward, the radius of motion will shrink with the cosine of the latitude, until it reaches a theoretical singularity at the North Pole. In order that angular momentum ($\omega^2 r$) is conserved the particle must accelerate, and this acceleration is observed to be eastward in the northern hemisphere and westward in the southern hemisphere. A movement by the particle back towards the equator would render the opposite effects to be observed. The action of the Coriolis force is to modify

tidal flows, particularly in estuaries and other partially enclosed areas such as sea lochs.

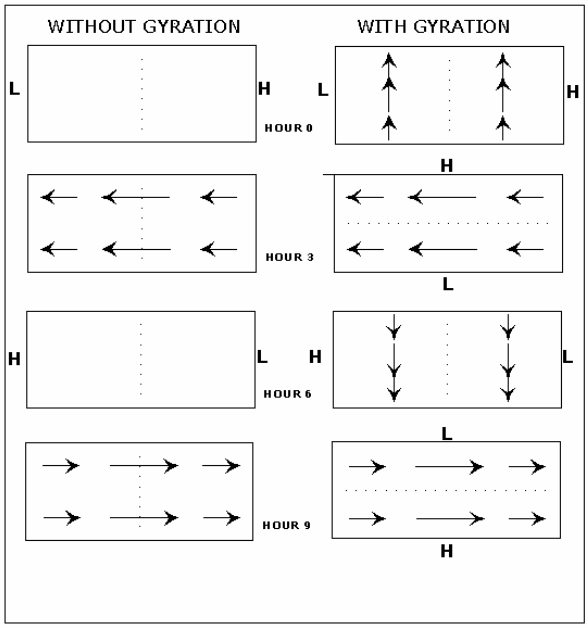

Figure 2-7: Gyratory modification of a standing wave within an enclosed basin [58].

In the absence of the gyratory forces described by Coriolis, a standing wave in a rectangular basin will alternate between high water at one end and low water at the other. At hour 0 (see Figure 2-7) there will be no current. At hour 3 there is a current flowing westward, and hours 6 and 9 are the reverse of 0 and 3 respectively. If the system is now subject to a gyratory motion, the wave will travel around the periphery of the basin in an anticlockwise manner, with high water at the periphery and unchanging low water in the centre of the basin. Instead of oscillating about a nodal line, the standing wave, at the frequency of the harmonic constituent that drives it, rotates about a nodal point, creating an amphidromic system. An amphidrome, therefore, is a position within the ocean where the net tidal forces produce zero tidal driven height variation.

An amphidromic point exists for each harmonic forcing frequency and it is this fact that explains the apparent difference in dominant frequency at

various sites. If an S2 harmonic driven amphidrome is closer to a particular area than an M2 amphidrome then the local tide will be S2 dominant [**59**].
Co-tidal lines emanate from the amphidrome in a manner similar to wheel spokes, with lines of co-range where the amplitude is the same for all points and co-phase where all points have the same phase lag (360^{o} = 24 hr) relative to their tide-producing force constituent. Amphidromic circulation is clockwise in the northern hemisphere and anti-clockwise in the southern hemisphere.

Ocean tides

As previously discussed, the ocean tides rotate about amphidromic points which suggests that any substantial body of water, where there is sufficient space available, will develop its own amphidromic system which will be linked with those of its neighbours via the tide producing forces. Since different areas are known to respond and resonate independently and with a variety of phase lag magnitudes, then any two neighbouring bodies of water will have to somehow negotiate their differences at their interface. Inspection of co-tidal maps illustrates that land masses, especially relatively small islands, play an important role in this negotiation. Co-tidal maps also show that the closer together any two co-phase lines are then the likelihood of there existing a substantial energy gradient between them is increased.
Most of the Atlantic coastal tides are semi-diurnal in nature, so the diurnal inequality which is readily seen in a mixed tide is quite small in tides of this area. This is largely due to the fact that the dimensions of the Atlantic basin give it a response that favours the semi-diurnal frequencies. The Pacific Ocean, being much larger, responds to both diurnal and semi-diurnal frequencies and this gives a substantial diurnal inequality to the tides of California and British Columbia on the west coast of the North American continent. According to King [**58**] the North Sea is too small to resonate to the astronomical forces, but it does resonate in response to the rhythm of the Atlantic Ocean, producing three amphidromic points. The natural position of these amphidromes would be equidistant from the coastlines of:

- Norway and East Scotland
- Denmark and North East England
- Belgium and East Anglia

In reality, these amphidromes are pushed eastward by the incoming tide, which enters from the northern end of the North Sea and rotates anticlockwise around the North Sea basin, pushing through the shallow water.

2.4.3 Tidal stream modifiers

Meteorological forces

Harmonic analysis of any tidal record will throw up residuals which represent elements in the tidal patterns that cannot always be satisfactorily extracted by the harmonic method. The regular warming of the oceans and associated onshore/offshore winds are discussed under radiational tides because of their relative regularity in certain parts of the world. In these areas, radiational tides are relatively straightforward to separate out with harmonic analysis. In other areas, particularly at higher latitudes, the weather can be much less regular and predictable and, since tidal streams are driven by periodic pressure head differences, atmospheric pressure can play a substantial part in their flow behaviour. Winter barometric pressure over the North Sea can range from 975 mb to 1025 mb in 24 hours and this represents a sea level change of approximately 0.5 m. Such barometric pressure variations can increase the local tidal range considerably, and therefore will have a significant impact on the pressure head available for stream driving. Surface wind effects if following or opposing a stream will create measurable surface velocity changes or raise the water levels in closed basins. The wind can also be split into prevalent and dominant components. The prevalent wind is the most common direction and the dominant wind is the one which has the most effect on local sea levels. Thus, on the western coasts of Britain, the prevalent and dominant winds are south-westerly, whilst on the east coast,

the prevalent wind is still south westerly i.e. offshore, whereas the dominant wind is northerly.

The basic predictability of tidal streams is not affected by these extraneous events but the periodic behaviour of tidal streams is much noisier in terms of data collection than tidal heights. Tidal stream activity is generally up to 90^{o} out of phase with the tidal height data, with high water slack and low water slack being at high water and low water respectively. Maximum tidal stream velocity generally occurs at the halfway point between high water and low water.

Bathymetry and topography

In narrow straits, such as the Pentland Firth (off Northern Scotland), which separates two tidal regimes, the flow is driven by a balance between pressure head and boundary layer friction and can be satisfactorily modelled using open channel hydrodynamics. Over large ocean regions the ratios of the astronomical forcing constituents are generally stable but this is frequently not the case in narrow straits which are heavily influenced by shallow water effects and reflection induced anomalies resulting from coastal effects.

The bathymetric and topographical dimensions of estuaries, basins and other funnelling features are fundamental to the characteristics of the flow behaviour. When decreasing depth is accompanied by decreasing width and basin dimensions corresponding to dominant wavelengths, the resulting tidal range is often very large. For example the Bay of Fundy on the east coast of Canada has a natural period of oscillation between 11.6 and 13 hours which corresponds to a number of semi-diurnal frequencies and creates a tidal range of up to 17 m.

Ocean tides generate a variety of forces dependent on the resonant response of the oceans to the individual astronomical forcing frequencies and further influenced by the water depth and the enhancing effects of the local topography and bathymetry. Coriolis forces tend to modify the standing wave, at each harmonic, into a rotating wave associated with an

amphidromic point, and it is the interaction of these rotating waves at certain locations that create the pressure head differences required to drive a tidal stream.

Tidal stream velocity

Tidal streams can be classified into two basic types: bi-directional and rotational. The bi-directional type, also referred to as hydraulic currents, are generally tightly constrained by topographical features into operating as a conduit between two bodies of water, a typical example being the Pentland Firth where the flow is generally east south-easterly or west north-westerly . Rotational flows are found in more open areas such as the North Sea and the Channel Isles. The rotational streams reflect the nature of the governing amphidrome(s) and are generally circular or large symmetrical ellipsoids in offshore areas, but tend to become tight, asymmetrical ellipsoids closer to shore.

For the time being, the development of tidal energy devices is focussed on the bi-directional model, which also exists at the entrance to sea lochs, fjords and bays, generally restricted by width and/or depth. These channels are very short in comparison with the tidal wavelength and are a balance of forces between pressure head and friction. The bottom friction or drag force, for a channel of length, L and width, W is given by

$$Drag = C_D L W \rho U^2 \qquad \textbf{(2-25)}$$

where C_D is the dimensionless drag coefficient, typically 0.002 at 1 m above the sea bed [**60**]. The force applied by the pressure head (F_P) for a channel of width, W and depth, z is given by

$$F_P = \rho g h W z \qquad \textbf{(2-26)}$$

where h represents the head difference across the channel. Equating the two forces given by ***(2-25)*** and ***(2-26)***, and solving for U:

$$U = \sqrt{\frac{zgh}{C_D L}} \qquad \textbf{(2-27)}$$

If h is found from the tide heights at each end of the channel, then the flow velocity U can be found, after allowing sufficient time for the flow to develop.

Velocity profiles

Tidal streams in coastal locations exhibit a significant friction loss at the seabed, and thus have a vertical velocity profile which can be modelled using a simple $1/7^{th}$ power law approximation as shown in Figure 2-8

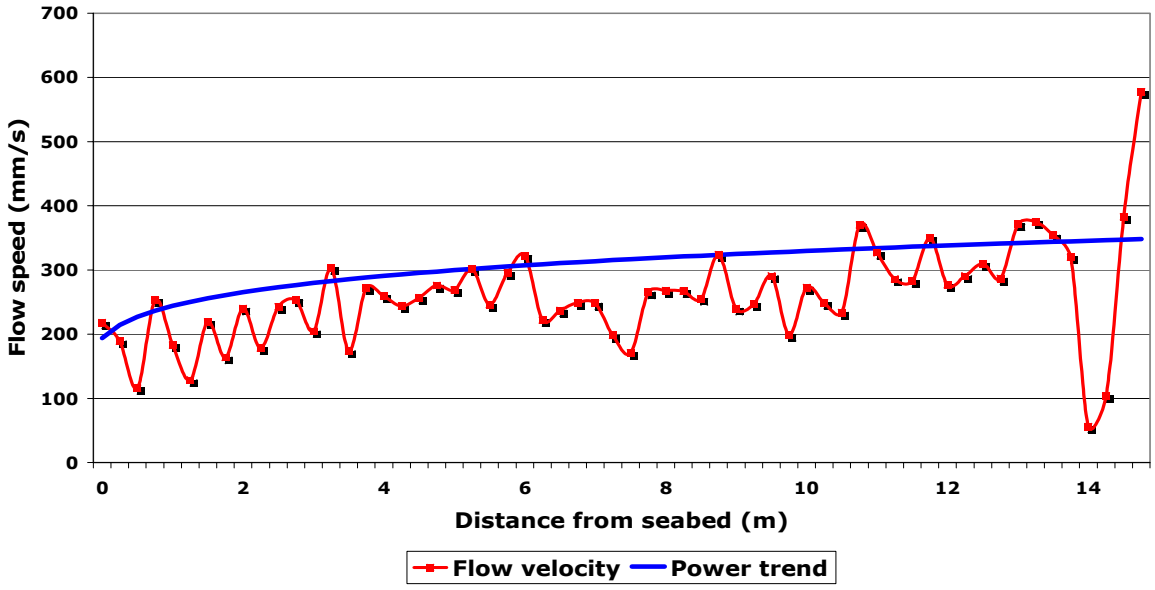

Figure 2-8: Burra Sound velocity profile

The interaction of tidal streams with the seabed produces a boundary layer, in which energy is lost to friction forces [**61**]. The Earth, rotating once every sidereal day, attempts to drag the lunar induced bulges around with it whilst the Moon's gravitational effects tend to hold them in place. The interaction of the water with the seabed induces turbulent eddies of decreasing scale that eventually dissipate as a small quantity of heat. Consequently, the Earth's angular momentum is decreased by the tidal friction induced between the water and the seabed, particularly in the shallower seas. The retardation thus applied, increases the day length by 1 second every 41000 years. It is therefore considered that, since the energy that a TSEC will extract is dissipated as heat anyway, the installation of multiple TSECs is unlikely to have any measurable effect on the Earth's rotation.

The existence of a velocity profile is an important consideration in the design and installation of tidal turbines, particularly horizontal axis models. If the

turbine is fixed relatively closely to the seabed, then, neglecting wave action and turbulence for the time being, the flow velocity seen by the turbine is going to vary from the uppermost blade tip to the lowermost blade tip. The result will be a potentially sizeable fluctuation in lift and bending moment for each blade coincident with the completion of one rotation. Avoidance of cavitation due to the blades proximity to the free surface will control the optimisation of the blade profile and limit it to the velocity and pressure experienced at its uppermost point. It is clear then, that the velocity profile of a proposed tidal stream site is an important component in the optimisation of the turbine, perhaps even in the choice of turbine type. A vertical axis crossflow turbine would see less vertical variance in velocity profile than a horizontal axis type and may therefore be better suited to shallow water installations.

Wave action

Gravity waves exist at the interface between any two fluids of different density, in this case air and seawater, and represent the different response of the two fluids to inertia and gravitational forces at the interface. The ratio of these forces form the basis of the Froude Number discussed under 4.3.1. Submerged tidal turbines will not generally be concerned with small amplitude, locally generated waves, but some accounting is necessary for relatively large swell waves. The wave speed (c) in any water depth is given by ***(2-28)*** [**62**],

$$c = \sqrt{\frac{g\lambda}{2\pi} * tanh\left(\frac{2\pi z}{\lambda}\right)} \qquad \textbf{(2-28)}$$

Where λ is the wavelength and z is the water depth (as before). If $z > \lambda/2$ then ***(2-28)*** reduces to ***(2-29)*** and wave speed depends on the wavelength.

$$c = \sqrt{\frac{g\lambda}{2\pi}} \qquad \textbf{(2-29)}$$

If $z < \lambda/20$ then the wave speed is determined by water depth and c is as given by ***(2-20)***. If $z > \lambda/20$ and $z < \lambda/2$ then ***(2-28)*** must be used.

In real seas there exist a large number of periodic wave constituents all with different amplitudes, frequencies and directions, dispersing over an ever increasing arc front from their point of origin. The superposition of these waves generates the randomly varying surface that is often observed, though closer observation over time will often reveal a small number of substantial, regular periodic waves that can be analysed using linear wave theory, which is developed in detail in [**63**]. The linear wave theory is used to generate a range of water wave properties, applicable to both deepwater and shallow water situations where $z < \lambda/2,$ which can usefully be applied to wave loading on a slender tubular structure via the Morison equation [**64**].

The Morison equation assumes that the wave properties are not significantly changed by the presence of the tubular member and that the total force due to waves is the sum of the inertia force (fluid acceleration) and drag forces (fluid velocity). The applied force per unit length (F) is given by ***(2-30)***,

$$F = C_m \rho V \dot{U}_n + C_D 0.5 \rho A |U_n| |U_n| \qquad \textbf{(2-30)}$$

where V denotes the volume of the tubular and $\dot{U}_n$ the fluid acceleration normal to the axis of the tubular. C_m is the inertia coefficient which is usually taken as the added mass coefficient i.e. a value of 1 for tubulars. U_n Is the component of velocity acting normally to the axis of the tubular and C_D is the drag coefficient for a tubular. Both C_D and C_m are dependent on the value of $Re.$

If the dimensions of the submerged structure are greater than 0.2λ, then the wave movement will be affected by the presence of the body and other analytical approaches are required.

Turbulence

The effects of small-scale turbulence on the boundary layer of a surface are discussed under 3.3.6. The immediate concern here is in the area of large-scale coherent turbulence such as vortices and shear flows. The interaction of

tidal streams with the bathymetry and topography that constrains them produces flow characteristics that are very different from those of the main flow, and capable of inducing large velocity fluctuations, with obvious implications for any device positioned in the flow stream. Inspection of Figure 2-9 shows a very complex flow regime of the southern tip of South Ronaldsay whereby the main east-going flow is drawing water in from the east coast of South Ronaldsay and spinning it rapidly through more than 360^{o} in a counter clockwise direction with a depthwise axis.

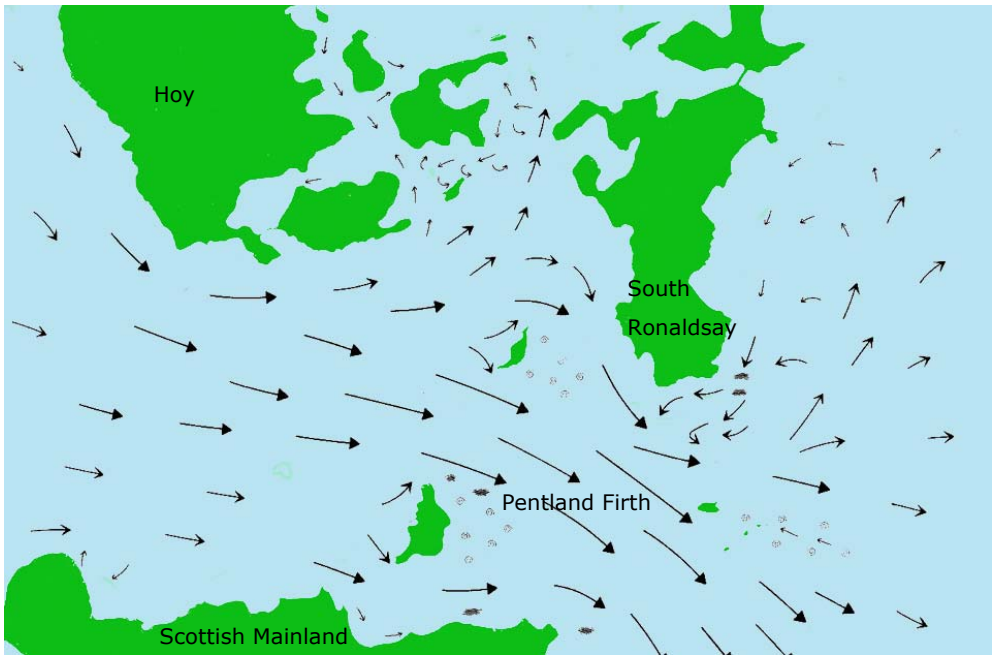

Figure 2-9: Graphical illustration of flow through the Pentland Firth.

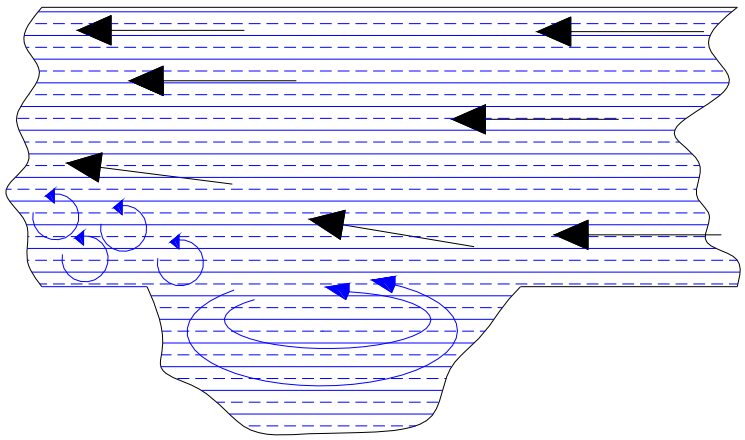

Figure 2-10: Section through trench in seabed east of Stroma and Swona

Bathymetrical features can also induce large scale turbulence. Figure 2-10 shows a sketch of a trench within the Pentland Firth that runs horizontally perpendicular to the dominant flow direction. The proportions are drawn to scale, indicating that the trench is a substantial feature relative to the main flow and that subsequently the flow characteristics close to the seabed and mid-depth will be influenced for considerable distances downstream.

The flow in the Pentland Firth is highly complex and notoriously difficult to predict, being very sensitive to meteorological influences in addition to the strong tidal forces. A contemporaneous account of a storm in December 1862 has the eastgoing flow clearing the vertical cliffs on the west of Stroma and depositing seaweed and shipwrecks on the top, a lift of 25 m [**65**].

2.4.4 Mooring loads and structural integrity

The true nature of tidal streams must be thoroughly understood before large-scale deployment of tidal stream energy converters can be safely and profitably undertaken. Although the marine environment will not deliver the same scale of unpredictable variation that the atmospheric environment is capable of on a daily basis, it is a much harsher environment and the structural loadings are inherently large. In addition, storm events such as the one described may increase structural and mooring loads to many times that

of the normal operational loading. It is not known at this time what represents the 100 year storm loading in terms of tidal stream pressures and velocities, but this will need to be established at some point in the future and fed into the calculations of mooring loads and structural integrity.

2.5 Chapter Summary

The timing and general magnitudes of tidal streams is a mature science and is generally well modelled at coarse scales, with a range of software and paper prediction information available. The individual characteristics of any given tidal stream are less well understood and this will impact on any projection of energy extraction or commercial benefits. It is known from historical accounts that extreme events are part of the long-term cycles of tidal behaviour, and it is also known that tidal streams drive parts of the marine food chain. Additionally, meteorological influences can play a substantial role in anomalistic events that may prove overwhelming for any devices deployed at the time. Devices are also at risk from flow events such as coherent turbulence and large-scale vortices that may travel for many kilometres and in any part of the water column.

Prediction of the available resource from existing charts and tidal stream atlases is of little value, the only way to find out how good the resource is at any one place is to acquire data from that one place, there are many areas where 50 m in any direction will produce a very different resource pattern.

Chapter 3 Hydrodynamic modelling

3.0 Chapter introduction

The mathematical modelling of tidal streams is still in its infancy, with very little hard data to provide appropriate boundary conditions or to validate the results against. Tidal streams can be modelled as a simple channel flow using a classical hydrodynamic approach, but mathematical analysis of fluid flow is, in reality, very complex, and solutions are frequently impossible without the application of simplifying assumptions.

Classical hydrodynamics addresses fluid flow problems by using idealised concepts such as an inviscid, incompressible fluid, which is treated as continuous and homogenous at all scales [**66**]. However, provided that the model is scaled properly and retains sufficient information to give a reasonably accurate solution, then the simplifications will still lead to a meaningful result. Many flow situations can be simply modelled using combinations of linear flow, flow from a source and flow into a sink. When a source and sink of equal strength are placed an infinitesimal distance apart, a doublet is created. Further combination of a doublet gives a good representation of the mathematical idea of flow around a cylinder or ellipse. A MathCAD model is given to illustrate the principle.

The hydrofoil is the single most important section property in any tidal stream device; it is the hydrofoil that is employed by turbine blades to extract energy from the flow, and it is the hydrofoil that provides the interface between the flow and the structure for the Sea Snail concept.

This chapter outlines the classical hydrodynamic concepts of flow around cylinders and hydrofoils that are required to understand the interaction of a tidal stream with a device placed in its path.

A mathematical model of tangential stresses and surface pressure distribution over a hydrofoil shape is developed and compared with related theory and empirical results. The mechanics of drag and lift applicable to hydrofoil sections are reviewed and the influence of the boundary layer on structural loading is discussed.

3.1 Hydrodynamic forces: tubulars and hydrofoils

The study of fluid flow around submerged streamlined bodies is well documented and readily available. What follows is a short review of the principal concepts in the analysis of flow around a tubular member and a hydrofoil.

3.1.1 Drag force on a stationary cylinder

In a Cartesian frame of reference, the simple case of flow around a stationary cylinder is visualised by combining a doublet at the origin with the stream flow of a uniform linear flow in the x direction. The appearance of stagnation points at the intersection of the cylinder with the x axis is consistent with flow around a cylinder, as is the acceleration of the flow at the intersection of the y axis. The acceleration is equal symmetrically about the axis of flow, and, whilst in reality the cylinder would experience drag force in the direction of flow, the non-rotating theoretical cylinder experiences no net lift. The drag force applied to the real cylinder is linked to the flow characteristics via the Reynolds number.

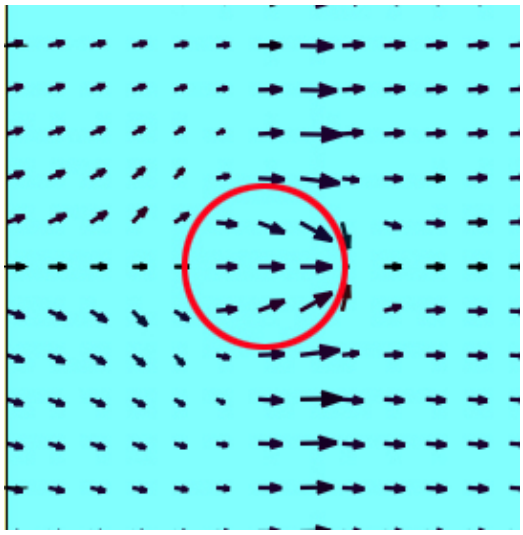

Figure 3-1: Vector plot of frictionless flow around a fixed cylinder.

The 0.214 m diameter steel tubulars used for the Sea Snail structure are assumed to have a typical commercial steel surface roughness, ε, of 4.5x10^{-5} m [**67**] and, therefore, a relative roughness (ε/d) of 2.1x10^{-4}. For a subcritical flow regime, Re <3x10^5, i.e. U <1.6 m/s, the tubulars can be considered to be smooth in sea water. The wake is completely turbulent, according to [**68**] but the boundary layer over the tubular is laminar and separates in a laminar manner.

For a critical flow regime where, 3x10^5< Re <3.5x10^5 and 1.6 m/s <U<1.8 m/s, the separation oscillates between laminar and turbulent but the boundary layer remains laminar. This oscillation in the separation behaviour creates a non-zero mean lift, which itself oscillates as the turbulent separation changes sides. The flow regime then remains in the super-critical band until Re ≈ 1.5 x 10^6, at which point, 8 m/s <U and the boundary layer separation is turbulent on both sides of the cylinder. The theoretical pressure distribution experienced by a stationary tubular of 0.214 m diameter in an ideal flow of 1 m/s is shown in Figure 3-2. The corresponding drag coefficient for this theoretical cylinder is C_D=6.

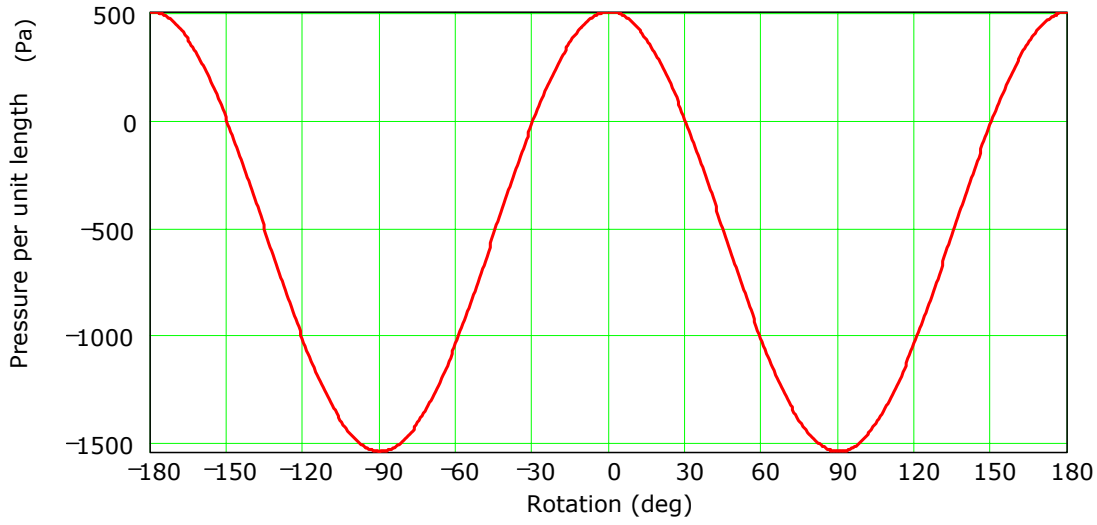

Figure 3-2: Theoretical pressure distribution about a stationary cylinder, per unit length

The drag coefficient for circular cylinders given by [**69**] suggest that for the sub-critical regime C_D remains within the range 0.95 – 1.2, until a sharp drop from C_D=1 to C_D= 0.3 is apparent, starting with the critical flow regime, for Re =3x10^5 and finishing at Re = 5x10^5. At Re = 1x10^6, which requires a flow velocity in excess of 5 m/s, C_D has recovered only as far as 0.38.

Since the Sea Snail is not intended to be trialled in flows exceeding 4 m/s, and 2 m/s represents the beginning of the super critical flow regime, i.e. Re >3.5 x 10^5 then an assumed C_D of 1 for all the structural tubulars comprising the Sea Snail, represents a reasonable factor of safety.

The method of analysis of drag forces applied to the complete Sea Snail structure is given in [**38**].

The following MathCAD sheets (Box 1) show the mathematical derivation of a doublet and linear flow and demonstrates the parameters that govern the numerical solution of the circulatory flow around a cylinder. The principle is subsequently used to model the lift forces on a rotating cylinder from which the Kutta-Joukowski condition [**70**] and conformal mapping of pressure distribution around a hydrofoil are derived. The MathCAD file is given on the attached CD, and the reader can experiment with variation of the linear flow components as well as the location and the strength of the source/sink values to produce a range of flow situations.

Combined doublet and linear flow

A combined doublet and linear flow is developed to illustrate the matehmatical principle that a combination of fundamental flow patterns can be used to model the circulatory flow around a cylinder. The doublet comprises a source and a sink in infinitesimal proximity (which is difficult to produce when mapping to a finite number of integer vertices) and the linear flow (U) can be mapped in any orientation by defining its u,v components accordingly. The resulting vector map is somewhat coarse, but the principle is readily apparent.

Define dimensions of array

$g := 0 .. 100$ $\quad h := 0 .. 100$

Define origin of source

$c := 46$ $\quad d := 50$

Map x and y co-ordinates onto the array

$x_g := -1 \cdot (d - g)$ $\quad y_h := -1 \cdot (c - h)$

Define strength of linear flow as a resultant of u and v

$Uu_{h,g} := 4\frac{m}{s}$ $\quad Uv_{h,g} := 0\frac{m}{s}$

Calculate the **linear** flow vector, U

$U_{h,g} := \sqrt{(Uu_{h,g})^2 + (Uv_{h,g})^2}$

Define strength of radial flow

$q := 20$ $\quad a := 0.1$

Define point **source** strength, Q

$Q := q\, m^2 s^{-1}$

Calculate radius from centre, (Origin)

$r_{h,g} := a\sqrt{(x_g)^2 + (y_h)^2}\, m$

Minimise effect of small radius at source

$$r_{h,g} := \begin{cases} r_{h,g} & \text{if } r_{h,g} > 3a\, m \\ 3 \cdot a\, m & \text{otherwise} \end{cases}$$

Calculate angle of point g,h from origin

$$\theta_{h,g} := \begin{cases} \text{if } h < c \\ \quad \begin{cases} \left(\operatorname{atan}\left(\frac{y_h}{x_g}\right) + 0\right) & \text{if } g < d \\ \left(\operatorname{atan}\left(\frac{y_h}{x_g}\right) + \pi\right) & \text{if } (g > d) \text{ if } 0 < x_g > 0 \end{cases} \\ \text{if } (h > c - 1) \\ \quad \begin{cases} \left(\operatorname{atan}\left(\frac{y_h}{x_g}\right) + \pi\right) & \text{if } g < d \\ \operatorname{atan}\left(\frac{y_h}{x_g}\right) + 0 & \text{if } ((g > d)) \text{ if } 0 < x_g > 0 \end{cases} \end{cases}$$

Bottom left

Top left

Bottom right

Top right

These equations deal with the infinite values found at the origin

$$\theta_{h,d} := \frac{\theta_{h,d+1} + \theta_{h,d-1}}{2}$$

$$\theta_{c,g} := \frac{\theta_{c+1,g} + \theta_{c-1,g}}{2}$$

Calculate horizontal component of radial flow, Ru

$$Ru_{h,g} := \begin{cases} \text{if } h < c \\ \quad \begin{cases} \frac{-1 \cdot Q}{2 \cdot \pi \cdot r_{h,g}} \cdot \cos(\theta_{h,g}) & \text{if } g < d \\ \frac{1 \cdot Q}{2 \cdot \pi \cdot r_{h,g}} \cdot \cos(\theta_{h,g}) & \text{if } g > d - 1 \end{cases} \\ \frac{1 \cdot Q}{2 \cdot \pi \cdot 1m} \cdot \cos(\theta_{h,g}) \quad \text{if } h = c \\ \text{if } h > c \\ \quad \begin{cases} \frac{-1 \cdot Q}{2 \cdot \pi \cdot r_{h,g}} \cdot \cos(\theta_{h,g}) & \text{if } g < d \\ \frac{1 \cdot Q}{2 \cdot \pi \cdot r_{h,g}} \cdot \cos(\theta_{h,g}) & \text{if } g > d - 1 \end{cases} \end{cases}$$

*

These equations deal with the infinite values found at the source origin

$$Ru_{h,d} := \frac{Ru_{h,d+1} + Ru_{h,d-1}}{2}$$

$$Ru_{c,g} := \frac{Ru_{c+1,g} + Ru_{c-1,g}}{2}$$

$$Rv_{h,g} := \begin{cases} \text{if } h < (c) \\ \quad \begin{cases} \frac{-1 \cdot Q}{2 \cdot \pi \cdot r_{h,g}} \cdot \sin(\theta_{h,g}) & \text{if } g < d \\ \frac{1 \cdot Q}{2 \cdot \pi \cdot r_{h,g}} \cdot \sin(\theta_{h,g}) & \text{if } (g > d - 1) \end{cases} \\ \text{if } h > (c) \\ \quad \begin{cases} \frac{-1 \cdot Q}{2 \cdot \pi \cdot r_{h,g}} \cdot \sin(\theta_{h,g}) & \text{if } g < d \\ \frac{1 \cdot Q}{2 \cdot \pi \cdot r_{h,g}} \cdot \sin(\theta_{h,g}) & \text{if } (g > d - 1) \end{cases} \\ \frac{2 \cdot Q}{2 \cdot \pi \cdot 2m} \quad \text{if } h = c \end{cases}$$

These equations deal with the infinite values found at the source origin

$$Rv_{c,g} := \frac{Rv_{c+1,g} + Rv_{c-1,g}}{2}$$

$$Rv_{h,d} := \frac{Rv_{h,d+1} + Rv_{h,d-1}}{2}$$

Combined flow is given by

$$Combu_{h,g} := Uu_{h,g} + Ru_{h,g}$$

$$Combv_{h,g} := Uv_{h,g} + Rv_{h,g}$$

$$Comb_{h,g} := Combu_{h,g} + i\,Combv_{h,g}$$

Combined Source and Linear flows

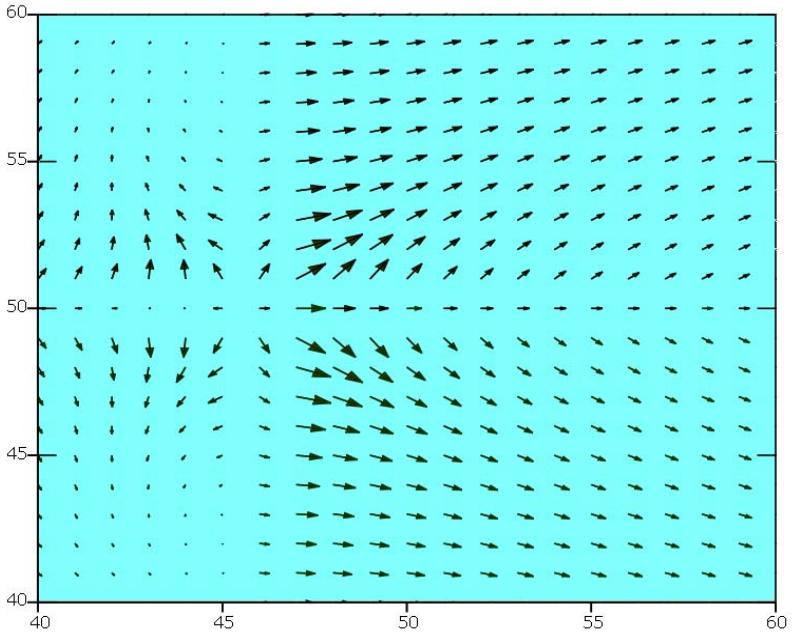

Combined Source and Uniform flow

Define strength of radial flow
(Note, negative value for a sink)

$q := -16$

Define point sink strength, Q

$Q := q\,m^2 s^{-1}$

Locate sink as close as possible to the source

$c := c + 1$

Map x and y co-ordinates onto the array

$x_g := -1 \cdot (d - g)$ $\quad y_h := -1 \cdot (c - h)$

$r_{h,g} := a\sqrt{(x_g)^2 + (y_h)^2}\,m$

Calculate horizontal component of radial flow, Ru

$$RSu_{h,g} := \begin{cases} \text{if } h < c \\ \quad \begin{cases} \frac{-1 \cdot Q}{2 \cdot \pi \cdot r_{h,g}} \cdot \cos(\theta_{h,g}) & \text{if } g < d \\ \frac{1 \cdot Q}{2 \cdot \pi \cdot r_{h,g}} \cdot \cos(\theta_{h,g}) & \text{if } g > d - 1 \end{cases} \\ \frac{1 \cdot Q}{2 \cdot \pi \cdot 1m} \cdot \cos(\theta_{h,g}) \quad \text{if } h = c \\ \text{if } h > c \\ \quad \begin{cases} \frac{-1 \cdot Q}{2 \cdot \pi \cdot r_{h,g}} \cdot \cos(\theta_{h,g}) & \text{if } g < d \\ \frac{1 \cdot Q}{2 \cdot \pi \cdot r_{h,g}} \cdot \cos(\theta_{h,g}) & \text{if } g > d - 1 \end{cases} \end{cases}$$

$$RSu_{h,d} := \frac{RSu_{h,d+1} + RSu_{h,d-1}}{2}$$

$$RSu_{c,g} := \frac{RSu_{c+1,g} + RSu_{c-1,g}}{2}$$

$$RSu_{c-1,g} := \frac{RSu_{c,g} + RSu_{c-2,g}}{2}$$

$$RSv_{h,g} := \begin{cases} \text{if } h < c \\ \quad \begin{cases} \frac{-1 \cdot Q}{2 \cdot \pi \cdot r_{h,g}} \cdot \sin(\theta_{h,g}) & \text{if } g < d \\ \frac{1 \cdot Q}{2 \cdot \pi \cdot r_{h,g}} \cdot \sin(\theta_{h,g}) & \text{if } (g > d - 1) \end{cases} \\ \text{if } (h > c) \\ \quad \begin{cases} \frac{-1 \cdot Q}{2 \cdot \pi \cdot r_{h,g}} \cdot \sin(\theta_{h,g}) & \text{if } g < d \\ \frac{1 \cdot Q}{2 \cdot \pi \cdot r_{h,g}} \cdot \sin(\theta_{h,g}) & \text{if } (g > d - 1) \end{cases} \\ \frac{10 \cdot Q}{2 \cdot \pi \cdot 1m} \quad \text{if } h = c \end{cases}$$

$$RSv_{c,g} := \frac{RSv_{c+1,g} + RSv_{c-2,g}}{2}$$

$$RSv_{c-1,g} := \frac{RSv_{c,g} + RSv_{c-2,g}}{2}$$

$$RSv_{h,d} := \frac{RSv_{h,d+1} + RSv_{h,d-1}}{2}$$

Combined doublet/linear flow is given by

$$CombuS_{h,g} := Ru_{h,g} + RSu_{h,g} + Uu_{h,g}$$

$$CombvS_{h,g} := Rv_{h,g} + RSv_{h,g} + Uv_{h,g}$$

$$CombS_{h,g} := CombuS_{h,g} + i\,CombvS_{h,g}$$

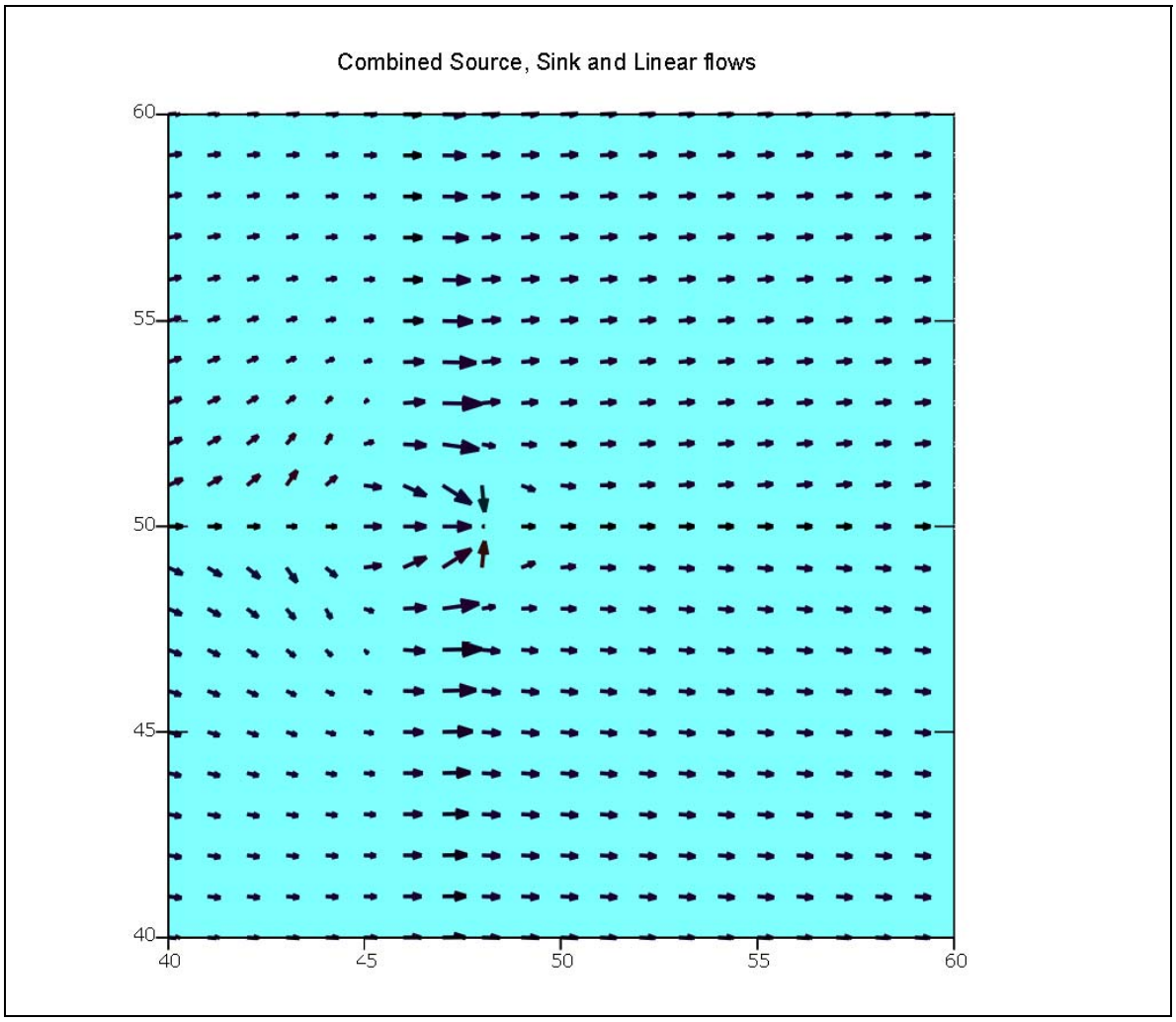

Box 1: MathCAD sheet for combined doublet and linear flow.

3.1.2 Lift forces on a rotating cylinder

Circulatory flow is an important concept in the modelling of hydrofoils and aerofoils. The flow pattern for a rotating cylinder can be represented by adding the circulatory flow due to an irrotational free vortex to the flow pattern for a stationary cylinder [**71**]. Referring to Figure 3-3

$$\psi = U\left(r - \frac{a^2}{r}\right)\sin(\theta) - \frac{\Gamma}{2\pi}\ln r \qquad \textbf{(3-1)}$$

Where Ψ is the stream function and Γ is the circulation around the cylinder.

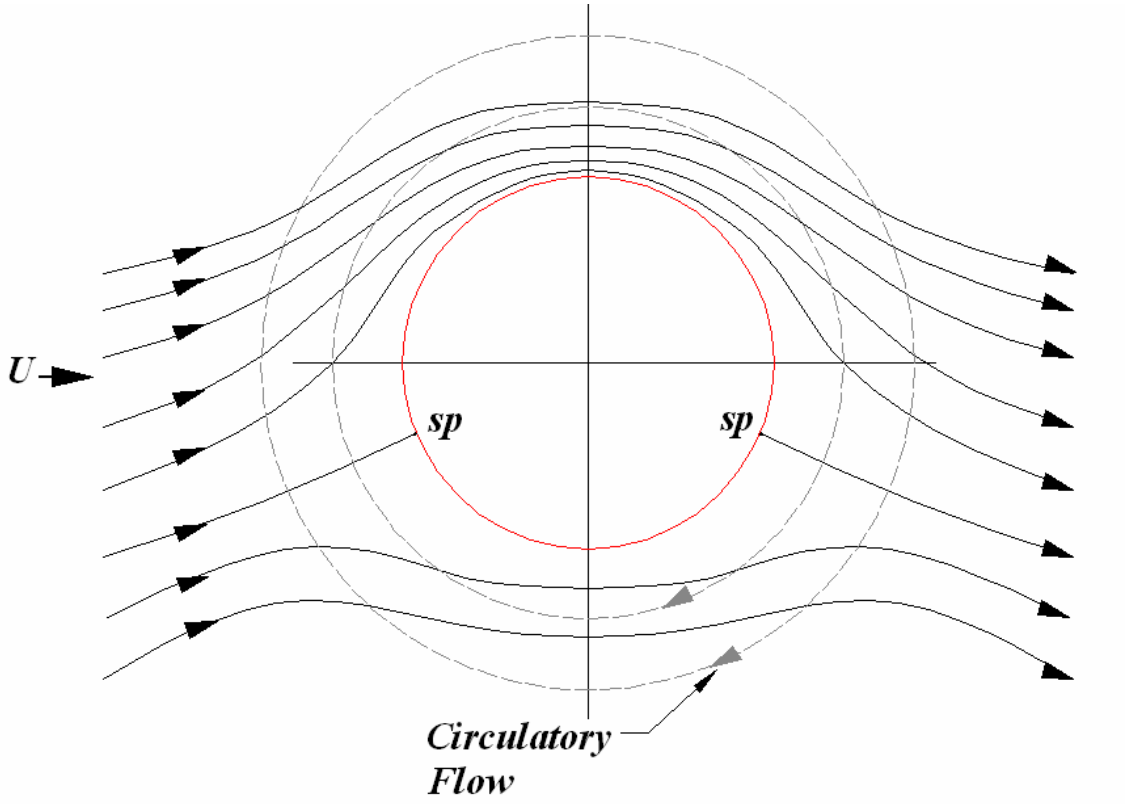

Figure 3-3: Frictionless flow around a 2-D cylinder, with circulation.

The circulatory flow in Figure 3-3 generates an increase in the velocity of the flow over the upper side of the cylinder and a decrease in flow velocity over the lower side, which, from Bernoulli's equation gives corresponding pressure variations and subsequent non-symmetrical force acting upon a symmetrical body[**72**].

$$U = \frac{\Gamma}{4\pi a} \qquad \textbf{(3-2)}$$

Equation ***(3-2)*** is known as the Biot-Savart Law, it describes the circulation (Γ) induced by a vortex line of infinite length. From Bernoulli, if the pressure at infinity is P_{inf} with a corresponding velocity of U, then

$$\frac{P - P_{inf}}{0.5\rho U^2} = 1 - \frac{U_\theta{}^2}{U^2} \qquad \textbf{(3-3)}$$

Setting $P_{inf} = 0$ for convenience and assuming a stagnation point [**73**] then,

$$\frac{P}{0.5\rho U^2} = 1 \quad \text{i.e.} \quad P = 0.5\rho U^2$$

Moving away from the stagnation point, the pressure distribution at any point on the surface is given by [**74**,

$$P = 0.5\rho U^2\left[1 - 4\sin^2\theta - \frac{4\Gamma\sin\theta}{2\pi a U} - \frac{\Gamma^2}{4\pi^2 a^2 U^2}\right] \qquad \textbf{(3-4)}$$

Inspection of Figure 3-3 suggests that, by symmetry, the resultant pressure force in the x direction (F_x) is 0, and this is confirmed by calculation in the MathCAD sheet in Box 2 on page 119.

The resulting lift force (L), in the Y direction (F_y) per unit length of cylinder is given by,

$$F_y = L = \rho U\Gamma \qquad \textbf{(3-5)}$$

This is a statement of the Kutta-Joukowski condition; the result is independent of the cross sectional shape or the dimensions of the cylinder. Its properties are of particular value in conformal transformation for 2D hydrofoil theory (p103) and it is discussed in greater depth later (p110).

Quantitative evaluation of lift on a rotating cylinder in an inviscid fluid

Define arbitrary values for components

Density of sea water, ρ $\quad \rho := 1025\frac{kg}{m^3}$

Diameter of cylinder, a $\quad a := 1m$

Velocity of flow, U $\quad U := 1\frac{m}{s}$

Strength of circulatory flow, Γ $\quad \Gamma := -2\frac{m^2}{s}$

$\theta := -\pi , -\pi + 0.01 .. \pi$

Define distribution of pressure on the cylinder surface, $p(\theta)$

$$p(\theta) := 0.5\cdot\rho\cdot U^2\cdot\left(1 - 4\cdot\sin(\theta)^2 + \frac{2\cdot\sin(\theta)\cdot\Gamma}{\pi\cdot a\cdot U} - \frac{\Gamma^2}{4\pi^2\cdot a^2\cdot U^2}\right)$$

Resultant pressure in the X direction is given by $\quad X := \int_0^{2\pi} p(\theta)\cdot a\cdot\cos(\theta)\ d\theta \quad X = -0\frac{N}{m}$

Resultant pressure in the Y direction is given by $\quad Y := \int_0^{2\pi} p(\theta)\cdot a\cdot\sin(\theta)\ d\theta \quad Y = -2050\frac{N}{m}$

Thereby confirming that the force applied per unit length of cylinder is given by, $\quad \rho\cdot U\cdot\Gamma = -2050\frac{N}{m}$

and that it is independent of the cylinder diameter, a

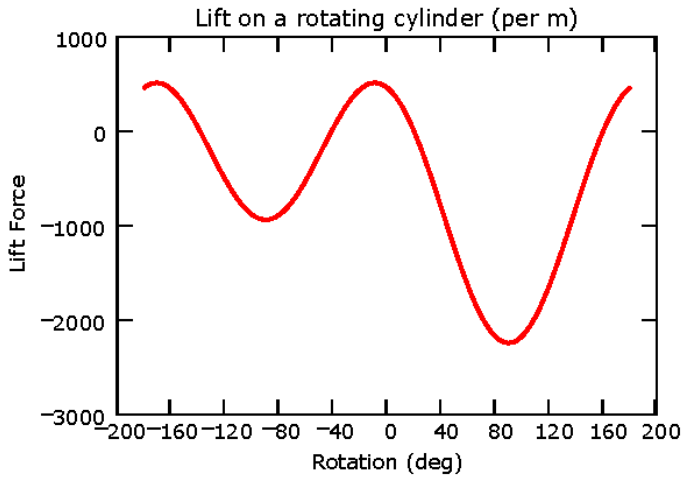

Box 2: Lift on a rotating cylinder

3.2 Development and analysis of hydrofoil profiles

Analysis of flow about a hydrofoil has been greatly advanced by FEA and similar numerical methods made accessible by the development of digital processing. However, the analytical and graphical predecessors can still be used to generate reasonable approximations of the lift and drag characteristics of hydrofoils without the comparatively substantial time commitment of a 3D numerical solution.

3.2.1 Conformal mapping from circle to hydrofoil shape

Conformal mapping is a mathematical method of extending the application of potential flow theory from flow around infinite cylinders to the visualisation of flow around an infinite hydrofoil. The essence of conformal mapping is that the post transform shape is made entirely from the pre-transform shape, including possessing the properties which were calculable at each point on the pre-transform shape; hence the calculable values from the flow around a rotating cylinder can be transferred to a two-dimensional circle and then transformed to a hydrofoil section profile.

The methodology is dependent on complex mathematics, by which process the pre-transform shape in the x-y plane is mapped onto the z-plane to become the post-transform shape. The easiest shape to manipulate for the purposes of elementary flow modelling is the circle, which, by altering the position of its centre relative to the origin, can be used to produce symmetrical hydrofoils, cambered hydrofoils and ellipses. The application of conformal mapping to hydrofoil shapes was originally developed by Joukowski and the resulting Joukowski Transformation formed the basis of much early theoretical work in hydrofoils.

Joukowski Transformation

The Joukowski transformation can be written as,

$$w = z + \frac{b^2}{z} \qquad \textbf{(3-6)}$$

Where z is the value in the source plane, w is the value in the complex mapped plane and b is the transformation factor. Since the initial function describes a circle then z must be a function of θ for $\theta = 0...2\pi.$ and the resulting complex equation of a circle is given by

$$z(\theta) = re^{i\theta} \qquad \textbf{(3-7)}$$

To map the circle co-ordinates into the shape of a symmetrical hydrofoil requires that the circle centre be shifted along the real axis by a factor of c, whilst a cambered hydrofoil requires an additional shift on the imaginary axis by a factor of k,

$$z(\theta) := \left[r \cdot e^{(i \cdot \theta)}\right] - b \cdot c + k \cdot i \qquad \textbf{(3-8)}$$

Substituting ***(3-8)*** into ***(3-6)*** gives the Joukowski mapping function

$$w(\theta) := \left[r \cdot e^{(i \cdot \theta)} - b \cdot c + k \cdot i\right] + \frac{b}{\left[r \cdot e^{(i \cdot \theta)} - b \cdot c + (k \cdot i)\right]} \qquad \textbf{(3-9)}$$

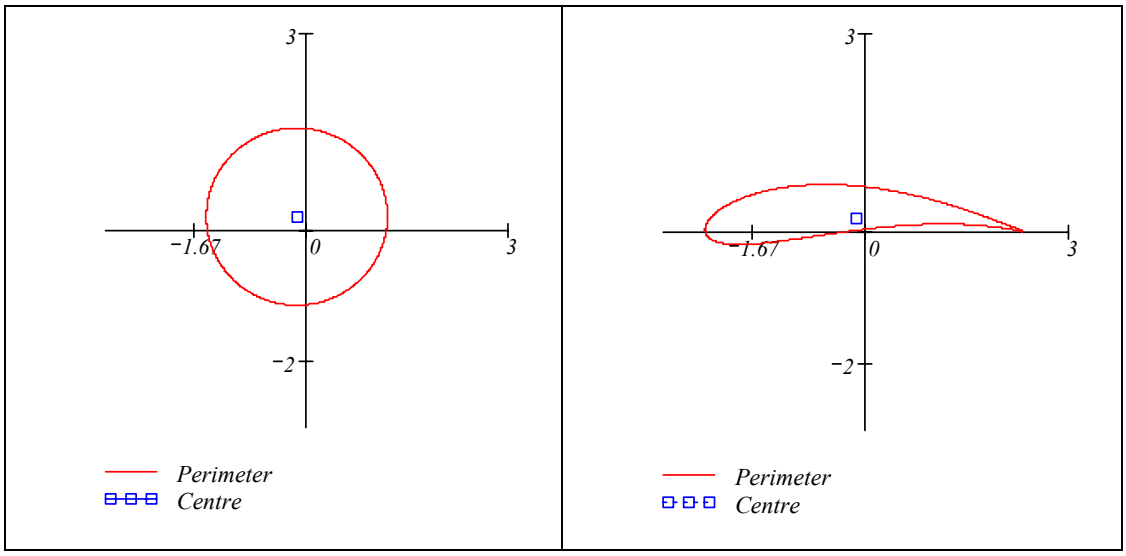

Figure 3-4: Joukowski transformation

3.2.2 Hydrofoil architecture and terminology

A hydrofoil is a lifting surface for use in water, which maximises its lift potential within the constraints of its section architecture and angle of attack,

whilst minimising its profile drag. In Figure 3-5, line *AB* is the chord length, *CD* the thickness, and the angle that the line *AB* makes with the mean free flow vector, U is the angle of attack α. *AE* is the span of the hydrofoil.

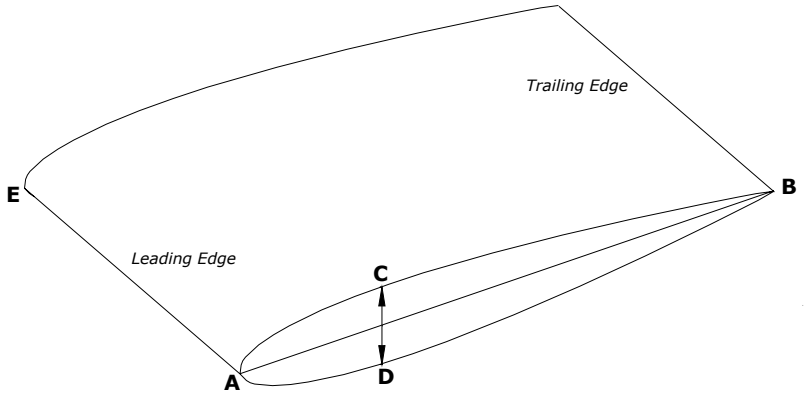

Figure 3-5: Hydrofoil nomenclature

The figure shown represents a NACA0013 section, which indicates that it was originally developed by the National Advisory Committee for Aeronautics (forerunner of NASA). The '00' shows that it is symmetrical, and '13' denotes that at its thickest point, (30% of chord length from the leading edge, *AE*) its thickness is 13% of chord. A rectangular or straight hydrofoil has its leading edge and trailing edge parallel and a constant chord length over the span, which makes for relatively easy fabrication. The planform is the shape of the hydrofoil when viewed perpendicular to the plane described by the chord line and the leading edge. The Aspect Ratio (AR) is the ratio of dimensions span^2/planform area, which equates to *AE*/*AB* for a rectangular hydrofoil, and has a considerable influence on the lift characteristics of hydrofoils where AR<3.

Given the wide variations in hydrofoil profiles, planform shapes and aspect ratios, some limiting conditions are necessary and, in terms of hydrofoil designs, this thesis is concerned only with the slow flow around a rectangular, low aspect ratio (LAR), symmetrical section hydrofoil operating at a depth (h) greater than two chord lengths (c) from the free surface (Figure 3-6). The Sea Snail uses hydrofoils of AR=0.833.

Geometrical and tabulated co-ordinates

The shape of a hydrofoil can also be drawn using equations, [***75***] and imported into design and drawing packages. For example, the following NACA 4-digit hydrofoil equation ***(3-10)*** describes the thickness distribution for a NACA0013 symmetrical hydrofoil with maximum thickness, t = 0.13, chord length, c = 1m, calculated at x = 1000 stations. a0, a1, a2, a3 and a4 are constants.

$$\frac{yt}{c} = \left(\frac{t}{c}\right)\cdot\left[\left(a0\cdot\sqrt{\frac{x}{c}}\right) - \left(a1\cdot\frac{x}{c}\right) - \left[a2\cdot\left(\frac{x}{c}\right)^2\right] + a3\cdot\left(\frac{x}{c}\right)^3\left[a4\cdot\left(\frac{x}{c}\right)^4\right]\right] \qquad \textbf{(3-10)}$$

$a0 := 1.4845 \quad a1 := 0.63 \quad a2 := 1.7580 \quad a3 := 1.4215 \quad a4 := 0.5075$

The availability of a function that describes the slope of a hydrofoil profile at individual stations about its perimeter also permits the mathematical analysis of the normal and axial pressure distribution on that perimeter (see DSP model, on page 113).

Modern hydrofoil design has moved away from description by equations and has developed computational models that can be tested and evaluated in virtual reality and the resulting profile can then be exported in tabulated format. The bi-directional Sea Snail concept requires hydrofoils that can accept a bi-directional flow and is therefore limited to symmetrical hydrofoil profiles.

3.3 Hydrodynamics of hydrofoils

The hydrodynamics of hydrofoils for fast marine vessel applications is generally concerned with high-speed (>20 m/s), surface proximate conditions, often leading to the hydrofoil itself operating in a super-cavitating condition. Other marine applications of streamlined appendages include stabiliser fins, rudders and keels.

The Sea Snail concept uses the flow velocities in tidal streams, which for present purposes can be considered to be less than 4 m/s, applied to symmetrical hydrofoils, to generate lift force that will supplement the inherent submerged weight of the structure alone. Lift is the usual term for the forces acting perpendicular to the drag forces on a body within a flow, but it should be borne in mind that the Sea Snail employs lift in a downward sense.

The forces acting on a hydrofoil that is far from any boundary can be reasonably determined with the same fluid mechanics tools that are applied to aerofoils, with appropriate modifications made to accommodate the different density and viscosity applicable to water. Important differences are that water will boil if the local vapour pressure is reduced sufficiently resulting in cavitation, and that tidal streams have a free surface.

If the hydrofoil is operating at less than two chords distance from the free surface, the generated lift may be significantly affected [**76**]. The increment of the angle of attack (α) required to achieve the same lift coefficient when proximate to the surface is plotted in Figure 3-6, [**77**].

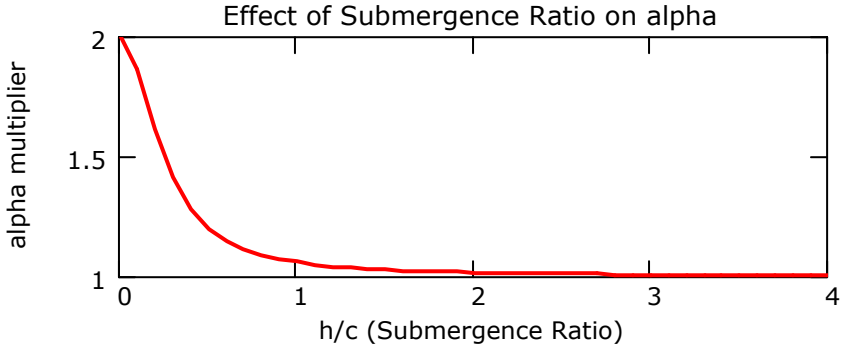

Figure 3-6: Effect of submergence ratio.

Where the submergence ratio (h/c) is given by:-

h = mean submerged depth of hydrofoil, and c = hydrofoil chord length

The definition of a fully submerged streamlined body can therefore be taken as when the body is operating at a depth which is at least two times greater than its chord.

3.3.1 Lift

Regardless of the body shape, the only mechanisms for communicating force to a body from a fluid are pressure, P and shear stress, τ. Both have units of Nm^{-2} but pressure always acts normally to the surface whilst shear acts tangentially due to the friction between the body and the fluid. The overall hydrodynamic forces R, and moments, M acting on the body can be found by integrating the distributions of P and τ over a finite lifting surface. The hydrodynamic force, R, is a resultant, and as such, can be separated into two components, lift L and drag D. The free stream velocity U is the velocity of the fluid stream ahead of the body and as yet, undisturbed by it. L is defined as operating perpendicular to U and D operates parallel to U.

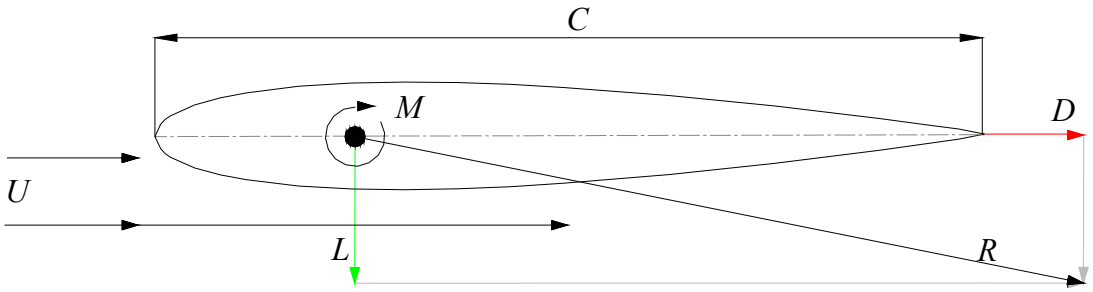

Figure 3-7: Symmetrical hydrofoil with α = 0

The chord, C, is the linear distance from the leading edge to the trailing edge of the lifting surface and, for a symmetrical hydrofoil in a neutral position, is parallel to U. For a symmetrical hydrofoil to achieve lift it must be orientated such that C is at an angle,α to U. For Figure 3-7, showing a symmetrical hydrofoil with no angle of attack, L = 0 and $M = 0$ and the only force applied

to the hydrofoil is drag, D due to the tangential shear stress, τ, therefore $R = D$.

For a symmetrical hydrofoil, as the angle of attack, α, increases (Figure 3-8), more of the free stream pressure is converted into lift force, by the creation of pressure differences above and below chord line, C, whilst the corresponding drag force increases more slowly. This effect holds until the flow over the lower surface becomes detached and lift is reduced or lost, as a consequence of α becoming too great, resulting in stall. The actual stall angle is a function of fluid properties, hydrofoil section and aspect ratio.

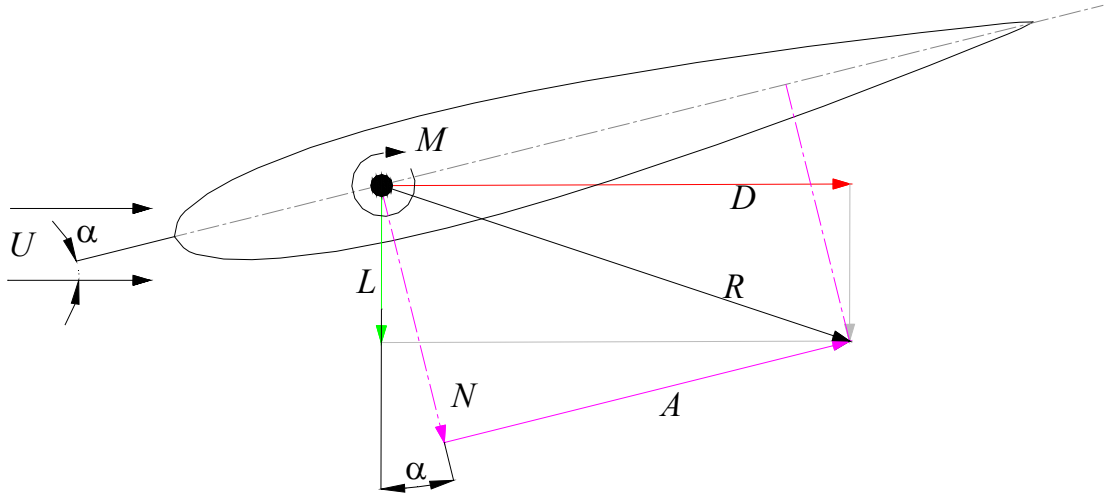

Figure 3-8: Symmetrical hydrofoil with α > 0

The resultant, R, can be represented by components parallel and normal to the chord, C, thus permitting representation of lift in terms of the angle of attack, α i.e. N = normal force acting perpendicular to chord line, C and A = axial force acting parallel to C, related by,

$$L = N\cos(\alpha) - A\sin(\alpha) \qquad \textbf{(3-11)}$$

$$D = N\sin(\alpha) + A\cos(\alpha) \qquad \textbf{(3-12)}$$

3.3.2 Circulation and the Kutta/Joukowski condition

In order to comply fully with the theoretical circulation (Γ) of flow around a hydrofoil, the flow velocity would need to be virtually infinite around the relatively sharp trailing edge found on all practical sections. Since, in reality, the flow is effectively prevented from negotiating the required turn, the position of this edge must control the circulation around the hydrofoil body as a whole. It is also apparent that the trailing edge must be the rearmost stagnation point, complimentary to the leading edge stagnation point, illustrated by the circulatory flow around a rotating cylinder model. The requirement that the circulation (Γ) has a physically real and proper value is known as the Kutta or Kutta/Joukowski condition and is fundamental to hydrofoil theory [**78**]. It depends on the combination of flow velocity, hydrofoil section and a range of values of α. If Γ is too low, then a stagnation point will appear on the low pressure side, and too high a value of Γ will generate a stagnation point on the high pressure side. For a range of values of α therefore, a particular hydrofoil will produce lift from a particular value of U. If the range of α is exceeded then that particular hydrofoil will stall under the prevailing flow conditions. It is this Kutta/Joukowski condition that dictates the suitability of a given hydrofoil section for a particular application.

Lifting Line Theory and Induced Drag

Early in the history of heavier than air flight (1911-18), Prandtl was the first to develop a practical theory for describing and predicting the properties of a finite wing, and his lifting line theory still forms the basis of modern numerical methods.

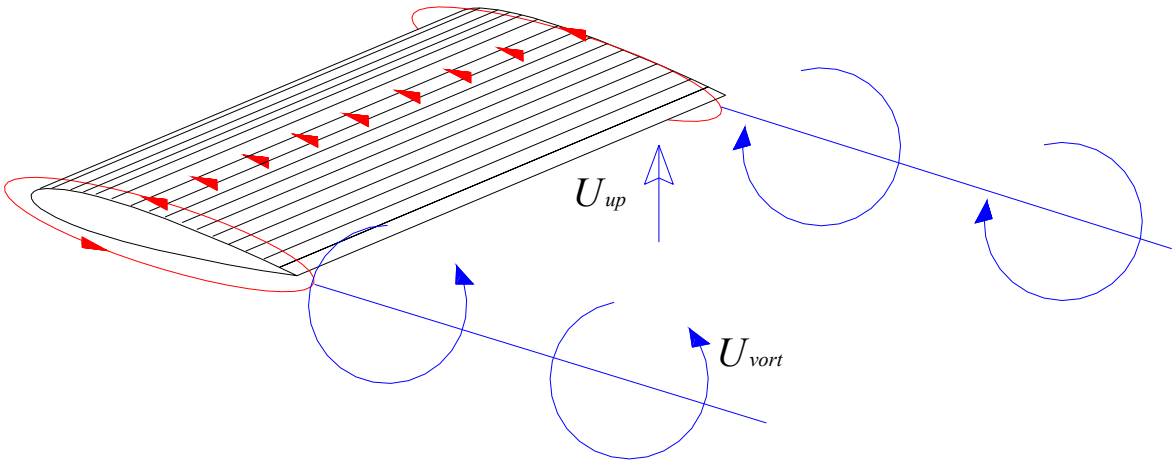

Figure 3-9: Single Horseshoe vortex pattern

It was developed for use in aircraft wings, but its application is appropriate to any lifting surface in a fluid. The visualisation consists of a bound vortex taking the place of the wing, whilst the limitation applied by Helmholtz's theorem that a vortex filament must either extend to the fluid boundary or form a closed path, is accommodated by allowing the vortex filament to extend to infinity in the wing tip free vortices.

The distinction between a bound vortex and a free vortex is that the free vortex moves with the same fluid elements in space, whilst the bound vortex is fixed to some location. The pattern resulting from the bound vortex and two free wing-tip vortices resembles a horseshoe, hence the name, horseshoe vortex.

The horseshoe vortex system allows the dissipation of the dynamic bound vortex around the finite hydrofoil, but the dissipation of the vortices creates an upwash immediately behind the hydrofoil. This upwash tends to reduce lift and increase drag by reducing the effective angle of attack [**79**]. From Prandtl's original work, [**80**], a straight vortex filament of infinite length induces an upwards velocity U_{vort} at a distance d according to,

$$U_{vort} = \frac{\Gamma}{2\pi d} \qquad \textbf{(3-13)}$$

If this vortex is a trailing vortex circulating about a hydrofoil edge, then on a transverse plane orthogonal to the hydrofoil section, the value of U_{vort} is halved. Denoting the span of the hydrofoil as l then, where the vortices meet at the centre (Figure 3-9) will be $l/2=d$ and the two vortices combine, giving

$$U_{up} = \frac{2\Gamma}{4\pi d/2} \qquad \textbf{(3-14)}$$

Substituting the Kutta-Joukowski theorem, from lift forces $L=F_Y$ ***(3-5)*** applied to a circulating cylinder,

$$L = \frac{\Gamma}{\rho l U} \qquad \textbf{(3-15)}$$

and recalling that U is the free stream velocity, then

$$U_{up} = \frac{L}{\pi l^2 U} \qquad \textbf{(3-16)}$$

If l is taken as $2d$, i.e. twice the distance from the hydrofoil centreline (where $l = d$) to the edge where $d=0$, then the resulting lift pattern, based on a NACA0013 hydrofoil of 2.5 m span, 3 m chord, flow speed of 4 m/s, C_L= 0.35, can be illustrated thus,

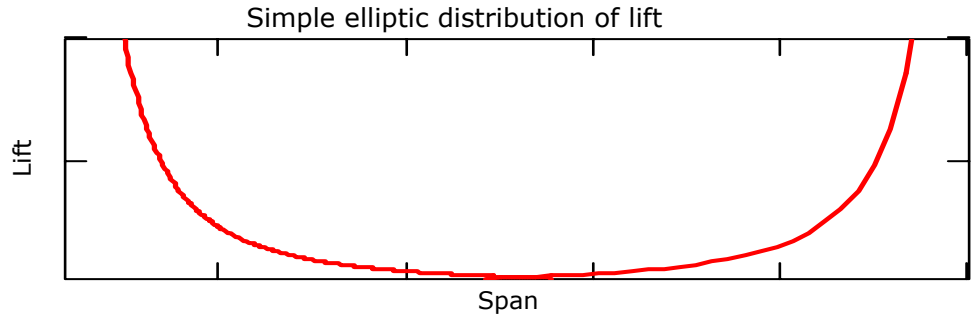

Figure 3-10: Simple elliptical lift

However, the simple elliptical lift concept from a single horseshoe vortex is not representative of real flow situations, particularly regarding the infinite upwash velocity at the hydrofoil edges. The more accurate system is to apply a large number of very small vortex filaments across the hydrofoil and integrate over the surface, with the result that $U_{up} = 2U_{vort}$.

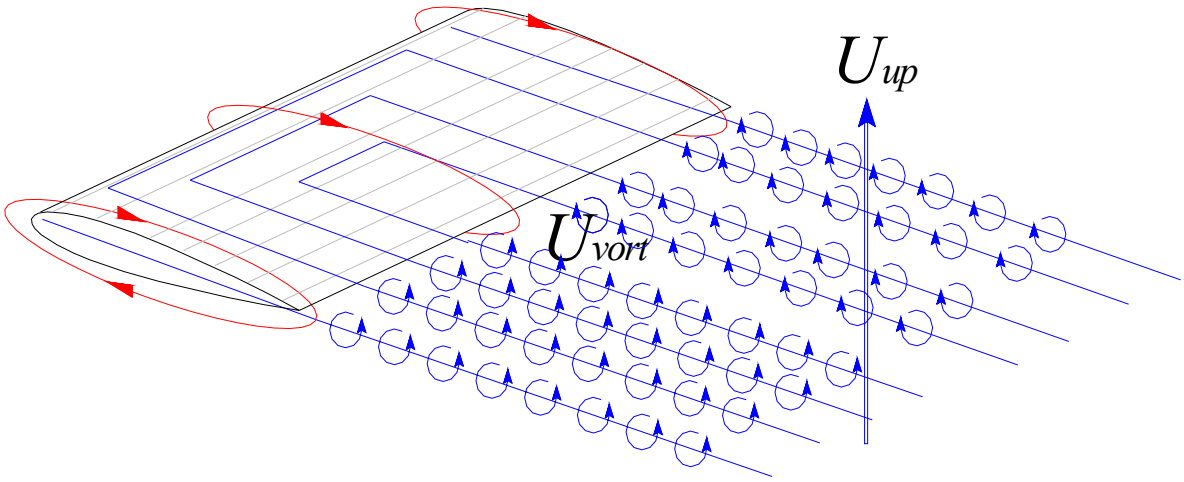

Figure 3-11: Multiple Horseshoe vortex pattern.

3.3.3 Distributed surface pressures (DSP) model

Referring to Figure 3-8, the hydrodynamic forces applied to any body are a function of pressure distribution (P) acting normally to the surface, and shear stress distribution (τ) acting tangentially to the surface. The combined effect of P and τ produces a resultant force vector (R) that can be decomposed into two orthogonal vectors, i.e. lift (perpendicular to the flow) and drag (parallel to the flow). The same resultant can be referenced to the chordline so that N represents the forces normal to the chord and A represents the component parallel to the chordline.

The hydrofoil profile can be plotted as hundreds (or thousands) of individual straight lines, the slope of which is given by differentiating ***(3-10)*** wrt x and using the sum of the surface profile angle at that point plus any additional angle of attack (α), to calculate the vector components of the incident flow U, which is assumed to progress from left to right with zero velocity component in the y direction. The DSP model utilises the fluid properties (via the Reynolds Number) to account for stress distribution from skin friction, but does not consider the onset of separation or the existence of turbulence within the flow, nor does it recognise the induced angle of attack. Since the model is based on the pressures applied to a section of an infinite hydrofoil,

it does not include end effects, thereby neglecting the effects of drag due to lift. The DSP model is developed from fundamentals and in Box 3 on the following pages and the lift and drag coefficients (C_L and C_D) applicable to the Sea Snail are found for a range of α, in a theoretical flow of 2 m/s. The particular solution required for comparison with later experimental and semi-empirical models of the Sea Snail concept is that of α = 15^{o}.

Calculation of normal pressure and shear stress distributions over the surface of an infinite length, symmetrical hydrofoil

The NACA 4 digit foil is given by the following equation.

$$\frac{yt}{c} = \left(\frac{t}{c}\right)\cdot\left[\left(a0\cdot\sqrt{\frac{x}{c}}\right) - \left(a1\cdot\frac{x}{c}\right) - \left[a2\cdot\left(\frac{x}{c}\right)^2\right] + a3\cdot\left(\frac{x}{c}\right)^3\left[a4\cdot\left(\frac{x}{c}\right)^4\right]\right]$$

where: $a0 := 1.4845$ $a1 := 0.63$ $a2 := 1.7580$ $a3 := 1.4215$ $a4 := 0.5075$

Number of stations for perimeter evaluation $i := 1 .. 1000$

Input desired thickness, t, $t := 0.13m$

Input desired chord length, m $c := 1m$

Calculate foil thickness at each station, x $x_i := 0.001m\cdot i$

$$y(x) := t\cdot\left[\left(a0\cdot\sqrt{\frac{x}{c}}\right) - \left(a1\cdot\frac{x}{c}\right) - \left[a2\cdot\left(\frac{x}{c}\right)^2\right] + a3\cdot\left(\frac{x}{c}\right)^3 - a4\cdot\left(\frac{x}{c}\right)^4\right]$$

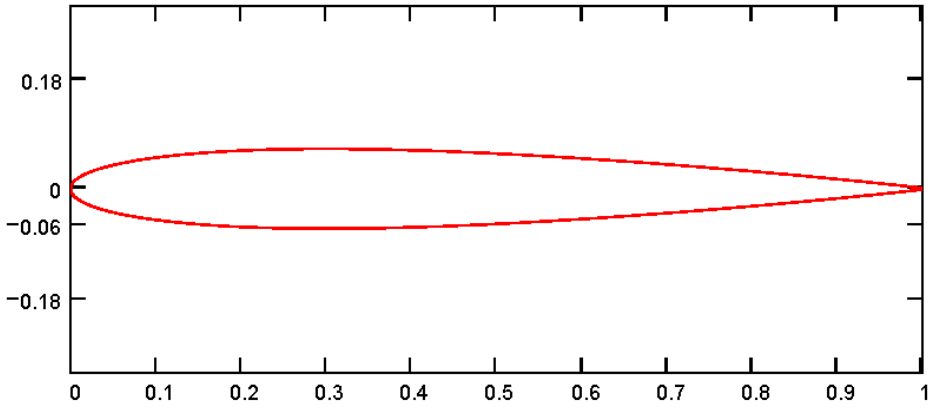

Leading edge radius is given by :- $R := c\cdot 1.1019\cdot\left(\frac{t}{c}\right)^2$ $R = 0.019\,m$

Trailing edge included angle is given by :- $te := 2\,atan\left(1.16925\frac{t}{c}\right)$ $te = 17.286\,deg$

Calculate perimeter of foil in metres $r_i := \sqrt{\left[x_i - \left(x_{i-1}\right)\right]^2 + \left(y\left(x_i\right) - y\left(x_{i-1}\right)\right)^2}$ $S_i := \sum_{i=2}^{i-1} r_i$

Perimeter of half of foil from LE to TE $Per := \sum_i r_i$ $Per = 1.022\,m$

Finding Surface Pressures.

The equation for the upper surface of the foil is given by :-

$$y(x) := t\cdot\left[\left(a0\cdot\sqrt{\frac{x}{c}}\right)-\left(a1\cdot\frac{x}{c}\right)-\left[a2\cdot\left(\frac{x}{c}\right)^2\right]+a3\cdot\left(\frac{x}{c}\right)^3-a4\cdot\left(\frac{x}{c}\right)^4\right]$$

Therefore the slope of the surface at any given station of x is given by the derivative of y(x), eg :-

$$\frac{d}{dx}t\cdot\left[\left(a0\cdot\sqrt{\frac{x}{c}}\right)-\left(a1\cdot\frac{x}{c}\right)-\left[a2\cdot\left(\frac{x}{c}\right)^2\right]+a3\cdot\left(\frac{x}{c}\right)^3-a4\cdot\left(\frac{x}{c}\right)^4\right]$$

Define the stations of x for the length of chord, c

$$x := 0.0001m, 0.0002m .. c$$

Calculate slope of surface for range of x

$$v(x) := \left[\frac{d}{dx}t\cdot\left[\left(a0\cdot\sqrt{\frac{x}{c}}\right)-\left(a1\cdot\frac{x}{c}\right)-\left[a2\cdot\left(\frac{x}{c}\right)^2\right]+a3\cdot\left(\frac{x}{c}\right)^3-a4\cdot\left(\frac{x}{c}\right)^4\right]\right]$$

Angle of attack,α

$$\alpha := \frac{\pi}{8}\cdot 0.667\cdot 1 \qquad \alpha = 15.007\,deg$$

Assuming a 1m length of infinite hydrofoil i.e. neglecting end effects

$$a := Per\cdot 1m$$

Assume tidal stream velocity, seawater density and viscosity

$$V := 2\frac{m}{s} \qquad \rho := 1024\frac{kg}{m^3} \qquad \mu := 1.14\cdot 10^{-3}\frac{kg}{m\cdot s}$$

Calculate Re No to establish surface drag

$$Re := \frac{\rho\cdot V\cdot c}{\mu} \qquad Re = 1.796\times 10^6$$

Surface coefficient of friction

$$Cf := 0.072\cdot Re^{(-0.2)}$$

Angle(θ) of line normal to the upper surface at station x is given by :-

$$\theta NU(x) := \operatorname{atan}(v(x)) - \frac{\pi}{2}$$

Angle(θ) of line normal to the lower surface at station x is given by :-

$$\theta NL(x) := \operatorname{atan}(-v(x)) + \frac{\pi}{2}$$

The flow velocity distribution on the upper surface of the hydrofoil is given by:-

$$VU(x) := \frac{V\cdot\sin\left(\frac{\theta NU(x)}{2}+\alpha\right)}{\sin\left(\frac{\theta NU(x)}{2}\right)}$$

The flow velocity distribution on the lower surface of the hydrofoil is given by:-

$$VL(x) := \frac{V\cdot\sin\left(\frac{\theta NL(x)}{2}+\alpha\right)}{\sin\left(\frac{\theta NL(x)}{2}\right)}$$

Ref: Grimson 1971, p106

From Bernouilli, the pressure distribution on the upper surface is given by:-

$$PU(x) := \left[0.5\cdot\rho\cdot V^2-(0.5)\cdot\rho\cdot(VU(x))^2\right]$$

and for the lower surface:-

$$PL(x) := \left[0.5\cdot\rho\cdot V^2-(0.5)\cdot\rho\cdot(VL(x))^2\right]$$

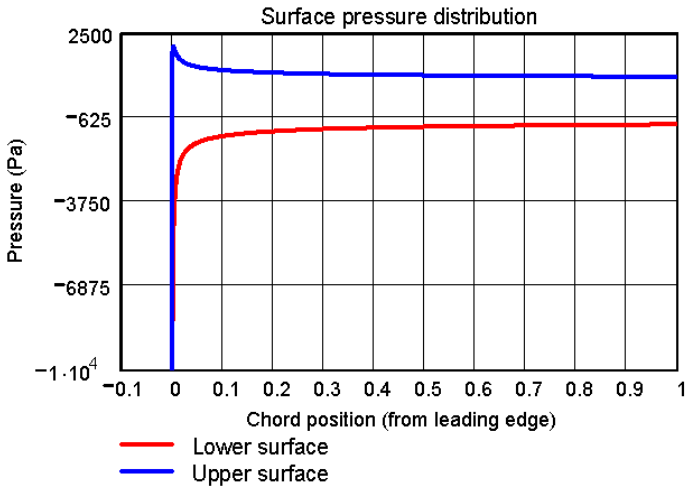

The total pressure, per m^2, acting on a 1 metre span of foil is found by integrating over the surface from the leading edge to the trailing edge, [Anderson, 2001 p19].

Finding normal pressures

The normal pressures acting on the upper surface are found from :-

$$Un := -\frac{1}{c}\left(\int_{0.0001m}^{1.022m} PU(x)\cdot\cos(\theta NU(x)) + PU(x)\cdot\sin(\theta NU(x))\,dx\right)$$

$$Un = 1.02\times 10^{3}\,Pa$$

Similarly for the lower surface,

$$Ln := \frac{1}{c}\left(\int_{0.0001m}^{1.022m} PL(x)\cdot\cos(\theta NL(x)) - PL(x)\cdot\sin(\theta NL(x))\,dx\right)$$

$$Ln = 979.153\,Pa$$

Summing normal pressures (NP) $NP := Un + Ln$ $NP = 1.999\times 10^{3}\,Pa$

Finding axial pressures

The axial pressures acting on the upper surface are found from :-

$$Ua := \frac{1}{c}\left(\int_{0.0001m}^{1.022m} -PU(x)\cdot Cf\cdot\sin(\theta NU(x)) + PU(x)\cdot\cos(\theta NU(x))\,dx\right)$$

$$Ua = 7.431\,Pa$$

Similarly for the lower surface

$$La := \frac{1}{c}\left(\int_{0.0001m}^{1.022m} PL(x)\cdot Cf\cdot\sin(\theta NL(x)) + PL(x)\cdot\cos(\theta NL(x))\,dx\right)$$

$$La = -65.125\,Pa$$

Summing axial pressures $AP := Ua + La$ $AP = -57.694\,Pa$

Finding Lift and Drag coefficients

Finding total lift pressure (L) for angle of attack (α)	$L := NP \cdot \cos(\alpha) - AP \cdot \sin(\alpha)$	$L = 1.945 \times 10^3$ Pa
Similarly for total drag pressure (D)	$D := NP \cdot \sin(\alpha) + AP \cdot \cos(\alpha)$	D = 461.833 Pa
Lift co-efficient (CL) is given by	$CL := \frac{L}{0.5 \cdot \rho \cdot V^2}$	CL = 0.95
Drag co-efficient (CD)	$CD := \frac{D}{0.5 \cdot \rho \cdot V^2}$	CD = 0.226

Box 3: Distributed surface pressures (DSP) model

The DSP model does not include end effects, which are of particular importance when using low aspect ratio hydrofoils. Mathematically, end effects are dependent on the energy dissipated by trailing vortices and are particularly difficult to model. An alternative approach to account for loss of lift and increase in drag due to end effects is now given and compared with other empirical data.

3.3.4 Lift induced drag

The pressure difference between the upper and lower surfaces also leads to the trailing vortices slipping round the hydrofoil edges, Figure 3-12, and a corresponding reduction in lift. In spite of this lift reduction, work has still been done on the fluid by the hydrofoil and energy has been dissipated in the edge vortices. The upwash combines with the freestream velocity U to produce a local relative flow [**81**], which reduces the effective angle of attack (α_{eff}) from that implied by the geometrical angle of attack α by an amount (α_{ind}). The local lift vector is therefore perpendicular to the relative flow, not the free stream vector, U and a component of drag is introduced whereby ***(3-17)***

$$D_{ind} = L \sin(\alpha_{ind})$$

D_{ind} is referred to as the induced drag and is particularly prevalent in the case of rectangular hydrofoils with low aspect ratio, because the span/chord ratio is relatively small and the edge vortices have a much greater influence than would be the case for high AR hydrofoils.

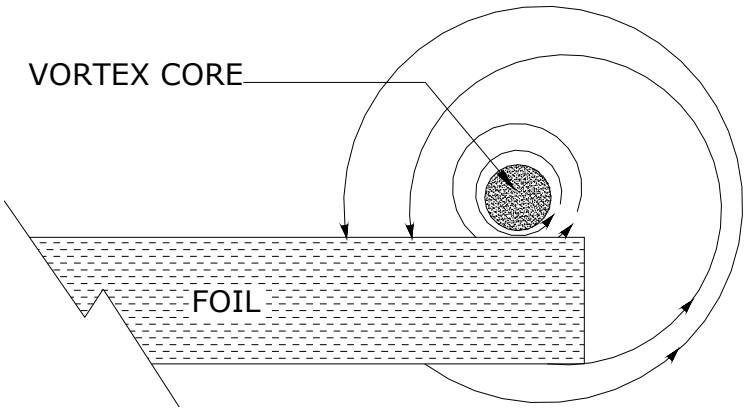

Figure 3-12: Hydrofoil edge vortex viewed chordwise.

Hoerner [**82**], suggests that, for LAR hydrofoils where AR<1, then α_{ind} = 0.5α.

As a result of the influence of the edge vortices, the lift force is spread over the entire surface of the hydrofoil and the lifting line theory is no longer applicable [**83**]. The deleterious effects can be reduced by use of appropriate endplates which minimise the ease with which the higher pressure above the hydrofoil can slip edgewise into the lower pressure zone below.

There is, however, a benefit to be realised from this edgewise flow; the feed of higher pressure flow into the lower pressure zone reduces the probability of flow separation on the low pressure side and thus reduces both the inclination to stall and the speed of transition to a stalled condition.

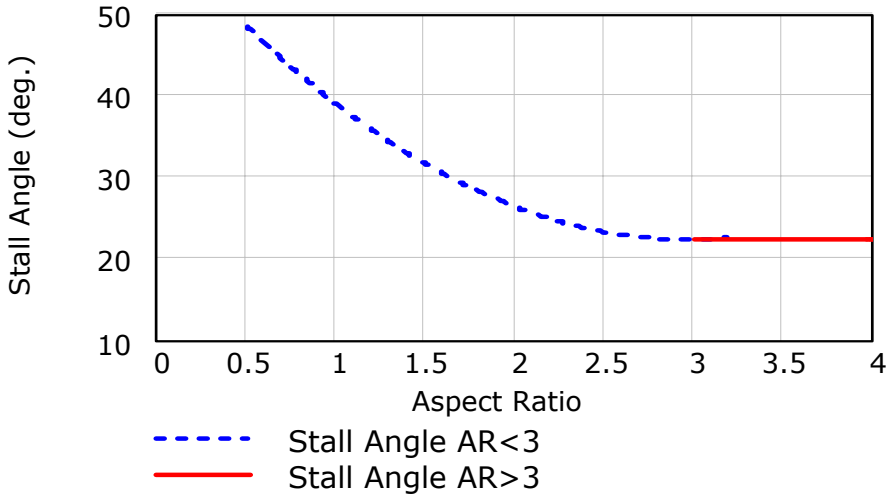

Figure 3-13: Stall angle of LAR hydrofoils

From equation ***(3-18)*** given by [**84**], the stall angle for LAR hydrofoils is plotted in Figure 3-13. The particular stall angle for the LAR hydrofoils used on the Sea Snail with AR=0.833, is given by,

$$\alpha_{stall} = 1.05 - 0.445AR + 0.075AR^2 = 0.793rads \approx 45^o \qquad \textbf{(3-18)}$$

The influence of the edgewise flow becomes more dominant as the AR decreases, thus permitting the use of larger values of α whilst actually reducing the risk of stall. LAR rectangular hydrofoils are known to be very effective, but there are difficulties in calculating the theoretical lift on a LAR hydrofoil because of the edge vortex effects.

There is a substantial body of theoretical and laboratory based data for hydrofoil performance. In reality, the hydrofoil response to a flow will also depend on the instantaneous temporal variations in the flow itself, as well as the hydrofoil characteristics, so any model will only represent the hydrofoil response under the immediate conditions prevailing.

For the reasons discussed, the edgewise flow means that the distributed surface pressures (DSP) model developed in Box 3 gives a somewhat optimistic result in terms of lift coefficients when compared with experimental recordings. For α=15^o, the DSP model for an infinite NACA0015

hydrofoil gives C_L= 0.94 which compares with C_L=0.43 from [**85**], for a square edged NACA0015 hydrofoil, where AR =1.

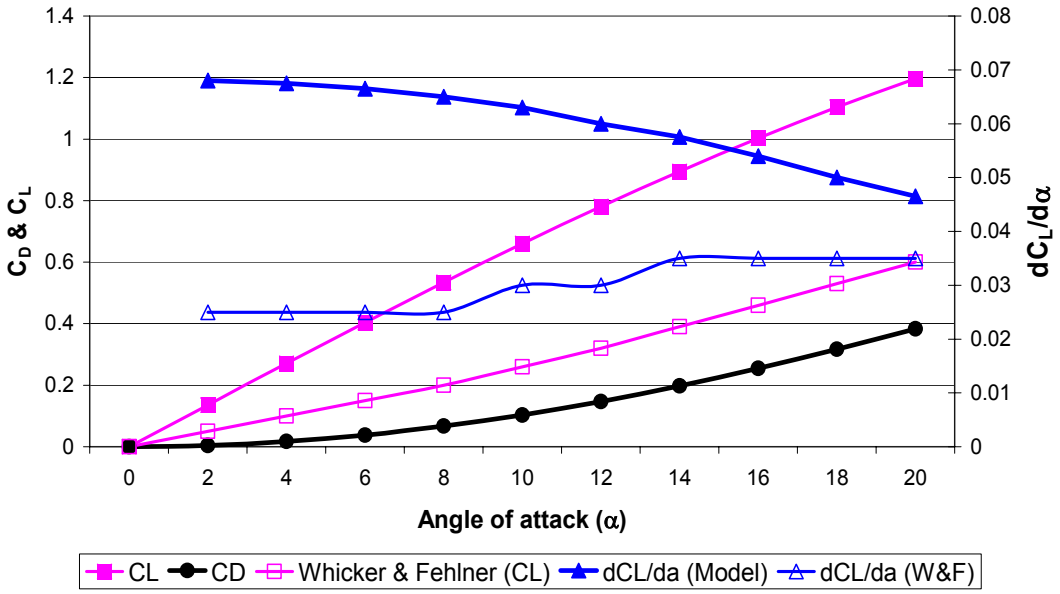

Figure 3-14: C_L from DSP model vs. Whicker & Fehlner

The ratio of dC_L to $d\alpha$ can be used as an approximate constant for a particular hydrofoil profile and thus allows a reasonable extrapolation of C_L for known values of α, or vice versa. For LAR hydrofoils it is given by [**86**], as

$$\frac{dC_L}{d\alpha} = 0.0274 * AR \qquad \textbf{(3-19)}$$

This gives for the Sea Snail hydrofoil (AR=0.833),

$$\frac{dC_L}{d\alpha} = 0.0274 * 0.8333 = 0.023 \qquad \textbf{(3-20)}$$

whereas Figure 3-14 suggests an average of approximately 0.06 for the distributed pressures model and 0.03 from the Whicker and Fehlner data. However, [**73**] shows that a finite hydrofoil is expected to have a lower ratio of dC_L to $d\alpha$ than an infinite span model.

3.3.5 Optimisation of lift

The optimisation of lift usually requires (or is a function of) minimisation of drag. Flow over a two dimensional section profile can be visualised mathematically and empirically, but three-dimensional considerations are required to develop an optimal model, particularly for LAR hydrofoils.

Boundary layer effects are managed by slots and slats on aircraft wings, either eliminating the boundary layer by suction [**87**] or re-energising it by permitting passage of high pressure flow through to the low pressure side. Similar arrangements are applicable to hydrofoils [**88**] for underwater naval applications. Both of these applications involve very high energy flows which are either due to the craft's motion relative to the free stream velocity (aircraft) or provided by high pressure pumps (underwater craft), and neither of these approaches are presently considered to be appropriate for use in the Sea Snail concept, though slots and/or slats may be an area for future investigation.

Therefore, the flow around the Sea Snail hydrofoils must be optimised to suit relatively slow flow velocities, with no external energy input to control the boundary layer. The remaining options are variation of α and the addition of endplates to the hydrofoils.

According to Hoerner, [**82**] for rectangular hydrofoils the height of the end plates (Eh) can be related to α and the chord length, c, by

$$Eh = 0.5\alpha c \qquad \textbf{(3-21)}$$

Application of ***(3-21)*** to the NACA0013 section hydrofoil results in a model scale endplate height of 56 mm. The addition of endplates is expected to culminate in an increase of the effective AR which Hoerner suggests is given by,

$$\Delta AR = 2(AR) * \alpha_{ind} * \frac{C}{SPAN} = AR\alpha\frac{C}{SPAN} \qquad \textbf{(3-22)}$$

Since ΔAR is a function of α, which is given by ***(3-18)*** as valid up to around 45°, then the effective AR can be found for any operational value of α up to the point of stall.

For the Sea Snail rectangular hydrofoil geometry, where $AR = \frac{C}{SPAN}$, with α = 15° (0.262 radians), ***(3-22)*** equates to

$$\Delta AR = 0.833 * 0.262 * 3 / 2.5 = 0.262$$

thereby implying an effective AR of,

$$0.833 + 0.262 = 1.095$$

and the C_L for this hydrofoil, with α=15°, is given by

$$C_L = 0.5\pi \sin(\alpha)\cos(\alpha)(AR + \alpha) = 0.53 \qquad \textbf{(3-23)}$$

and thereby demonstrates the disparity between the infinite hydrofoil model and the LAR model.

The lift coefficient will also affect the drag coefficient, particularly as has been shown, in the case of LAR hydrofoils. The induced drag on an LAR hydrofoil can be modelled as [**89**],

$$C_D ind = C_L\left(\frac{\alpha}{2}\right) \qquad \textbf{(3-24)}$$

giving an additional induced drag for the Sea Snail hydrofoils where α = 15° and C_L=0.53, of 0.06. The variation of C_L and $C_D ind$ with the effective AR is shown in Figure 3-15.

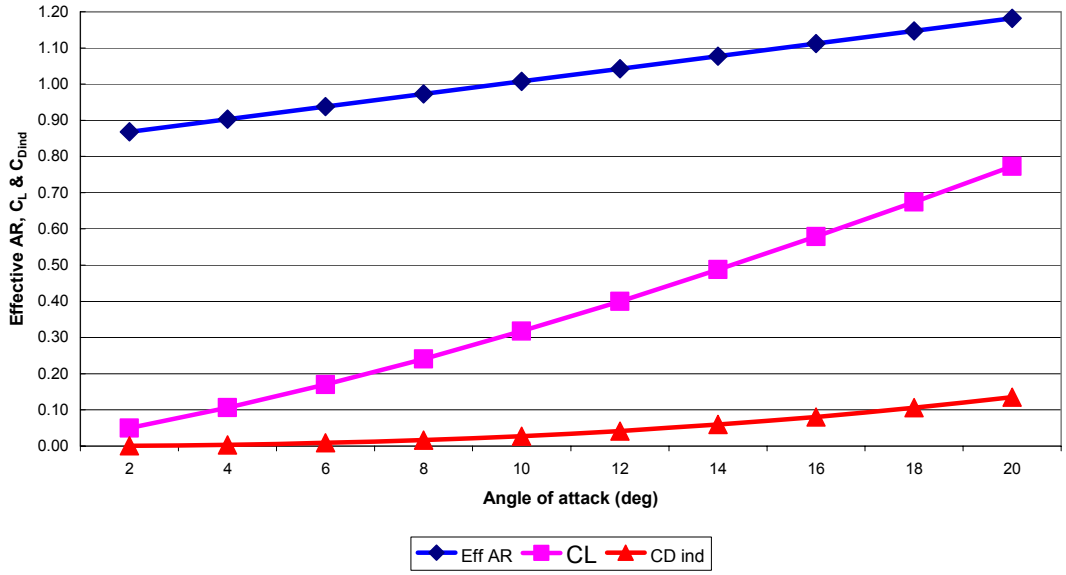

Figure 3-15: Effective AR, C_L, Induced Drag Coefficient ($C_D$ind)

3.3.6 Drag

Drag is the undesirable, but inevitable component of the relative motion of a body and a fluid, and its minimisation is (usually) one of the major objectives of any hydrodynamic engineering project. A body, moving relative to a fluid will experience a resistive force that is proportional to the square of the relative velocity, the area presented by the body perpendicular to the freestream vector and the density of the fluid(s) in the space occupied by the body.

The fluid motion will be disturbed by the presence of the body, and the disturbance is left as a trailing wake of ever decreasing turbulent eddies, redirected flow, organised vortices or, in the case of free surface interactions, as wave energy. The energy dissipated by the disturbance is equal to the energy used in maintaining the body stationary relative to the flow, by resisting drag and/or generating lift, and is eventually distributed as low grade heat.

The disturbance of the fluid, which is taken to be seawater, is imparted by a number of different mechanisms, i.e. surface or skin drag which depends on the development and characteristics of the boundary layer; form (or pressure) drag, which depends on the shape that an object presents

perpendicular to the freestream vector; interference drag, whereby the proximity of multiple bodies influences the flow relative to both, and drag-due-to-lift, which was discussed under 3.3.1. These mechanisms, though different in their individual actions are not independent in origin, for instance, the turbulent eddies that contribute much to the pressure drag, are triggered by the boundary layer separation that occurs due to an adverse pressure gradient on the surface of the body.

Surface drag (Skin Friction)

The flow immediately adjacent to the surface of the body is predominantly influenced by the characteristics of the boundary layer. The energy dissipated at the body/fluid interface is a function of the surface finish of the body and the fluid's viscosity.

The boundary layer is sensitive to any pressure gradient imposed on the flow, in the direction of flow. For example, in Figure 3-16, the pressure at A decreases in the direction of flow i.e. $\delta p/\delta X < 0$, leading to a favourable pressure gradient; the pressure at B is constant, i.e. $\delta p/\delta X = 0$, and the pressure at C and D increases with direction of flow, i.e. $\delta p/\delta X > 0$ giving an adverse pressure gradient [**90**]. Following a fluid particle through the flow from A to D illustrates the principle.

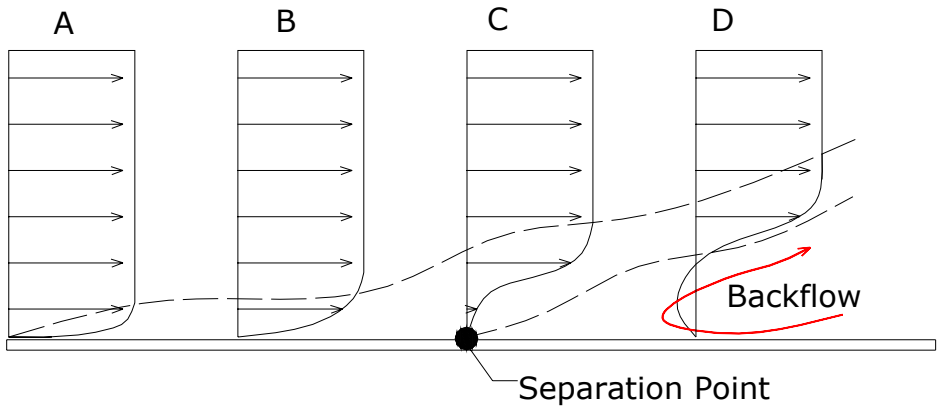

Figure 3-16: Effects of pressure gradient on boundary layer.

The presence of the surface generates a net retarding force on the particle, which is tending to decrease its momentum at A, but the pressure of flow behind pushes the particle onward through region B where it encounters the adverse pressure gradient at C. The particle must then either separate from the boundary and follow the line of constant pressure away from the surface (form a wake), or come to a halt where it will become instrumental in deflecting other particles away from the surface.

The fluid downstream (at D) of the separation point (at C), is made up of low energy particles that are forced upstream by the pressure gradient downstream. This process continues until either the flow has completed its association with the body and moved on, or a discontinuity in the body surface alters the pressure gradient again. Since a turbulent boundary layer carries more energy than a laminar boundary layer, it is better able to resist the separation forces applied by an adverse pressure gradient. This is the explanation for the drag on a circular cylinder, discussed under 3.1.1, suddenly changing at Re = 5 x 10^5. In the region of the critical Reynolds number, the drag coefficient of a sphere in turbulent flow is approximately 0.2 of that for laminar flow.

Form drag (Pressure drag)

The discontinuity that exists at the trailing edge of a streamlined body will also produce the flow reversal effect discussed; the better the streamlining, the smaller the flow reversal, but there will always be a flow reversal. The backflow in either case leads to the creation of a vortex and, for a trailing edge at relatively slow flow velocities, the vortices will be produced from alternate sides of the body, generating a vortex street. As the velocity increases, a highly confused turbulent wake is generated which dissipates energy in the form of large scale, pressure-reducing eddies. Thus, the body is affected by the presence of a volume at its trailing edge that is at a lower pressure than the flow on its leading edge, and the body has a tendency to move into the volume of lower pressure. From this, it follows that the greater

the energy dissipated by turbulence behind a body, the greater the pressure difference and the higher the drag force experienced.

The objective of streamlining is to minimise the adverse pressure gradient that occurs behind the point of maximum thickness of a body and thus delay the point of separation by minimising the flow reversal opportunities.

Interference drag

The implications of form drag continue into interference drag. The vortices leaving the surface of one structure will continue for a considerable distance downstream and, since the vortices are volumes of variable velocity and pressure, they will influence the pressure gradient within the boundary layer of any downstream surface. Anyone who has travelled by air through turbulence will be well aware of the shock loading that can be created by metre length scale, coherent turbulence. Interference drag for an array of hydrofoils will be defined by the relative spatial positions of the hydrofoils and the level of turbulence induced by the leading hydrofoil, mainly due to the characteristics of the vortex shedding. The DSP model gives a C_D of 0.22 for the Sea Snail hydrofoils. With the additional C_{Dind} given by ***(3-24)*** this suggests a value of C_D=0.28 for a NACA0013 hydrofoil with AR=0.833 and α = 15^o. For the Sea Snail hydrofoil array, the additional effects of interference drag are clearly illustrated in Chapter 4 where the results of the tow tank testing are discussed.

Minimisation of drag

The minimisation of drag is therefore concerned primarily with the shape of a body as presented to the mean flow vector, and to a lesser extent with the surface finish of a body. Much of the work required to maximise the lift of a hydrofoil will also reduce its drag.

Hydrofoils have been developed with the thickest section closer to the mid-chord area in order to push the area of adverse pressure gradient toward the trailing edge, thereby also shifting the point of separation closer to the trailing edge and reducing the linear distance for backflow to form. Surface

finish (such as golf ball dimples) may have an influence in the management of the boundary layer, though in real marine flows, the boundary layer is almost certainly fully turbulent anyway.

3.3.7 Body forces

In addition to the hydrodynamic forces applied to the surfaces and structure of any marine device by the fluid flow, there are additional forces acting due to gravity and buoyancy. In a fluid, gravity and buoyancy will act on the entire structure in a manner proportional to the mass of the structure and the volume of fluid displaced by the structure. Any submerged structure will displace a volume of fluid equivalent to its own volume and the overall buoyancy force, which is the sum of the buoyancy forces experienced by individual components, acts at the centroid of the submerged structure. The buoyancy forces applicable to the centroid of the Sea Snail structure are discussed under 4.2.1 .

3.4 Chapter summary

The fundamental concepts of flow around a hydrofoil have been developed from the flow patterns associated with cylinders, both stationary and rotating, and the lift generated by a rotating cylinder in an inviscid fluid is shown to be independent of the shape around which it is mapped. Subsequently, the pressure variation around a 2D circle is mapped onto a hydrofoil shape using complex numbers, thus demonstrating the Kutta-Joukowski condition. The dependence of the Kutta Joukowski condition on a theoretical circulatory flow is shown via a numerical MathCAD model which employs the combination of a doublet flow and a linear flow.

Creation of a hydrofoil profile from a parameterised equation allows the straightforward modelling of the distribution of normal and axial dynamic pressures acting on the hydrofoil perimeter. The Distributed Surface Pressures (DSP) model can be applied to any hydrofoil (or aerofoil) whose profile can be described by an equation. The concept of the lifting line was explained and the dissipation of energy through trailing vortices has been demonstrated to be the cause of the lift-induced drag that affects the flow over low aspect ratio (LAR) hydrofoils. The importance of the boundary layer was discussed and its influence on both skin drag and pressure drag resulting in a turbulent wake explained.

All of these concepts and models are subsequently used in designing experiments to demonstrate the viability of the Sea Snail proposal as a self-securing device. After completing the description of the design of the Sea Snail, Chapter 4 describes the application of hydrodynamic theory to experimental models at $1/7^{th}$ scale, both in a stream and in a laboratory tow tank.

Chapter 4 Experimental Modelling of the Sea Snail

4.0 Chapter introduction

This chapter discusses the early conceptual and mathematical modelling of the Sea Snail. The original project was a substantial device, 15 m long, 7.6 m high, 10 m wide and weighing approximately 20 tonnes, it was always intended that it would be trialled at sea.

The conceptual and mathematical model of the Sea Snail is developed and its response to the forces applied by a flow of water is shown. The basic functions were outlined in 1.1 and, though the resulting structure failed to provide recorded data from its at-sea trials, the following design analysis explains the reasoning for the layout of the hydrofoil array and therefore has implications for the subsequent experimental work.

Two model experiments were conducted using the hydrofoils and their array pattern at $1/7^{th}$ scale to determine the lift and drag forces applicable to the hydrofoils and to assess the potential effects of flow interaction between them. The first experiment used an array of hydrofoils positioned in a small river, with α ranging from 0^o to 16^o, and measured the lift and drag forces acting on the full array of 6 hydrofoils in a flow velocity of 0.7 m/s. The second experiment was carried out in a towing tank environment and used one set of 3 hydrofoils. Each individual hydrofoil was instrumented for lift and drag forces with α=15^o and the assembly was towed at a range of velocities from 1 m/s to 3 m/s. The resulting data from both experiments is statistically analysed and described in terms of standardised normal distribution about an estimated mean for each record, ensemble of records, and for the full set of data.

The challenges and applications of scaling and physical similarity are discussed in the context of dimensionless coefficients and the method proposed by Froude is used to extrapolate the experimental data to full scale.

4.1 Detailed design

Following on from the conceptual design given in section 1.5 the concept became increasingly refined and, by the third stage concept, the hydrofoil dimensions and their internal positioning systems were being finalised and the support structure had evolved into a set of formed tubes with bolted joints, capable of being transported in kit form on a standard articulated lorry trailer.

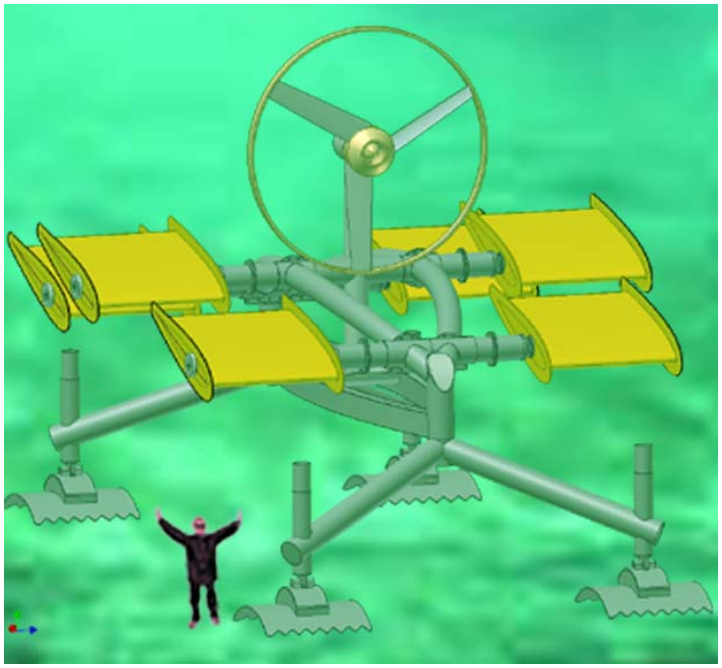

Figure 4-1: Sea Snail support frame, concept 3

Discussions with the fabricators indicated that the formed tubing would present difficulties in accurate alignment and cutting, which would require the design and manufacture of jigs. The extra cost and time made this option untenable, but the essential form and function of the structure was now clear.

The distribution of the hydrofoils was considered to be acceptable, though not necessarily optimal, and the kit format was the most appropriate methodology for fabrication, transportation and assembly. The difficulties of the formed tube approach could be overcome by using a pin-jointed frame made up of straight tubulars with clevises at each end, locating into tangs

formed as part of the end and intermediate assemblies, as shown in Figure 4-2.

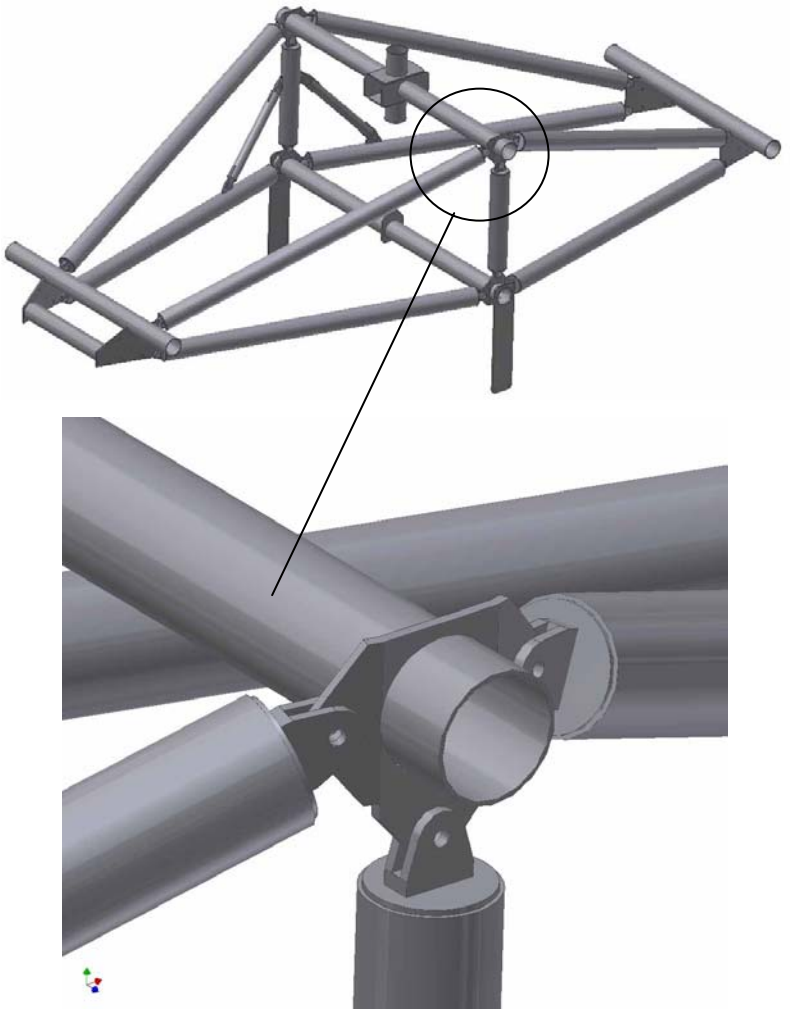

Figure 4-2: Detail of pin-jointed structure.

Thus the fourth development of the concept (Figure 4-3) is, with minor detailing differences, the as-built device, shown in Figure 4-4 to Figure 4-7. Significant structure dimensions are given and all drawings are on the attached CD for detailed dimensions.

Figure 4-3: Sea Snail assembly, side view

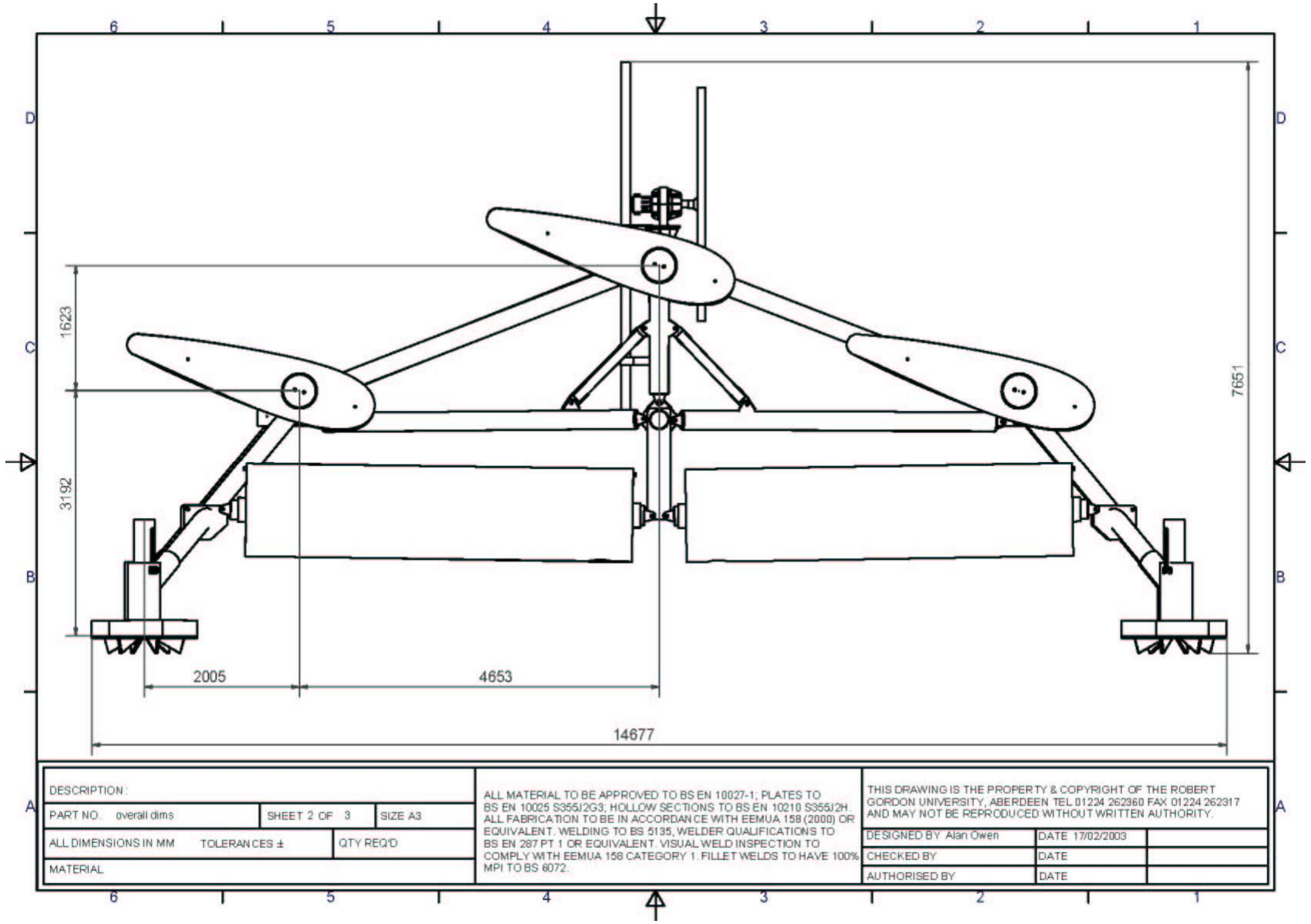

Figure 4-4: Sea Snail assembly, dimensioned side view.

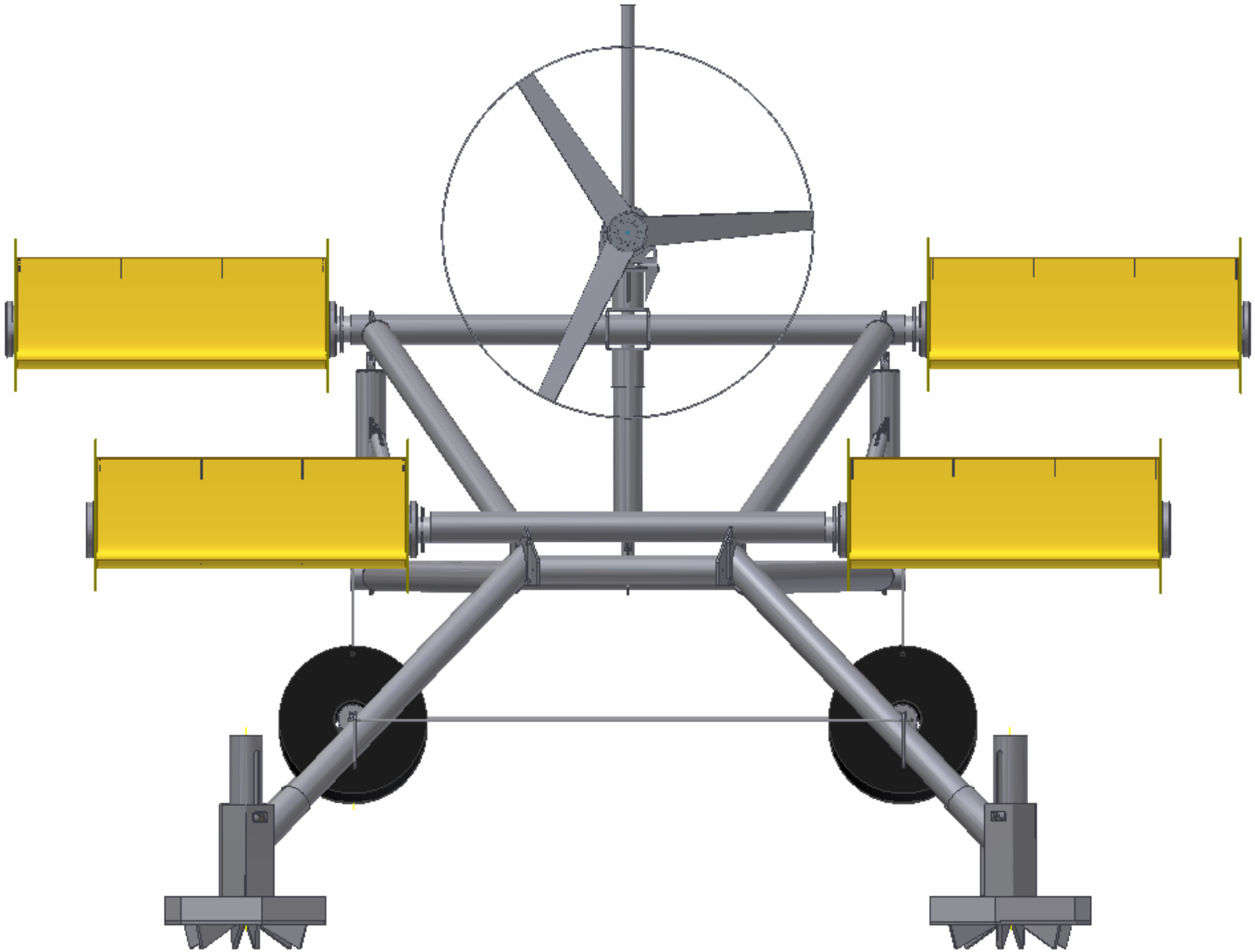

Figure 4-5: sea Snail assembly, front view

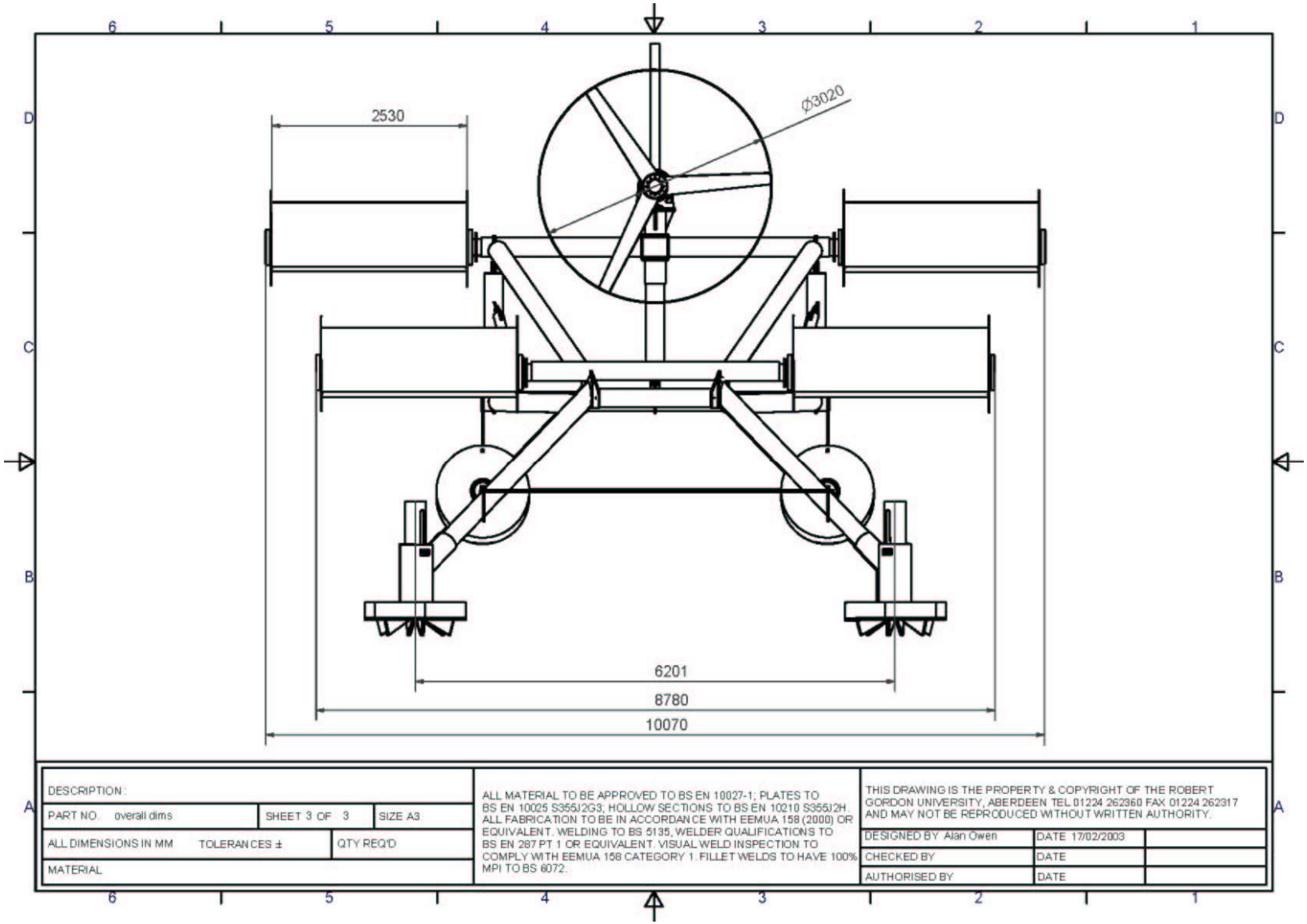

Figure 4-6: Sea Snail assembly, dimensioned front view

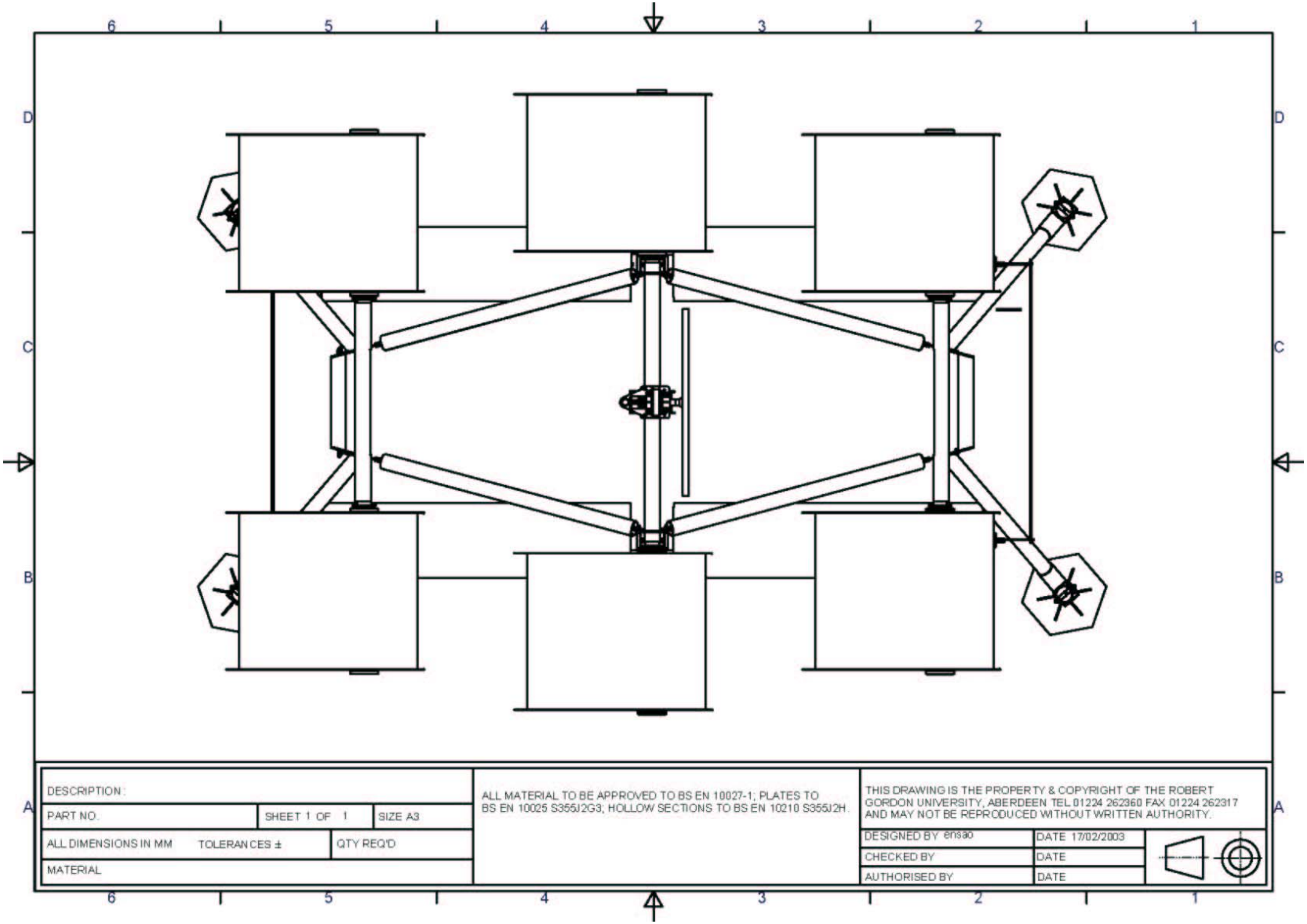

Figure 4-7: Sea Snail assembly, Plan View

4.2 Operational mathematical model

If a steady, uniform, bidirectional, fully turbulent flow is assumed, the deployed Sea Snail can be simply modelled as two separate entities; as a set of hydrofoils and as a tubular steel frame with a turbine centrally mounted.

4.2.1 Overturning and restorative moments

Designed for a bidirectional flow, the Sea Snail responds to reversals in the tidal stream flow by allowing its lifting surfaces to be repositioned by the flow itself. When no flow is present, the lifting surfaces, being positively buoyant align themselves vertically and, as the tidal stream flow increases, sufficient force is generated to press the lifting surfaces down onto their stops, (Figure 4-8) and apply a downward pressure to the structure.

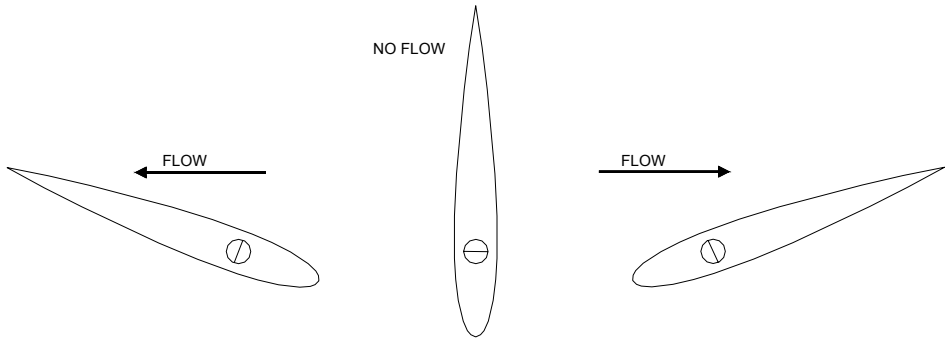

Figure 4-8: Hydrofoil response to changes in flow direction

The serrated steel feet are then pushed into the seabed material (usually bedrock in vigorous streams) and the Sea Snail is thus prevented from moving laterally. The flow of the tidal stream also applies an overturning moment to the structure and its turbine about the rearmost feet. The calculation of the overturning moment is carried out as follows:-

The frontal view (Figure 4-9) is sliced horizontally such that each slice represents 0.3 m on the full size device. With the exception of the hydrofoils and the turbine, any components viewed through this slice are given a drag coefficient [**91**] based on their section as presented to the flow, e.g. for cylindrical tubes denoted by (C), C_D =0.35; for cylinders end on (Ce) with

length/diameter = 5, C_D = 0.8; and for square sections perpendicular to the flow, C_D = 2.1. Denoting the distance of the slice above the seabed by 0.3 m x Z, the total overturning moment (M_F) is then calculated using ***(4-1)***.

$$M_F = \sum_{Z=1}^{25} 0.5 C_D \rho A U^2 Z \qquad \textbf{(4-1)}$$

The overall C_D for the structure (excluding hydrofoils) is found from the C_D of the individual areas to be 0.54. Application of symmetry permits the frontal area of the Sea Snail to be calculated for half of the structure and then doubled. Importing of the drawing at full scale into a CAD programme and using the calculate area tool gives a reasonable level of accuracy.

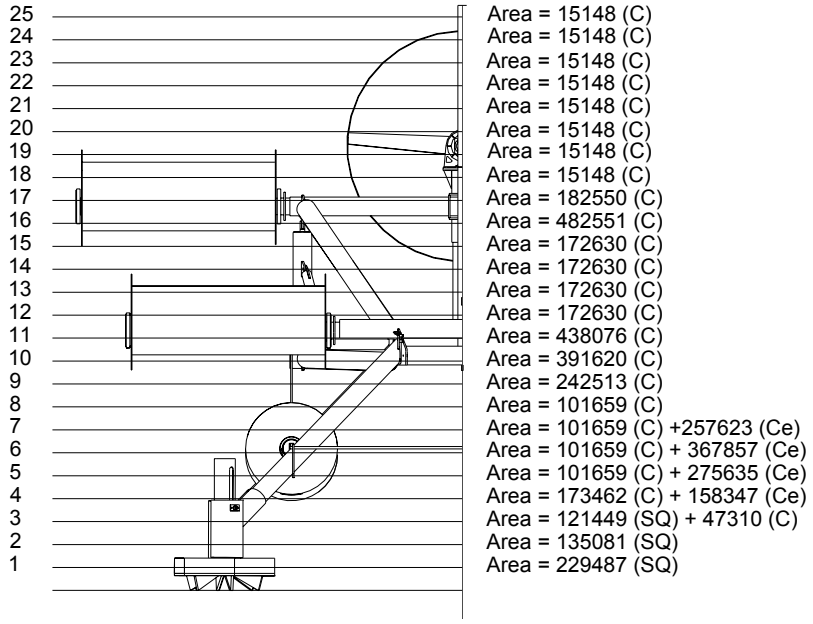

Figure 4-9: Areas (mm^2) of structure presented to flow.

Summing the moments for all the components in each slice (including the components that are replicated at the rear of the structure, e.g. legs), plus the hydrofoil drag, gives a total overturning moment for the structure. The product of the net mass of the individual component assemblies (after buoyancy is considered) and the lateral distance from the rear feet to the centre of mass of that assembly, gives the inherent device restoring moment, without lift augmentation from the hydrofoils, shown in Table 4-1.

Table 4-1: Inherent restorative moments.

Inherent device net restorative moments due to mass, (Nm)					
Assembly	qty	distance from rear feet (m)	mass (kg)	buoyancy (kg)	moment (Nm)
Upper cross member	1	6.7	407	30	24779.08
Lower cross member	1	6.7	419	30	25567.8
End frame	1	11.3	318	30	31925.66
End frame	1	2	318	30	5650.56
Hydrofoil assembly	2	11.3	1013	1527	-113957
Hydrofoil assembly	2	6.7	1013	1527	-67567.4
Hydrofoil assembly	2	2	1013	1527	-20169.4
Foot assembly	2	13.34	1325	83.5	324938.8
Leg assembly	2	12.38	462	30	104930.9
Leg assembly	2	0.97	462	30	8221.565
Side tube	2	6.85	270	30	32255.28
Side tube	2	4.3	270	30	20247.84
Centre strut	2	6.7	81	5	9990.504
Lower strut	2	9.52	214	30	34367.96
Lower strut	2	4.36	214	30	15739.95
Upper strut	2	9	228	30	34962.84
Upper strut	2	4.3	228	30	16704.47
Turbine assembly	1	6.7	767	20	49098.07
Buoyancy tank	2	9.5	137	30	19943.73
Buoyancy tank	2	3.84	137	30	8061.466
Total	n/a	n/a	16363	10079	565692.9

The positional integrity of the Sea Snail depends on the resultant sum M_R of the overturning moments due to flow M_F, the inherent restorative moments due to mass M_I, and the restorative moments due to lift M_H derived from the hydrofoils.

$$M_R = \sum (M_I + M_H - M_F) \qquad \textbf{(4-2)}$$

The value of M_F and M_I can be calculated from knowledge of the structure in terms of its dimensions, mass and surface area perpendicular to the flow. However, knowledge of the lift and drag forces generated by the hydrofoils is required to compute the value of M_H and consequently the net moments applicable to the complete structure. The overturning moment due to the drag on the hydrofoils is a function of α as well as flow speed, U, and must therefore be calculated discretely from the main structure and summed with the frame moments.

The velocity profile of the tidal stream is assumed to correlate with a modification of the 1/7th Power Law ***(4-3)*** proposed by Prandtl, [**92**], though a variety of other velocity profile approximations are applicable, such as the 1/10th power law or the half-depth power law in [**93**].

$$U(z) = U\left(\frac{z}{h}\right)^{\frac{1}{7}} \qquad \textbf{(4-3)}$$

Where: z indicates height from seabed (m), U is the freestream surface velocity (m/s) and h is the overall depth (m). Lift force is calculated using ***(4-4)*** and the value of C_L for the LAR hydrofoils is calculated from ***(3-23)*** in Chapter 3

$$F_{Down} = 0.5 C_L \rho A U^2 \qquad \textbf{(4-4)}$$

The initial model used to estimate the slip forces and overturning moments incorporates the reduction in weight of the structure as the moments are applied and assumes the coefficient of Coulomb friction between the feet and the seabed to be 1.

The mathematical solution is approached using the theoretical Distributed Surface Pressures (DSP) method and the Low-Aspect-Ratio (LAR) hydrofoils empirical method, both developed in Chapter 3. For both models, taking the unit lift force generated by the lead hydrofoils as 1, then the lift force on succeeding hydrofoils is assumed to be 0.8 for the central hydrofoils and 0.56 for the trailing hydrofoils.

4.2.2 The Distributed Surface Pressures model

The DSP model is developed and discussed in Chapter 3 and the model is utilised here to illustrate the theoretical infinite-span hydrofoil behaviour for α=15°. From Box 3 on p118, the lift and drag coefficients are given by the DSP model as 0.95 and 0.23 respectively, and substitution of these into the calculations gives the overturning and restorative moments as in Figure 4-10.

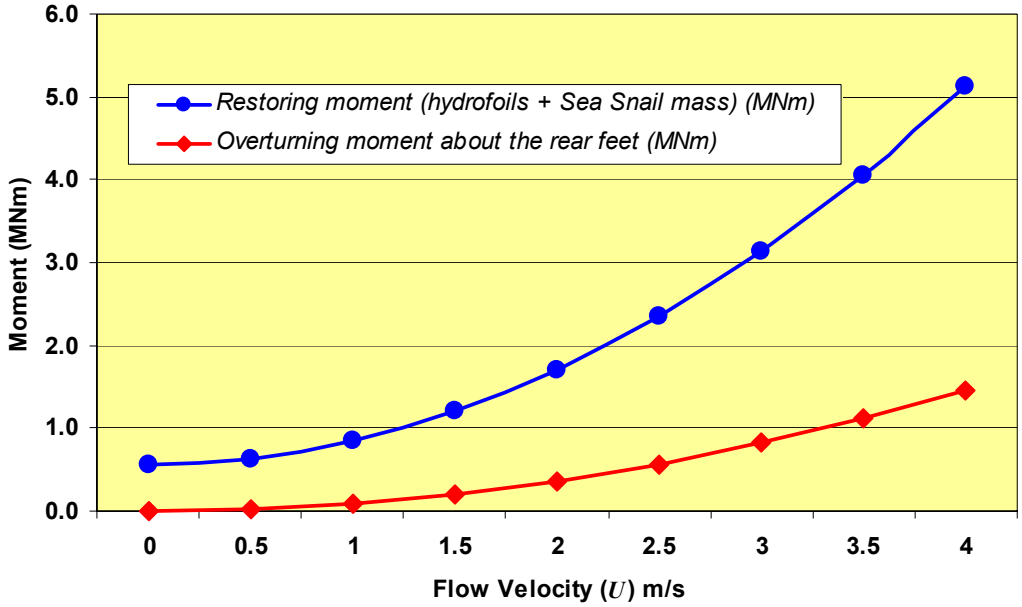

Figure 4-10: Moments for α=15°, DSP Model

The theoretically high value of C_L suggests that the restorative moment from the hydrofoils will consistently exceed the overturning moment applied to the complete structure, Figure 4-10, for all flow velocities.

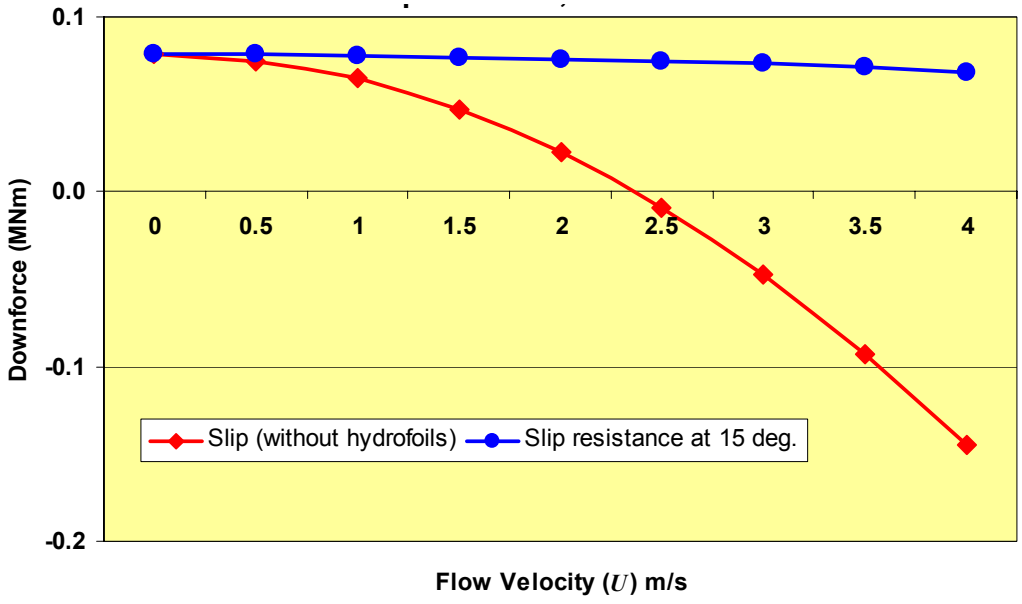

Figure 4-11: Slip resistance for α=15°, DSP Model

From Figure 4-11, the hydrofoils will apply sufficient downforce to the structure to maintain position in flows in excess of 4 m/s, though the margin of safety is slowly declining with increased values of U.

4.2.3 Low-Aspect-Ratio hydrofoil model

Based on the hydrodynamic theory developed in Chapter 3, in addition to the drag calculated from the DSP model, the induced drag due to a LAR hydrofoil configuration must be accounted for. The LAR model gives C_L and C_D for a hydrofoil with end plates at α=15° of 0.53 and 0.21 respectively. The LAR model also gives a modified value for the effective aspect ratio (AR_{eff}) and the additional drag force induced by the generation of lift. The overturning and restorative moments applied to the Sea Snail structure for U < 4 m/s, are given in, Figure 4-12, having been corrected for AR_{eff} and induced drag.

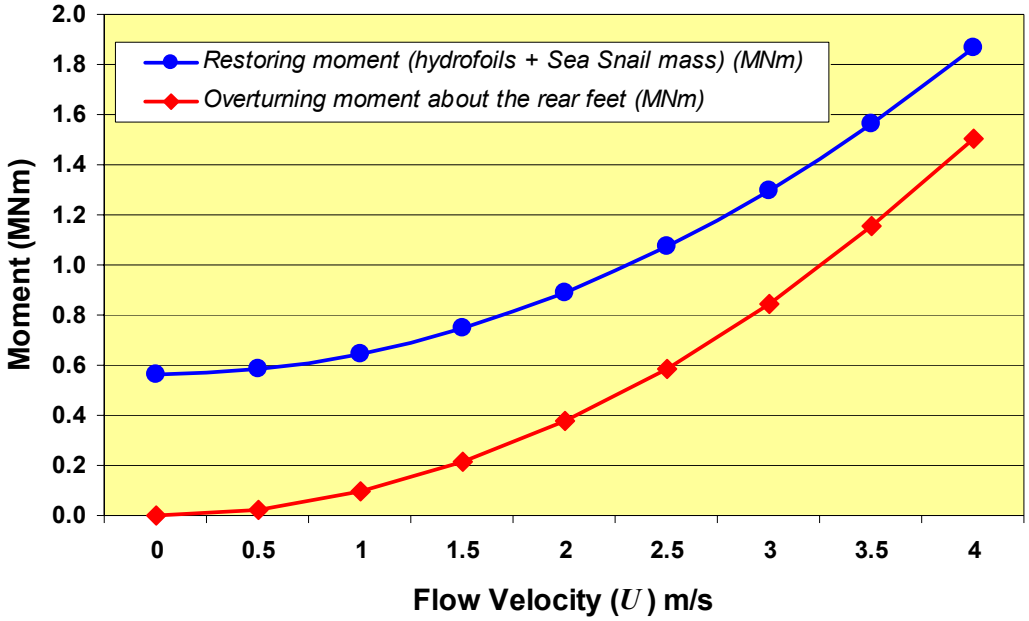

Figure 4-12: Moments for α = 15°, LAR model

The LAR model shows a decreasing level of confidence in the positional integrity of the Sea Snail as the flow velocity increases, though the safety margin is still approximately 0.35 MNm at U=4 m/s. The slip resistance is also less optimistically modelled by the LAR approach, and suggests that the current Sea Snail configuration will start to slip for values of U >4 m/s.

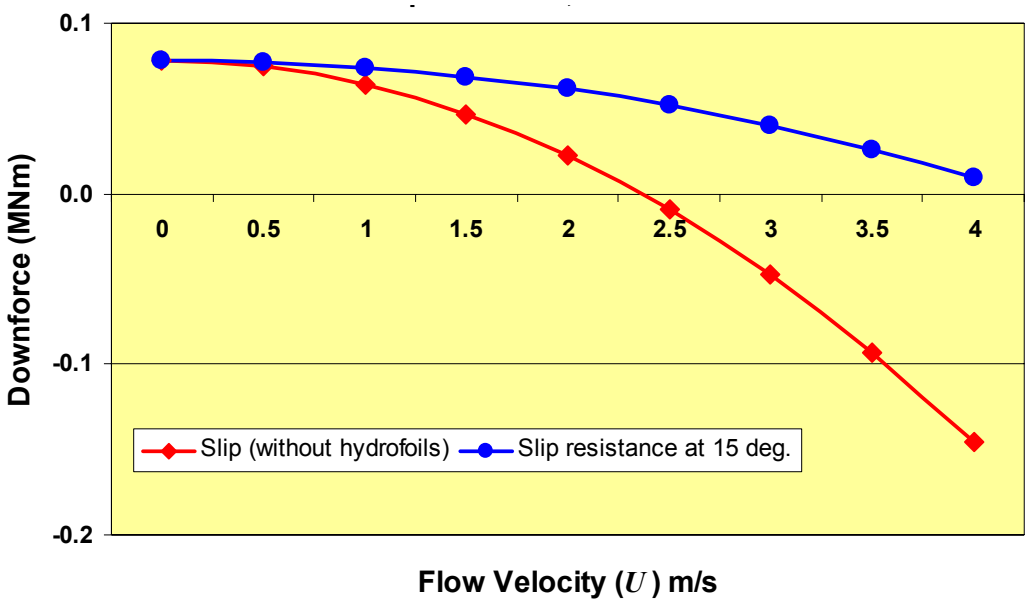

Figure 4-13: Slip resistance for α =15°, LAR model

Both the DSP and LAR models indicate that resistance to slip is of greater concern than the application of a restorative moment to prevent overturning and in reality this will be substantially dependent on the nature of the seabed and the design of the Sea Snail feet.

The DSP and LAR models both show that a structure can potentially be made secure within a vigorous flow by manipulating the fluid's kinetic energy through designed structure properties and streamlined lift surfaces positioned at an effective angle relative to the free stream vector. However, there is obvious disparity of hydrofoil performance between the two models and a solution is required to give a more accurate representation of the hydrofoil system. Ideally, the solution also needs to indicate the nature of the interdependency of the hydrofoils and thus remove the assumption of decaying efficacy from lead hydrofoil to trailing hydrofoil. Physical testing at scaled dimensions was therefore employed to measure the effects on a hydrofoil array of the same proportions as the Sea Snail device.

4.3 Validation of the Sea Snail model

Unfortunately, the sea trials of the Sea Snail (see appendix 2) failed to recover data from the instrumented device at sea and therefore the hydrodynamic component of the proposal needed to be validated by a different experimental approach. Budgetary and other constraints dictated that the new experiments would need to be on a more modest scale, at approximately $1/7^{th}$ of the original Sea Snail size. It was decided that a river test should be undertaken, and later an opportunity arose for a tow tank test model to be developed. The design, methodology and results of these river and tow-tank experiments is now described and discussed.

The common experimental requirement of both the river test and the tow tank models is to demonstrate that the Sea Snail concept has a valid connection between theory and practice via controlled experiments where scale effects are understood and accounted for. The Sea Snail model made assumptions based on a theoretical hydrodynamic analysis of the complete structure, regarding the values of C_D and C_L for the hydrofoils that would be required to maintain a secure position. The experimental procedures are therefore designed to show that these values of C_D and C_L can be delivered by an array of symmetrical hydrofoils in the original designed pattern, with one detail change that is considered to be of minimal influence, i.e. to accommodate the turbine, the upper middle hydrofoils on the original Sea Snail are ¼ span offset outboard of a line connecting the centre span points on the leading and trailing hydrofoils on the same side. According to [**94**], this outboard effect may be beneficial. For scale model simplification, all of the hydrofoil span centres are held to the same line for both river and towing models.

4.3.1 Scaling and physical similarity

Hydrodynamic analysis, as described in Chapter 3 is an invaluable start to developing and proving a concept, but physical modelling is often required to complete the study, particularly as in the Sea Snail concept, where the flow from one surface has a direct effect on the flow over another surface.

Provided that the test device and the full-scale device are physical similar, i.e. the ratio of the magnitudes of certain selected properties are the same at all points for both devices, then the results may be scaled. The physical quantities required to maintain physical similarity are geometric, kinematic and dynamic, i.e. length, motion and force.

The *geometric* ratio is usually given as the defining scale factor and many coefficients employ some characteristic dimension in their relationships. For structures such as the Sea Snail, provided that the chosen dimension is relevant to the test (e.g. hydrofoil chord), then scaling is straightforward, but if the dimension is not necessarily related to the overall dimensions of the structure (e.g. surface finish), this must be allowed for where possible. The hydrofoils of the Sea Snail and its scale models were manufactured using the same process, so the surface finishes are essentially the same, whilst their principal dimensions have a scale factor of seven.

Kinematic similarity requires geometric similarity as a primary condition, but since motion includes an element of time, then the time intervals must also be similar in the same ratio as the geometry. Kinematic similarity permits the assumption that flow past a geometrically similar boundary is kinematically similar, but the validity of this assumption decreases with distance from the boundary due to difficulties in maintaining the geometrical similarities of the streamlines.

A fixed ratio of forces is required for *dynamical* similarity to be achieved, but fluids contain many different force mechanisms (pressure, gravitational, viscosity etc) and it is impossible to maintain all forces at the desired ratio at all times. It is therefore desirable to select the forces that are most important for the model testing and to maintain their dimensional, kinematic and dynamic similarity wherever possible, neglecting those forces of minor importance. Selection of the appropriate coefficients from the range available for modelling purposes can be made by determination of the dominant forces applicable to the full scale device, since it is usually knowledge of the magnitude of forces acting that is desired, and in this instance surface tension and fluid compressibility are of no concern.

For a submerged hydrofoil, which may have free surface effects, the forces acting within the fluid are due to viscosity, pressure and gravity. In addition, the fluid possesses a hypothetical reaction force (inertia force) due to the movement of any given particle [**95**] that is the negative resultant of the applied force on that particle. Since fluid/device interaction requires that there is some acceleration of the fluid, then inertia will always be present and, by selecting the appropriate force, a dimensionless coefficient descriptor of a force ratio can be deduced from knowledge of the selected force and the inertial force. If surface tension is irrelevant to the problem and compressibility effects are negligible, then the vector sum of the viscous, gravity, pressure and inertia forces applied to the hydrofoil must complete a force polygon.

Fluid modelling coefficients

The testing of models is the principal method by which the design of a substantial marine based device can be best informed. Any solid body moving through a real fluid will experience a drag force, opposing its motion, and the dimensional analysis of a test model is required to ensure that, as far as is practicable, the ratio of the principal forces acting is maintained constant for the model and the full sized device. For marine purposes the dominant non-dimensional groups are those represented by the Reynolds Number,***(4-5)*** which indicates the relationship between the inertial forces and viscous forces acting on the body, and the Froude Number ***(4-6),*** which is the relationship between inertial forces and gravity forces, indicated by the generation of waves (by a surface piercing body) or disturbance of the free surface by a submerged body.

$$\mathrm{Re} = \frac{inertia}{viscous} = \frac{\rho U d}{\mu} \qquad \textbf{(4-5)}$$

Where μ is the absolute viscosity and d is some characteristic dimension. Assuming that the fluid properties remain constant, then if the model dimension d_m is scaled to full size d by a scale factor of, say, $d_m=0.1d$, the

velocity will need to increase by the inverse of the scale factor (i.e. 10) to maintain the same Reynolds Number.

$$Fr = \frac{inertia}{gravity} = \frac{U}{\sqrt{dg}} \qquad \textbf{(4-6)}$$

However, if the equivalent scaling is required to maintain the Froude Number identical then the velocity will need to increase by the square root of the inverse of the scale factor. It is therefore impossible to run a model that affects the free surface behaviour, which satisfies both the Reynolds Number and Froude Number identities simultaneously.

The semi-empirical approach taken [**96**], is that the total resistance offered by the fluid to the movement of the object is assumed to be the sum of three components,

a) wave-making resistance
b) skin friction
c) eddy-making resistance

The wave making resistance (a) is assumed to be independent of viscosity and therefore of Re, whilst (b) is assumed to be entirely Re dependent. The eddy making resistance (c) is considered to be small for surface craft and is usually included as a component of the resistance due to (a). However, for a fully submerged device producing no surface waves, the eddy making resistance will be the principal force driven by pressure differences.

The outcome of these simplifications is to define the total resistance (R_{total}) in terms of Re and Fr as in equation ***(4-7)***

$$R_{total} = R_{SF} + R_{PF} \qquad \textbf{(4-7)}$$

The skin friction (R_{SF}) can be estimated using thin flat plate theory with an equivalent wetted surface area and moving at the same velocity, end-on, through the water. Having established the value of the skin friction

resistance, the remaining resistance (R_{PF}) can then be attributed (without differentiation) to wave–making and eddy-making resistances.

The eddy-making resistance is due to pressure differences between two points in the flow and the ratio of pressure force to inertial force is represented by the Newton number, Ne, otherwise known as the Euler Number (Eu).

$$Eu = \frac{\Delta p}{\rho U^2} \qquad \textbf{(4-8)}$$

The function of a hydrofoil is to generate lift and minimise drag, both of which are functions of pressure, and since Eu is independent of any surface geometry, the pressure distribution acting on the surface of the hydrofoil is independent of scale. This subject is discussed further under 4.5.

Other dimensionless coefficients important in the analysis of fluids (though not applicable here) are,

- the Mach number (Ma), which relates the inertia forces to elastic forces due to compressibility, and thus the object's velocity to the local velocity of sound. The flow velocities of interest here (<3 m/s) do not approach the velocity of sound in water (~300 m/s)
- the Weber number (We) which relates the inertia force to surface tension force and is generally applicable to small objects in stationary or very slow-moving water.

4.4 River model experiment

Subject to the demands of physical similarity discussed, the river test model is required to illustrate the lift and drag forces applicable to a hydrofoil array at full scale flow velocity of ~2 m/s, sized and distributed at a geometrical scale of 1/7th of the full scale Sea Snail device. The depth of the river indicates that surface waves will be generated by the flow over the hydrofoils, and that Froude scaling will therefore be applicable, but that the full pressure-driven hydrofoil wakes will not be formed.

Calculation of Froude scaling for hydrofoil array in field test

Full scale flow velocity, U	$U = 2\,m/s$
Full scale characteristic dimension (chord), L	$L = 3\,m$
Calculate Fr	$Fr = \frac{U}{\sqrt{Lg}} = 0.369$
Scale factor model, SF	$SF = 0.142$
Calculate scale length, L_S	$L_S = L * SF = 0.425\,m$
Calculate scale flow velocity, U_S	$U_S = U\sqrt{SF} = 0.757\,m/s$
Check Fr scaling identity	$\frac{U_S}{\sqrt{L_S g}} = 0.369$

From which, a mean river flow velocity (U_S) of 0.76 m/s will provide suitable conditions for modelling the structure at an equivalent full scale flow velocity of 2 m/s.

Based on the Froude scaling discussed, the river test model can be expected to indicate the forces applicable to, and the likely response of, the full scale device at a realistic flow velocity but close to the surface. The design and assembly of an appropriate system for measuring and recording the force data generated by the river test model is now discussed.

4.4.2 Experimental background

The river test model is required to emulate the hydrofoil distribution of the full scale Sea Snail and render information regarding the distribution of the applied forces due to lift and drag over a range of α. Determination of these forces at scale dimensions will indicate the required sensitivity of the data acquisition system. Good quality sensor technology with fine levels of accuracy and repeatability is readily available and relatively inexpensive.

Applied Forces

The expected lift force magnitude can be calculated using equation ***(1-1)*** with values of C_L=0.9, A=0.43 m x 0.35 m =0.1505 m^2, which gives a lift force per hydrofoil of 68 N in an assumed flow of ~1 m/s, and therefore a total of 410 N for the full rig.

Assuming a value of C_D=0.2 for the hydrofoils, the same process gives a total hydrofoil drag F_D of 90 N in addition to the skin friction drag F_{SF} applied to the central plate, given by,

$$F_{SF} = 0.5\rho A U^2 C_F \qquad \textbf{(4-9)}$$

where, $C_F = \frac{1.33}{\sqrt{Re}} = 0.00203$, Re=4.3 x10^5 and A is the wetted surface area of the plate (1.2 m^2),

$$F_{SF} = 0.5\rho A U^2 C_F = 1.22\ N$$

The mechanisms for adjusting the angle of attack of the foil sets will also apply a drag force to be accounted for, e.g. the nylon bobbins that secure the foil pairs to the central plate will apply a drag force, F_{NB}=10 N, as will the M4 studding and swivels for height adjustment of the hydrofoils, F_{ST}=1.6 N, giving a total expected drag force,

$$F_{total} = F_D + F_{SF} + F_{NB} + F_{ST} \approx 103\ \text{N}$$

Force Measurement

The measurement of applied forces can be achieved by measuring the change in size of a solid object as a function of strain. A bonded resistance strain gauge will change in size along with the object to which it is bonded, resulting in a change of resistance within the strain gauge that is proportional to the level of applied strain. A number of individual strain gauges can be encapsulated into a single unit to form a load cell offering load sensing along different axes or in opposite directions on the same axis. The fractional change in resistance is proportional to the change in size of the object and the two changes are equated using a Gauge Factor (GF) which is a constant for any one load cell. The change in resistance is actually very small, of the order of 10^{-1} ohms, so a typical strain gauge load cell incorporates one (or more) strain gauges (Rv) as part of a Wheatstone bridge to convert the change in resistance to a change in voltage [**97**], given by ***(4-10)***

$$\Delta Vout = V\,sup\left(\frac{\Delta Rv}{Rv + R2}\right) \qquad \textbf{(4-10)}$$

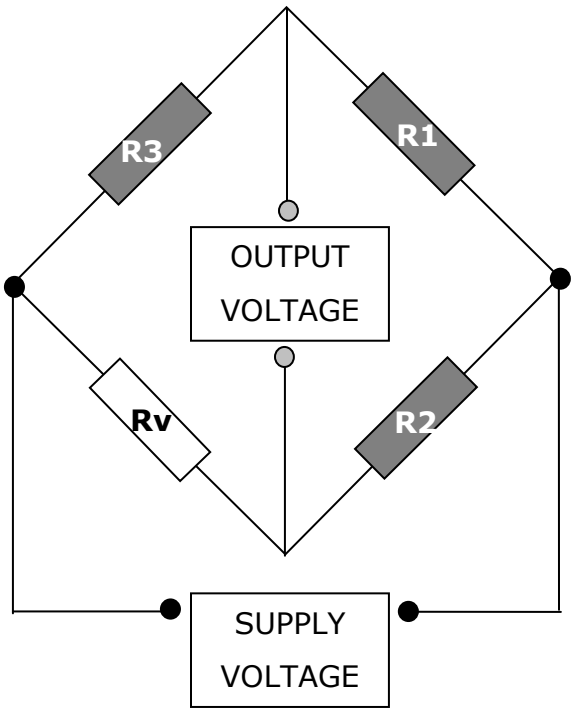

The strain gauge is a well-tested force measurement technique and good levels of accuracy, repeatability and robustness are available in relatively inexpensive units. The full specification of the Tedea Huntleigh 615 (TH 615) load cells used in this and the tow tank experiment is given in appendix 3. The TH 615 unit is protected to IP67 and is calibrated during production to a rated output tolerance of 0.002 mV/V, thereby permitting use of multiple units without the need for individual calibration of each load cell unit. The Ingress Protection (IP) rating of 67 is based on the international standard IEC 60529 for protection of electrical equipment, which is previewed at [**98**]. The two digits '6' and '7' refer to a value on two separate sliding scales, from 0 to 6 and from 0 to 8 respectively, the first of which describes protection against solids, and the second describes protection against liquids. The first digit, in this case '6', demonstrates that the load cell enjoys total protection against dust, and the second digit '7' states that the load cell is protected against immersion in liquids up to 1 m depth. The load cells are rated at 2000 N each and operate in tension and compression. The total error as specified by the manufacturer complies with the OIML R60 standards, [**99**], and is given as ±0.03% of rated output.

Load Cell Calibration

The load cells were calibrated in turn using a sequence of 10 N weights and the resulting voltage output noted to be compliant with the manufacturers test data sheet (appendix 4).

4.4.3 Site survey

The river test device was deployed into the Ebrie Burn, close to its confluence with the River Ythan at Bridgefoot near Ellon, Aberdeenshire, identified on the Ordnance Survey Landranger series map (sheet 30) at OS REF: 922324. The location of the site was identified from local knowledge and the owners approached for access permissions before survey commenced.

The surveyed test site offered a reasonably consistent water depth of 0.6 m ± ~0.05 m across a substantial part of the stream, and a symmetrical flow

profile parallel to stream sides. The stream bed in the test site was of coarse gravel with minimal aquatic plant growth. A small amount of site preparation was required upstream, and a number of small rocks were repositioned to improve the flow on its arrival at the test site. A trial frame with two experimental hydrofoils was deployed for illustration purposes and two locations within the site were surveyed for depth dependent velocity profile using a Valeport 002, impeller driven, open channel flow meter (Figure 4-14). The impeller rotates at an angular velocity proportional to the flow velocity and operates a magnetic reed switch as it does so. The resulting pulse frequency (n) is thus proportional to the flow velocity and the value of n can be converted to flow velocity (m/s) using the calibration equation given with the device. The full specification is given in appendix 5.

Figure 4-14: Valeport 002 Pulse counter flow meter.

Figure 4-15: Test location showing stream bed and water depth.

The flow conversion factor given in the flow meter documentation for n is 0.039 + (0.1071n) and the results are plotted in Figure 4-16.

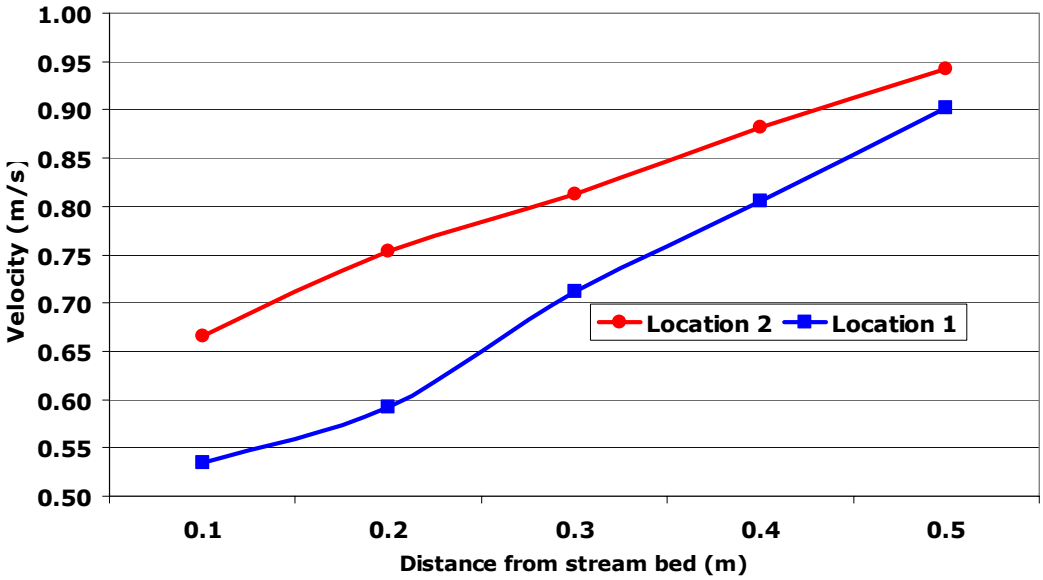

Figure 4-16: Velocity profiles of sites within the test location

The velocity profiles are almost linear rather than being described by a simple power law, and are both characteristic of a supercritical flow on a mildly sloping bed [**100**]. Location 2 was chosen as it offered the least velocity profile variation, and its position within the stream was marked relative to each bank using locally acquired, environmentally benign position markers.

4.4.4 Experimental equipment design

Full manufacturing drawings, including dimensions, materials and off-the-shelf component details for the river test device are given on the accompanying CD.

In addition to cost and portability, the design specification of the river test model had to fulfil a number of requirements regarding its hydrodynamic purpose, in that it must present an assembly of foils to a flow stream whilst minimising its own distortion of that flow. The frame must be capable of providing a stable and rigid structure, upon which sensitive measurement systems may be mounted and from which the angle of attack of the hydrofoils can be adjusted without disturbing the structure's position on the stream bed. An undertaking was given to the site owners that no trace would

be left of the device and that at no time would the stream be inaccessible to fish and wildlife.

Fabrication of the hydrofoil half-shells (Figure 4-22) is a straightforward moulding process in GRP using XY co-ordinates from the NACA 4 digit symmetrical hydrofoil profile created using the equations given in [**75**]. The hydrofoils are principally supported by, and are able to rotate around, steel tubulars fixed normal to a central plate. Their angle of attack is controlled by threaded rod supporting the tail of the hydrofoil. Thus, the lift created by the interaction of the hydrofoils with the flow stream is transferred to the longitudinal bar supporting the central plate. This bar is able to rotate about its axis whilst being attached at each end to full bridge strain gauge load cells, two of which measure the lift (red dotted indicator in Figure 4-17) and drag (blue indicator in Figure 4-17) forces applied to the front of the bar by the hydrofoil array, whilst a third measures the lift force being applied to the rear of the bar by the hydrofoil array (see Figure 4-20).

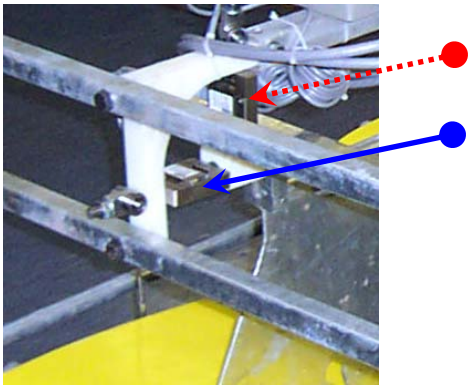

Figure 4-17: Load cell detail, drag and front lift.

The restrained end of each load cell is mounted on a small carriage using 25x10x6 sealed roller bearings as wheels, thus permitting any small movement normal and parallel to the load cell plane of operation.

The overall structure drag force is minimised by arranging the hydrofoils in such a way that the supporting structure presents as little frontal area as possible (see Figure 4-19). The end frames were adjustable in height so that

a range of stream depths could be accommodated if local weather conditions resulted in a change of stream depth.

By permitting the hydrofoil assembly to rotate about a longitudinal axis (see Figure 4-21, inset), no rolling moment is applied to the load cells.

The river test device was fully assembled in the laboratory (see Figure 4-23) and checked for operational function, structural integrity and any assembly snags. Once assembled, the rig was loaded to check the load cells' calibration and consistent return to zero when unloaded. This was achieved by placing 10 N weights in a distributed pattern for lift measurement and applying a horizontal load via a spring balance for drag measurement. The load cell supply voltage was delivered by an RS7221 data scan unit which energised each load cell at the point of acquisition with a controlled 24 V voltage, thus ensuring a consistent voltage response from each load cell.

Figure 4-18: RS7221 Datascan ruggedised field unit

The data scan unit and a fused connection block for each channel was built into a ruggedised Peli® water and impact resistant case appropriate for arduous field work (see Figure 4-18). A copy of the RS7221 specification document is given in appendix 6 or can be found at [**101**]. The RS7221 unit was connected to a Sony Vaio laptop via RS-232 protocol and the calibration

data (Table 4-2) was recorded by the software supplied with the RS7221 unit into a standard .CSV file on the laptop.

Table 4-2: Calibration data for river test model.

Temperature Sensing		Lift force Load Cells		Drag force Load Cell	
Zero point R (Ohm)	100	Zero load output (V)	0	Zero load output (V)	0
Increase in R (Ohm/^{o}C)	0.384	Rated load (mV/V)	2	Rated load (mV/V)	2
Temp (^{o}C)	20	Input (V)	24	Input (V)	24
R value (Ohm)	7.68	Rated Load (kg)	200	Rated Load (kg)	200
Supply Voltage (V)	1.8	Rated Load (N)	1962	Rated Load (N)	1962
Bridge fixed R (Ohm)	100				
Bridge output (V)	0.933	V @ rated load (mV)	48	V @ rated load (mV)	48
	293		1962		1962
Display scale factor	2.604	Display scale factor	40.875	Display scale factor	40.875
Offset for ^{o}Kelvin	273	Foil structure offset (N)	-210.1		0.0

The RS7221 Datascan unit was powered by two portable 12 V 60 AH lead acid batteries, capable of supporting the unit for about 10 days continuously at 500 mA, thus obviating concerns regarding instrument voltage variation over the testing period of approximately 2 hours.

The following fabrication drawings and photographs of the assembled river test model illustrate the arrangement and positioning of the data acquisition components.

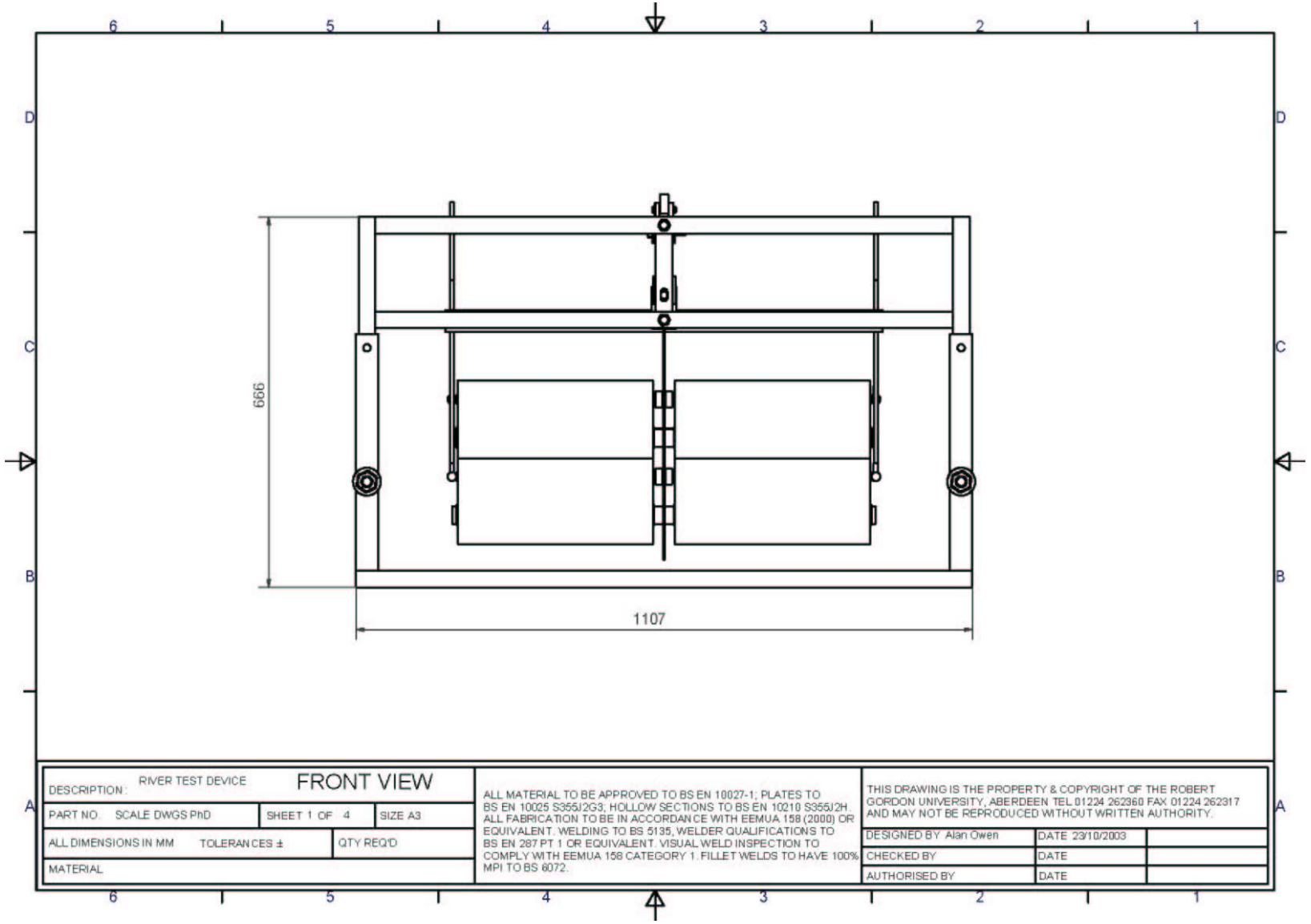

Figure 4-19: River test model; front view.

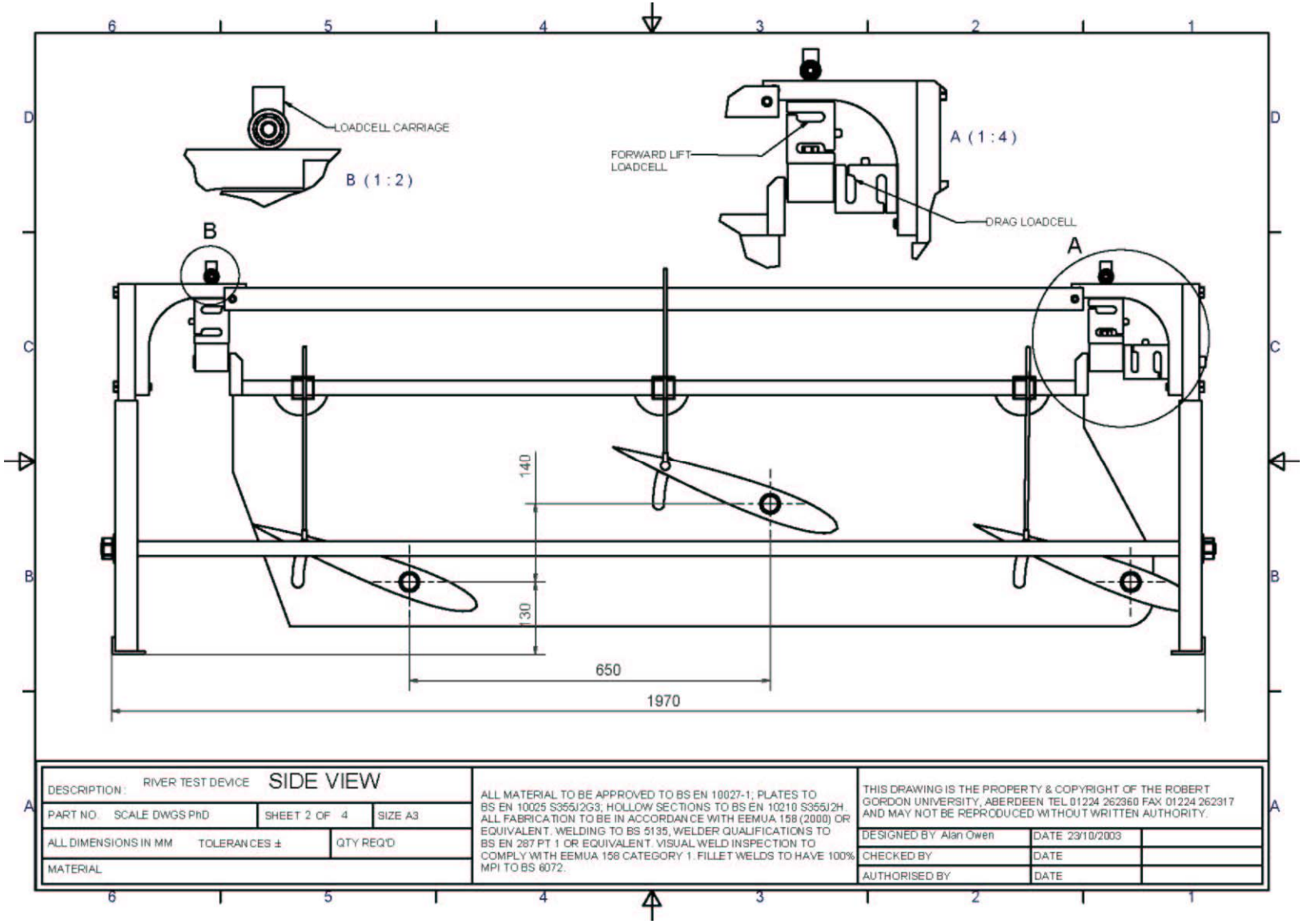

Figure 4-20: River test model; side view.

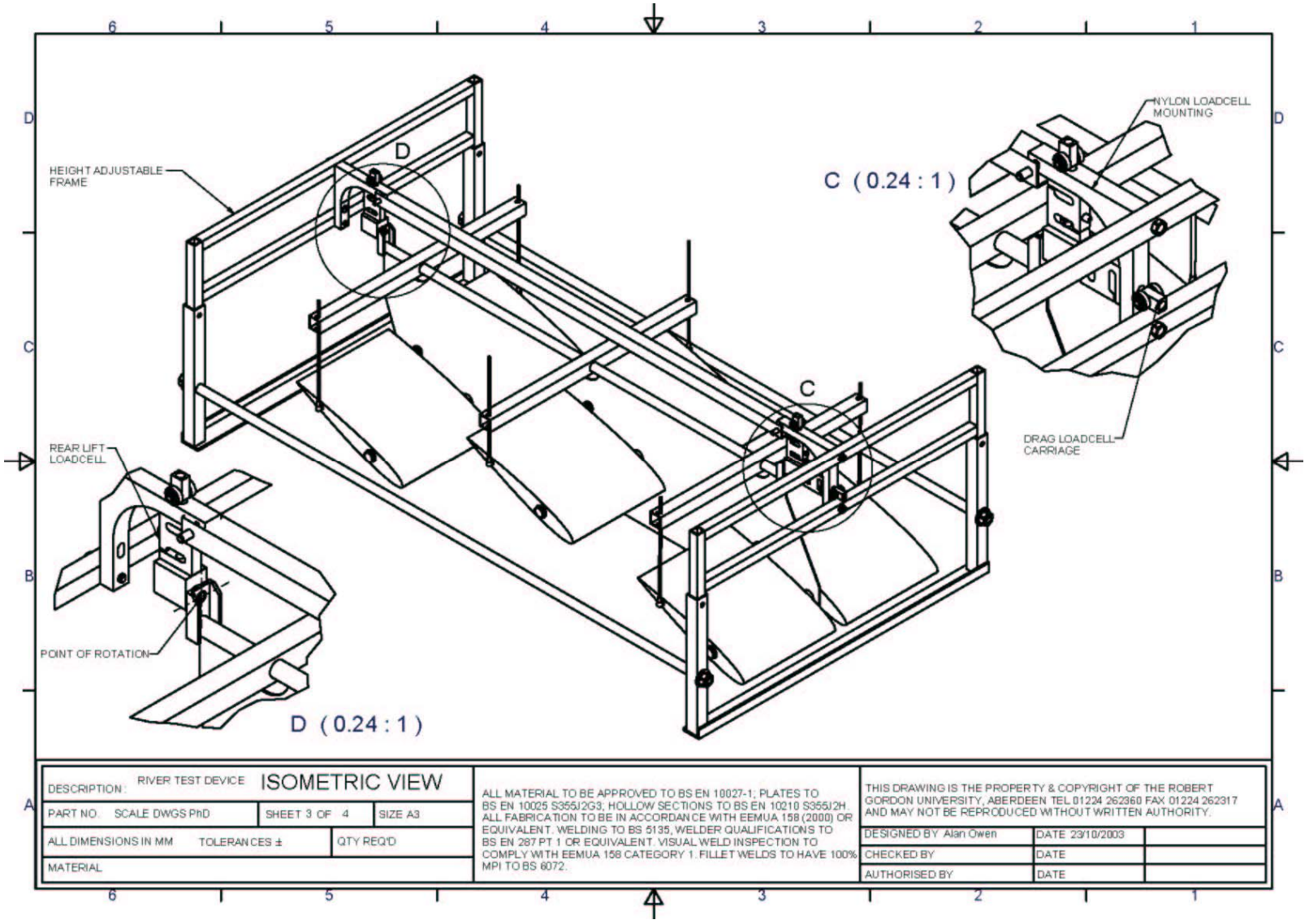

Figure 4-21: River test model; isometric view.

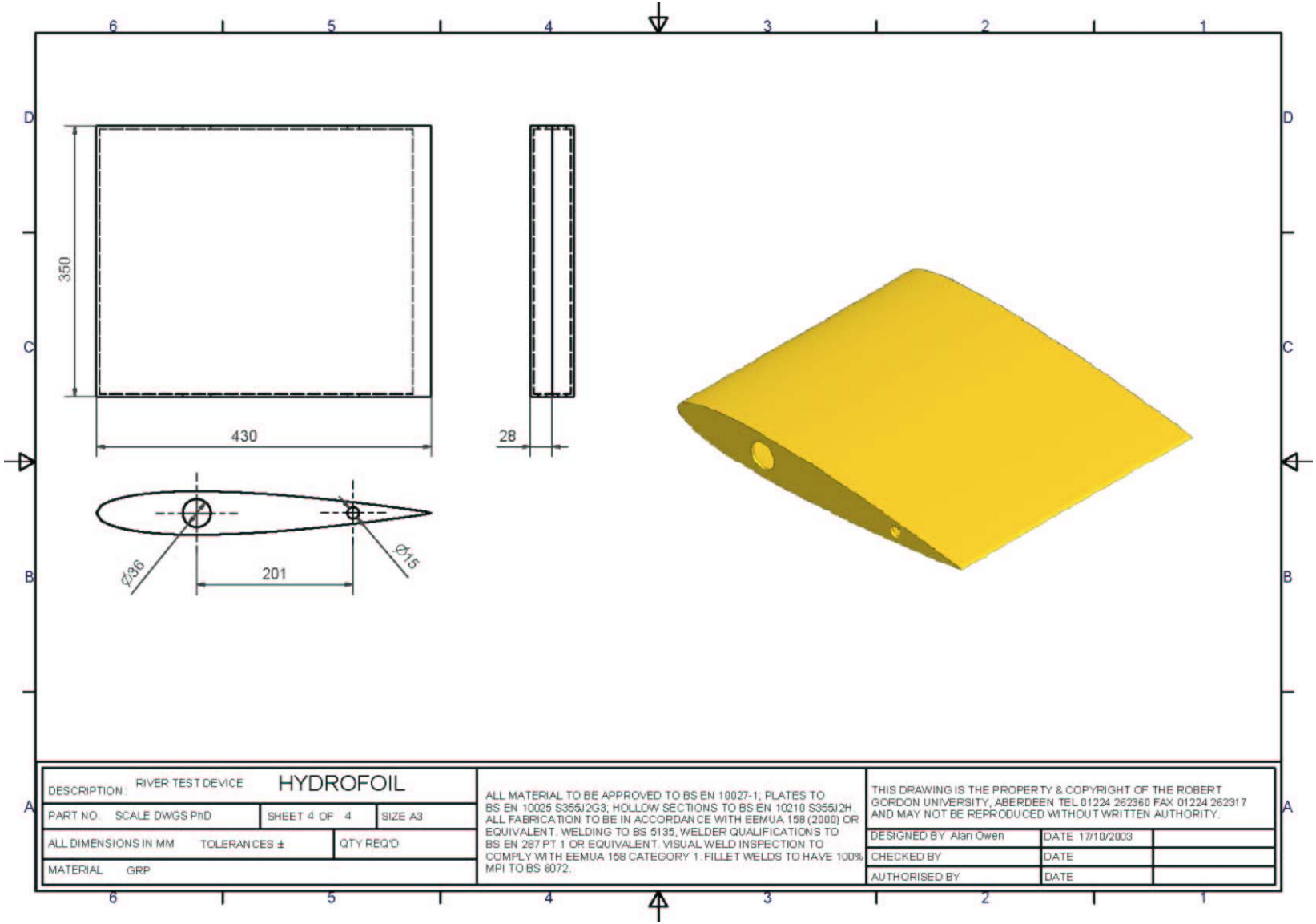

Figure 4-22: River test model; hydrofoil dimensions.

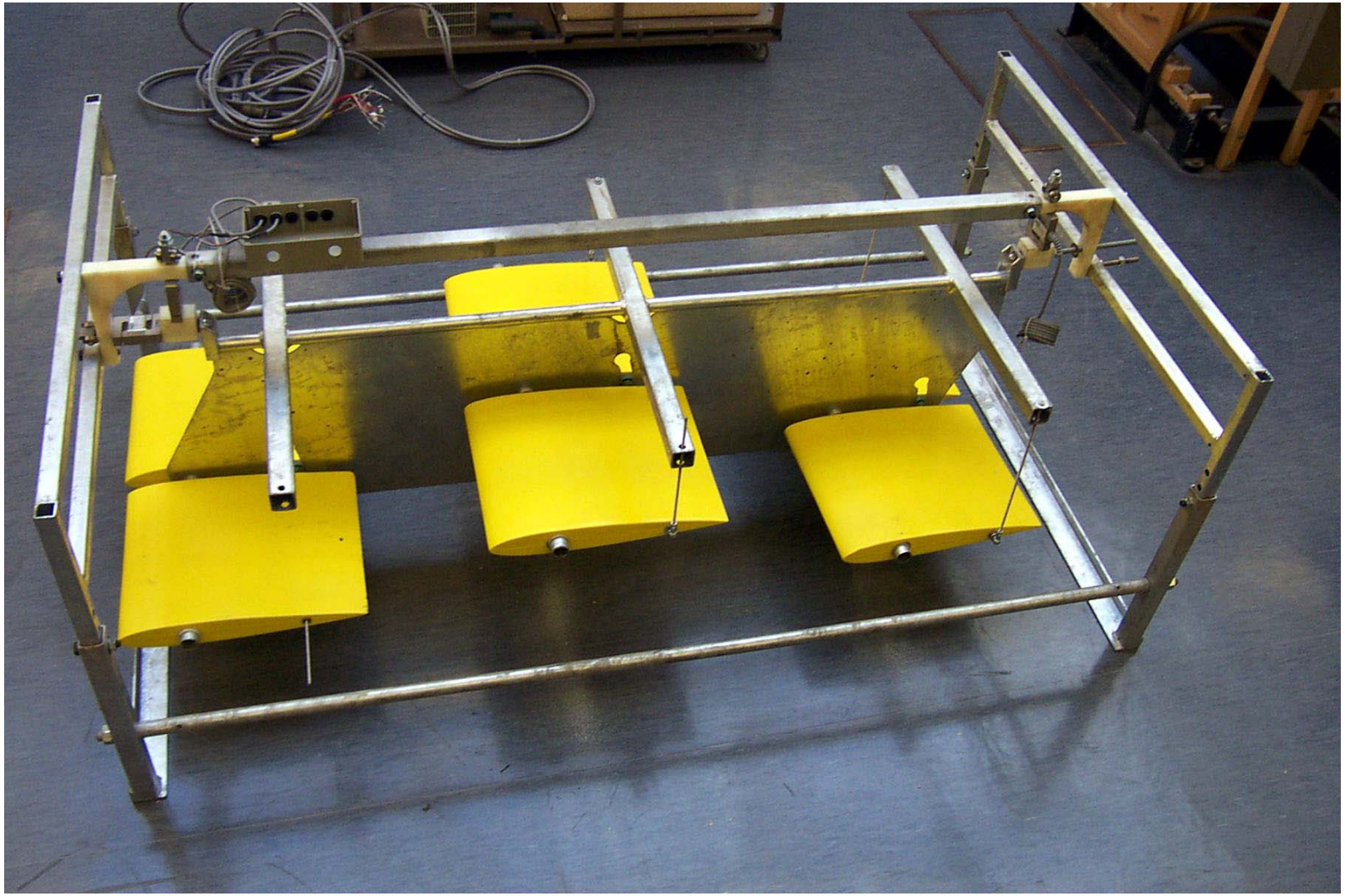

Figure 4-23: River test model during assembly

Figure 4-24: River test model awaiting deployment

4.4.5 Experimental procedure

The weather conditions at the site were cold, air temperature around 5^{o} C, and a very light breeze. During the week preceding the test there had been little rain within the catchment area of the Ebrie Burn and the water depth was approximately 10 mm less than that surveyed. The site is sheltered by a raised roadway to the north and a small stand of pine trees to the east. The surrounding topography is generally low hills and the burn was running at a level about 0.5 m below its bank tops at the site.

The device was positioned in the flow at the location previously identified during the site survey and made level across the stream with its longitudinal axis approximately parallel to the stream surface.

Figure 4-25: River test model in position.

The Valeport 002 flow meter was affixed to the leading frame such that the impeller was centrally located between, and at the same level in the flow as, the leading edges of the two leading hydrofoils; see Figure 4-26.

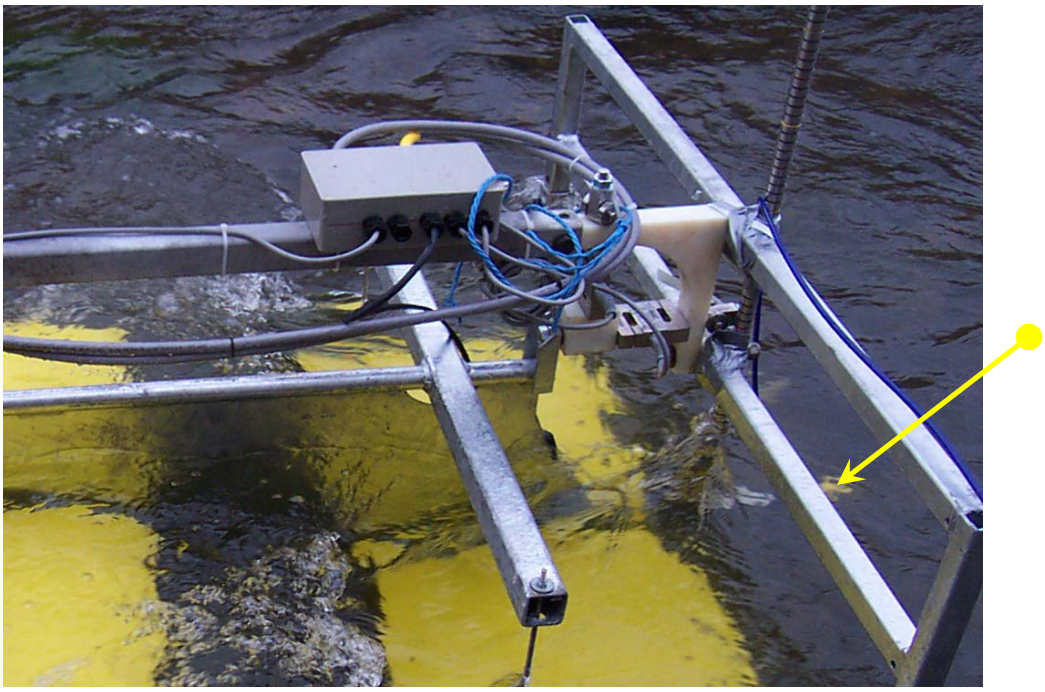

Figure 4-26: Position of Valeport flow meter

By allowing sufficient slack in the adjustment of the angle of attack for the hydrofoils, the hydrofoils were allowed to find their own no lift position within the flow. Since the chord line of a symmetrical section hydrofoil is coincident with its zero lift axes, the hydrofoil will position itself within the flow at the point of least resistance. By taking this position as zero lift, it mitigates the need to level the device precisely with respect to the flow. The angle of zero lift, relative to the frame, was later measured as 3^{o}, which correlated with the mild slope of the stream bed implied by the previously discussed velocity profile. The device was left undisturbed for approximately 20 minutes to allow for any short-term settlement.

The zero lift position of each M4 hydrofoil adjuster was marked and the first set of readings taken. The distance between centres of the hydrofoil pivotal axis and the attachment of the M4 adjustment was 201 mm, giving a tangential distance of 3.5 mm per degree increase of the angle of attack. Since M4 thread has a standard pitch of 0.7 mm, then 5 complete rotations of each adjusting nut gives 1 degree increase in the angle of attack to a good approximation. This permitted each hydrofoil to be adjusted from above the

water surface without the need to measure the angle of attack directly. After adjustment of the hydrofoils, the personnel exited the water and a 30 second interval was allowed for the flow to settle before acquiring concurrent measurements of lift at the front and rear of the device, overall drag on the hydrofoil assembly, flow velocity and water temperature, for a minimum of 60 seconds. The flow velocity data was recorded independently of the force data, care being taken to ensure that flow velocity was averaged over a concurrent period for each of the 17 off tests at increments of 1^{o}. After completion of the experiment, the river test model was removed and the site checked for debris prior to departure.

4.4.6 Data processing

The original sampled data files (extension .DIF) are included on the attached CD as are the processed data files and the data manipulation VBA® routines. The .DIF file is a .CSV format file with a different extension and is accessible by Microsoft® Excel ®. Each file is time and date stamped by the acquisition software and each file is numbered sequentially as the value of α is increased. The angle of attack of the hydrofoils relative to the supporting framework is notated as α_1, whilst α applies to the angle of attack relative to the flow. Therefore, for any value of α_1, $\alpha = \alpha_1 - 3^{o}$. The file named 'data1.DIF' holds the data taken for $\alpha=0^{o}$, so 'data2.DIF' holds the data for $\alpha=1^{o}$, etc.

The acquisition software (Orchestrator) has sampled the data at 20 Hz, but the RS7221 unit only samples at 1 Hz, resulting in multiple samples of the same reading in the original file. A short Visual Basic ® (VB) routine was used to open each of the 17 original .DIF files in numerical sequence, extract the data at 1hz intervals and write the sampled variables into a record of 61 data points per .DIF file as ensembles of data in the file 'dataAll.xls'. A sample of the ensemble header for $\alpha=0^{o}$ is given in Table 4-3. The ensemble header contains a hyperlink to its file of origin so that all processed data can be traced back if required. The temperature value varies from 7.68^{o} C to 7.78^{o} C for the duration of the field experiment and is therefore considered to be a constant and neglected in the remainder of the analysis.

Table 4-3: Sample data ensemble header, α=0°.

					Variation from mean		
Source	data.1.DIF			α 0			
Time (s)	Front lift(N)	Drag(N)	Rear Lift(N)	Temp(°C)	Fr Var	Dr Var	Rr Var
0	-179.61	27.4	-201.85	7.68	-1.79	0.32	1.09
1.04	-177.67	28.24	-207.03	7.68	0.15	1.16	-4.09
2.03	-178.77	25.71	-203.7	7.68	-0.95	-1.37	-0.76
3.02	-174.34	26.55	-206.3	7.68	3.48	-0.53	-3.36
4.01	-173.23	27.96	-200.37	7.68	4.59	0.88	2.57
5.05	-183.21	24.58	-201.85	7.68	-5.39	-2.50	1.09
6.04	-182.38	25.99	-205.19	7.68	-4.56	-1.09	-2.25

```
For p = 10 To 34
    a = ((p - 22) / 4)  ' sets class limits from -3 to +3, step 0.25
    If a < 0 Then c = 0.005 ‘ sets the class boundaries
    If a = 0 Then c = 0
    If a > 0 Then c = -0.005
    Cells(p, 4).Value = a + c  'sets the column of 'z' values for the standard
                               normal curve, -3 to +3
    Cells(p, 5).Value = 0 ' sets all existing frequency data to zero
    Cells(p, 6).Value = 0 ' sets all existing frequency data to zero
    Cells(p, 7).Value = 0 ' sets all existing frequency data to zero
Next p

s = Cells(74, 9).Value 'fetches calculated value of Standard Deviation for the
                       front lift force data
For i = 9 To 69 'FOR LOOP moves from 0 to 61st line fetching (X-mu)
  x = Cells(i, 13).Value'reads the value of the cell selected by the FOR
                         LOOP,(X-mu)
  For p = 10 To 34 ' FOR LOOP to seek correct class limit
     z = x / s   'standardise (X-mu) to sigma
     If z < 0 Then c = 0.005
     If z = 0 Then c = 0
     If z > 0 Then c = -0.005    ' Sets the class boundaries
     DoEvents
     If Val(z) < Val((p - 22) / 4) Then Cells(p, 5) = Cells(p, 5).Value + 1:
GoTo out
        'If the value of x i.e.(Xbar-Sigma) fits into a class limit, count one
         and add it to the tally monitoring that class limit, then exit the 'p'
         Loop. Otherwise continue with the 'p' Loop until the correct class
         limit is found.
    Next p
out:
Next i  ' repeat for next data value of (X-mu)
```

Figure 4-27: Sample VBA code for frequency distribution.

In addition, it is assumed that the data will correspond to a normal distribution.

For each of the 17 ensembles (Figure 4-28 (***a*** to ***p***)), representing α=0° to 16°, the Microsoft ® Excel® mean (μ), minimum, maximum, standard deviation (σ), mode and median functions are applied to the data for the three principal records, Front Lift Force, Drag Force and Rear Lift Force, and the values are recorded at the bottom of the ensemble. The value of σ is then used in a short VBA routine to calculate the standardised normal distribution [**102**] for each record.

The code in Figure 4-27 gives the routine for calculating the frequency distribution for the Front Lift force variation, as a function of σ, and the same routine was used for each record in the ensemble.

The raw data for each value of α, (normalised to zero, but otherwise as recorded) is plotted in Figure 4-28 (***a*** to ***p***) on the following pages; note that lift force is recorded as increasing in the negative sense. The fluctuation in all of the readings is obvious and there is a strong general correlation within the data, particularly between the front lift force and the drag force, suggesting that the flow velocity fluctuated significantly during the 60 second sample period. In addition, the drag force data suggests that the hydrofoils are being drawn positively upstream at low angles of attack.

Figure 4-28: Also see subsequent pages – Data plots for all values of α

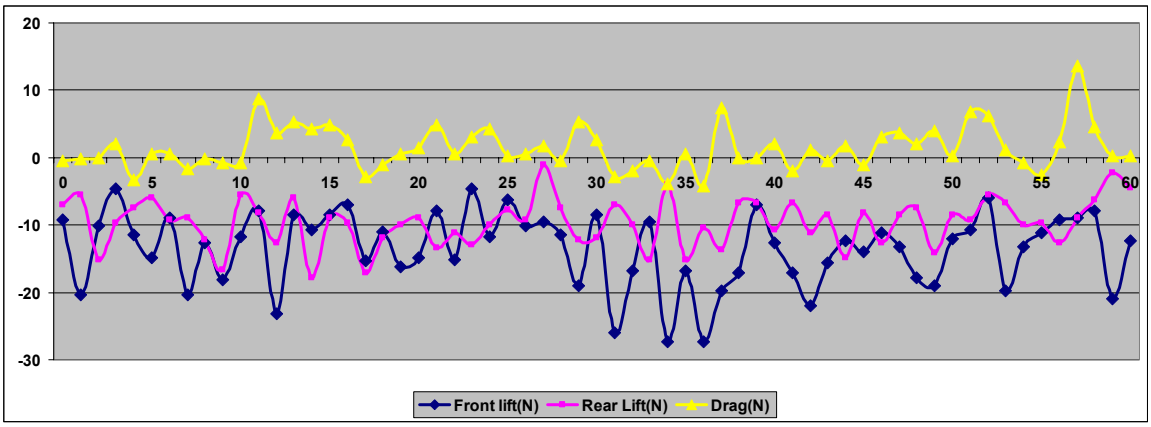

Figure 4-28(a) α= 1°

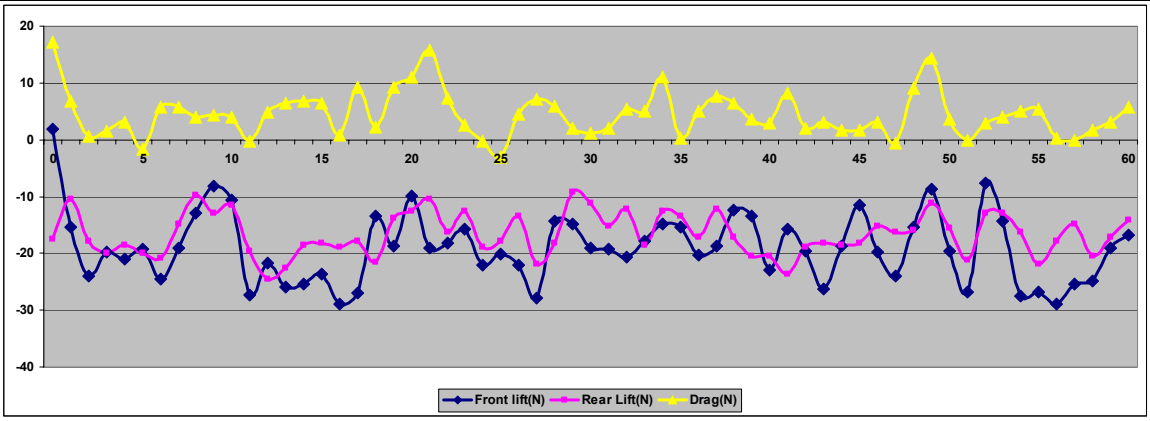

Figure 4-28(b) α= 2°

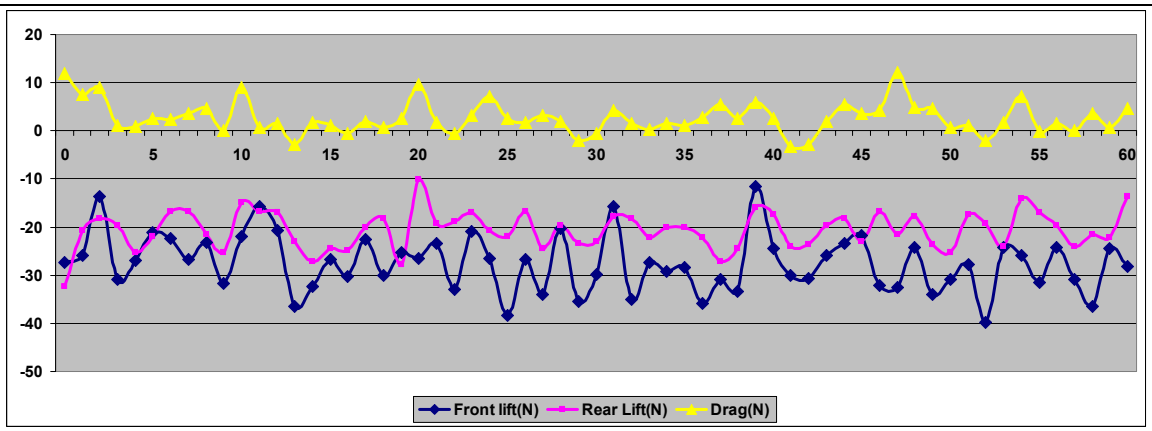

Figure 4-28(c) α= 3°

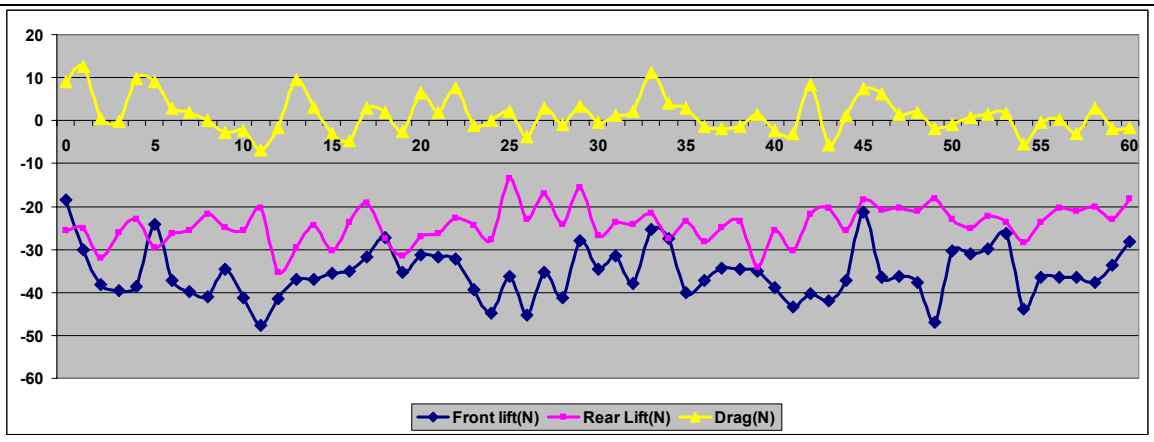

Figure 4-28(d) α= 4°

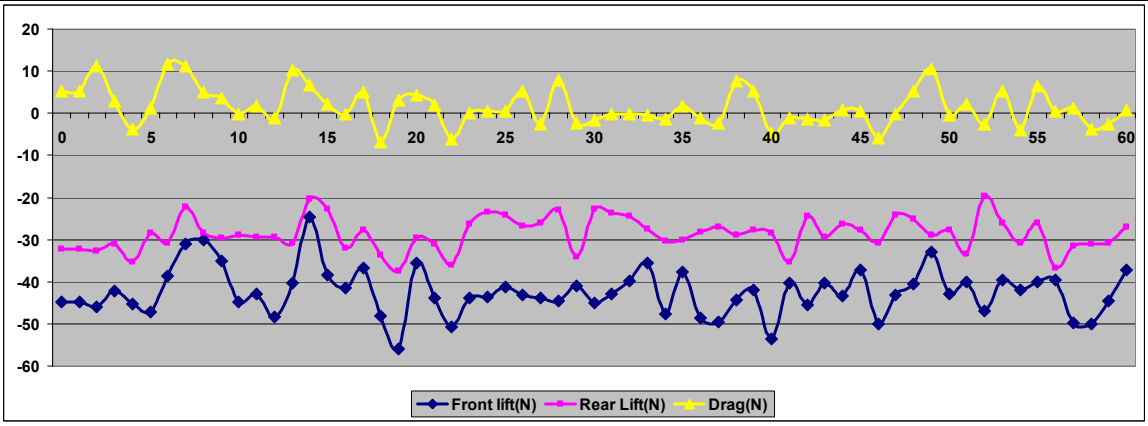

Figure 4-28(e) α***= 5°***

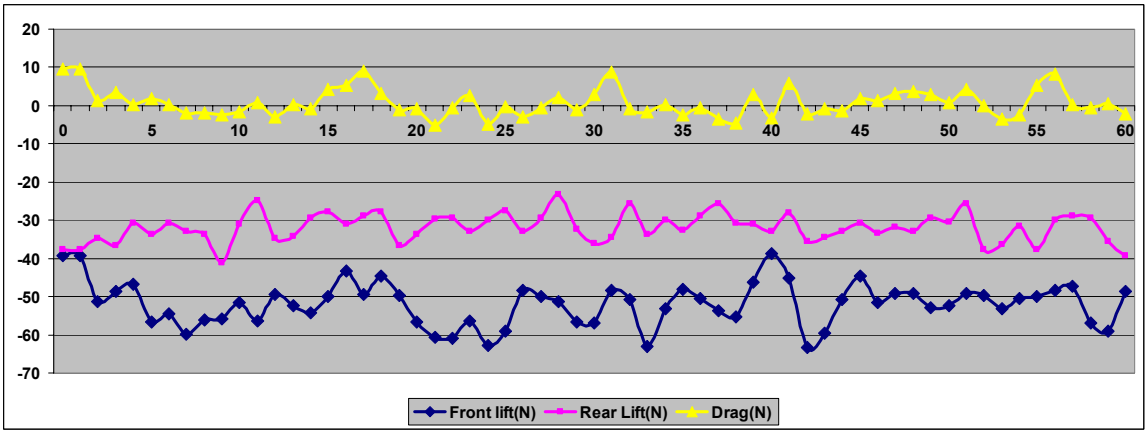

Figure 4-28(f) α***= 6°***

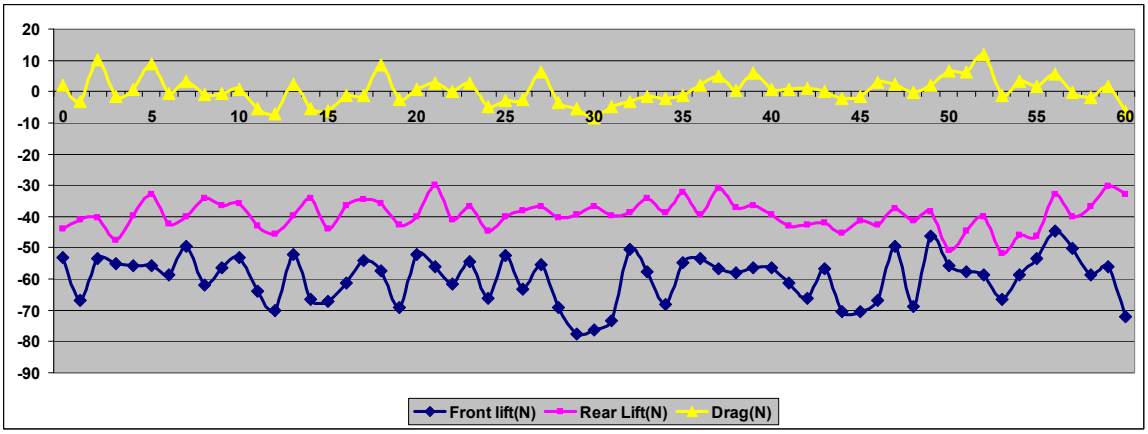

Figure 4-28(g) α***= 7°***

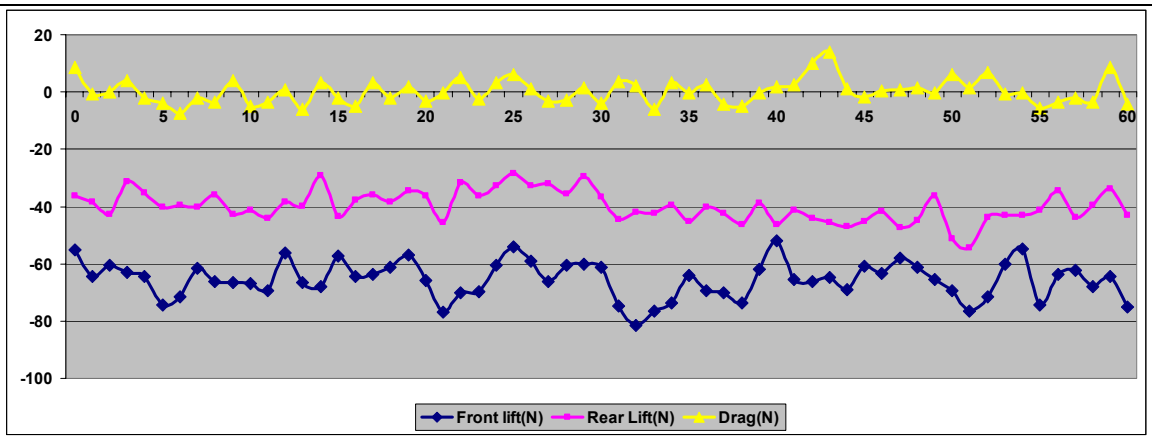

Figure 4-28(h) α= ***8°***

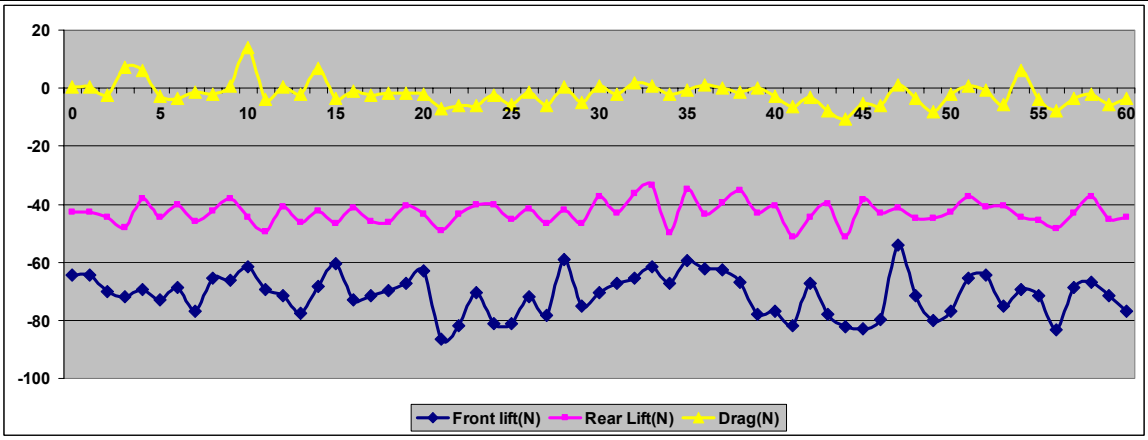

Figure 4-28(i) α= ***9°***

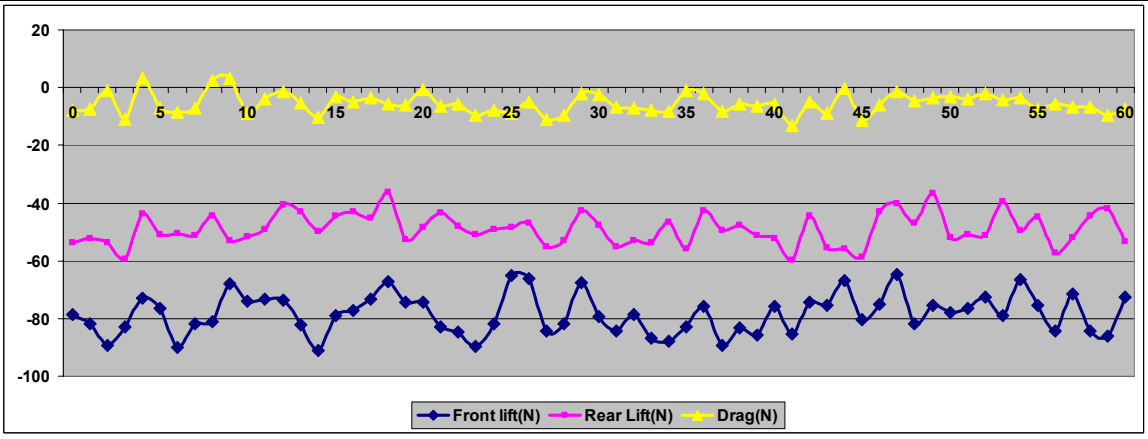

Figure 4-28(j) α= ***10°***

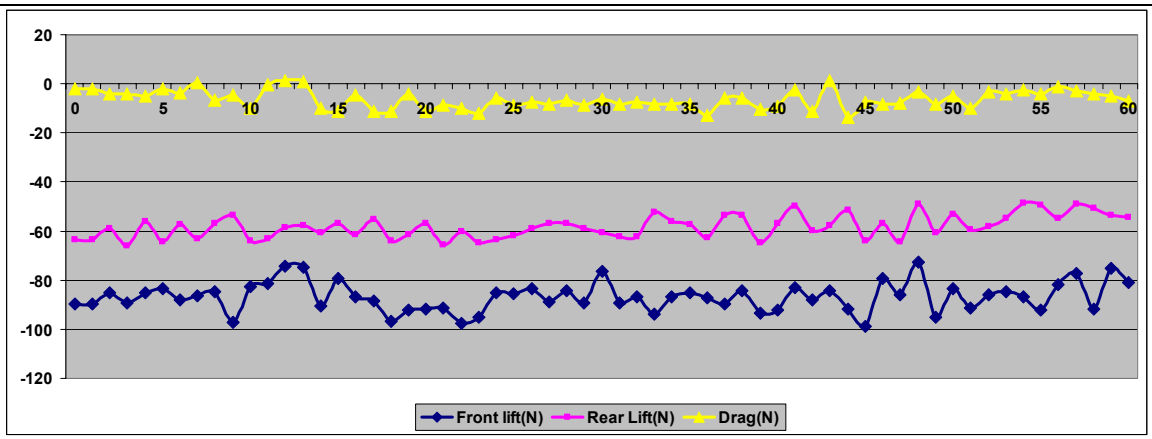

Figure 4-28(k) α= ***11°***

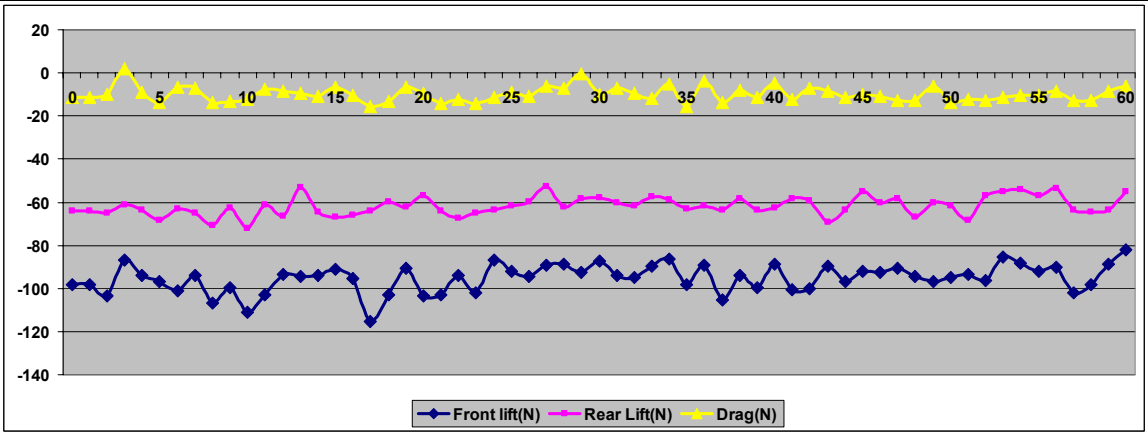

Figure 4-28(l) α= ***12°***

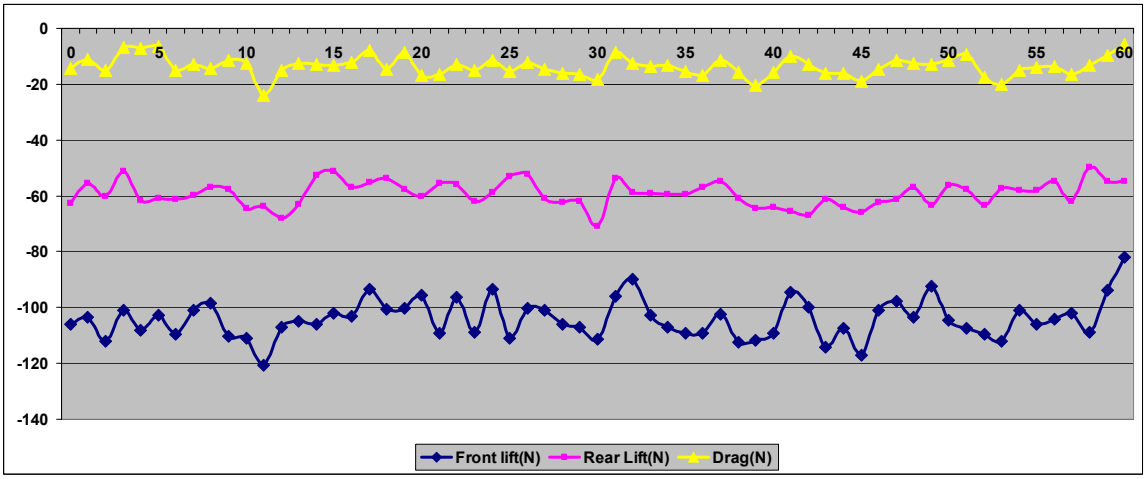

Figure 4-28(m) α= ***13°***

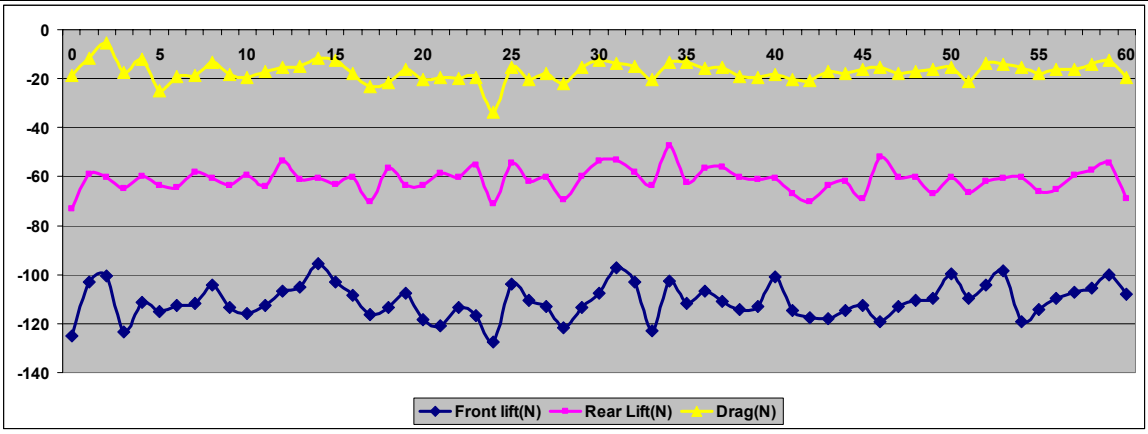

Figure 4-28(n) α= ***14°***

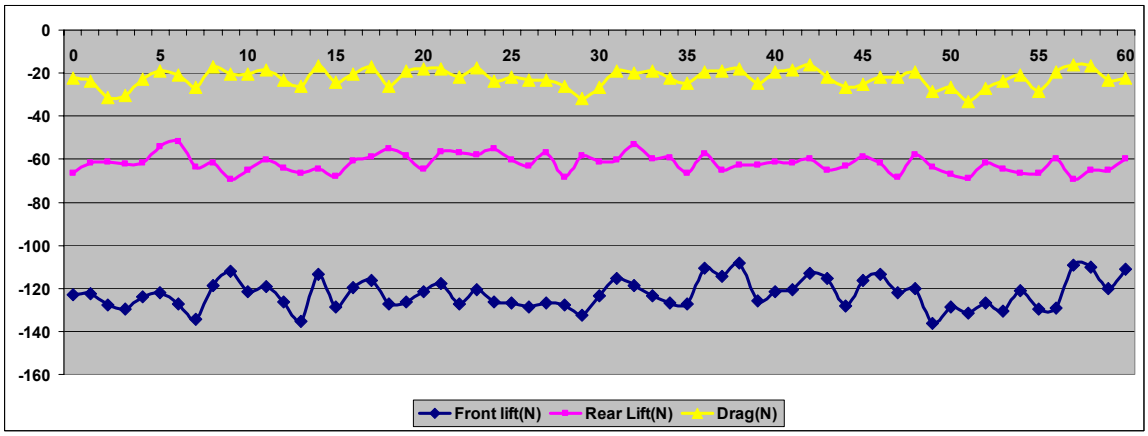

Figure 4-28(o) α= ***15°***

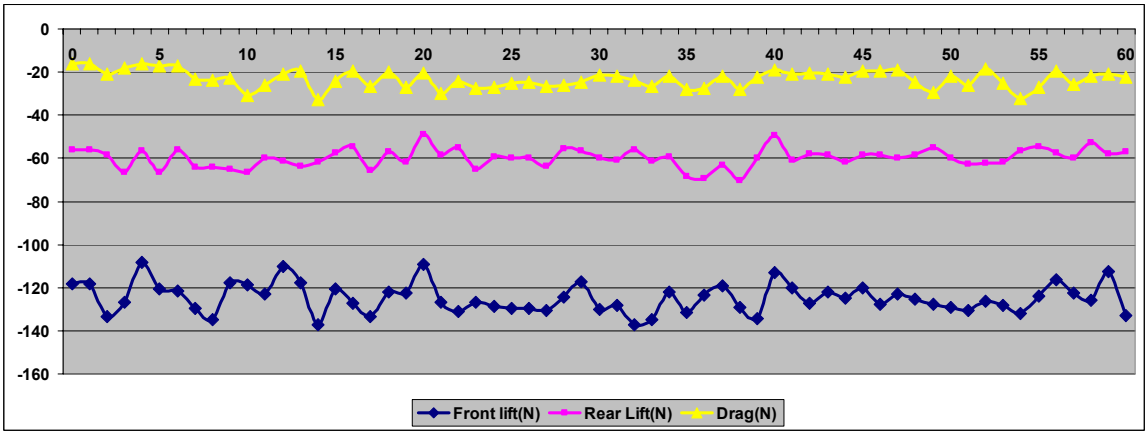

Figure 4-28(p) α= ***16°***

4.4.7 Statistical confidence

The distribution of the error about the estimated mean (μ) of each record in the ensemble gives the Standardised Normal Frequency Distribution for the record. As an example, the frequency distribution for α=10° is given in Figure 4-29.

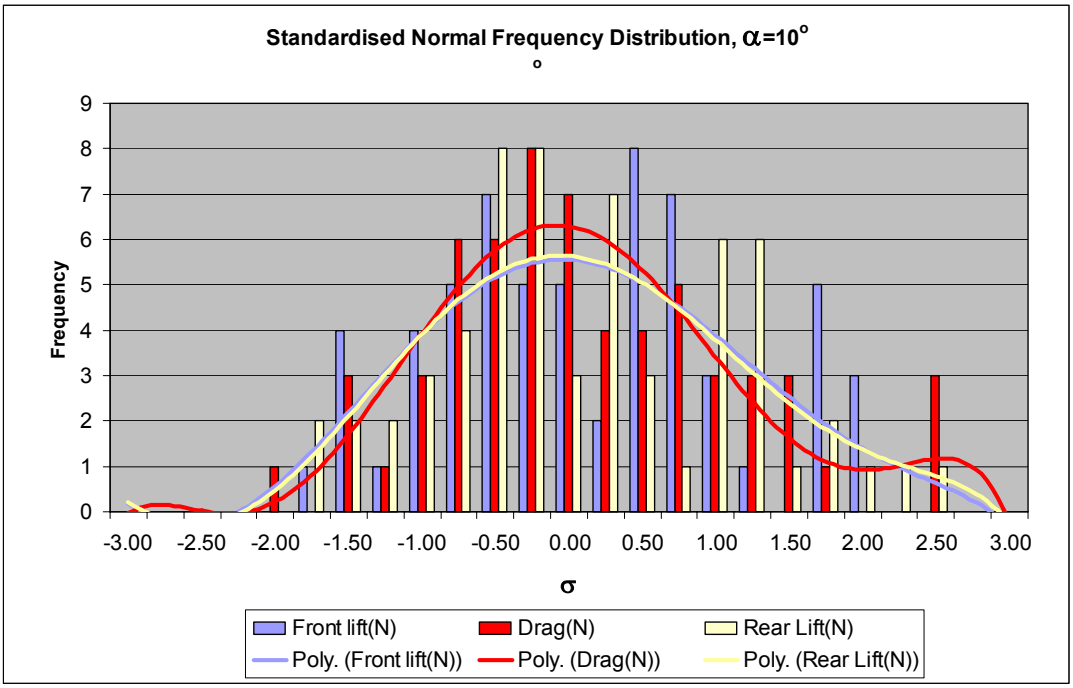

Figure 4-29: Example frequency distribution of data.

The frequency distribution allows an estimate to be made of the probability that any given variable lies between the class intervals $\pm\sigma$ or $\pm2\sigma$ or $\pm3\sigma$. The recorded data is given to 2 decimal places so the class limits are set to multiples of 0.25σ between -3σ and $+3\sigma$ and the class boundaries are defined as the class limits $\pm0.005\sigma$, where the sign is opposite to that of the class limit, e.g. -2.50σ is bounded at $-2.50\sigma + 0.005\sigma = -2.495\sigma$. The data in Figure 4-29 shows the frequency distribution for each of the principal records, and a 6th order polynomial is applied to indicate the trend of the data, which suggests that a normal distribution is likely.

Calculation of the probability indicates that the data can be expected to fall within the first two class intervals ($\pm\sigma$ and $\pm 2\sigma$) with a confidence level of,

Table 4-4: Confidence levels for data for α=10°

	Front Lift force	Drag Force	Rear Lift force
σ	75%	75%	70%
2σ	100%	95%	97%

Whilst the ensemble for α=10° is suggestive of a normal distribution, and the confidence levels also fit with such a distribution, the requirements of random data input suggests that the distribution should become more normalised as the number of samples increases.

The following three plots (Figure 4-29, Figure 4-30 and Figure 4-31) show the mean frequency distributions for all ensembles for each of the three principal records. For comparison, each mean frequency distribution is plotted alongside a standardised normal curve using the equation,

$$z = \frac{1}{\sqrt{2\pi}} e^{-0.5z^2} \qquad \textbf{(4-11)}$$

Having established that the estimated mean value of each record is representative of the applied force, the estimated mean of each record from the first ensemble (i.e. α=0°) is subtracted from the estimated mean of each subsequent record, therefore defining itself as zero.

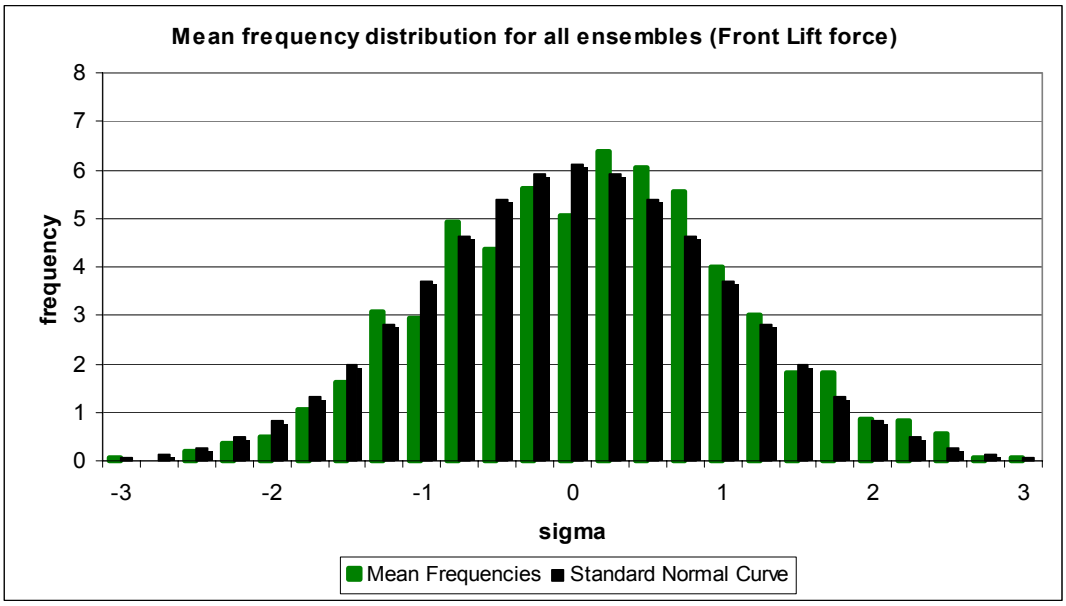

Figure 4-30: Front Lift force

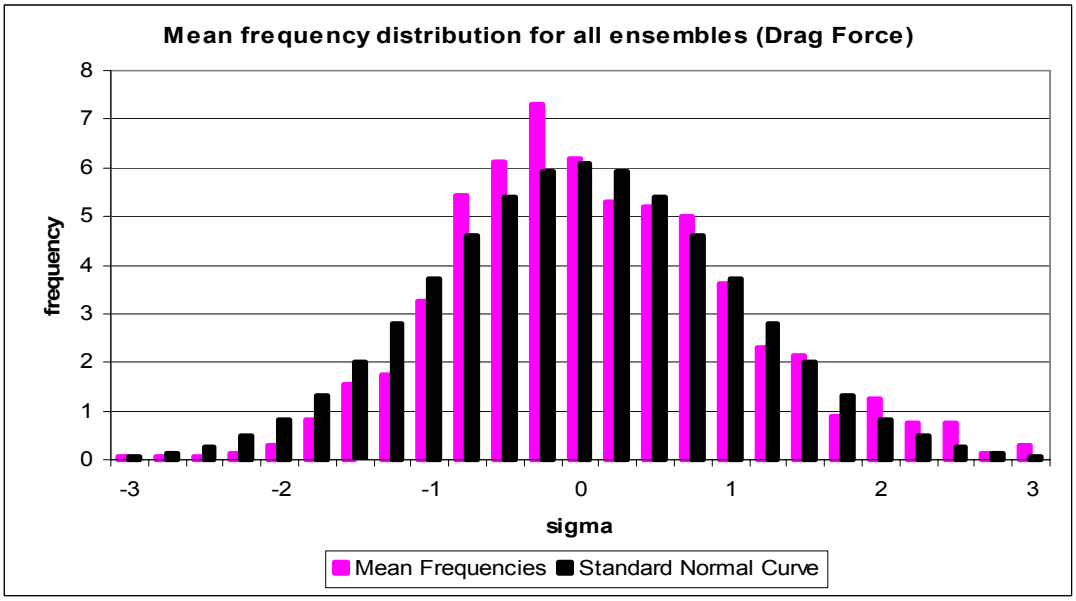

Figure 4-31: Drag Force

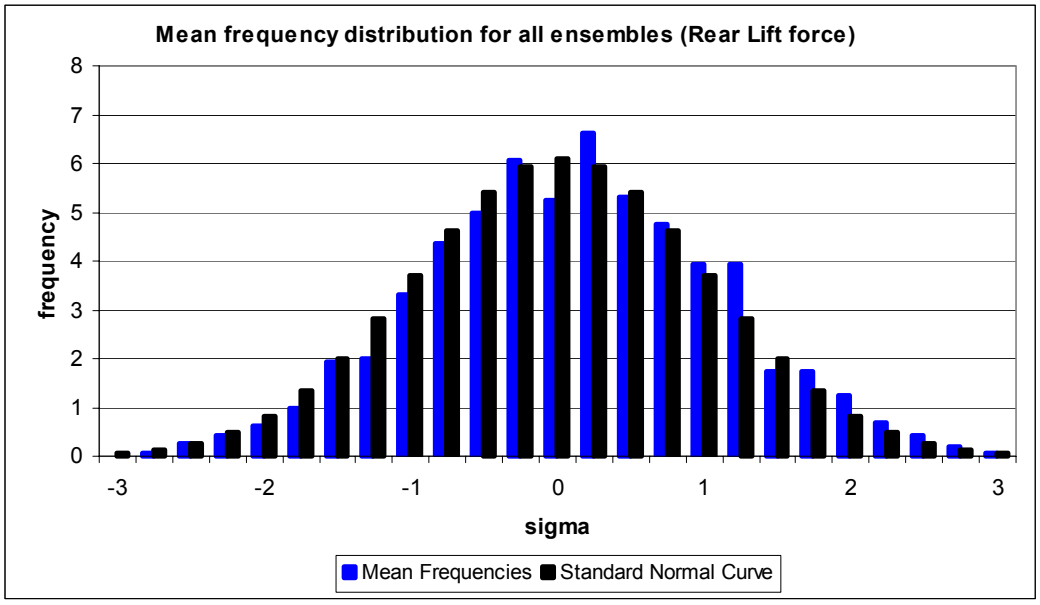

Figure 4-32: Rear Lift force

The statistical coefficients (Standard deviation, mean, median, mode, confidence at 1σ and confidence at 2σ) for each record are given in Table 4-6 for each value of α. In almost all cases, the mean and the median are very similarly valued, thus reinforcing the premise that the estimated mean values are indicative of the actual applied force for each record.

Table 4-5: Summary of confidence levels

	Front	Drag	Rear	Equation
σ	74%	78%	73%	74%
2σ	96%	96%	97%	97%

The integral of equation ***(4-11)*** gives the confidence levels of σ and 2σ as 68.3% and 95.5% respectively, but the use of finite class intervals distorts the count, resulting in the equation giving 74% and 97% respectively as given in Table 4-5. However, the confidence levels of the data correspond well with the requirements of a standardised normal distribution curve and the recorded data can therefore be expected to comply with the confidence levels implied by such a distribution.

	angle of attack (α^0)	1	2	3	4	5	6	7	8	9	10	11	12	13	14	15	16
Front Down Force	σ	5.49	6.14	5.91	6.01	5.61	5.65	7.55	6.35	7.14	6.87	5.93	6.45	6.98	7.16	6.88	6.81
	μ	-13.52	-19.03	-27.52	-35.49	-42.48	-51.95	-59.67	-65.44	-71.04	-78.41	-86.82	-95.25	-104.13	-110.91	-122.62	-124.88
	median	-12.33	-19.27	-27.31	-36.47	-42.85	-51.17	-57.55	-64.77	-70.31	-78.63	-86.68	-94.17	-104.71	-111.93	-122.75	-125.80
	mode	-7.89	-18.99	-30.92	-36.47	-44.79	-56.72	-58.66	-64.21	-71.42	-81.69	-85.30	-94.17	-109.16	-103.05	-127.46	-126.91
	Conf σ	75%	74%	75%	75%	75%	75%	72%	70%	70%	75%	75%	75%	79%	72%	72%	72%
	Conf 2σ	95%	98%	93%	97%	93%	95%	97%	97%	98%	100%	95%	95%	95%	97%	98%	95%
Drag Force	σ	3.23	4.01	3.30	4.33	4.43	3.58	4.27	4.29	4.11	3.49	3.66	3.43	3.47	3.99	4.12	4.00
	μ	1.43	4.52	2.70	1.38	1.61	0.78	0.32	0.23	-1.91	-5.49	-6.23	-9.85	-13.58	-17.13	-22.31	-23.18
	median	0.60	3.98	2.01	1.16	0.60	0.32	0.03	-0.25	-2.22	-5.60	-6.72	-10.39	-13.77	-17.15	-21.66	-22.50
	mode	0.60	3.13	2.57	2.85	5.38	0.32	0.60	-0.25	-2.22	-5.60	-4.19	-7.01	-12.92	-15.46	-21.66	-20.81
	Conf σ	77%	82%	79%	75%	79%	82%	72%	80%	85%	75%	69%	82%	75%	82%	74%	77%
	Conf 2σ	97%	95%	95%	97%	95%	92%	97%	97%	95%	95%	97%	97%	95%	97%	97%	98%
Rear Down Force	σ	3.56	3.71	3.94	4.25	3.98	3.75	4.69	5.39	3.96	5.49	4.77	4.40	4.46	4.99	4.14	4.35
	μ	-9.64	-16.59	-20.64	-24.23	-28.65	-31.99	-39.46	-39.88	-42.83	-48.96	-58.21	-61.73	-59.23	-61.27	-61.93	-59.79
	median	-9.28	-17.06	-20.02	-24.09	-28.91	-31.88	-39.66	-40.03	-42.99	-49.28	-58.17	-62.25	-59.29	-60.77	-61.88	-59.66
	mode	-8.91	-17.80	-16.69	-25.58	-30.76	-32.99	-40.03	-36.32	-44.47	-44.47	-57.06	-63.36	-57.06	-60.40	-66.32	-59.66
	Conf σ	72%	70%	77%	75%	69%	72%	72%	75%	72%	70%	69%	74%	79%	74%	75%	77%
	Conf 2σ	95%	100%	97%	93%	97%	97%	95%	97%	97%	97%	98%	97%	97%	97%	97%	95%

Table 4-6: Statistical coefficients for all records

4.4.8 Experimental Results

Having established that the data correspond with the expectations of a standardised normal distribution, the estimated mean of each record is used as the accepted value of applied force for the three records of each ensemble, i.e. Front Down force, Drag Force and Rear Down force in addition the change in flow velocity recorded from the Valeport flow meter. The estimated means at each value of α then form a dataset for each of the applied forces, and are plotted in Figure 4-33.

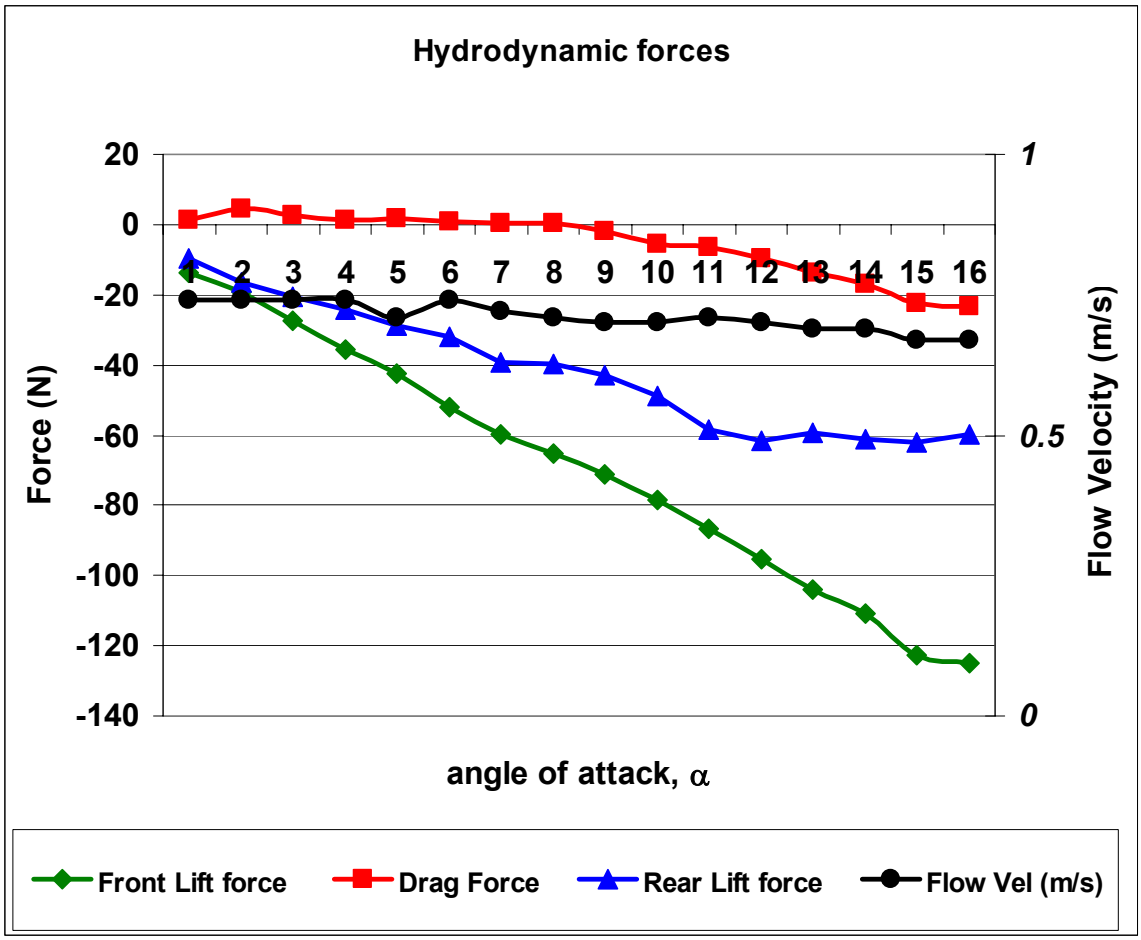

Figure 4-33: Results of the river model test.

The dimensionless coefficients of drag and lift for each α are computed from the results and tabulated alongside the recorded flow velocity immediately upstream of the river test model.

Table 4-7: Lift and Drag coefficients for the river test model.

angle of attack (α), degrees	Flow Vel (m/s)	C_D	C_L	C_L (front)	C_L (rear)
1	0.74	-0.006	-0.096	-0.112	-0.080
2	0.74	-0.019	-0.148	-0.158	-0.137
3	0.74	-0.011	-0.199	-0.228	-0.171
4	0.74	-0.006	-0.247	-0.294	-0.201
5	0.71	-0.007	-0.320	-0.382	-0.258
6	0.74	-0.003	-0.348	-0.430	-0.265
7	0.72	-0.001	-0.434	-0.522	-0.345
8	0.71	-0.001	-0.474	-0.589	-0.359
9	0.7	0.009	-0.527	-0.658	-0.396
10	0.7	0.025	-0.589	-0.726	-0.453
11	0.71	0.028	-0.652	-0.781	-0.524
12	0.7	0.046	-0.726	-0.882	-0.571
13	0.69	0.065	-0.778	-0.992	-0.564
14	0.69	0.082	-0.820	-1.056	-0.584
15	0.67	0.113	-0.932	-1.239	-0.626
16	0.67	0.117	-0.933	-1.262	-0.604

According to [**103**], hydrofoils operating within 2 chord lengths of the surface require that a correction factor be applied to α to obtain a certain value of C_L. For the river test model, the 1st and 3rd (front and rear) hydrofoils are within 0.64 chord from the surface and the 2nd (central) hydrofoils are within 0.35 chord from the surface, and therefore require a correction factor of 1.2 and 1.3 respectively. For example, at α=16°, the average of 2 pairs of hydrofoils at 1.1 and 1 pair at 1.2 is 1.13, therefore the lift obtained at α=16° in the river test should be obtained at α~14° for a submergence ratio >2.

4.4.9 Discussion – River test model

The flow in the Ebrie Burn was fully turbulent, maintained a constant temperature and no changes in colour or turbidity were noted during the period of the experiment. It is therefore reasonable to expect then that the fluid properties remained constant. The flow velocity was measured using an

axial flow pulse counter and averaging over the sampling period for each value of α, thus no information was retained regarding the variation of flow velocity during the sampling period, though the pulse counter is audible in operation and it was obvious that the flow velocity was fluctuating. Fluctuations are readily apparent in the sampled data and it is assumed that these would have been contemporaneous with the flow. Indeed for most ensembles, the correlation between the load force signals is visually apparent, though no attempt has been made to formally correlate the records since it is the estimated means for each record that are required to relate to the mean flow velocity given by the flow meter.

From inspection of Figure 4-33, the front lift force is a linear function of the value of α. There is insufficient subsequent data to extrapolate the apparent change at 16°, which may be the onset of stall, or an anomaly in the data similar to the levelling out of the rear lift force at α = 13°. Notwithstanding this, the front lift force is also effectively linear until α =15°, from which point it remains constant whilst the rate of increase of the drag force grows markedly. The inference of the preceding is that for values of α>15°, the flow leaving the front and/or middle foils is affecting the flow over the middle and/or rear foils, increasing the drag and stagnating the value of the rear lift force. At α=15°, all estimated mean values show a tendency toward level, indicating that α=15° is perhaps the maximum performance limit for this hydrofoil array pattern under the prevailing conditions.

The magnitude of the lift created is clearly a function of α whilst the corresponding decrease in upstream flow velocity is due to the advancing flow stagnation point emanating from the leading edge of the leading hydrofoils. Scaling the recorded data up to a full size Sea Snail, comparing

and Figure 4-16 suggests that using a model velocity of 0.7 m/s is a reasonable assumption, which applied to the Froude scaling gives,

Calculation of Froude scaling for hydrofoil array at full scale

River model scale flow velocity, U	$U = 0.7\,m/s$
River model scale dimension (chord), L	$L = 0.425\,m$
Calculate Fr	$Fr = \frac{U}{\sqrt{Lg}} = 0.343$
Scale factor model, SF	$SF = 7.06$
Calculate full scale length, L_F	$L_F = L * SF = 3\,m$
Calculate full scale flow velocity, U_F	$U_F = U\sqrt{SF} = 1.86\,m/s$

The experimental values can be expected to reflect full scale values in a flow of 1.86 m/s but only at appropriately scaled depth.

Summary of river model experiment

Statistical analysis demonstrates the normal distribution of the acquired data, which is valid for extrapolation to full scale at a flow velocity that can be considered appropriate and realistic for the flow within a tidal stream. The scaled velocity is of the order at which the hydrofoil array is expected to deliver a positional benefit to the full scale Sea Snail structure. However, proximity to the surface will make extrapolation of the results to a fully submerged, full-scale device potentially unreliable.

The experiment demonstrated that for values of α>12°, some interference exists in the flow between the lead hydrofoils and the trailing hydrofoils that increases the overall drag and stagnates the rear lift force, but gives no detail of the forces applicable to each hydrofoil in the array.

4.5 Tow tank testing

The river test model demonstrated the range of forces acting on the complete array at varying angles of attack but gave no indication of the interaction between succeeding foils in the array, and pressure drag was not properly accounted for due the models' proximity to the free surface.

A general solution to these difficulties was identified, and a tow tank model built, using the same hydrofoil units as those employed in the river model test so that dimensional similarity (including surface finish) of the hydrofoils, between the two model tests is unity. The Centre for Marine Hydrodynamics Acre Road tow tank facility at the Department of Naval Architecture and Marine Engineering (Glasgow) [**104**] was made available for one afternoon, courtesy of the Supergen Marine research project, (EPSRC Reference GR/S26958/01) [105].

The use of models in a towing tank is an established methodology, and the previous river test shows that the relatively controlled environment of the towing tank laboratory is to be preferred to river testing. The Acre Rd towing tank is 75 m in length, 4.2 m wide and the depth can be varied to a maximum of about 2.2 m. A wave maker is positioned at one end, and a beach equivalent at the other. No waves were used for this experiment. The towing carriage is a substantial steel 'I' beam structure and runs on steel rails at the sides of the tank, driven by electric motors. The test model is attached to the underside of the carriage which provides the reaction point and datum for the forces applied by the water to the model.

The towing tank is not an ideal environment, but represents a better level of control over many of the variables found in open water. The tow tank does not represent an infinite environment and wall effects may need to be accounted for. Towing a model, even a fully submerged model, will produce waves that radiate away from it as it moves through the water. According to [**106**] a fully submerged hydrofoil will generate a theoretical wave pattern leaving the ends of the hydrofoil at 19.5^{o}. If these waves are reflected back by the tank walls, before the model has moved forward sufficiently, then the

waves will interfere with the model. The dimensions of the model in relation to the tank width (Figure 4-34) shows that the waves created by the model in an undisturbed fluid will not be reflected back to the tank centreline before the model has moved away. Also, the waves created by the leading tubular uprights of the support frame will meet behind the 3rd hydrofoil.

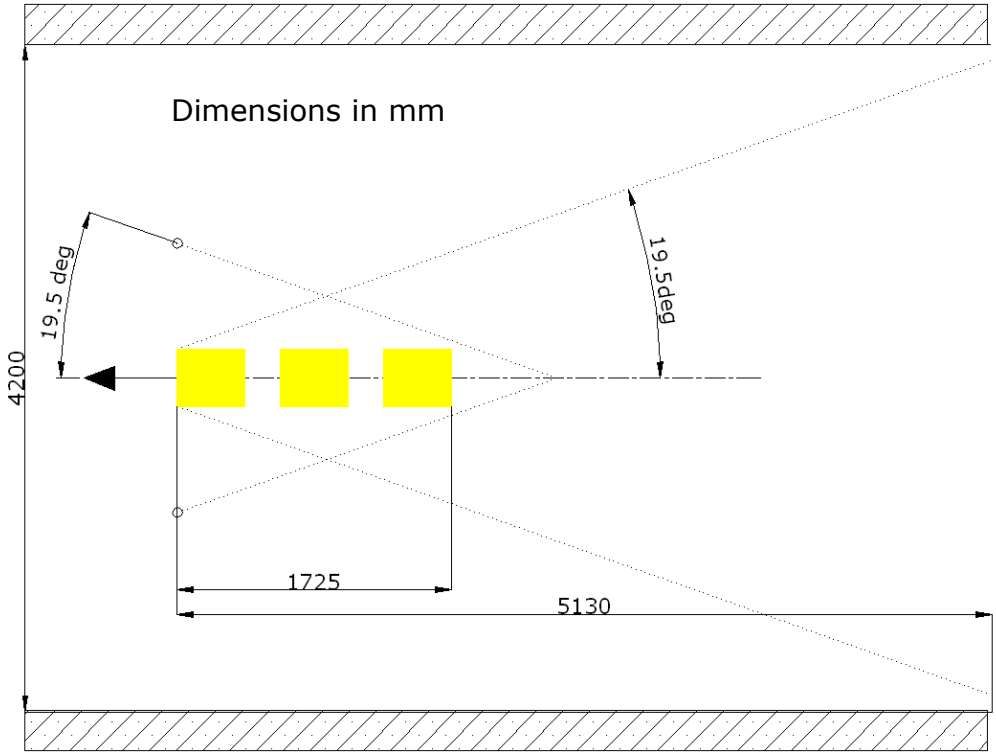

Figure 4-34: Plan view of the model in relation to tow tank width.

The entrained water within the tank will be disturbed by the movement of the model and turbulence will be induced. Provided that sufficient time is allowed to elapse between runs, then the turbulence will have dissipated sufficiently to be of little concern to the hydrofoils.

4.5.1 Scaling and physical similarity

As discussed in Chapter 3, the requirement to avoid Froude scaling, and by implication, enable Reynolds scaling, is that the hydrofoil must be submerged by at least two chord lengths from the free surface.

An additional factor to be considered in using the towing model is represented by the Strouhal number (St) which is applicable for values of $Re<2x10^5$. Vortex shedding, whereby vortices are shed alternately from the upstream side of a round tube is very sensitive to the value of Re and can induce considerable vibration if encountered. The lowest value of Re for the towing model frame tubing (OD=32 mm) is $3.2x10^5$ and therefore is expected to be clear of the maximum applicable for forced vibration.

Calculation of Reynolds scaling for tow tank hydrofoil array

Full scale flow velocity, U	$U = 2\,m/s$
Full scale dimension (chord), L	$L = 3\,m$
Calculate Re	$Re = \frac{\rho UL}{\mu} = 6 * 10^6$
Scale factor model, SF	$SF = 0.142$
Calculate tow tank scale length, L_{ST}	$L_{ST} = L * SF = 0.425\,m$
Calculate tow tank scale flow velocity, U_{ST}	$U_{ST} = \frac{\mathrm{Re}^* \mu}{\rho L_{ST}} = 14.1\,m/s$

Thus for Reynolds scaling, if a maximum towing carriage velocity of 3.0 m/s is assumed (given the tank length and allowing for acceleration/deceleration times) then results will only be indicative of full scale conditions at 0.43 m/s, i.e. 0.143 m/s full scale equates to 1 m/s towing carriage velocity. Whilst this is by no means ideal, it is also not unusual in the field of hydrodynamics model testing that accurate scaling requires substantial facilities capable of high speed flows.

Continuing from the discussion at 4.3.1, an alternative view can be taken that, since the Reynolds Number represents the ratio of inertia force to viscous force, then at high values of Re, the viscous forces are negligible in comparison with the inertial force, i.e. in this case at full scale $6x10^6$:1 and at model scale $8.5x10^5$:1. Since both values of Re are well into the turbulent region and therefore the difference between laminar and turbulent flows

avoided, it is found that the effect of friction is much less important than that of inertia [**107**].

A further semi-empirical method detailed in [**108**] uses the concept that any one of the dimensionless coefficients associated with fluid mechanics (Re, Fr, Ma, We) are all ratios between the inertia force and one other, with the third side of the force polygon being made up of the (as yet) unknown pressure forces. The total resistance is made up of skin friction (R_{SF}) and pressure force (R_{PF}),

$$R_{total} = R_{SF} + R_{PF}$$

where it is considered that the skin friction is entirely dependent on Re, but as shown, it is not possible to keep Re equivalence within the capabilities of the towing carriage. However, by maintaining Fr equivalence, it is postulated that the residual resistance will continue to be proportional (at some level) from the model to full scale, that the frictional resistance can be estimated from calculation of Re for the full scale, and that the total resistance of the full scale device can be estimated from the sum of R_{SF} and R_{PF}. The process is demonstrated under section 5.4.

4.5.2 Experimental background

The interaction of the hydrofoils and their associated wake effects influences the overall effectiveness of the concepts self-fixing capabilities, and the hydrofoil array itself requires significantly more work to identify its optimum spatial relationship. The objective of the tow tank test is to observe the interdependent behaviour of the hydrofoils when operating as part of an array as opposed to stand-alone.

Cascaded aerofoils are common in rotodynamic machinery, and cascaded hydrofoils are found on high-speed surface craft, but both are of limited application to this work, since the former are usually operating in compressible flows and the latter are close to the free surface. In addition, published material [**109**] generally refers to cascades as resembling steep steps or vertical stacks, whereas the Sea Snail application is more accurately described as tandem [**110**].

Applied forces

With the resources available, there was only sufficient time for testing at two values of α; 0°, to establish the zero lift resistance of the hydrofoils, and approximately 15° to emulate the full scale Sea Snail arrangement.

Based on previous data from the river test model, C_D and C_L at α=15° will be of the order of 0.1 and 1.2 respectively. This suggests that a down force of approximately 700 N and a drag force of approximately 70 N will be applied to the hydrofoils at 3 m/s.

4.5.3 Experimental equipment design

The tow tank model is easily dismantled and portable in three pre-assembled modular units to avoid detailed recalibration on assembly.

Figure 4-35: Tow tank hydrofoil array

Each individual module comprises one hydrofoil mounted on its shaft, with adjustment for α and attachment points for load sensing cables. An upright tube at each end of the hydrofoil shaft and a cross tube at the top completes the module and carries the load cell attachment.
The design minimises the support frames interference with the flow and allows location of the load cells above the waterline, whilst rigidly supporting the hydrofoils at a submergence of at least 0.85 m, (2 x chord length).

The test rig (shown in Figure 4-35), allows adjustment of α from zero to a maximum of 35^{o} for each hydrofoil, independent of the other hydrofoils. The lift and drag forces applied to the hydrofoils are transmitted to load cells (as used in the river test model) by means of cables similar to those used for cycle braking systems. The frame is assembled from 32 mm x 4.5 mm aluminium alloy tubing and commercially available fittings secured with M12 hexagonal-socket headed setscrews. Engineering drawings of the machined components are given on the attached CD, and assembly drawings are given on the following pages.

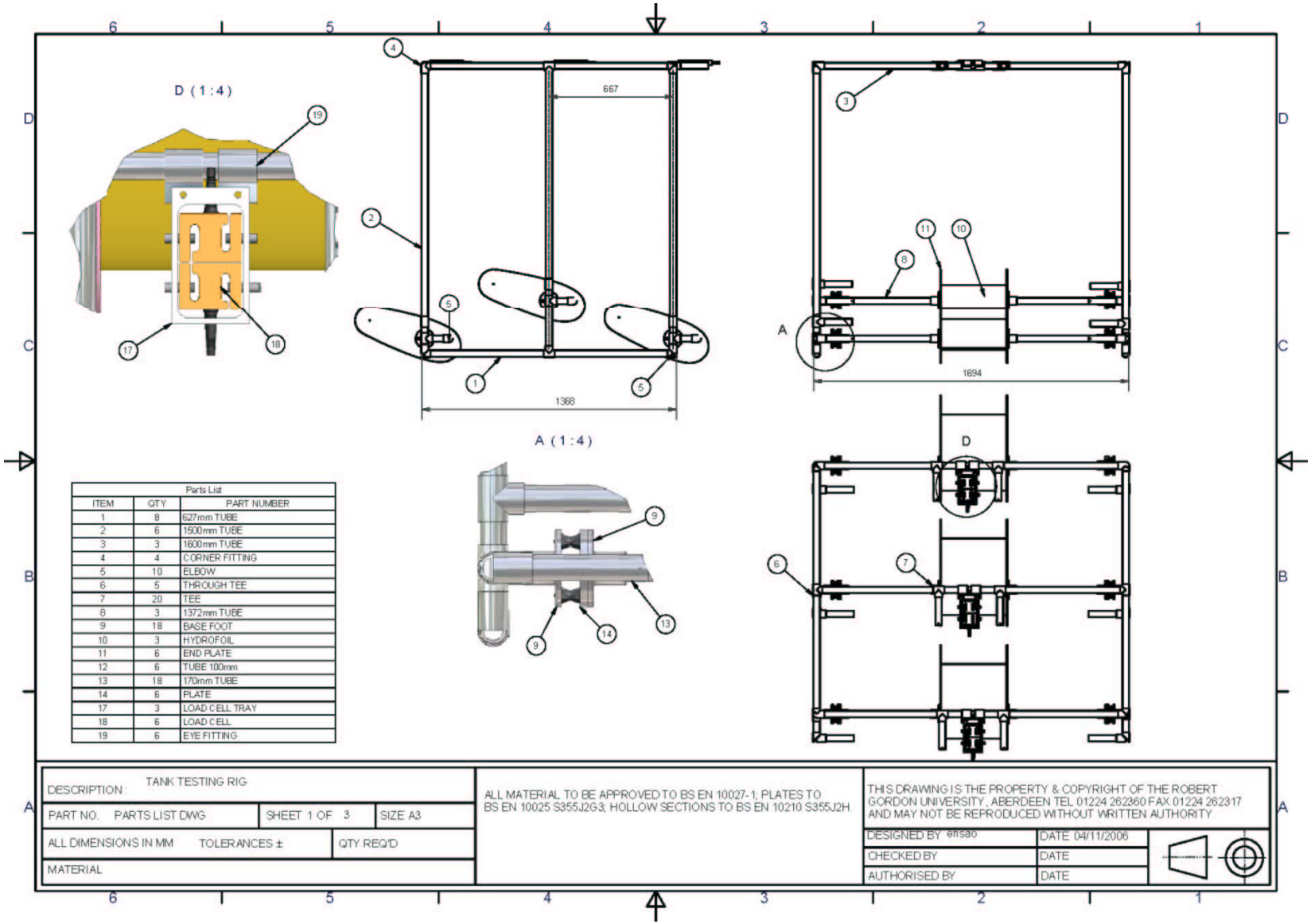

Figure 4-36: Parts list and assembly detail, tow tank model

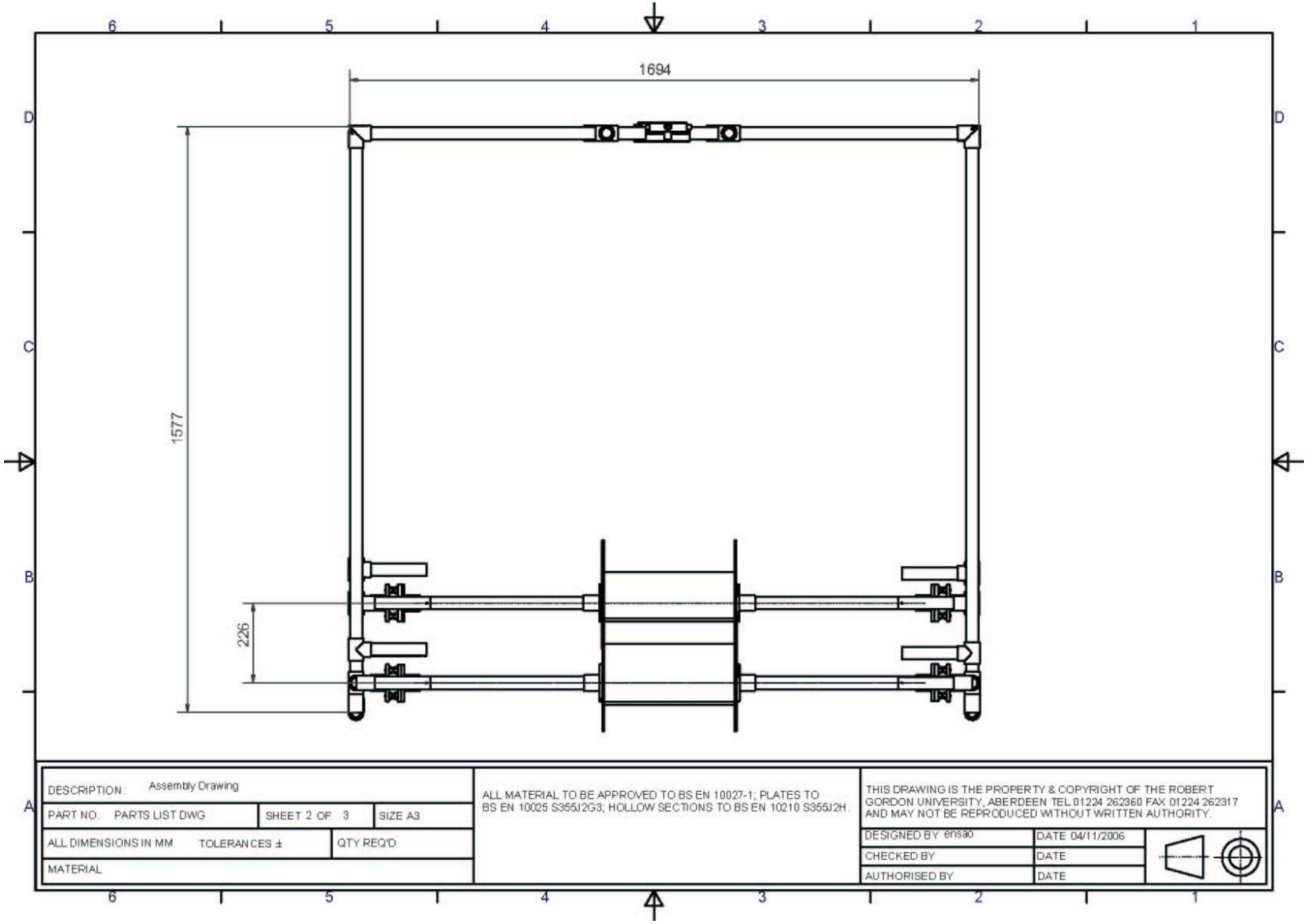

Figure 4-37: Assembly drawing, tow tank model, front view

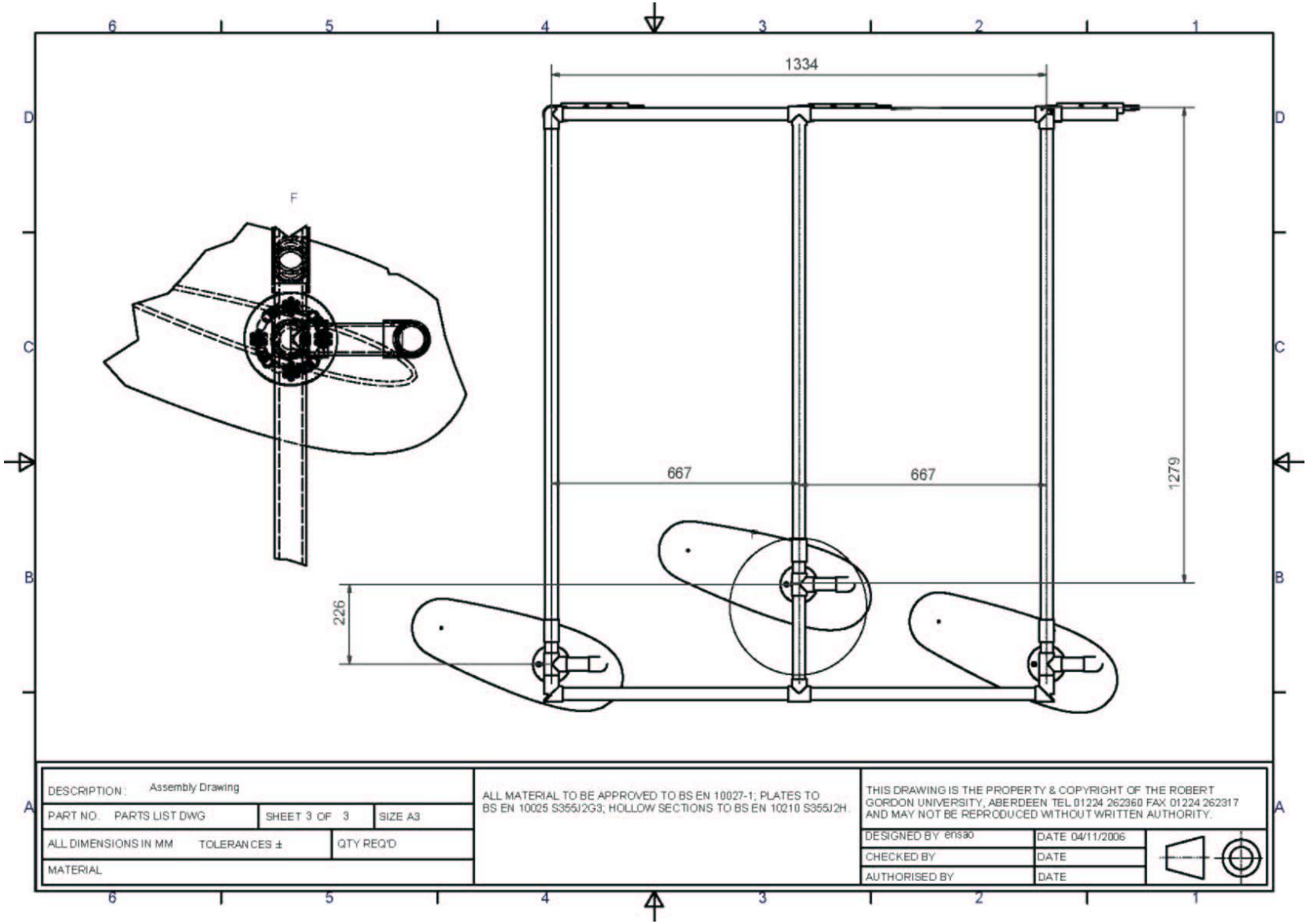

Figure 4-38: Assembly drawing, tow tank model, side view

The frame is inherently stiff chordwise with the hydrofoils and spanwise in a horizontal plane, and is diagonally tensioned spanwise perpendicular to the flow, with 1.5 mm diameter steel cables.

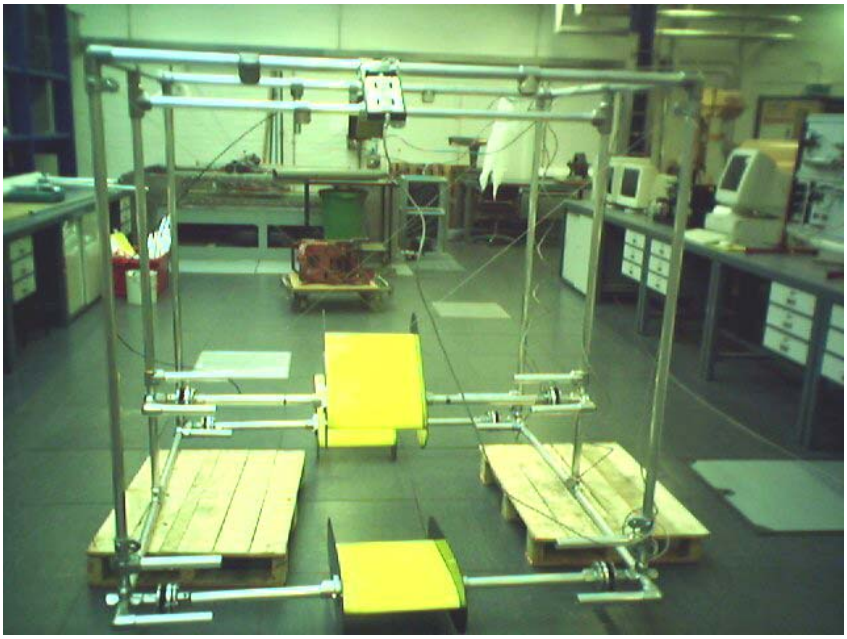

Figure 4-39: Assembly of the tow tank model

The hydrofoils are fixed to horizontal lengths of aluminium tubing, isolated from the main frame by 4 rubber mountings at each end, to minimise any frame stresses being transmitted to the hydrofoils and possibly distorting the load cell readings. The bushes are attached to slotted plates that permit adjustment of α independently of the frame structure. The load cell cable outer sleeves are located in short stub tubes approximately 100 mm from each hydrofoil shaft centreline, and the inner (force transmitting) cables are passed through drillings at each end of the hydrofoil support shaft, with the drag sensing cables acting horizontally and the lift force sensing cables acting vertically, as shown in Figure 4-40. The red dashed arrow indicates the lift force outer sleeve, the black dotted arrow indicates the lift force sensing cable and the blue solid arrow indicates the drag force sensing cable.

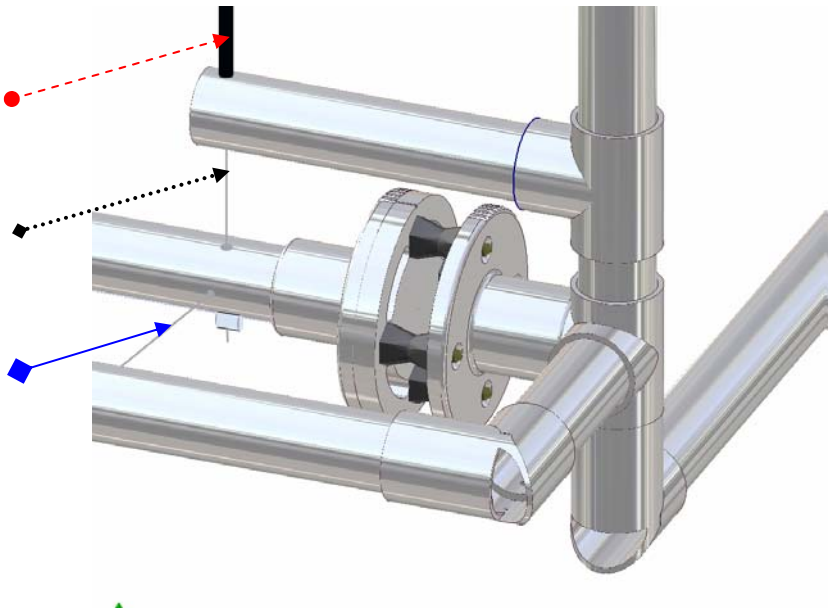

Figure 4-40: Foil mount assembly, showing cable alignment.

The hydrofoils are identical to those used in the river test model but with the addition of polystyrene end plates sized as per the appropriate theory outlined in Chapter 3.

Figure 4-41: Hydrofoil with additional end plates.

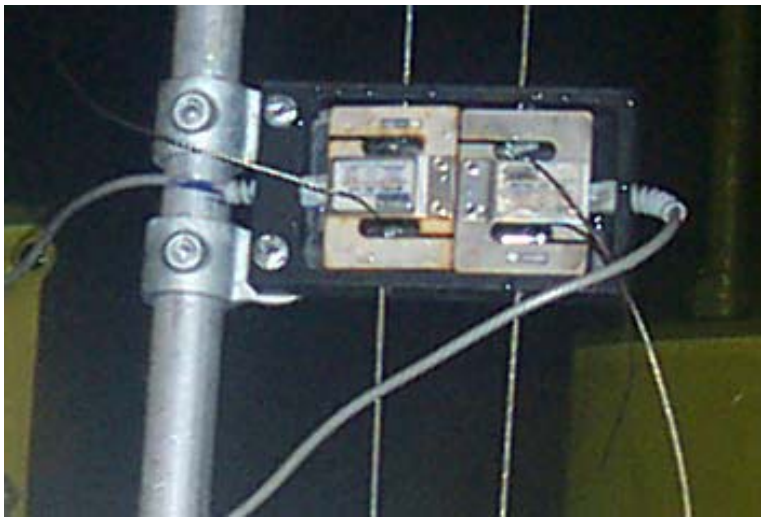

Figure 4-42: Close up of load cells mounted on the frame.

The load cells are supported in nylon trays at the top of the frame, clear of the water line, as the IP67 rating infers that the load cells are water resistant to 1 m but are not suitable for long-term immersion, which requires IP68 rating. The two drag sensing cables from each end of the hydrofoil mounting shaft are connected to opposite sides of the same load cell, thereby measuring the total drag force applied to the shaft with one load cell. The lift force sensing cables are similarly connected to a single load cell. Thus a pair of load cells mounted on each modular frame can remain calibrated to the hydrofoil on that frame during transportation and re-assembly.

The entire frame was assembled in the laboratory, load-tested and calibrated using 245 N weights (25 kg mass). The return to zero is found to be very sensitive to cable routing, and silicone fluid lubrication between the force sensing cables and their outer sleeves, coupled with greater attention to bend radii reduces the error to an acceptable percentage of the expected applied force. The Tedea Huntleigh 615 load cells used in the tow tank rig have a standardised full scale output consistent to within 0.1%, therefore (as for the river test model) the data is on a consistent scale across all six load cells with no requirement for calibration between load cells.

The tow tank model data acquisition unit was a Datascan RS7321 unit similar to the unit used for the river test. The Datascan unit was powered using a

240 V to 12 V 500 mA switch mode power supply, and the load cells were powered with a purpose built, 4 output, 12 V DC controlled voltage unit to ensure a consistent voltage feed to the Wheatstone bridges.

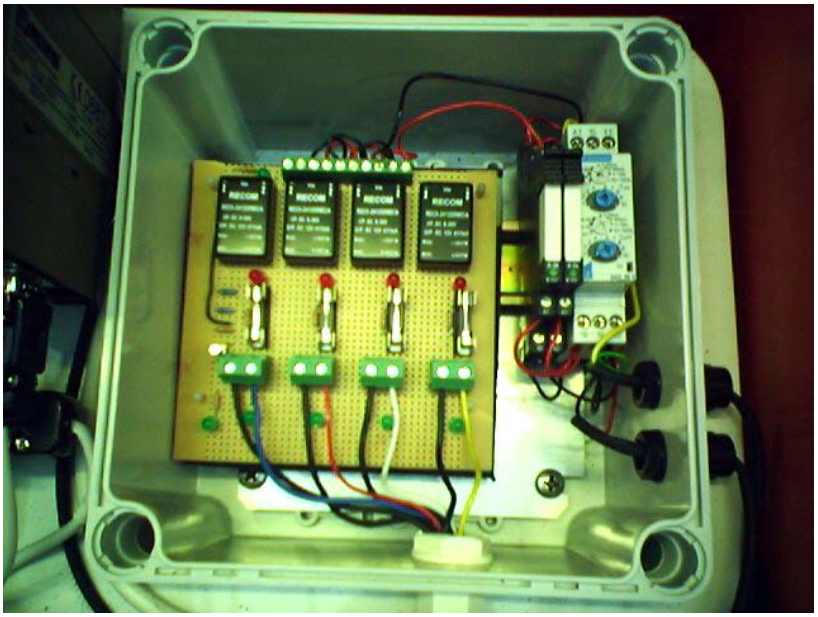

Figure 4-43: Four output 12 V DC regulated voltage supply

Table 4-8: Calibration data for towing model

Average differences	0-245	68.75	70.00	67.00
	245-490	65.75	69.50	68.25
Average scales	0-245	3.56	3.50	3.66
	245-490	3.73	3.53	3.59
Overall difference		68.21		
Overall scale		3.59		

Each hydrofoil was loaded 4 times in turn with 25 kg and 50 kg (245 N and 490 N respectively) and the differences recorded. The average signal change between 0 N-245 N and 245 N-490 N for each hydrofoil therefore reflects the signal value of the applied force, i.e. 68.21 and this value therefore represents an applied force of 245 N, giving a scale factor of 245/68=3.6.

4.5.4 Experimental procedure

The testing was undertaken at The Centre for Marine Hydrodynamics Acre Road tow tank facility on the afternoon of Monday 11th December 2006, with the assistance of Charles Keay and his staff.

Figure 4-44: Towing model installed at the Acre Road facility.

The towing model was assembled and the hydrofoils individually tested for lift force response using the same 25 kg mass as was used for the initial calibration. Installation was challenging due to the overall frame dimensions and the towing model was awkward to handle, though not heavy. The towing model was clamped to the underside of the towing carriage (Figure 4-45 and Figure 4-46) and the hydrofoil end plates aligned with the streamwise axis of the carriage frame, to ensure correct alignment with the flow as seen by the hydrofoils. The first run was performed with the hydrofoils set at α=0° and a carriage velocity of 1 m/s to obtain a baseline drag force applicable to each hydrofoil. Time constraints restricted the subsequent testing to taking

measurements at α=15° for carriage velocities of 1.0, 1.5, 2.0, 2.5 and 3.0 m/s.

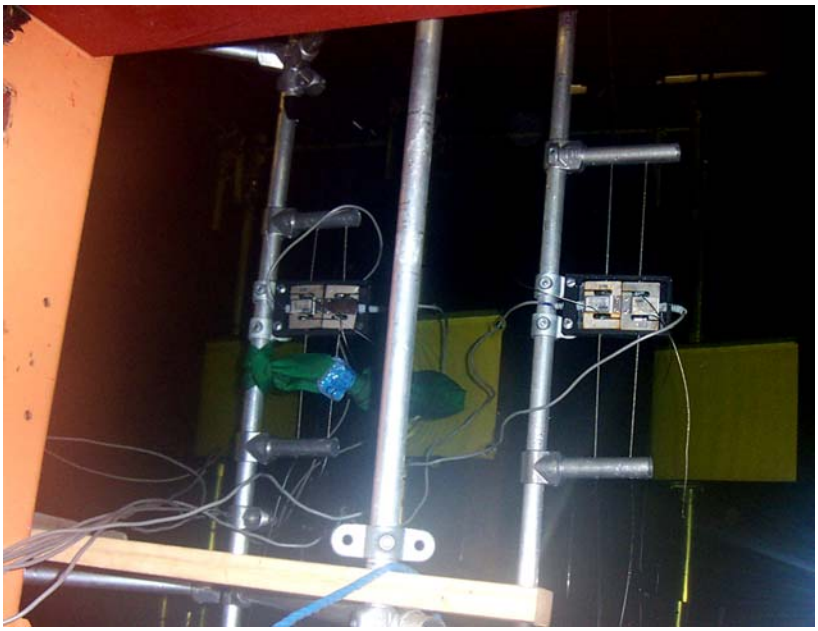

Figure 4-45: Tow tank test rig installed (viewed from above).

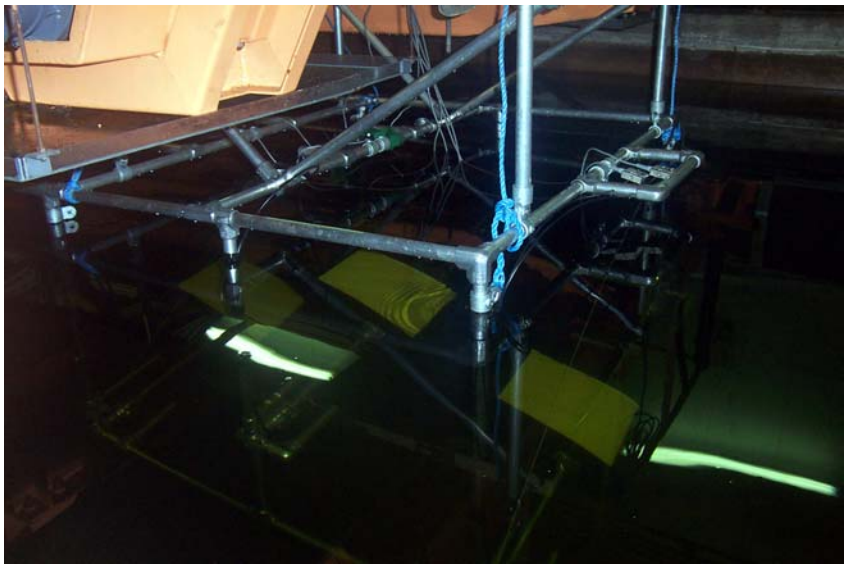

Figure 4-46: Towing test model mounted on the towing carriage

The water level in the tow tank was set at 2.1 m, which gave a submergence depth for the uppermost hydrofoil of 1m (i.e. >2 x chord), thereby avoiding the dissipation of energy in wave generation. The RS7321 unit was initiated

prior to the commencement of each run so that the acceleration component of the carriage would be observable, and the consistent steady velocity period would be extractable from the complete record during data processing. After each run, the carriage was returned to its start position and approximately 5 minutes allowed between runs for the tow tank water to settle. Since the hydrofoils were operating at submergence >0.85 m, surface waves were not important, but the water was observed for any tendency to circulate, which could have affected the relative velocity of the hydrofoils and the water. None was noted. The secure attachment of the device was checked after each run and a visual check made of the hydrofoils' position and integrity. Data were sampled at 4 Hz intervals and a typical run length of the towing carriage was approximately 60 m from start to stop. Starting at 1 m/s, successive runs increased in velocity by 0.5 m/s up to a maximum of 3 m/s, resulting in datasets of different lengths for the increasing velocities.

The towing model was removed from the tank and a final confirmation taken of hydrofoil position and structural integrity prior to dismantling the towing model and returning to Aberdeen.

4.5.5 Data processing

The real-time data were recorded in CSV files by the RS7321 unit onto an ASUS laptop PC, with a new file being created for each run. The complete, original recorded files are given on the attached CD.

The principal data of interest are the data recorded at a constant carriage velocity (shaded green in Figure 4-47), with established hydrofoil circulation for each run, neglecting the acceleration (shaded buff in Figure 4-47) and deceleration phases of the towing carriage. Inspection of the data shows that the carriage achieves this constant velocity for approximately 30 m over the duration of the test, but the increase in velocity for each run reduces the number of data samples from 30 at 1 m/s to 10 at 3 m/s. For every run, there are measurements of lift and drag forces applied to each hydrofoil, (numbered 1, 2 and 3 where hydrofoil 1 is the lead), generating an ensemble of six records, at a sampling frequency of 1 Hz. The data is assumed at the

outset to comply with a standardised normal distribution, and this is subsequently shown to be an appropriate statistical approach. For consistency, the same spreadsheet and coded routine applied to the river test model was used and the mean, minimum, maximum, standard deviation, mode and median are found for each record.

Time	1.17E+09					
Filename	towtank.cnf					
	Tow					
Recorder	Tank					
Time	Lift 1	Drag 1	Lift 2	Drag 2	Lift 3	Drag 3
1.17E+09	-74.29	-216.96	-395.96	-393.08	-196.11	-163.85
1.17E+09	-74.29	-216.74	-395.96	-393.3	-196.33	-164.07
1.17E+09	-60.1	-217.63	-396.18	-393.08	-196.11	-164.07
1.17E+09	-60.1	-218.07	-395.74	-392.63	-196.11	-164.07
1.17E+09	-74.29	-208.53	-397.52	-406.83	-192.34	-163.4
1.17E+09	-74.29	-218.73	-407.28	-419.47	-191.45	-162.52
1.17E+09	-74.29	-219.62			-186.13	-159.63
1.17E+09	-88.47	-225.39			-183.69	-155.64
1.17E+09	-74.29	-220.07	-375.33	-430.12	-185.02	-150.32
1.17E+09	-88.47	-184.8	-350.05	-416.81	-193	-138.56
1.17E+09	39.35	-116.04	-254.45	-390.86	-158.18	-115.49
1.17E+09	124.46	-64.13				-62.26
1.17E+09	153	-51.27				-23.22
1.17E+09	153	-47.94	-184.58	-322.1	-61.25	-10.13
1.17E+09	167.18	-44.61	-181.03	-322.76	-57.03	0.73
1.17E+09	181.36	-41.06	-174.82	-318.55	-51.71	12.93
1.17E+09	181.36	-39.07	-175.48	-319.66	-53.04	16.92
1.17E+09	181.36	-38.18	-173.93	-321.43	-49.94	18.92
1.17E+09	181.36	-42.39	-169.72	-317	-45.5	22.46

Figure 4-47: Sample data ensemble header for U=2 m/s

The standardised normal distribution is found for each record at each velocity as previously discussed, and the confidence levels (Table 4-9) of the data are found to represent a reasonable fit to the normal distribution curve (Figure 4-48), though the tendency is for values to be above average.

Table 4-9: Average confidence levels for each hydrofoil for all velocities

	Lift 1	Drag 1	Lift 2	Drag 2	Lift 3	Drag 3	Average
σ	98%	70%	75%	69%	77%	78%	78%
2σ	98%	100%	95%	100%	98%	100%	98%

The reference standardised normal distribution as given by ***(4-11)*** is again used as the comparator.

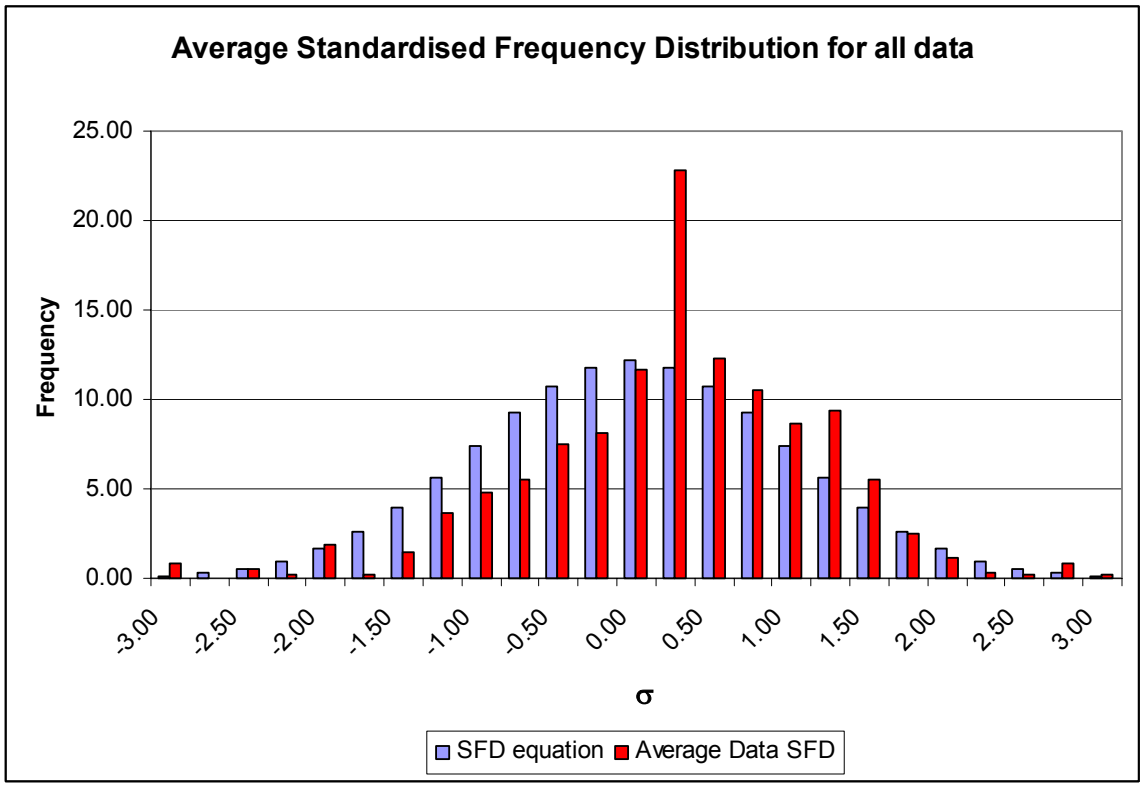

Figure 4-48: Standardised normal frequency distribution for towing model

The towing model necessarily produces less data points than the river test model and it is this that renders the standardised frequency distribution slightly unbalanced. The estimated mean and the median of each record are, for most of the data, very similarly valued with a maximum variance of approximately 2%, thus suggesting the data is well centred about the estimated mean. The SFD equation ***(4-11)*** gives confidence levels that data will fall within σ and 2σ as 74% and 97% respectively for randomly distributed samples. The towing model data offers comparative confidence levels for σ and 2σ as 75% and 96% respectively, thus the data can be accepted as being representative within the requirements of the standardised normal distribution curve.

During static load calibration of the rig it was found that the hysteresis effects generated by friction in the load sensing cable system tended to

prevent the load cells reliably returning to their zero load position, thereby shifting the zero-crossing point. This was essentially random in its nature and could not be reduced to a satisfactory zero band unless an external returning force was applied to the hydrofoil. It was additionally found that if the hydrofoil was subjected to a small fluctuating dynamic force, then the load cell response would return to within a reasonable approximation of its original starting point. From this, it was postulated that, when subjected to the dynamic fluctuations of a relative flow, the system would self-return to a baseline position whilst the towing carriage returned to its start position. Numerically, this position is represented by taking an average of the signal values for each load cell at the lead-in (shaded yellow in Figure 4-47) of each run and subtracting the result from the data signal at each point.

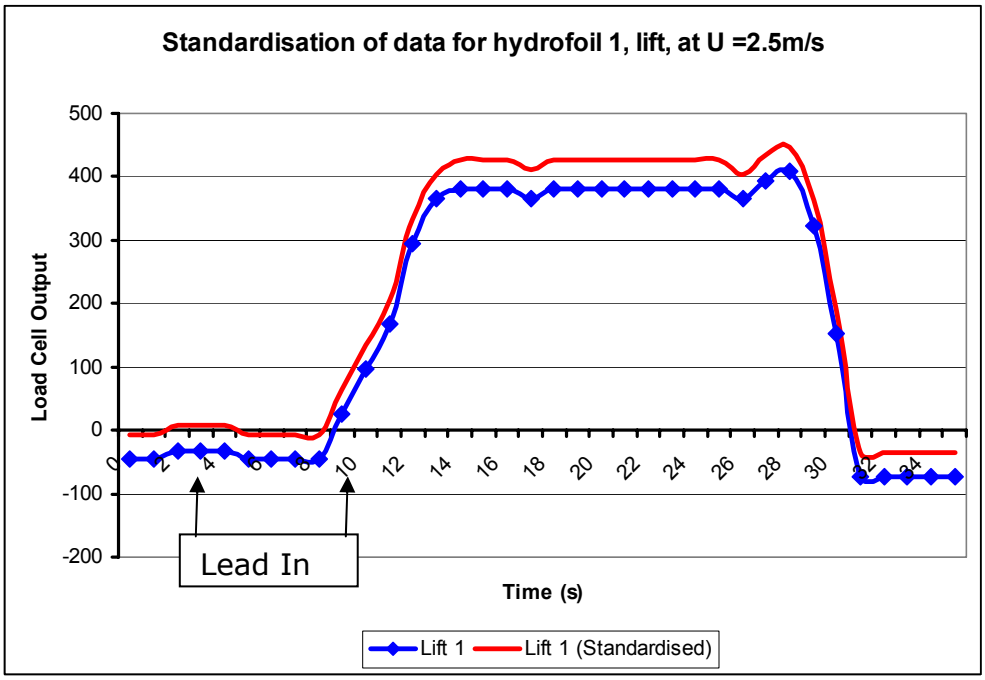

Figure 4-49: Standardisation of data.

As is shown in Figure 4-49, the data is shifted along the ordinate and the estimated mean value of the constant velocity section of the signal is standardised as accurately as possible relative to zero. To accommodate the lift and drag forces applied to the hydrofoil tube and attached fittings (that are measured by the load cells but are not dependent on the value of α), the

standardised data for the forces applied at $\alpha=0^o$ and U=1 m/s (Figure 4-50) are used to extrapolate correction factors for higher values of U. The C_D for the hydrofoil tube and fittings (based on $Re= 3.2x10^4$ for 32 mm OD. tubing) is given by [**111**] as approximately 1.2 in a flow of 1 m/s.

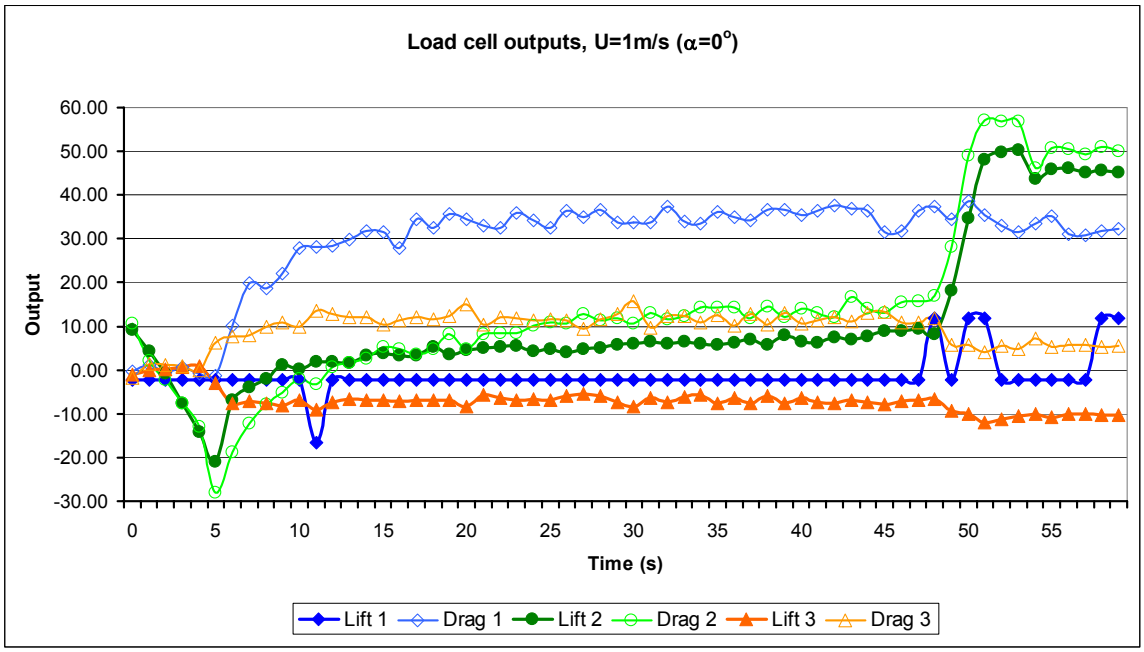

Figure 4-50: Load cell outputs for U=1 m/s and $\alpha=0^o$

Subsequently, for values of U>1.5 m/s, where $Re>5x10^6$, the value of C_D can be taken as 0.65 for an infinite cylinder (i.e. length/diameter ratio >5), perpendicular to the flow.

Table 4-10: Lift and Drag corrections

Corrections for hydrofoil support structure lift and drag forces						
	Lift 1	Drag 1	Lift 2	Drag 2	Lift 3	Drag 3
Mean (1 m/s)	-2.36	34.58	5.48	10.50	-6.82	11.77
Mean (1.5 m/s)	-2.88	42.14	6.68	12.80	-8.32	14.34
Mean (2 m/s)	-5.12	74.91	11.88	22.75	-14.78	25.49
Mean (2.5 m/s)	-8.00	117.05	18.57	35.54	-23.10	39.83
Mean (3 m/s)	-11.52	168.55	26.74	51.18	-33.26	57.36

4.5.6 Experimental results

The experimental results for α=15^{o} are presented for each carriage velocity U sequentially, commencing with U=1 m/s using a pair of plots for each value of U.

The output from the load cells, via the data acquisition unit, is calibrated such that each gradation represents 1 N of force. Prior to installation, each load sensing cable was pre-loaded to ensure that no slack remained in the cabling system. As a result, each load cell channel data value was offset by an unknown but consistent amount, which is later removed by standardisation in the data processing stage, as described. Thus the following full data plots, titled "Load cell outputs" for each value of U from 1 m/s to 3 m/s, show the correct scale of each measured force, but not the correct relative magnitudes, hence the ordinate of each plot is labelled only as 'Output'. These plots contain the full records for each run up to a maximum of 60 seconds.

The data plots titled "Standardised Force Magnitude" show the correct values of applied force for each load cell and thereby, their correct relative magnitudes. The "Standardised Force Magnitude" plots only hold the data for the period during which the carriage is assumed to be maintaining a steady velocity, since this is the consistent data that will allow the calculation of consistently applied forces and therefore, the appropriate values of C_D and C_L for each value of U.

U=1 m/s

At U=1 m/s, (Figure 4-51), the start of the run is seen at t=3 s and the lift and drag forces applied to the 1st and 3rd hydrofoils follow the acceleration of the carriage and are both steady from t=10 s.

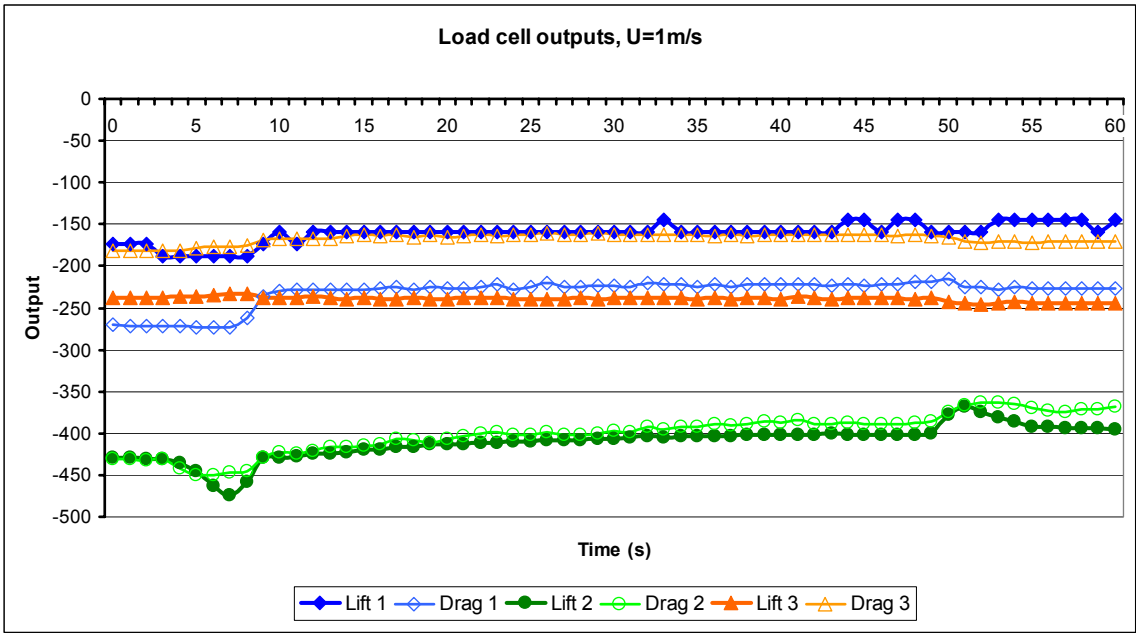

Figure 4-51: Load Cell Outputs for Umax=1 m/s

The forces applied to the second hydrofoil both reduce as the carriage accelerates from rest, before increasing sharply to follow a small but constant increase over the period of constant velocity from t=10s to t=46s . At t=48s where the towing carriage is decelerated to a halt, the lift and drag forces on the 1st and 3rd hydrofoils reduce marginally, whilst those applied to the 2nd hydrofoil both increase sharply before settling again.

Examination of data from t=10 s to t=40 s (Figure 4-52) shows the fluctuations in greater detail and the consistent rise in lift and drag forces applied to the 2nd hydrofoil, from 0 N to 26 N and 0 N to 39 N respectively, is clearly visible. The lift force on the 1st hydrofoil is effectively constant at 24 N whilst the accompanying drag rises from 6 N to 16 N over the period. For the 3rd hydrofoil, both lift and drag forces are constant at around 6 N.

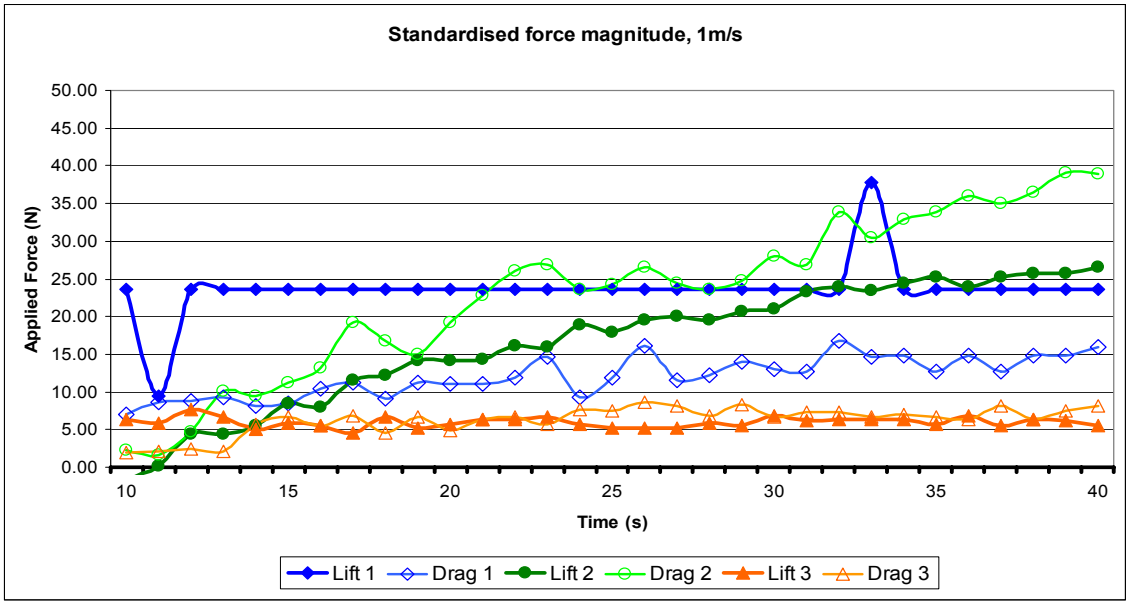

Figure 4-52: Force magnitudes at U =1 m/s

U=1.5 m/s

At U =1.5 m/s (Figure 4-53) the run starts at t=7 s and the 2nd hydrofoil begins to respond immediately but in the opposite sense to that expected, repeating the starting pattern seen for U=1 m/s.

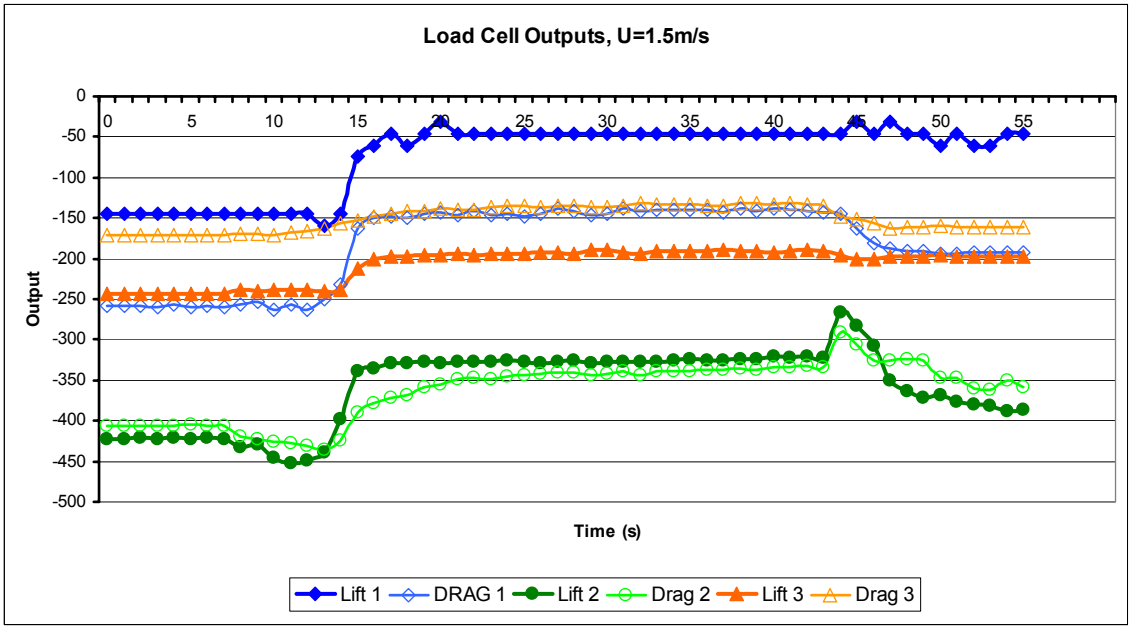

Figure 4-53: Load cell outputs for Umax =1.5 m/s

Subsequently, both lift and drag forces build up rapidly from t=13 s with the increase in drag lagging the increase in lift. The response of the 1st and 3rd hydrofoils lags that of the 2nd hydrofoil by about 1 s. The 1st hydrofoil is oscillatory in its starting response and the lift force continues to oscillate until t=21 s when lift is fully established. The 3rd hydrofoil generates less lift force and drag force than the 1st and 2nd hydrofoils, and is much less steep in its response to the velocity change. At t=42 s when the carriage is decelerated, the 2nd hydrofoil responds with a sharp increase in both lift and drag, before settling again, whilst the 1st and 3rd hydrofoils do not exhibit the same response. The run ends at t=50 s.

The time taken for the towing carriage to cover the 30 m at a constant velocity reduces from 30 s at 1 m/s to 20 s at 1.5 m/s and the window of

constant velocity data (Figure 4-54) therefore reduces to 20 s also. The lift forces generated by the 1st and 2nd hydrofoils are constant at around 105 N and 95 N respectively, but the 1st hydrofoil experiences greater drag force (~75 N) than the 2nd hydrofoil (~60 N). The 3rd hydrofoil maintains a consistent lift force of ~60 N and a drag force of ~20 N. All applied forces are more constant at U=1.5 m/s than was the case at U=1 m/s.

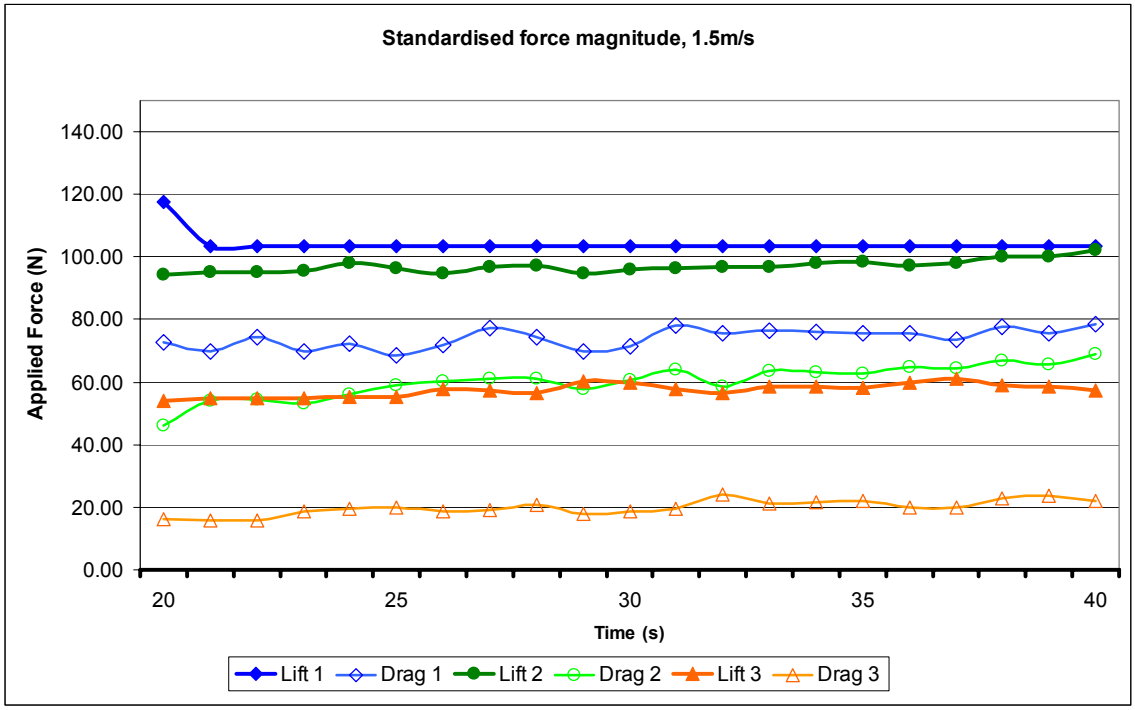

Figure 4-54: Force magnitudes at U=1.5 m/s

U=2 m/s

For U=2 m/s (Figure 4-55) the run starts at t=5 s and the 2nd hydrofoil is the first to respond, though the rate of response is less steep than the 1st hydrofoil which takes a further 2 seconds to begin to develop drag forces, and 3 seconds to initiate lift forces.

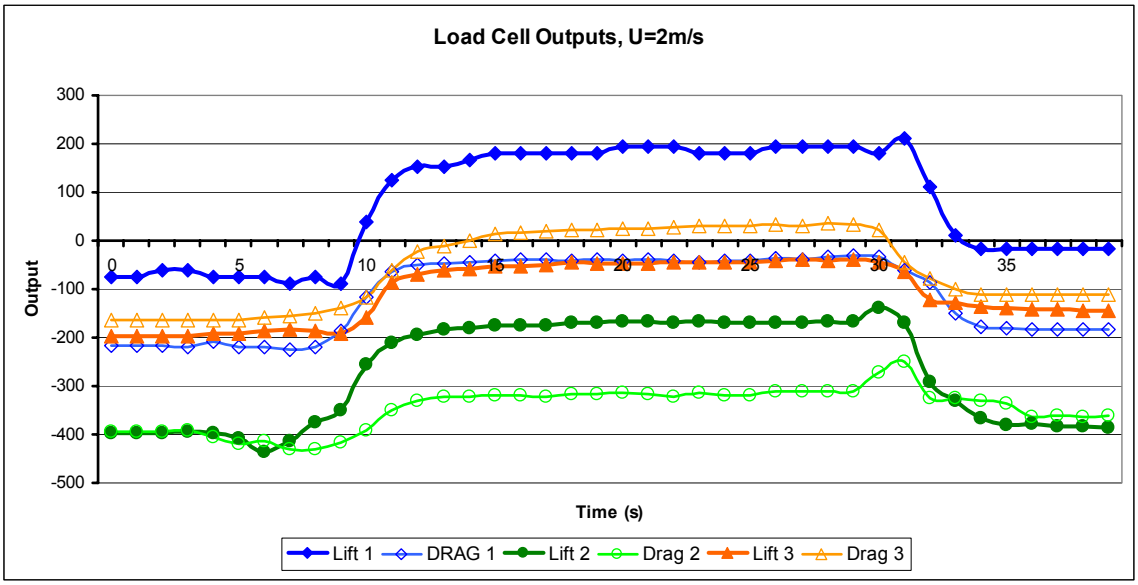

Figure 4-55: Load cell outputs for Umax=2 m/s

The 3rd hydrofoil begins to develop both lift and drag forces at t=6 s and tends to follow the same rate of increase as the 2nd hydrofoil. All hydrofoils have fully established lift force and drag force at t=14 s and maintain a steady response until the carriage is decelerated at t=29 s, at which point, the 2nd hydrofoil, consistent with previous runs, generates a sharp rise in both lift force and drag force before falling away. The 1st hydrofoil exhibits a similar but less marked response after a 1 s lag, but only in the lift force. The run ends at t=35 s.

At U=2 m/s the data window is now reduced to 15 s in length (Figure 4-56). The lift force generated by the 1st hydrofoil is consistent at around 250 N whilst the corresponding drag force is 100 N. The 2nd hydrofoil produces less lift force (210 N) but also less drag force (~60 N) whilst the 3rd hydrofoil generates equivalent magnitudes of lift force and drag force at ~160 N. All of the results are steady within the window of constant velocity.

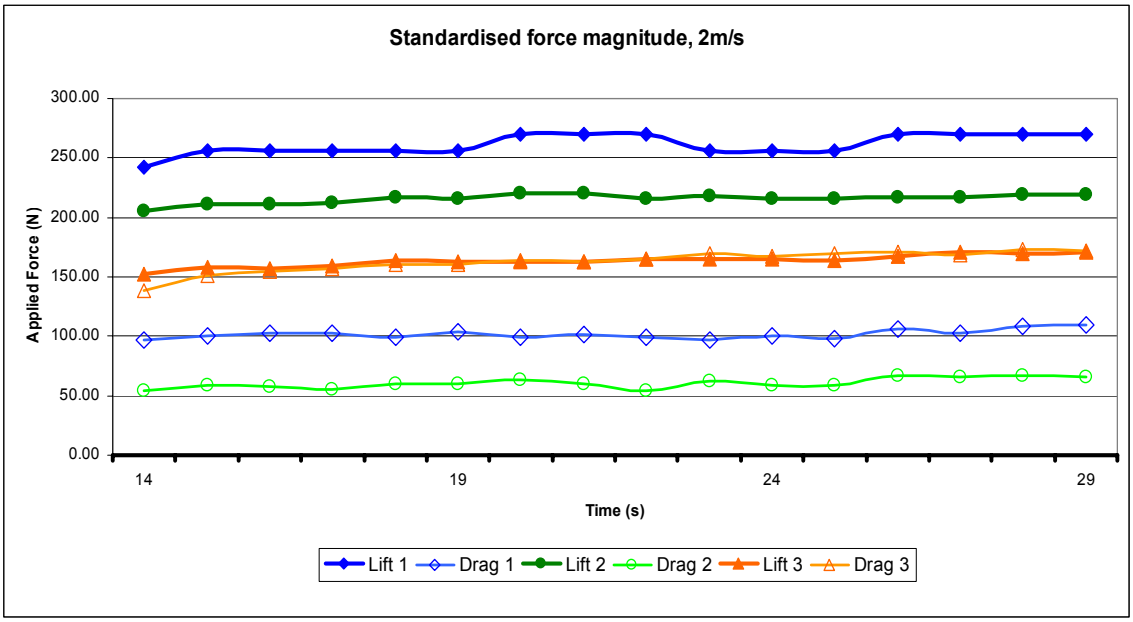

Figure 4-56: Force magnitudes at U=2 m/s

U=2.5 m/s

For U=2.5 m/s (Figure 4-57) the run starts at 4 s and the pattern of initiation alluded to in the previous records is now more marked i.e. the 2nd hydrofoil begins to generate lift force and drag force, albeit in the opposite sense to that expected, several seconds before the first hydrofoil initiates, with the 3rd hydrofoil beginning to develop lift force and drag force approximately 1 s later than the 1st hydrofoil. The drag force on the 2nd hydrofoil no longer tracks the corresponding lift force, but increases slowly as the distance covered increases. With this one exception, all forces are steady at t=14 s until t=26 s.

At the point of carriage deceleration, both the 1st and 2nd hydrofoils experience an increase in lift force, and the 2nd hydrofoil also experiences an increase in the applied drag force. This is consistent with the pattern of applied forces from the previous run at 2 m/s.

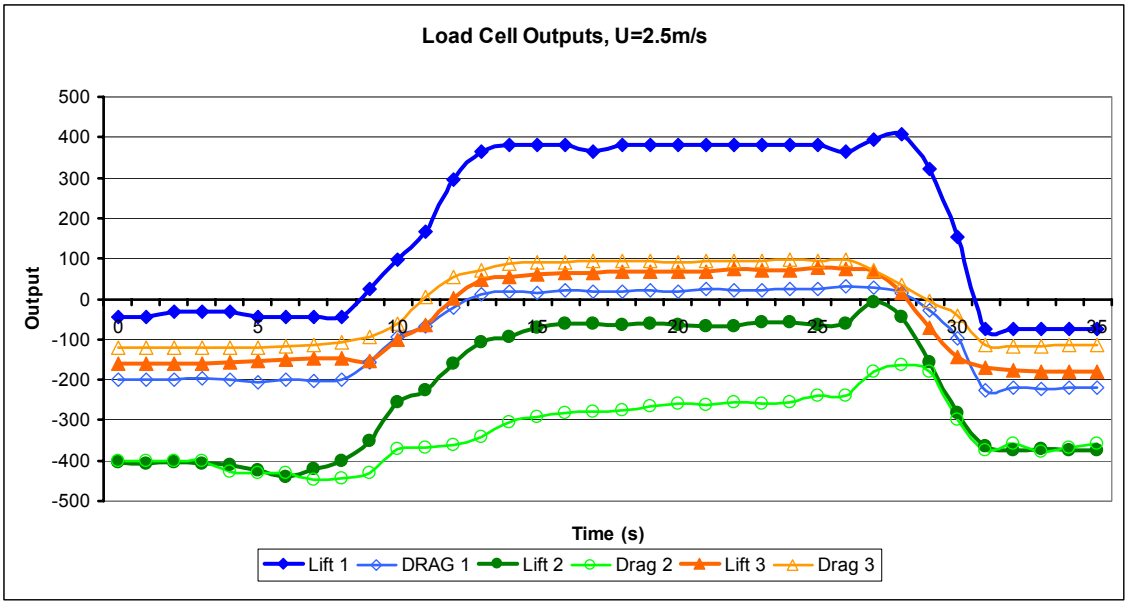

Figure 4-57: Load cell outputs for Umax=2.5 m/s

At a constant U=2.5 m/s the record of interest is of 12 s duration (Figure 4-58) and the applied lift forces and drag forces vary little with time. The 1st hydrofoil generates a lift force of 425 N (a substantial increase from U=2 m/s) and a drag force of 100 N, (essentially unchanged from U=2 m/s), whilst the 2nd hydrofoil produces 300 N of lift force and 100 N of drag force.

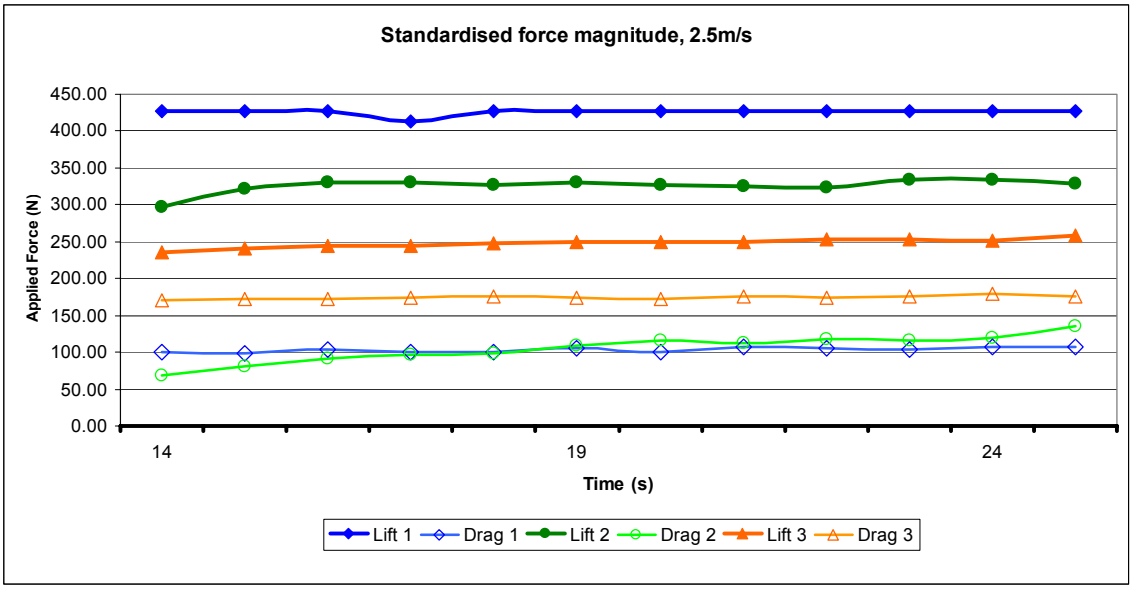

Figure 4-58: Force magnitudes at U=2.5 m/s

The 3rd hydrofoil generates 250 N of lift force (again, a substantial increase from U=2 m/s) and a drag force of approximately 175 N which is a relatively small increase from 160 N at U=2 m/s.

U=3 m/s

At U=3 m/s (Figure 4-59), the run starts at t=5 s and the 1st and 2nd hydrofoils both respond immediately, again in the opposite sense to expectation, with the 3rd hydrofoil initiating much more slowly. At t=7 s, all of the hydrofoils are increasing their lift force contribution at the same rate, with the drag forces of the 1st and 2nd hydrofoils maintaining a reduced rate of change. At t=11 s, the 1st and 3rd hydrofoils are beginning to level off to their constant velocity values. However, the 2nd hydrofoil has apparently stalled with a value of lift corresponding to the at-rest measurements, and the drag force value remaining constant. The situation remains unchanged until the carriage is decelerated at t=22 s, when a brief but sharp rise is recorded before all values settle when the carriage halts.

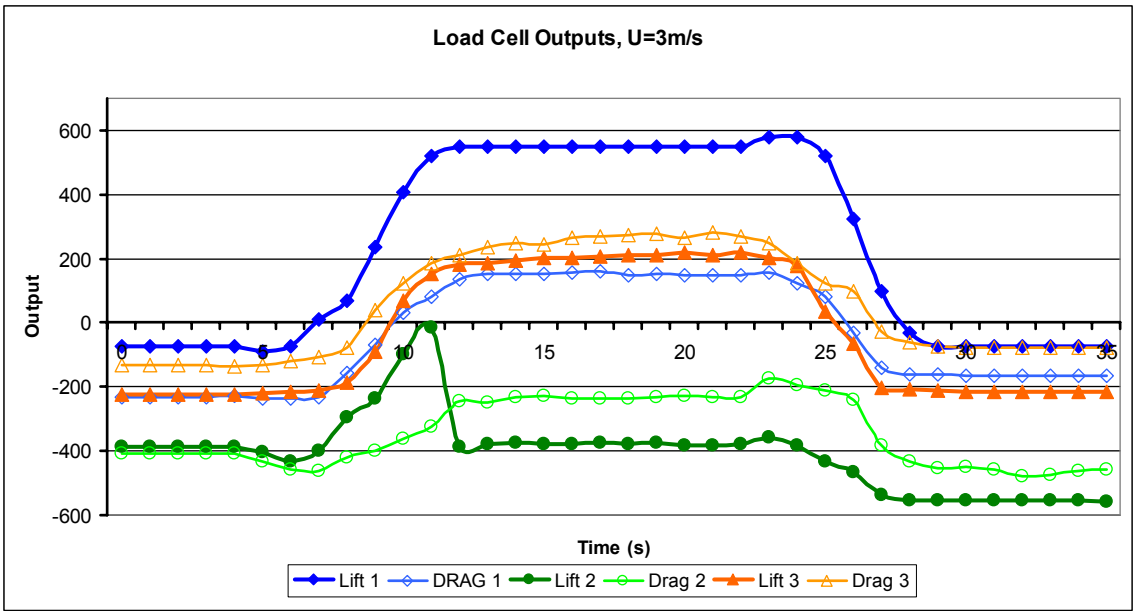

Figure 4-59: Load cell outputs for Umax=3 m/s

The constant velocity data window (Figure 4-60) exists for 10 s at 3 m/s. The lift force and drag force applied to the 1st hydrofoil are 640 N and 210 N respectively, both remaining steady for the duration of the constant velocity section. The 2nd hydrofoil has stalled completely and its applied drag force remains consistent at 125 N, whilst the 3rd hydrofoil experiences slowly increasing lift force and drag force, from ~430 N to ~460 N and ~280 N to ~350 N respectively.

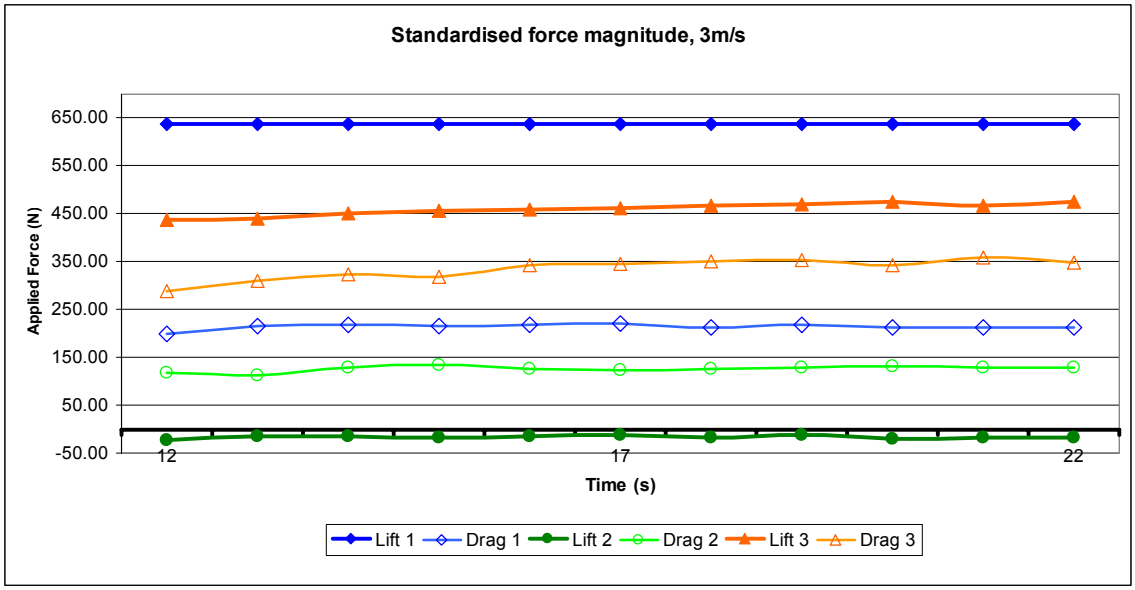

Figure 4-60: Force magnitudes at U=3 m/s

4.5.7 Discussion- Towing test model

The water within the tank remained unchanged during the experiment, and the temperature of the water would not have changed substantially during the 2 hours of testing, therefore the fluid properties can be assumed to have remained constant throughout. It is further assumed the carriage velocity was consistent with the velocity values requested on the day. Whilst the hysteresis of the load sensing cable system is not ideal, the sensitivity of the operational readings at U=1 m/s is in the region of ±2 N which gives a high degree of consistency at higher values of U. The use of correction factors extrapolated from the drag and lift forces applied to the structure for α=0^{o} and U=1 m/s, represents an additional source of error, with the drag force applied to the 1st hydrofoil being most at risk. There is justification for the 1st hydrofoil carrying the biggest drag load, in that it would have been advancing through an undisturbed stationary body of water, whereas the drag forces applied to the 2nd and 3rd hydrofoils would be reduced by virtue of advancing through the turbulence induced by the 1st hydrofoil assembly. After this first 'zero' run, all subsequent tests would have been through water disturbed by the previous test and therefore incorporating a degree of turbulence, notwithstanding the settling time of 5 minutes allowed between tests.

Using the same Froude scaling methodology that was applied to the river test model, the drag resistance results of the towing model are applicable to full scale flows in the range of 2.64 m/s to 7.93 m/s and comparison with the river test model requires that the towing model test results be extrapolated to 0.7 m/s.

It is clear from the lift coefficients plotted in Figure 4-61 that the lift forces are proportional to the increase in carriage velocity up to approximately 2 m/s, at which point the coefficients stagnate up to 2.5 m/s carriage velocity. At a carriage velocity of 2.5 m/s the lift coefficients of the 1st and 3rd hydrofoils increase slowly, but the middle hydrofoil stalls at flow velocities >2.5 m/s and intimation of this is indicated by the drop in C_L for the 2nd and 3rd hydrofoils at 2.5 m/s (Table 5-1) The lift coefficients for the 1st and 3rd hydrofoils show an increase as soon as the 2nd hydrofoil has stalled.

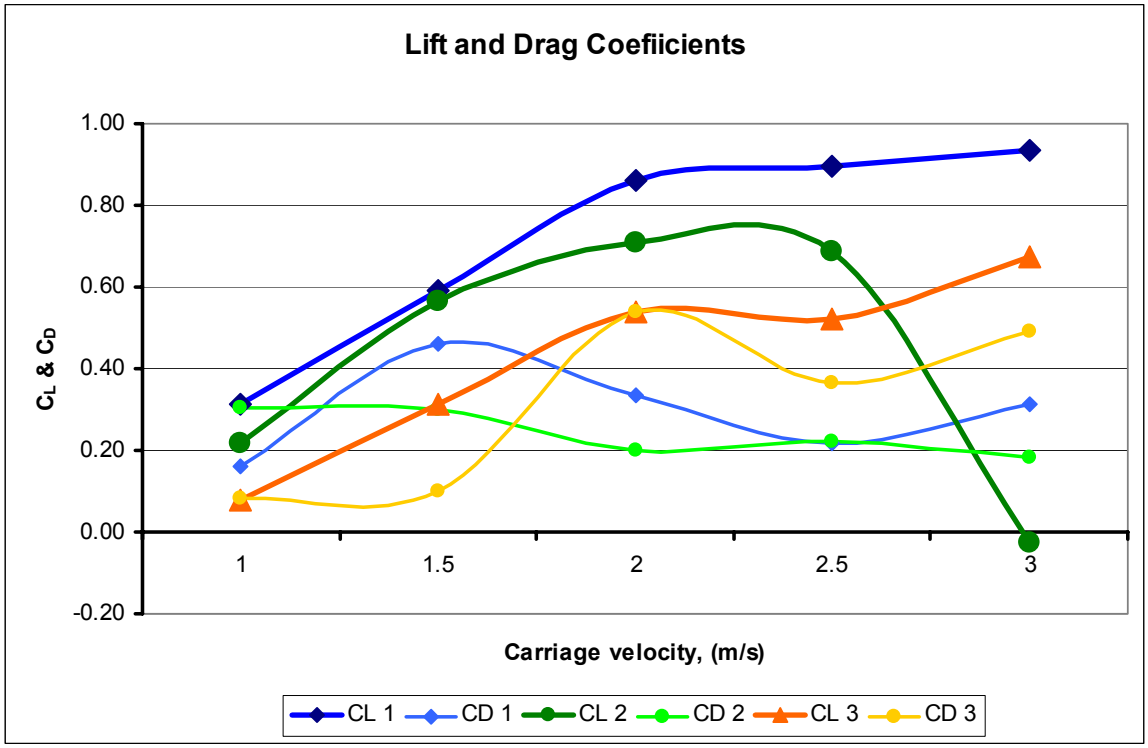

Figure 4-61: Drag and lift coefficients of tandem hydrofoils

The drag coefficient of the 2nd hydrofoil decreases slowly from 0.3 to 0.2 over the range of U, whilst at U=1.5 m/s, an increase in the 1st hydrofoil C_D corresponds with a stagnant C_D for the 3rd hydrofoil. At U=2 m/s the situation reverses when the C_D for the 3rd hydrofoil increases sharply to 0.5 at the same time that the C_D for the 1st hydrofoil drops to 0.35. This implies that at velocities of 1.5 m/s, the drag of the 2nd and 3rd hydrofoils is being partially borne by the leading (1st) hydrofoil, (this has a counterpart in motor racing known as slipstreaming) but at 2 m/s the 3rd hydrofoil is taking more drag loading, to the benefit of the 1st and 2nd hydrofoils. The Lift/Drag ratio at 2 m/s is 2 and at 1.5 m/s it is 1.7. The best lift/drag ratio is achieved at U=2.5 m/s (2.6) whilst at 3 m/s it has dropped to 1.6 due to the loss of lift contribution from the middle foil.

Summary of towing model experiment

The data falls within the confidence intervals of a normal distribution and represents the relationship of the hydrofoils in terms of lift forces and drag

forces applied whilst being moved through a stationary body of water. The test velocities are higher than would be desirable for direct comparisons with the river test model, but are generally of similar order and can therefore be extrapolated with a degree of confidence.

4.6 Chapter Summary

The Sea Snail concept has been developed from a basic spreadsheet model through the application of Low-Aspect-Ratio hydrofoil theory from Chapter 3 to laboratory and field trial models. The concept of using the lift forces from hydrofoils to add downforce to the weight of a submerged frame in a moving flow has been shown to be valid, and the particular array pattern used behaves as intuitively expected, i.e. the lift force decreases from the leading hydrofoil to the trailing hydrofoil whilst the drag force increases. The challenges of developing meaningful experiments from limited resources were met and the compliance of the tests with the demands of the principal dimensionless coefficients was demonstrated.

The river model using Froude scaling demonstrated the variation of lift forces and drag forces applicable to a tandem hydrofoil set at a sequence of angles of attack for a consistent velocity.

The towing model illustrated the variation in lift force and drag force between the hydrofoils at a constant angle of attack for different flow velocities, including the stall of the central hydrofoil at 3 m/s.

The results of the mathematical modelling and the experiments will be brought together and discussed in Chapter 5.

Chapter 5 Discussion and Conclusions

5.0 Chapter introduction

The release of the Stern Report on climate change [**112**] has added a sense of commercial urgency to the academic and scientific identification of the questions posed by climate change. During the four years spanned by this project, the UK energy security issue has become more focussed and is now given much greater political attention than before. The UK (and other energy dependent economies) has identified renewables as a necessary component of its energy supply, and that access to marine renewables is an advantage.

The exploitation of tidal streams is difficult, but the potential energy benefits are substantial and predictable. If the recent proposals [**113**] to raise the level of Renewable Obligation Certificates (ROC's), is approved, then a sizeable barrier to commercial generation is removed.

Regardless of the economic manipulation, marine renewables are unlikely to generate the same level of profit that hydrocarbons enjoy, and therefore the installation of marine turbines must be cost effective. In addition, experience clearly indicates [**114**] that attempting to install very large devices without having developed the skills and knowledge from small installations carries many unforeseen risks that potential investors are understandably wary of.

This thesis has proposed a support structure that is cost effective, easily fabricated, applicable to a broad range of bi-directional sites and capable of supporting any of the present energy conversion technologies described in Chapter 1.

5.1 Devices and moorings

The range of tidal energy device proposals is expanding at great speed, reminiscent of the explosion of ideas for wind energy in 1960's and 1970's, most of which have been left behind by the three-bladed axial devices that are now operating cost-effectively (albeit with ROC support) throughout the UK. The linear momentum theory suggests that the forces applied to an axial or crossflow turbine are (for a given flow velocity) a function of the area that the turbine presents perpendicular to the flow. From a reaction standpoint then, the supporting structure will be required to resist the same lateral force for either type of turbine for a given power output. However, it is possible that a crossflow turbine can be carried by a shorter structure than that required by an axial turbine, thus reducing the restoring moment required, whether the turbine is surface mounted or seabed mounted. Crossflow turbines have the additional advantage of being omni-directional with reference to the horizontal flow direction and thereby simplifying much of the structural and power transmission systems. However, at present crossflow turbines are very sensitive to tip-speed ratio and may not be applicable over a broad range of flow velocities.

The major cost in tidal stream energy exploitation is the supporting structure and mooring system and a significant component of that is the boat hire required for the works.

Gravity fixings are an attractive option allowing onshore fabrication of the complete structure prior to the onsite installation of the support, followed by the attachment of the turbine and power train. It has been shown that although using concrete as a gravity anchor is relatively cheap, the mass required for anchoring tidal turbines is considerable, even with the addition of reinforcing. Concrete behaves very well under a compressive load, but turbine anchoring is largely a tensile requirement and consequently requires a mass twice the gravitational design requirement. Thus a 5 m diameter turbine generating 100 kW in a 3 m/s stream requires approximately 211 dry tonnes of concrete as a gravitational base or 2 x 150 dry tonnes as a

gravitational anchor for a positively buoyant device, and cranage would be 1479 tonne metres and 900 tonne metres respectively.

The optimal operation of a tidal turbine requires good alignment of the turbine with the freestream flow vector and for a gravity base to achieve this will require seabed preparation. The combined effects of scour and the mass of a gravity base in addition to the cyclic loading of the tidal streams will almost certainly shift the alignment of the turbine over a period of time thus reducing its effectiveness as a power generator. Due to the combination of turbine load and buoyancy, positively buoyant devices will only achieve correct alignment at one flow velocity and therefore will not be optimal at lower velocities or risks being driven to the seabed at higher velocities. A partial solution to this is to provide separate buoyancy to support the tether cables, but additional buoyancy units will increase the horizontal and vertical loading on the anchors, and will automatically be in the upstream path of the turbine.

The monopile installation is probably the most satisfactory methodology from a purely engineering perspective, offering a rigid structure with tight positional control. The tubular cantilever is inherently strong and, with the hydrocarbon based experience from the North Sea, the effect of marine forces on tubulars is a well understood discipline, making the structural design relatively straightforward. The capability to bring the turbine and nacelle to the surface for maintenance and repair offers a reasonably safe working environment, though major overhauls still require that the turbine/gearbox/generator assembly is returned to a land-based facility. The challenge for monopile installations is the cost of the highly specialised workboat required for drilling the socket whilst remaining on site in a strong flow. Waiting time for weather is a significant and unpredictable factor in the process and a few days of poor weather could render a device unprofitable before it has been commissioned.

Use of diving personnel to install large devices in tidal streams is hazardous and time consuming due to the very short dive times available between flows

and divers cannot work in flows >0.5 m/s [**115**] Use of rock bolts is therefore an unlikely fixing method given that the number of drillings and the size of the drillings are approximately inversely proportional, thereby making the dive time required essentially constant for a given fixing strength required.

The commercial viability of tidal stream energy requires the development and availability of cheap, reliable technology that can be easily and safely installed with minimal disturbance to its host environment. The Sea Snail concept fulfils all of these requirements. It is easily fabricated from standard steel tubulars and transported as a flat-pack system to a quayside close to the deployment site. Assembly is straightforward and can be undertaken with a readily available crane and skilled but non-specialist labour.

Once assembled, it can be towed to site on integral buoyancy floats and sunk into position by flooding the tanks. Positioned on the seabed, it can be remotely levelled using a hydraulic ram on each leg and underside of each foot can be customised according to the seabed conditions e.g. serrated teeth for scoured rock conditions or short spikes for softer materials

The complete Sea Snail unit weighs around 22 tonnes with a 5 m diameter turbine and requires a cranage capability of around 200 tonne metres, considerable less than existing proposals

5.2 Tidal streams

The exploitation of tidal stream energy is but one strand of the power generating mix that the world will need in the 21st century. It is a viable and predictable resource for those regions that have it, but the current level of understanding of the resource is very simplistic, and substantial claims have been extrapolated from historical information taken from charts and tidal atlases. Most device designs have been validated against well behaved laboratory-based flows or towing tank experiments, but the world of real tidal stream flows is far more variable with fluctuations caused by bumps, hollows and trenches. Additional forcing input from waves and meteorological influences will create pressure and velocity changes that are difficult to predict or quantify. The implications for mooring and support systems are that static devices will have to be heavily over-specified (and therefore expensive) to reliably resist the poorly understood range of applied forces. If a device can respond dynamically by increasing its performance in proportion to the same range of forces being applied to the turbine then it does not require such levels of over-specification.

5.3 Sea Snail models and hydrodynamics

The hydrodynamics of fully immersed bodies is well understood, though the analysis of low-aspect-ratio hydrofoils is better served by the addition of empirical laboratory results to the mathematical theory. The combined results of the mathematical modelling, tow tank testing and field work demonstrate that an array of hydrofoils, distributed in a particular pattern can be employed to secure a piece of static equipment within a vigorous flow. The early model, developed from a set of assumptions regarding the numerical values of C_L and C_D , showed that both slippage and overturning of the structure would occur in a narrow velocity band of 1.8 – 2.5 m/s and that neither failure mode exists in isolation. Careful attention to the geometry of the structure, in combination with the lift force from the hydrofoils, significantly improved the devices' resistance to overturning but also impacted on the logistics management of the sea trials device.

The early work on the Sea Snail structure illustrated the design areas that required further and deeper understanding, principally the interaction of the flow between adjacent hydrofoils. The field test model confirmed that the leading hydrofoil would generate the greatest lift force, and also illustrated the advancement of the flow stagnation point with the increased value of α. The tow tank testing showed that the hydrofoils do operate at decreasing values of C_L according to their position in the array, as intuitively expected, and that at high flow velocities (≈3 m/s) for this array pattern at the dimensions used, the middle hydrofoil is stalled completely by the disturbed flow leaving the lead hydrofoil.

5.3.1 Wakes and Stall

The wake of a hydrofoil is a measure of the velocity (and therefore pressure) differential of the upper and lower flows as they re-engage at the trailing edge of the hydrofoil and the fundamental theory is generally covered under 3.3.6 on page 124. The effects of wake development on the hydrofoil array used in this work are distorted by the close proximity of the hydrofoils. The

separation of flow from the low-pressure side is an inevitable result of the fluid being unable to follow the surface boundary smoothly due to the hydrofoil being overloaded either in terms of its angle of attack or the velocity of the flow over its surfaces. As a result, the separated flow contains regions of rotational flow and the boundary layer breaks down taking with it the irrotational model of the flow around a hydrofoil beyond the boundary layer. All flow of practical value leaving a hydrofoil trailing edge will develop a wake; if there were no velocity or pressure variation then no lift will have been generated and the hydrofoil will have performed no purpose.

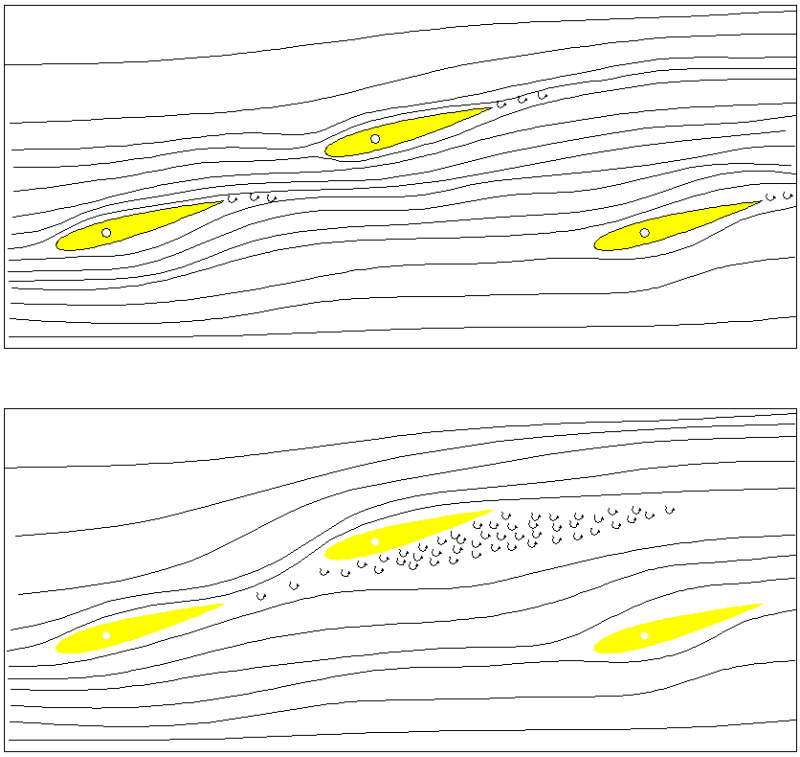

Figure 5-1: Sketch of attached and detached flow over the hydrofoil array

In the towing test model, the interaction of the trailing hydrofoils with the wake of their upstream companions for flows <2.5 m/s would generally have been similar to the upper panel in Figure 5-1, whereby the turbulence in the wake of the lead hydrofoil will not affect the flow over the 2nd hydrofoil provided that the streamline containing the turbulence does not subsequently encompass the 2nd hydrofoil. In the lower panel of Figure 5-1, the rotational

turbulent eddies are within the same streamline as the flow arriving at the 2nd hydrofoil and the boundary layer of the 2nd hydrofoil is reduced by this effect. As a result, the 2nd hydrofoil is unable to establish circulatory flow and all lift is lost, though the drag remains consistent, see Figure 4-61.

The idealised model of a wake is discussed under 3.3.2 on page 110 and its effects on the induced angle of attack, upwash and end effects.

The symmetrical NACA0013 hydrofoil shape is hydrodynamically efficient and will not create undue pressure drag. There are profile modifications methods of reducing the pressure drag such as making the maximum thickness of the hydrofoil occur nearer to the trailing edge, thus shifting the negative pressure point closer to the trailing edge also. However this has the effect of allowing the hydrofoil to stall quicker than with a standard NACA0013.

The hydrofoil array pattern used in the Sea Snail project was chosen intuitively and it is recognised that much more work is required to identify the optimal hydrofoil distribution for this type of application.

5.4 Synthesis of full scale data from test models

5.4.1 Drag Forces from towing model

As discussed under 4.3.1, there exists a contradiction under ordinary laboratory conditions between Reynolds Number scaling and Froude Number scaling for calculation of the total resistance to the flow created by a device or structure. The semi-empirical solution proposed by Froude, and used heavily in naval architecture and model ship testing, divides the total resistance of a structure to a flow into two components,

$$R_{total} = R_{SF} + R_{PF} \qquad \textbf{(5-1)}$$

Where the skin friction resistance is

$$R_{SF} = 0.5 C_F \rho A U^2 \qquad \textbf{(5-2)}$$

And the residual or pressure force resistance is

$$R_{PF} = 0.5 C_R \rho A U^2 \qquad \textbf{(5-3)}$$

For the coefficients, C_F is an empirical skin-friction coefficient widely given as

$$C_F = 0.074 (Re)^{0.2} \qquad \textbf{(5-4)}$$

And C_R is the coefficient of the pressure force resistance and is a function of Froude and Newton (or Euler) numbers. If both Fr and Eu are made the same for both model and prototype, then $C_R(F_R,E_U)$ will be the same for both and R_{PF} for the model will be the same as R_{PF} for the prototype, hence

$$C_R = \frac{R_{PF}(m)}{0.5 \rho A_m U_m^{\ 2}} = \frac{R_{PF}(p)}{0.5 \rho A_p U_p^{\ 2}} \qquad \textbf{(5-5)}$$

Consequently

$$C_R = \frac{R_{PF}(m)}{R_{PF}(p)} = \frac{0.5 \rho A_m U_m^{\ 2}}{0.5 \rho A_p U_p^{\ 2}} = \frac{A_m U_m^{\ 2}}{A_p U_p^{\ 2}} \qquad \textbf{(5-6)}$$

If the bodies are geometrically similar then lengths will be proportional by a scale factor (n) and areas will be proportional by n^2 so,

$$\frac{A_m}{A_p} = \frac{1}{n^2} \qquad \textbf{(5-7)}$$

Since it has been specified that model and prototype have the same value of Fr then,

$$\frac{U_m{}^2}{U_p{}^2} = \frac{\sqrt{A_m}}{\sqrt{A_p}} = \frac{1}{n} \qquad \textbf{(5-8)}$$

Substituting ***(5-8)*** and ***(5-7)*** into ***(5-6)*** gives,

$$\frac{R_{PF}(m)}{R_{PF}(p)} = \frac{1}{n^3} \qquad \textbf{(5-9)}$$

so

$$n^3 R_{PF}(m) = R_{PF}(p) \qquad \textbf{(5-10)}$$

and the total resistance of the prototype hydrofoil, given by ***(5-1)***, is

$$R_{total} = 0.5 C_F \rho A_p U_p{}^2 + n^3 R_{PF}(m) \qquad \textbf{(5-11)}$$

The pressure force resistance can be found from the towing model resistance as follows, for a scale factor of 7, which gives a model towing velocity of 0.76 m/s as representative of 2 m/s full scale, as discussed for the river test model.

The value of C_F is calculated, based on the value of Re for the towing model,

$$C_F = 0.074(Re)^{0.2} = 5.85 * 10^{-3}$$

$$R_{SF} = 0.5 C_F \rho A_m U_m{}^2 = 0.256\ N$$

The total drag resistance on the model is measured and the values found at U=1m/s for hydrofoils 1, 2 and 3 respectively from left to right are,

$$Rm_{total} = 12.07\ N \quad 23.14\ N \quad 6.24\ N$$

Therefore the residual resistance, R_{PF} is,

$$R_{PF} = Rm_{total} - R_{SF}$$

$$R_{PF} = 11.81\ N \quad 22.88\ N \quad 5.98\ N$$

Assuming that drag forces are only proportional to $U^{2,}$, find the model pressure drag forces at 0.76 m/s, $R_{PF(0.7)}$

$$R_{PF(0.7)} = R_{PF} * 0.76^2 = 6.8\,N \quad 13.21\,N \quad 3.46\,N$$

Calculate the prototype scale (Subscript (*p)*) properties. First, find the residual resistance on the full scale Sea Snail, $R_{PF(p)}$

$$R_{PF(p)} = n^3 * R_{PF(0.7)}$$

$$R_{PF(p)} = 2341\,N \quad 4534\,N \quad 1186\,N$$

The value of $C_{F(p)}$ is calculated, based on the value of Re for the full scale Sea Snail,

$$C_{F(p)} = 0.074(Re)^{0.2} = 3.263 * 10^{-3}$$

$$R_{SF(p)} = 0.5 C_{F(p)} \rho A_p U_p{}^2 = 48.943\,N$$

So the total resistance of the full scale hydrofoils for one side of the Sea Snail in a flow velocity of 2 m/s is,

$$R_{total(p)} = R_{PF(p)} + R_{SF(p)} = 2390\,N + 4583\,N + 1325\,N + 49\,N = 8347\,N$$

A full set of six hydrofoils can be expected to offer a resistance to the flow of 16694 N at 2 m/s.

5.4.2 Lift forces from towing model

Since only pressure forces are acting, the lift forces applied to a hydrofoil are only a function of Eu, provided that the hydrofoil is submerged by a depth greater than twice its chord. Since Eu has no geometry dependence, then if the velocities are equivalent, the pressures are also equivalent.

$$\frac{P_m}{\rho U_m} = \frac{P_p}{\rho U_p} \qquad \textbf{(5-12)}$$

From the lift force equation, $F_L = C_L 0.5 \rho A U^2$ if the pressures are equivalent then the force per unit area is the same for both and the pressure is independent of area. Therefore, the value of C_L for the model is the same as the value of C_L for the full scale Sea Snail at any given test velocity and can be used to calculate the lift forces generated by the Sea Snail hydrofoils, but with a significant proviso; the separation distance between the hydrofoils is a

function of the scale factor. This means that the loss of lift created by the 2nd hydrofoil being forced to operate in the wake of the 1st hydrofoil is due to their close proximity at 1/7th scale, and not to the hydrofoil array pattern. At this scale the linear distance between the trailing edge of the 1st hydrofoil and the leading edge of the 2nd hydrofoil is 271 mm, which is covered in 0.09 s by a flow of 3 m/s. For the same phenomenon to occur at Sea Snail dimensions, would require a tidal stream velocity of 21 m/s. From the towing model data the values of C_L for the hydrofoils are:-

Table 5-1: Lift coefficients for the towing model.

C_L from towing model			
U (m/s)	C_L *1*	C_L *2*	C_L *3*
1	0.31	0.22	0.08
1.5	0.59	0.57	0.31
2	0.86	0.71	0.54
2.5	0.90	0.69	0.52
3	0.94	-0.02	0.67

In terms of lift force generated, the values in give the optimal operational conditions for the Sea Snail as 2.5 m/s. Subtracting the additional overturning moment generated by the hydrofoil drag from the additional restorative moment generated by the hydrofoil lift based on the values of C_L obtained from the towing model test, the net restorative moments attributable to the hydrofoils on the Sea Snail would be:-

Table 5-2: Net restorative moment for Sea Snail hydrofoils

Net restorative moment from hydrofoils (from towing data)							
			1 m/s	1.5 m/s	2 m/s	2.5 m/s	3 m/s
Hydrofoil 1, Restorative	*lift*	*MNm*	0.0271	0.1152	0.2993	0.4873	0.7311
Hydrofoil 1, Overturn	*drag*	*MNm*	0.0038	0.0086	0.0153	0.0233	0.0329
Hydrofoil 2, Restorative	*lift*	*MNm*	0.0112	0.0657	0.1464	0.2211	-0.0113
Hydrofoil 2, Overturn	*drag*	*MNm*	0.0110	0.0246	0.0440	0.0676	0.0960
Hydrofoil 3, Restorative	*lift*	*MNm*	0.0012	0.0108	0.0331	0.0503	0.0932
Hydrofoil 3, Overturn	*drag*	*MNm*	0.0020	0.0045	0.0079	0.0119	0.0166
Total restorative	*lift*	*MNm*	0.0395	0.1916	0.4789	0.7587	0.8130
Total overturn	*drag*	*MNm*	0.0169	0.0377	0.0671	0.1029	0.1455
Total Net	*lift-drag*	*MNm*	0.0227	0.1540	0.4117	0.6558	0.6675

Comparison of the net restorative moments with the overturning moments (Figure 5-2) shows that the Sea Snail would benefit from a surplus of approximately 750 kNm, and that when summed with the submerged weight of the Sea Snail, the net downforce (Figure 5-3) represents a no-slip confidence level of over 200%.

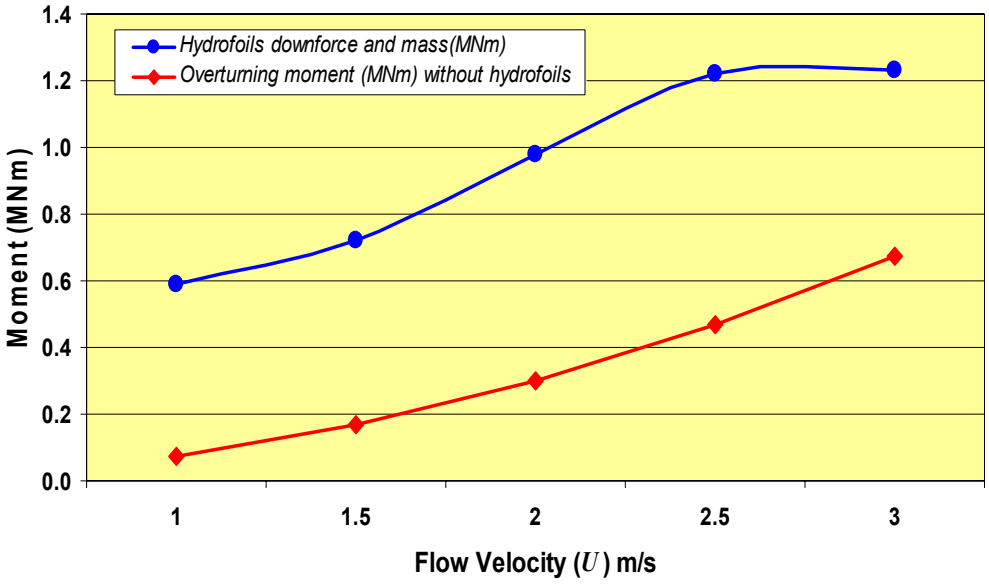

Figure 5-2: Comparison of overturning and restorative moments.

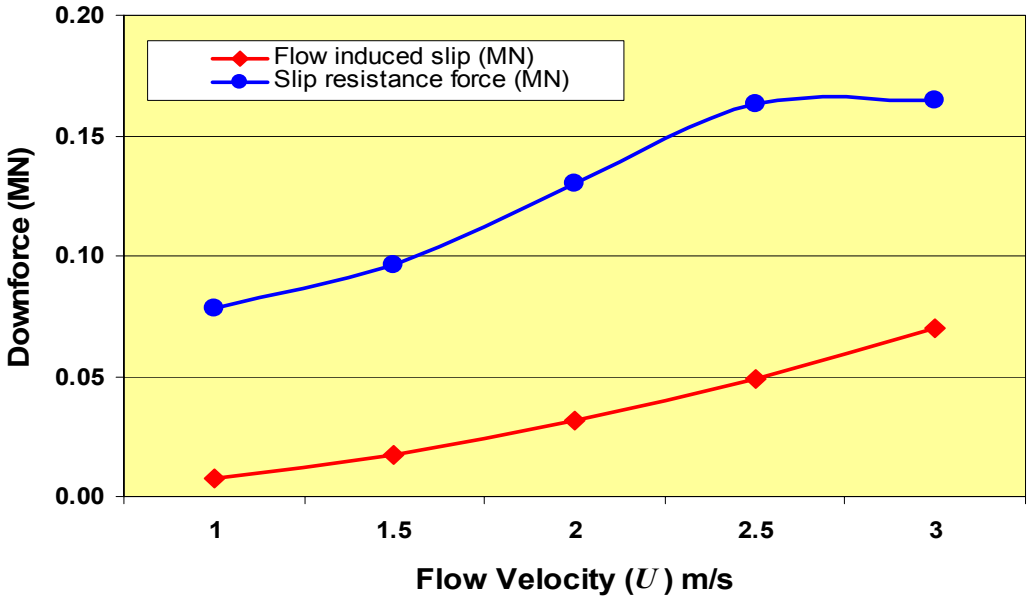

Figure 5-3: Comparison of flow induced slip and slip resisting forces.

5.4.3 Test and model data comparison

The river test model produced data from a range of values of α but only for one flow velocity, 0.76 m/s, and the data for comparison will be taken from α=15°.

The towing test model measured the lift and drag forces applied to each hydrofoil, whereas the river test model measured total drag force and split the lift force measurement between front and rear. Taking the average values of C_D and C_L from the experimental rigs gives the following comparisons,

Table 5-3: Test and model coefficients comparison

Source	Free stream Velocity (m/s)	C_D	C_L
River model α = 15°	0.76	0.12	0.93
Towing model α = 15°	0.76	0.18	0.70
DSP model	2.0	0.23	0.95
Low Aspect Ratio Model	2.0	0.18	0.53
Averages		0.18	0.78

The towing model gives good general agreement with the averaged results from the other models. The river test model recorded less drag force than is indicated by the other models and this is due to the 2nd hydrofoils proximity to the surface preventing the full wake expansion and the corresponding pressure drop that creates the form drag.

Tandem wings

The arrangement of the hydrofoils on the Sea Snail reflects its intended function as a turbine carrier and fulfils the requirements of handling by crane, amongst other priorities. The initial thinking was that the lead hydrofoils would be little affected by the flow over the trailing hydrofoils and that the distance between the lead hydrofoils point of action and the overturning axis would allow the generation of sufficient restoring moment from 1 pair of hydrofoils.

Subsequent theoretical analysis, in addition to the towing model test results, has shown that the Sea Snail hydrofoil configuration behaves more as a case

of tandem wings [**116**]. Generally, work involving hydrofoil interaction examines hydrofoils in cascades or ladders, where there is a distinct sandwiching of the flow between hydrofoils, and common endplates form part of the hydrofoil cascade structure. The fore and aft hydrofoils of fast boats do operate as tandem hydrofoils but the low relative velocity between the water and the hydrofoils on the Sea Snail makes extrapolation of data from hydrofoil boats unsuitable. The Sea Snail device, which proposed to position the 2nd hydrofoil ¼ span outboard of the 1st and 3rd hydrofoils would benefit from the canard arrangement so created, whereby the downwash leaving the leading hydrofoil outer end will contribute to the lift effect on the 2nd hydrofoil.

Novel contribution

The Sea Snail is protected by patents, either approved (Europe) or pending (U.S. and Australia). The application of hydrofoils to secure a stationary device in a moving flow is unprecedented and the principle is applicable to any vigorous flow, not necessarily tidal by nature. The capability to quickly and cost effectively deploy energy conversion equipment, with minimal environmental disturbance is a significant advance in the application of marine renewable energy. The simplicity of the supporting structure makes it easily fabricated with basic metalworking tools, and it does not, therefore rely on cutting edge technological support for its use.

Future work

- Subsequent to this thesis, an omni-directional model is being developed using the same concept that has been described herein, with a particular applicability to the vertical axis crossflow turbine proposals.
- The hydrofoil array pattern requires optimisation and it is additionally considered possible that hydrofoil alignment could be used to accentuate the flow at the turbine.
- The concept is appropriate for development as a river based device.

- The UK has a surfeit of tidal stream resource due to the existence of multiple amphidromic systems in the North Sea, English Channel, Irish Sea and North Atlantic, operating at different levels of resonance and phase difference, often at opposite ends of relatively narrow channels. Successful deployment and operation of tidal stream devices will require a full understanding of the flow characteristics and turbulent behaviour of these localised streams, as opposed to the simple acceptance of tidal velocities marked on charts and tidal stream atlases.

5.5 Conclusions

1) Low aspect ratio, symmetrical profile hydrofoils can be used to secure a static device in a moving flow.
2) The Sea Snail concept is a significant contribution in the development of tidal stream energy.
3) The hydrofoil array pattern used in this project is capable of securing a 5 m diameter turbine in a 3 m/s flow, but it is not necessarily an optimal pattern.
4) The Sea Snail concept requires fewer resources to achieve the same goal as a gravity base, a gravity anchor, or a drilled and grouted pile.
5) The Sea Snail concept is 90% lighter than the nearest equivalent gravity base system.
6) The Sea Snail concept as developed in this thesis is appropriate for bi-directional flows, thus making it applicable to large areas of many tidal stream sites.

References

1 Bryden IG, Couch SJ. ME1-Marine energy extraction: tidal resource analysis. Renewable Energy 2006;31: p133-139

2 MacKay DJC. Under-estimation of the UK tidal resource. Cambridge: [2006 Dec 7; 2007 June 3] Available from: www.inference.phy.cam.ac.uk/sustainable/book/tex/TideEstimate.pdf

3 Trapp AD. *The Engineering Business Limited, Stingray Tidal Stream Power Generator.* [Page on the internet]. Newcastle-upon-Tyne: The Engineering Business; c.2006 [2006; 2007 June 3]. Available from: http://engb.com/downloads/M0200301.pdf

4 Salter SH. Theta-Islands for flow velocity enhancement for vertical axis generators at Morecambe Bay. World Renewable Energy Conference. Aberdeen: 2005

5 Fraenkel PL. Marine Current Turbines: An emerging technology. paper for Scottish Hydraulics Study Group seminar; Glasgow 19/03/2004: p5.

6 Germanischer Lloyd, 14 Guideline for the certification of ocean energy converters (draft). 2005

7 Fraenkel PL. Marine Current Turbines: An emerging technology. paper for Scottish Hydraulics Study Group seminar; Glasgow 19/03/2004: p 4.

8 Bahaj AS, Myers LE. Fundamentals applicable to the utilisation of marine current turbines for energy production. Renewable Energy 2003; 28: p2205-2211.

9 Personal comment, I.G. Bryden

10 Bryden IG. Tidal energy. Encyclopaedia of Energy. 2004; 6: p148.

11 Twidell J, Weir T. Renewable energy resources. London: E&FN Spon; 2000, p213-216

12 Bryden IG, Couch SJ, Owen A, Melville GT. Tidal Current Resource Assessment. Proc IMechE (A) Journal of Power and Energy 2006;

13 Twidell J, Weir T. Renewable energy resources. London: E&FN Spon; 2000, p224

14 Ainsworth D, Thake J. *Final report on preliminary works associated with 1MW tidal turbine. URN Number 06/2046* [Page on the internet]. London: Department of trade and Industry; c.2000-2007 [2007; 2007 January 4]. Available from:

http://www.dti.gov.uk/files/file35033.pdf

15 Vauthier P. *Kite soars to new depths*. [Page on the internet]. Ontario: International Water Power and Dam Construction, Wilmington Media Ltd.; c.2007 [2007; 2007 January 4]. Available from: http://www.waterpowermagazine.com/storyprint.asp?sc=2034904

16 Marsh G. Tidal Turbine harness the power of the sea. Reinforced Plastics 2004 Jun; p44-47.

17 Gajanayake PA, Furukawa A, Okuma K, Applicability of Darrieus-Type turbine for extra low head tidal power generation. Int. J. Offshore and Polar Eng. 1998 Dec;8(4) ISOPE.

18 Salter SH. Proposal for a large, vertical-axis tidal-stream generator with ring cam hydraulics. 3rd European Wave Energy Conference: 1998 Oct; Greece

19 Kiho S, Shiono M, Suzuki K, The power generation from tidal current turbines by Darrieus turbine. 1996 WREC.

20 Low head tidal power Davis,B.V. Energy Conversion Engineering Conference, 1997. IECEC-97. Proceedings of the 32nd Intersociety Volume 3, Issue , 27 Jul-1 Aug 1997 Page(s):1982 - 1989 vol.3

21 Calcagno G, Salvatore F, Greco L, Moroso A, Eriksson H. Experimental and numerical investigation of an innovative technology for marine current exploitation: the Kobold turbine, Proc. 16th IOPEC, 2006 vol:1 part:1 pp323-30

22 *Enermar.* [Page on the internet]. Messina: Ponte di Archimede International S.p.A; c.2005-2007 [2007; 2007 January 4]. Available from: http://www.pontediarchimede.com/language_us/progetti_det.mvd?RECID=2&CAT=002&SUBCAT=&MODULO=Progetti_ENG&returnpages=&page_pd=p

23 T-06-00217-00-REP Potential applications for Flettner rotors and Turbosails in tidal stream turbines, Report for the DTI by Oreada. URN Number 05/636.

24 Schonborn A, Chantzidakis M, Development of a hydraulic control mechanism for cyclic pitch marine current turbines. Renewable Energy In Press; 2006: (Source: ScienceDirect)

25 Harris RE, Johanning L, Wolfram J, Mooring systems for wave energy converters: a review of design issues and choices. Unpublished paper produced as part of

the Supergen Marine Consortium work
26 Berteaux HO, Buoy Engineering, New York:John Wiley & Sons; 1976, pp266-7
27 Aubeny C, Murff JD, Simplified limit solutions for the capacity of suction anchors under undrained conditions, Ocean Engineering 32 2005; p864–877
28 Teng HH, Applied offshore structural engineering, Houston: Gulf Publishing; 1984,p95-8
29 Bryden IG, Naik S, Fraenkel P, Bullen CR. Matching tidal current plants to local flow conditions. Energy 1998; 23(9): p699-709.
30 Orme JAC, Masters I. Analysis and comparison of support structure concepts for tidal stream turbines. Unpublished paper.
31 Marsh G, Tidal Turbine harness the power of the sea. Reinforced Plastics 2004 Jun p46.
32 The Engineering Equipment and Materials Users Association (EEMUA). Construction specification for fixed offshore structures in the North Sea. 158; 2000.
33 Le Tirant P. Seabed reconnaissance and offshore soil mechanics. Editions Technip: Paris; 1979, p109.
34 Fraenkel PL. Marine Current Turbines: An emerging technology. paper for Scottish Hydraulics Study Group seminar; Glasgow 19/03/2004: p 7.
35 Berteaux HO, Buoy Engineering, New York:John Wiley & Sons; 1976,p135-148
36 Joosten H. Elastic mooring of navigation buoys. International ocean systems 2006; 10(5):
37 Patel MH. Dynamics of offshore structures. London: Butterworths; 1989, pp283-337.
38 Owen A, Bryden IG, Prototype Support Structure for Sea Bed Mounted Tidal Current Turbines. Proc I Mech Eng, Part M, Journal of Engineering for the Maritime Environment, 2006
39 Kerr A, Cowling MJ, Beveridge CM, Smith MJ, Parr, Effects of marine biofouling on optical sensors. ACS, Environment International,1998; 24(3): pp 331-343.
40 Yebra DM, Kiil S, Dam-Johansen K, Anti-fouling technology past, present and future. Progress in organic coatings 2004;50 pp75-104.

41 Pickard GL, Emery WJ, Descriptive Physical Oceanography. 5th Ed. Oxford: Butterworth Heinemann; 1995. p180-1.
42 UNEP/GRID-Arendal, *World ocean thermohaline circulation*, UNEP/GRID-Arendal Maps and Graphics Library, 2000, Available from: http://maps.grida.no/go/graphic/world-ocean-thermohaline-circulation> [Accessed 2007 January 11]
43 Cartwright DE. Tides, a scientific history. Cambridge: Cambridge University Press; 1999.
44 Darwin GHD. The Tides and Kindred Phenomena. 3rd Ed. London: John Murray; 1911.
45 Pond S, Pickard GL. Introductory dynamical oceanography. 2nd ed. Oxford: Butterworth-Heinemann; 2003. p261
46 Darwin GHD. The Tides and Kindred Phenomena. 3rd Ed. London: John Murray; 1911.
47 Munk WH, Cartwright DE. Tidal Spectroscopy and Prediction. Philiosophical Transactions, Royal Society of London, A, 259, 1966 p533-581.
48 Pugh DT, Tides Surges and Mean Sea Level Avon GB: Bath Press; 1987. p63.
49 Boon JD. Secrets of the tide. Chichester: Horwood; 2004. p21
50 Pugh DT. Changing sea levels. Cambridge: Cambridge University Press; 2004, p65.
51 Cartwright DE. Tides, a scientific history. Cambridge: Cambridge University Press; 1999, p198.
52 Pond S, Pickard GL. Introductory dynamical oceanography. 2nd ed. Oxford: Butterworth-Heinemann; 2003, p273.
53 Pond S, Pickard GL. Introductory dynamical oceanography. 2nd ed. Oxford: Butterworth-Heinemann; 2003, p275.
54 Charlier RH. Tidal energy. New York: Van Nostrand Reinhold Company Inc; 1982, p96.
55 Pugh DT, Tides Surges and Mean Sea Level Avon GB: Bath Press; 1987. p181.
56 Boon JD. Secrets of the tide. Chichester: Horwood; 2004. p39
57 Darwin GHD. The Tides and Kindred Phenomena. 3rd Ed. London: John Murray;

1911. p89
58 King CAM. Beaches and Coasts, London: Edward Arnold; 1959, p34-5.
59 King CAM. Beaches and Coasts, London: Edward Arnold; 1959, p27-8.
60 Pugh DT. Changing sea levels. Cambridge: Cambridge University Press; 2004, p118.
61 Roy AE. Orbital Motion. 2nd Ed, Bristol: Institute of Physics; 1982.
62 Wright J, Colling A, Park D. Waves tides and shallow water processes. 2nd Ed, Oxford: Butterworth-Heinemann & Open University; 2002 p22
63 Patel MH, Dynamics of offshore structures. London: Butterworths;1989 p121
64 Patel MH, Dynamics of offshore structures. London: Butterworths;1989 p188
65 *A historical perspective, drawn from the Ordnance Gazetteer of Scotland: A Survey of Scottish Topography, Statistical, Biographical and Historical, edited by Francis H. Groome and originally published in parts by Thomas C. Jack, Grange Publishing Works, Edinburgh between 1882 and 1885*. [Page on the internet]. Edinburgh: University of Edinburgh; c.1995-2007 [2007; 2007 January 15]. Used with permission from The Gazetteer for Scotland; available from: http://www.geo.ed.ac.uk/scotgaz/features/featurehistory6716.html#
66 Lamb H. Hydrodynamics. 6th Ed, Cambridge: University Press; 1957.
67 Avallone EA, Baumeister T. Marks standard handbook for mechanical engineers. 10th ed. Boston (Mass): McGraw-Hill; 1996. p3-48
68 Mutlu Sumer B, Fredsoe J. Hydrodynamics around cylindrical structures. Singapore: World Scientific; 1999, p3.
69 Schlichting H. Boundary layer theory. 6th ed. New York: McGraw-Hill; 1968, p17.
70 Shames IH, Mechanics of fluids. New York: McGraw-Hill; 1962, p246
71 Douglas JF, Gasioreck JM, Swaffield JA. Fluid Mechanics. 3rd Ed, Singapore: Longman Scientific and Technical; 1995, p379.
72 Vallentine HR. Applied hydrodynamics. SI Ed, London: Butterworths; 1969, p122-123.
73 Grimson J, Advanced fluid dynamics and heat transfer. London:McGraw-Hill; 1971. p106

74 Douglas JF, Gasioreck JM, Swaffield JA. Fluid Mechanics. 3rd Ed, Singapore: Longman Scientific and Technical; 1995, p225.

75 Mason F. *Geometry for Aerodynamicists.* [Page on the internet]. Blacksburg: Virginia tech; c.1993-2007 [2007 April 23; 2007 January 5]. Available from: http://www.aoe.vt.edu/~mason/Mason_f/CAtxtAppA.pdf.

76 Daskovsky M. The hydrofoil in surface proximity, theory and experiment. Pergamon; Ocean Engineering.2000; 27pp1129-1159

77 Hoerner S. Fluid dynamic lift. 2nd ed. Bakersfield CA: Mrs Liselotte A. Hoerner; 1985. p 8-7

78 White FM. Fluid Mechanics. 4th Ed. Singapore: WCB/McGraw-Hill; 1999. p524.

79 Fox RW, McDonald AT. Introduction to fluid mechanics. 2nd ed. New York: John Wiley & Sons; 1978. p 441.

80 Prandtl L. Fluid dynamics. London: Blackie & Son; 1949. p209

81 Anderson JD. Fundamentals of aerodynamics. 3rd ed (intn'l). Singapore, McGraw-Hill; 2001. p354.

82 Hoerner S. Fluid dynamic lift. 2nd ed. Bakersfield CA: Mrs Liselotte A. Hoerner;1985.p17-6.

83 Hoerner S. Fluid dynamic lift. 2nd ed. Bakersfield CA: Mrs Liselotte A. Hoerner;1985.p17-1.

84 Lloyd ARJM. Seakeeping, Chichester: Ellis Horwood; 1989, p62.

85 Whicker LF, Fehlner LF. Free stream characteristics of a family of low-aspect-ratio, all-movable control surfaces for application to ship design. Revised ed. 1958, p22.

86 Hoerner S. Fluid dynamic lift. 2nd ed. Bakersfield CA: Mrs Liselotte A. Hoerner;1985.p17-3.

87 Prandtl L. Fluid dynamics. London: Blackie & Son; 1949. p202.

88 Rogers EO, Donnelly MJ. Characteristics of a dual-slotted circulation control wing of low aspect ratio intended for naval hydrodynamic applications. Reno, AIAA, 42nd Aerospace Sciences Meeting, Jan 2004.

89 Hoerner S. Fluid dynamic lift. 2nd ed. Bakersfield CA: Mrs Liselotte A. Hoerner;1985;p17-2.

90 Fox RW, McDonald AT. Introduction to fluid mechanics. 2nd ed, New York: John Wiley & sons; 1978, p420.

91 Douglas JF, Gasioreck JM, Swaffield JA. Fluid Mechanics. 3rd Ed, Singapore: Longman Scientific and Technical; 1995, p811.

92 Douglas JF, Gasioreck JM, Swaffield JA. Fluid Mechanics. 3rd Ed, Singapore: Longman Scientific and Technical; 1995, p336.

93 Commission of European Communities, DGXIII, The exploitation of tidal and marine currents, Program JOULE II. Report: EUR16683 EN. No. JOU2-CT93-0355 p25.

94 Hoerner S. Fluid dynamic lift. 2nd ed. Bakersfield CA: Mrs Liselotte A. Hoerner; 1985. p 20-13

95 Massey B. Mechanics of Fluids. 7th Ed. Cheltenham: Stanley Thornes (Publishers) Ltd; 1998, p172

96 Massey B. Mechanics of Fluids. 7th Ed. Cheltenham: Stanley Thornes (Publishers) Ltd; 1998, p185

97 Elgar P, Sensors for measurement and control, Harlow: Pearson Education Ltd; 2001, p80

98 *International standard IEC 60529.* [Page on the internet]. Geneva: International Electrotechnical Commission; c.2007 [2007; 2007 June 3]. Available from: http://webstore.iec.ch/preview/info_iec60529%7Bed2.1%7Den_d.pdf

99 *International organisation of legal metrology* [Page on the internet]. Paris: OIML Secretariat; c.2007 [2007 May 31; 2007 June 3]. Available from: http://www.oiml.org/

100 Roberson JA, Cassidy JJ, Chaudry MH. Hydraulic Engineering, Boston: Houghton Mifflin; 1988 p202

101 RS Components Ltd. *RS Datascan data acquisition system.* [Page on the internet]. Northampton: RS Components Ltd; c.2002-2007 [2007 June 1; 2007 June 3]. Available from: http://docs-europe.electrocomponents.com/webdocs/001a/0900766b8001a9c6.pdf

102 Jordan DW, Smith P. Mathematical techniques, 2nd Ed, Oxford: Oxford

University Press; 1998, p697

103 Hoerner S. Fluid dynamic lift. 2nd ed. Bakersfield CA: Mrs Liselotte A. Hoerner; 1985. p 8-7

104 *Acre road Hydrodynamics Laboratory.* [Page on the internet]. Glasgow: Universities of Glasgow and Strathclyde; c.2007 [2007; 2007 June 3]. Available from: http://www.na-me.ac.uk/facilities/cmh.htm

105 *Details of grant.* [Page on the internet]. Swindon: Engineering and Physical Sciences Research Council; c.2003-2007 [2007; 2007 June 3]. Available from: http://gow.epsrc.ac.uk/ViewGrant.aspx?GrantRef=GR/S26958/01

106 Hoerner S. Fluid dynamic lift. 2nd ed. Bakersfield CA: Mrs Liselotte A. Hoerner; 1985. p 8-6

107 Hunsaker JC, Rightmire BG. Engineering applications of fluid mechanics, New York: McGraw-Hill; 1947, p120

108 Berteaux HO, Buoy Engineering, New York:John Wiley & Sons; 1976, pp75-7

109 Iga Y et al, Numerical study of sheet cavitation break-off phenomenon on a cascade hydrofoil, CAV2001, 4th Int. Symposium on Cavitation, Californian Institute of Technology, 2001

110 Matveev KI, Matveev II. Tandem hydrofoil system, Ocean engineering, 28, 2000, pp253-261

111 Massey B. Mechanics of Fluids. 7th Ed. Cheltenham: Stanley Thornes (Publishers) Ltd; 1998, p344

112 Stern N. *Stern Review on the Economics of Climate Change.* [Page on the internet]. London: HM Treasury; c.200-2007 [2007 Feb 12; 2007 January 5]. Available from: http://www.hm-treasury.gov.uk/independent_reviews/stern_review_economics_climate_change/stern_review_report.cfm

113 *Consultation on Review of ROS (Support for Wave and Tidal Power) 2006.* [Page on the internet]. Edinburgh: Scottish Executive; c.2000-2007 [2007; 2007 January 5]. Available from: http://www.scotland.gov.uk/Resource/Doc/115084/0028289.pdf

114 *Renew on line.* [Page on the internet]. Milton Keynes: Energy and environment research unit; c.2000-2001 [2001; 2007 January 5]. Available from: http://eeru.open.ac.uk/natta/renew96(4).html

115 Williams RV Nielsen JB. Modelling of currents in Yell Sound, Proc SUT Modelling the offshore environment, vol 12,p227-8, April 1987

116 Hoerner S. Fluid dynamic lift. 2nd ed. Bakersfield CA: Mrs Liselotte A. Hoerner; 1985. p 20-12